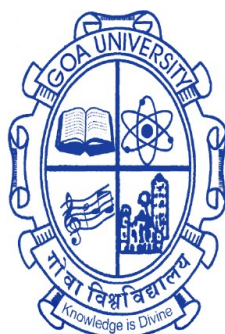# ISOLATION OF MARINE NATURAL PRODUCTS AND SYNTHESIS OF BIOACTIVE MOLECULES USING CHIRON APPROACH

A Thesis submitted in partial fulfillment for the Degree of

DOCTOR OF PHILOSOPHY

in the School of Chemical Sciences
Goa University

By

Lima Rodrigues
School of Chemical Sciences
Goa University
Goa

December *2023*

DECLARATION

I, Lima Rodrigues hereby declare that this thesis represents work which has been carried out by me and that it has not been submitted, either in part or full, to any other University or Institution for the award of any research degree.

Place: Taleigao Plateau.   Lima Rodrigues

Date :   PhD Candidate

                                                                         School of Chemical Sciences

                                                                         Goa University, Goa

CERTIFICATE

We hereby certify that the work was carried out under our supervision and may be placed for evaluation.

Prof. S. G. Tilve   Prof. V. M. S. Verenkar

Research Guide   Co-guide

School of Chemical Sciences   School of Chemical Sciences

Goa University,Goa   Goa University, Goa

Dedicated to my Parents,

Mr. Carlos Rodrigues & Mrs. Etelvina D. Rodrigues

And to my Husband, Mr. Rosnelo Fernandes

ACKNOWLEDGEMENT

Contents

2　Chemical transformation of natural elemol to elemoxide and investigation of tyrosinase inhibition studies

to evaluate its potential for COVID-19 treatment

List of Abbreviation

General abbreviations

FDA	-	Food and Drug Administration
EU	-	European Union
EMA	-	European Medicines Agency
PICS	-	Preintegration complexes
MTB	-	Microbacterium Tuberculosis
IC_{50}	-	Half maximal inhibitory concentration
EC_{50}	-	Half maximal effective concentration
HIV	-	Human immunodeficiency viruses
SEO	-	Seaweed essential oil
SD	-	Standard deviation
cc	-	Colum chromatography
R_f	-	Retention factor
TLC	-	Thin layer chromatography
UV	-	Ultraviolet
IR	-	Infrared
NMR	-	Nuclear Magnetic Resonance
DEPT	-	Distortionless Enhancement by Polarization Transfer
LCMS	-	Liquid chromatograpgy mass spectrometry
HRMS	-	High resolution mass spectrometry
ESI	-	Electron spray ionisation
TOF	-	Time of flight
HSV	-	Hepes simplex virus
Equiv	-	Equivalent
anhyd	-	Anhydrous
rt	-	Room temperature
SARS	-	Structure-activity relationship studies
COVID-19	-	Coronavirus disease 2019
FDA	-	Food and Drug Administration
RNA	-	Ribonucleic acid
PDB	-	Protein Data Bank
RdRp	-	RNA-dependent RNA polymerase
B. E	-	Binding energy
Ki	-	Inhibition constant
NOESY	-	Nuclear Overhauser Effect Spectroscopy
COSY	-	Correlated Spectroscopy

Abbreviations of units

μM	-	Micromolar
IU/mL	-	International Units Per Milliliter
mg/mL	-	Milligram per milliliter
ng/mL	-	Nanogram per milliliter
μg/mL	-	Microgram per milliliter
mmol	-	Millimoles
M	-	Molarity
GI_{50}	-	Concentration of a drug that reduces total cell growth by 50%
Kcal/mol	-	Kilo calories per mole
Hz	-	Hertz

Abbreviations of reagents and solvents

EA	-	Ethyl aceate
Hex	-	Hexane
MeOH	-	Methanol
$CHCl_3$	-	Chloroform
CH_2Cl_2	-	Dichloromethane
THF	-	Tetrahydrofuran
$PhCH_3$	-	Toluene
m-CPBA	-	*meta*-Chloroperbenzoic acid
$LiAlH_4$	-	Lithium aluminium hydride
$AlCl_3$	-	Aluminium trichloride
$Hg(OAc)_2$	-	Mercury(II) acetate
$NaBH_4$	-	Sodium borohydride
NaOH	-	Sodium hydroxide
Cs_2CO_3	-	Cesium carbonate
I_2	-	Iodine
$PhSiH_3$	-	Phenylsilane
$PdCl_2(PPh_3)_2$	-	Dichlorobis(triphenylphosphine)palladium(**II**)
CuCl	-	Copper(I) chloride
DCE	-	Dichloroethane
$RuCl_2(p\text{-}cymene)_2$	-	Dichloro(p-cymene)ruthenium(II) dimer
CuOAc	-	Copper(I) acetate
KO^tBu	-	Potassium *tert*-butoxide
n-BuLi	-	*n*-Butyllithium
$HClO_4$	-	Perchloric acid
CH_3COOH	-	Acetic acid
Na_2S	-	Sodium sulfide
Na_2S_4	-	Disodium tetrasulfide
NaSH	-	Sodium hydrosulfide
CS_2	-	Carbon disulfide

(NH$_2$)$_2$CS	-	Thiourea
AcSH	-	Thioacetic acid
KSAc	-	Potassium thioacetate
BnSH	-	Benzyl mercaptan
Rh$_2$(OAc)$_4$	-	Rhodium(II) acetate
PhH	-	Benzene
PMB-Cl	-	4-Methoxybenzyl chloride
HCl	-	Hydrochloric acid
NaIO$_4$	-	Sodium periodate
H$_2$O	-	Water
MsCl	-	Methanesulfonyl chloride
H$_2$SO$_4$	-	Sulphuric acid
CuSO$_4$	-	Copper(II) sulfate
TsCl	-	4-Toluenesulfonyl chloride
BnBr	-	Benzyl bromide
NaH	-	Sodium Hydride
DMF	-	Dimethylformamide
EtOH	-	Ethanol
H$_2$	-	Hydrogen
Pd-C	-	Palladium on carbon
TFA	-	Trifluoroacetic acid
PPh$_3$	-	Triphenylphosphine
DABCO	-	1,4-Diazabicyclo[2.2.2]octane
K$_2$CO$_3$	-	Potassium carbonate
CSA	-	Camphorsulfonic acid
CH(OMe)$_3$	-	Trimethoxymethane
(*i*-Bu$_2$AlH)$_2$	-	Diisobutylaluminium hydride
Br$_2$	-	Bromine
NEt$_3$	-	Triethylamine
KOH	-	Potassium hydroxide
TBDPSCl	-	tert-Butyldiphenylsilyl
TBAF	-	Tetra-*n*-butylammonium fluoride
NaHCO$_3$	-	Sodium bicarbonate
AIBN	-	Azobisisobutyronitrile
BuSn$_3$H	-	Tributyltin hydride
TBAI	-	Tetra-*n*-butylammonium iodide
SOCl$_2$	-	Thionyl chloride
DMAP	-	4-Dimethylaminopyridine
PdCl$_2$(dppf)$_2$	-	[1,1′-Bis(diphenylphosphino)ferrocene]dichloropalladium(II)
TBS-Cl	-	*tert*-Butyldimethylsilyl chloride
*p*TSA	-	*p*-Toluenesulfonic acid
Pd(PPh$_3$)$_2$Cl$_2$	-	Palladium(II)bis(triphenylphosphine) dichloride
LiCl	-	Lithium chloride
KMnO$_4$	-	Potassium permanganate

List of Tables

List of Figures

Chapter 1

Chapter 2

Chapter 3

List of Schemes

Chapter 1

Chemical investigation of marine algae *Enteromorpha* sp. and marine sponge *Cinachyra cavernosa*

1.1. Introduction

Nature has a vital role to play in the development of drug prototypes. In the past 20 years, around 50% of commercial drugs were derived or inspired from natural products.[1] Lately, bioactive natural products from marine sources are emerging to be a subject of intense study. The marine ecosystem makes up around 95% of the earth's biosphere and is an abundant resource of biologically active metabolites. The secondary metabolites from the marine ecosystem are distinct from those of the terrestrial ecosystem due to genetic diversity. The organisms dwelling in the ocean are put through discrete physical and chemical environmental conditions like light penetration, salt concentration, temperature, pressure, radiation exposure, oxygen concentration, etc. Marine organisms also have to defend themselves against predators, compete for space and protect themselves from infections. In order to survive all these conditions, marine organisms have to adapt persistently and in this process, they develop novel fascinating bioactive metabolites. Therefore, scientists vigorously exploit the secondary metabolites from marine sources in hope of discovering medicinally valuable natural products. Exploring novel metabolites from marine sources will not only benefit pharmaceuticals but also other sectors such as the food industry, agriculture, cosmetics, other biomedical applications, etc.[1]

From the 1900s to date, countless bioactive secondary metabolites were isolated from marine sources.[2] A bioactive marine natural product vidarabine **1** was isolated from cone snail *Conus magus* (Figure 1.1). A synthetic equivalent of vidarabine **1** (i.e ziconotide) is approved by the FDA as an analgesic drug.[3] In 2010, eribulin mesylate **2**, a synthetic macro-cyclic ketone analogue of halichondrin B (a molecule isolated from the marine sponge *Halichondria okada*) received FDA approval for the treatment of metastatic breast cancer.[3] Trabectedin **3** isolated from the ascidian *Ecteinascidia turbinata* has been approved in the European Union (EU) by the European Medicines Agency (EMA) as an anti-cancer agent for the use in the treatment of soft tissue sarcoma andplatinum-sensitive ovarian cancer.[3] Lamellarin *α*-20-sulphate **4**, from an Arabian Sea ascidian, inhibited HIV-integrase, strand transfer activity, preintegration complexes (PICS) and also, inhibited live virus.[4] Extraction from the
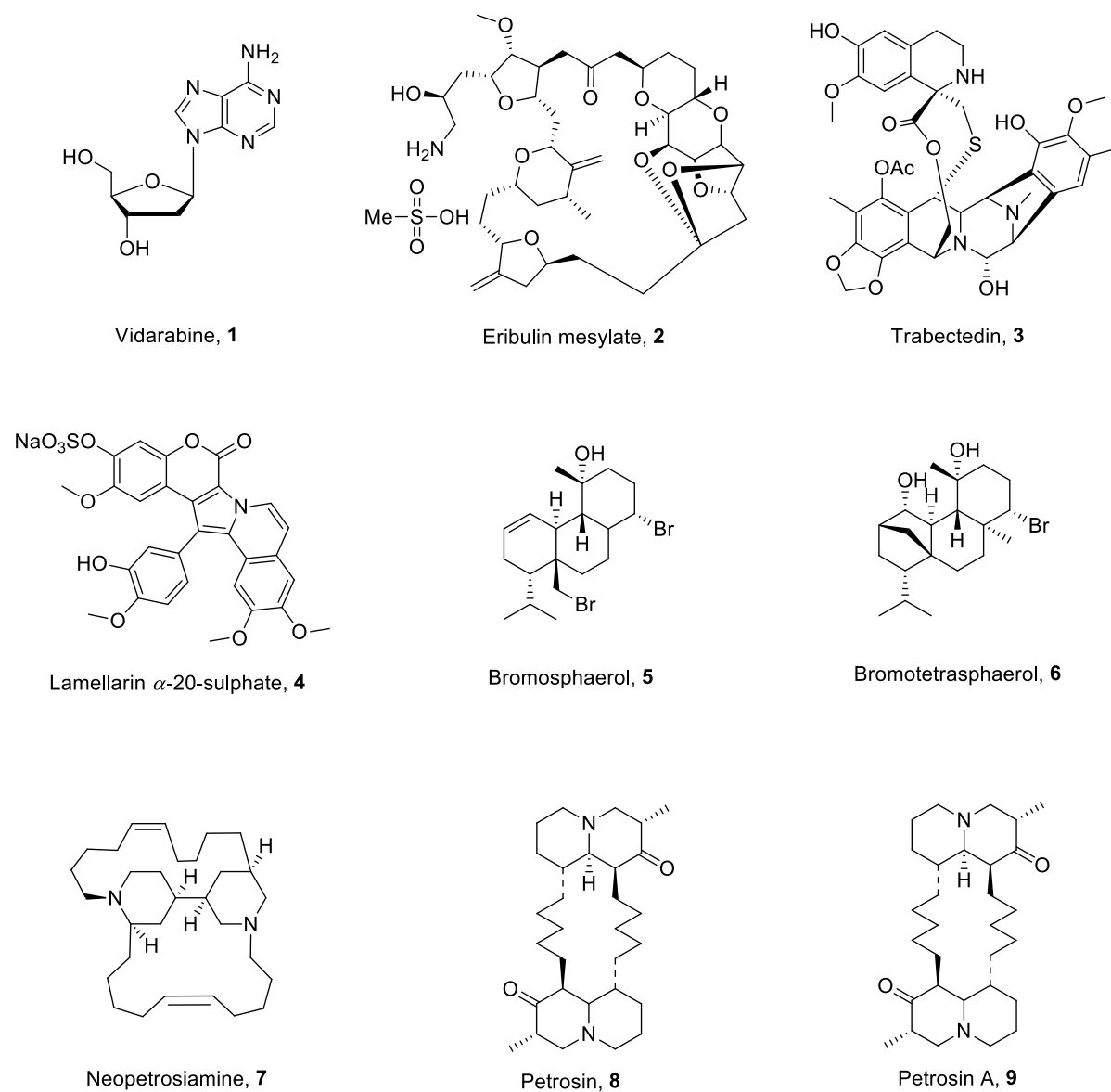
Figure 1.1: Structures of some bioactive metabolites **1-9** from marine sources.

Cosmopolitan red algae *Sphaerococcus coronopifoluis* led to the isolation of antifouling agents bromosphaerol **5** and bromotetrasphaerol **6** ($EC_{50} = 0.51$ and 0.99 μM, respectively).[5] Neopetrosiamine A **7** isolated from sponge *Neopetrosia proxima* exhibited strong microbacterium tuberculosis (MTB) activity.[6] Anti-HIV agents petrosin **8** and petrosin A **9** were isolated from the Indian marine sponge *Petrosia similis*. Both **8** and **9** inhibited HIV-1 replication at IC_{50} 41.3 and 53 μM, respectively.[7]

Chapter 1

Scope of the present study

The marine ecosystem is a valuable source of bioactive metabolites. In the present study, we targeted secondary metabolites from two marine sources: a marine alga, *Enteromorpha* sp. and a marine sponge, *Cinachyra cavernosa*. The marine samples were collected from Anjuna Goa, as these species were less explored for their chemical constituents and hence there is a need to feel the research gap of identification of new chemical entities from these sources. The overall process followed for isolation in this chapter is illustrated in figure 1.2.
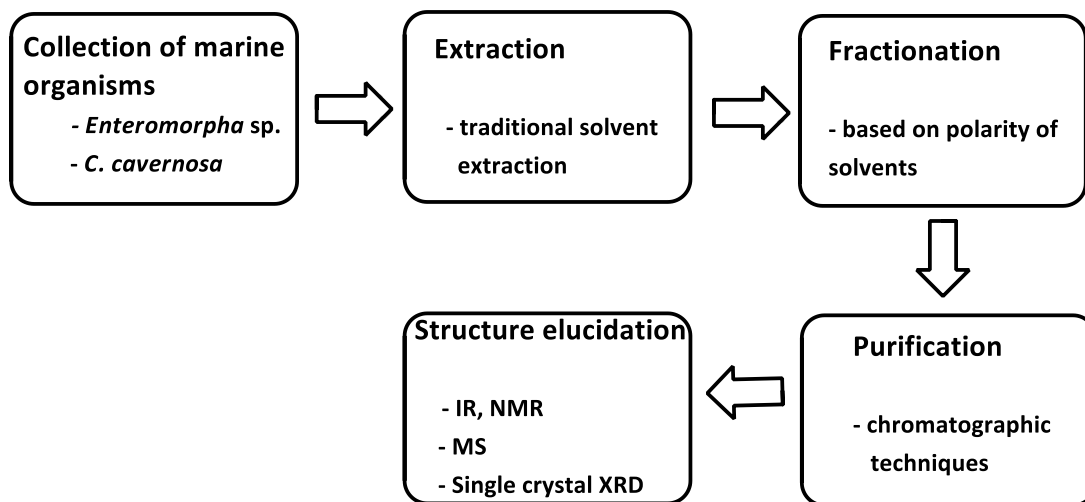
Figure 1.2: Outline of the isolation process of metabolites from marine sources.

Section A: Isolation of secondary metabolites from *Enteromorpha* sp.

1.2. Introduction

Marine algae (seaweeds) are chlorophyll-containing entities, made up of either a single cell or many cells and exist as colonies or as simple tissues. It is one of the essential parts of the marine ecosystem which performs a vital role in producing biomass in the ocean. To get rid of settling organisms, most marine algae produce chemically active metabolites in their vicinity.[8,9] Recently, in 2019, anti-Alzheimer's Disease (AD) drug, acidic oligosaccharide or GV-971 **10** was discovered in marine brown algae (Figure 1.3).[1] This promising molecule passed phase III of clinical trials and is used in the treatment of mild to moderate AD.[1] Studies proved that marine algae also display intriguing properties such as anti-cancer, anti-allergic, anti-coagulant, anti-viral, anti-inflammatory, anti-obesity, *etc.* along with anti-fouling abilities.[9] Marine algae are known to inherit metabolites like phlorotannins, sulphated

polysaccharides, lectins, terpenes, fatty acids, steroids, alkaloids, etc. For instance, 8,8'-bieckol **11**, a phlorotannin from *Ecklonia cava* portrayed HIV-1 reverse transcriptase & protease inhibition (IC$_{50}$ = 0.5 µM) (Figure 1.3).

GV-971, **10**
n = 1-9; m = 0,1 or 2; m'= 0 or 1

8,8'-Bieckol, **11**

Sulphated glucuronogalactan, **12**
R = SO$_3^-$

R = OH, **13**
R = OAc, **14**
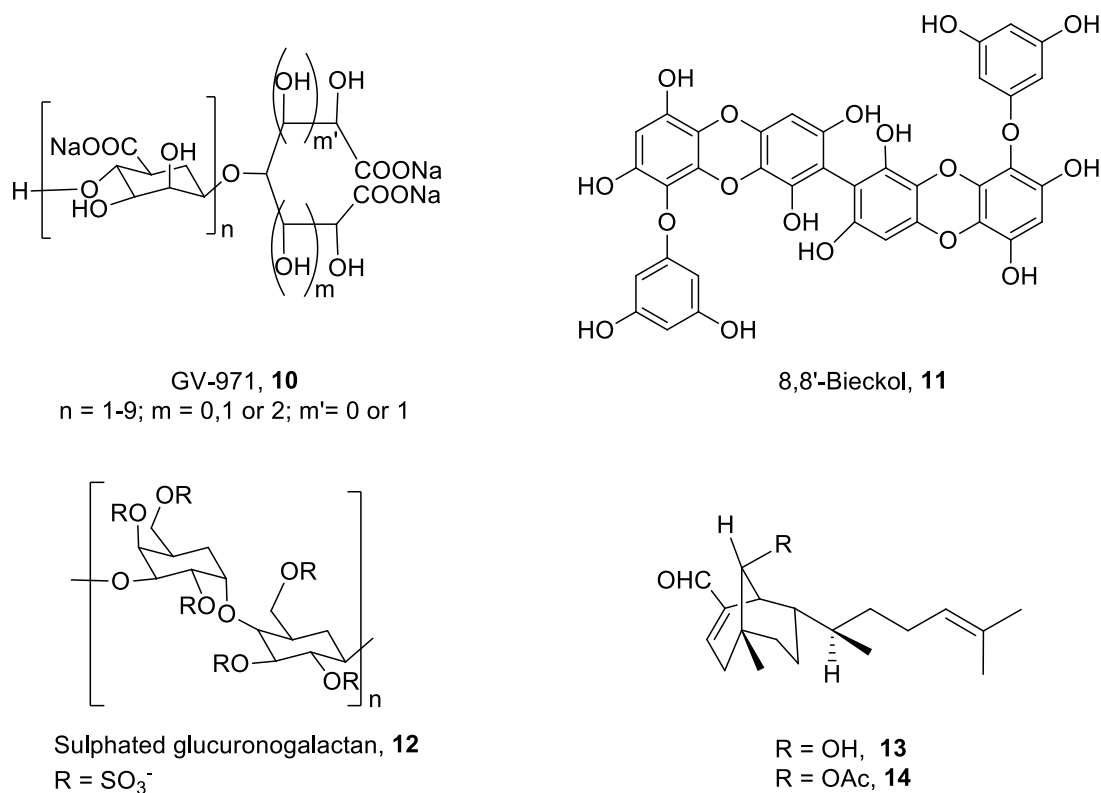
Figure 1.3: Structures of selective bioactive metabolites **10**-**14** from marine algae in the literature.

Sulphated glucuronogalactan **12**, a sulphated polysaccharide from *Schizymenia dubyi*, diterpenes **13** &**14** from *Dictyota menstrualis* showed HIV-1 reverse transcriptase inhibition (IC$_{50}$ = 5 µg/mL, 10 µM & 35 µM, respectively) (Figure 1.3). Not only this, a citrate buffer extract of marine algae *Schizymenia pacifica* inhibited HIV reverse transcriptase and HIV replication at an inhibitory concentration dose of 0.0095 IU/mL.[2,8]

Scope of the present study

Marine green macro-algae *Enteromorpha* sp. associated with the phylum *Chlorophyta*, class *Chlorophyceae*, order *Ulvales*,family *Ulvaceae*, genus *Enteromorpha* is disseminated worldwide in the tidal zones, rock pools and river mouths. Sometimes, the episodic large accumulations of massive macroalgal blooms, like *Enteromorpha* sp. in a limited area can

have damaging impacts on other organisms and can be a marine disaster. This phenomenon is called 'green tide'.[10] As acknowledged in Chinese material medica, *Enteromorpha sp*. has been extensively utilized as a nutritional food and in herbal remedies to treat various diseases.[11,12] Thus, *Enteromorpha sp*. is an excellent marine resource for discovering valuable bioactive secondary metabolites.

1.3. Objectives

1. The objective of the present study is to isolate, purify and characterize the secondary metabolites from marine algae *Enteromorpha* sp.
2. To discover novel structures with potent biological activity from a marine algae *Enteromorpha* sp.

1.4. Literature review of metabolites isolated from marine algae *Enteromorpha* sp.

Compared to terrestrial plants, seaweeds constitute a higher proportion of essential fatty acids (EFA). Two categories of EFAs which play a vital role in maintaining good health are Omega-3 and Omega-6 acids. Omega-3 fatty acids are obtained from linolenic acid and Omega-6 acids from linoleic acid. The major fatty acid components in the saponified ether extract of *Enteromorpha intestinales* were palmitic acid (hexadecanoic acid), palmitoleic acid ((9Z)-hexadec-9-enoic acid), linoleic acid ((9Z, 12Z)-octadeca-9,12-dienoic acid) and linolenic acid ((9Z, 12Z, 15Z)-octadeca-9,12,15-trienoic acid). The EFA play an essential role in the maintenance of cardiac cells and the high composition of unsaturated fatty acids may guard against Parkinson's disease.[13,14] Also, the seaweed essential oil (SEO) from *Enteromorpha* sp. significantly inhibited lipid peroxidation (EC_{50} = 287.06 μg/mL), which is the major reason for the deterioration of nutrition in food. The major component of the SEO extracted from *Enteromorpha Linza* (by microwave-assisted hydrodistillation) and bio-oils extracted from *Enteromorpha prolifera* (by liquefication of algae in sub-/supercritical alcohol) was hexadecanoic acid. Thus, SEO from *Enteromorpha* sp. can be employed as a food preservative and dietary supplement.[15,16] Besides this, sulphated heteropolysaccharides (also known as "Ulvans") represent approximately >50% of the dry *Enteromorpha* sp. algal weight.[17–19] These results clearly explain the nutritional values of *Enteromorpha* sp. and its potential as a nutritional food preservative.

Pheophytin A, **15**
(chlorophyl-related compound)

Isofucosterol, **16**

R = H   Cholesterol, **17**
R = CH₃ 24-Methyl cholesterol, **17a**

Phytol, **18**
(diterpene alcohol)

Ethyl [2-(benzylsulfanyl)-4-
(4-nitrophenyl)-1*H*-imidazol-
1-yl]acetate, **19**
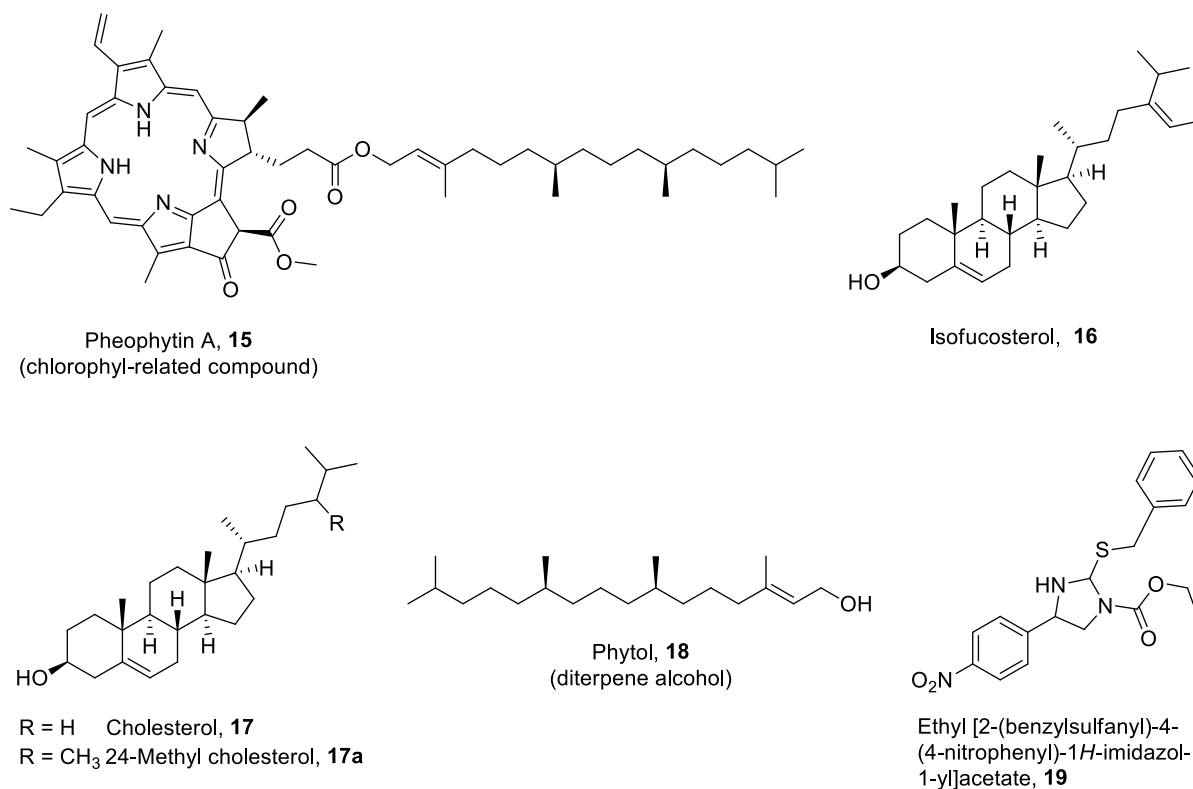
Figure 1.4: Structures of metabolites **15-19** isolated from *Enteromorpha* sp. in the literature.

In the year 1997, U. Okai and K. Higashi-Okai isolated, a chlorophyll related compound, pheophytin A **15** from methanol:acetone (1:1) extract of *Enteromorpha prolifera* having anti-inflammatory properties (Figure 1.4).[20] In 1983, J. Agard *et al*. identified sterols (28-isofucosterol **16**, cholesterol **17** & 24-methyl cholesterol **17a**, hydrocarbons (*cis*-7-heptadecene, *n*-eicosane, *n*-octadecane &*n*-nonadecane), fatty acids (palmitic acid/ hexadecanoic acid & oleic acid/(9*Z*)-octadec-9-enoic acid) and phytol **18** in the hexane extract of *Enteromorpha prolifera* and studied the seasonal variation of these phytochemicals.[21] Later in the year 2011, S.M.M. Shanab *et al*. isolated ethyl[2-(benzylsulfanyl)-4-(4-nitrophenyl)-1*H*-imidazol-1-yl]acetate **19** from the anti-oxidant active ethyl acetate fraction from *Enteromorpha compressa* (Figure 1.4).[22]

1.5.   Results and discussion

The isolation of metabolites from the marine algae *Enteromorpha* sp. is broadly divided into three parts: extraction and bioactivity study of the crude sample, purification of metabolites and structure elucidation of metabolites.

Chapter 1

1.5.1. Extraction and bioactivity study of the crude sample

To extract the metabolites from the algae, the algal solid material was soaked in methanol at room temperature. This is called solid-liquid extraction. The solvent was allowed to diffuse in the cells of the algae and to solubilize the metabolites. The solvent was filtered and concentrated under vacuum on a rotary evaporator at low temperature to give a crude methanol extract. One of the traditional use of *Enteromorpha* sp. extracts has been in cosmetic compositions which were directly applied to the skin.[11] We thought to investigate the role of the *Enteromorpha* extract in the inhibition of tyrosinase enzyme, which is the key enzyme that bio-catalyses melanin production. Excess melanin leads to melanoma (skin cancer). Hence, this study could help in solving many skin related ailments. Primarily, crude methanol extract of *Enteromorpha* sp. was tested for its ability to inhibit tyrosinase enzyme (for the details of tyrosinase enzyme inhibition see Chapter 2, Section B) (Figure 1.5). Crude
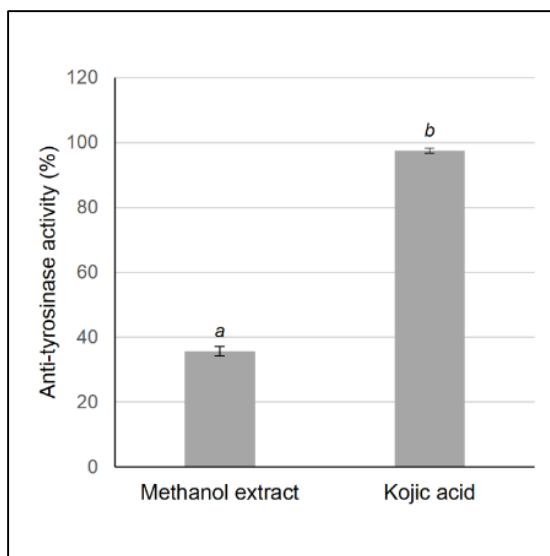
Figure 1.5: The *in vitro* anti-tyrosinase activity of crude methanol extract of *Enteromorpha sp.* at the concentration 0.6mg/mL for L-tyrosine. Error bars indicate the standard deviation (SD) of the triplicates. Kojic acid was used as positive control. [a,b]Different superscripts are statistically significant at $p < 0.05$ as measured by *post hoc* Tukey's HSD test, performed by ANOVA. Comparisons between means were performed by student's t-test. The software used was IBM® SPSS Statistics v.23.0 program for Windows.

methanol extract of *Enteromorpha* sp. portrayed moderate tyrosinase inhibition (35.70 ± 1.40 % at the concentration 0.6 mg/mL for ʟ-tyrosine) compared to the reference kojic acid (97.5 ± 0.80 % at the concentration 0.6 mg/mL for ʟ-tyrosine) (Figure 1.5).

1.5.2. Purification of metabolites

To further purify the crude methanol extract of *Enteromorpha*, it was partitioned between two immiscible solvents. This is called liquid-liquid extraction. The crude methanol extract was partitioned between hexane, ethyl acetate, *n*-butanol and water to obtain hexane fraction, ethyl acetate fraction, *n*-butanol fraction and aqueous fraction. The outline of complete fractionation by silica column chromatography is depicted in figure 1.6. In the present work, we directed our focus on the isolation of constituents from hexane and ethyl acetate fraction.
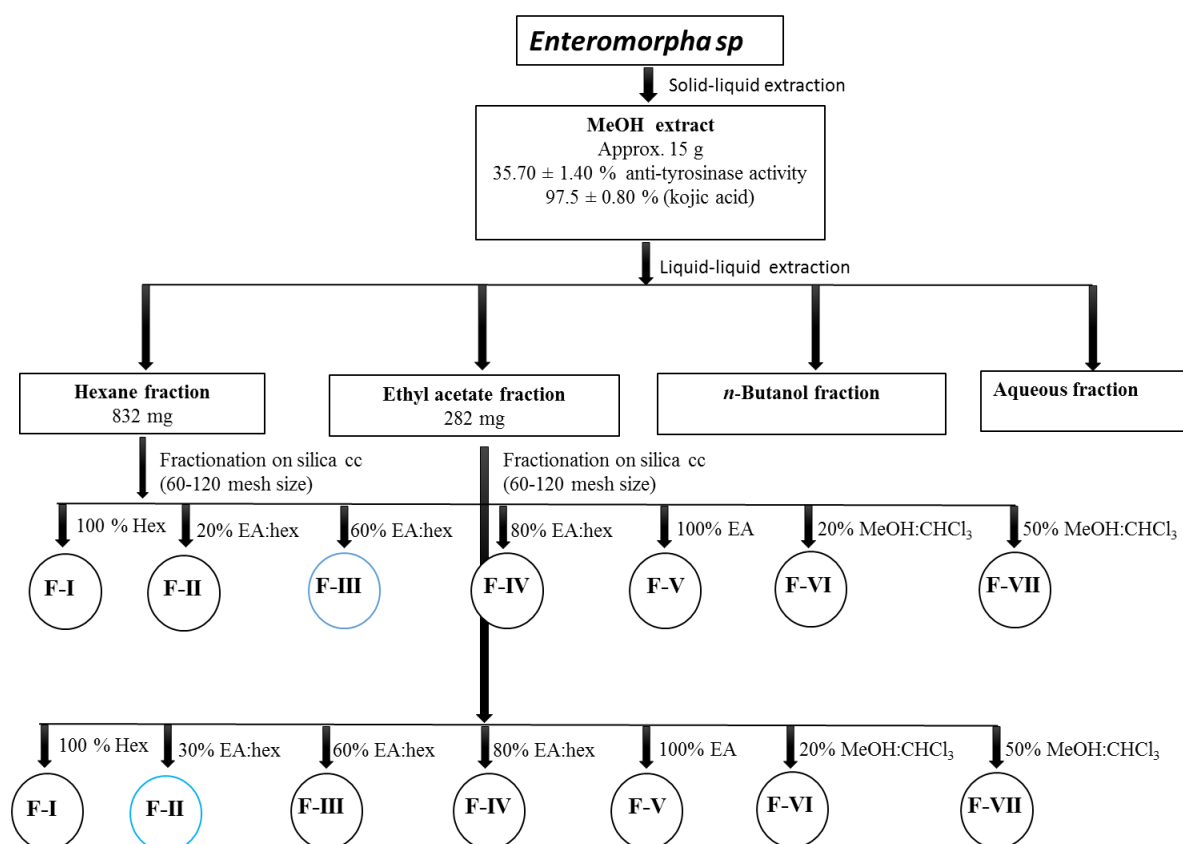
Figure 1.6: A brief outline of the extraction and fractionation process of metabolites from *Enteromorpha* sp. in the present work.

The hexane fraction was subjected to successive column chromatography over silica gel using mixtures of hexane, ethyl acetate, chloroform and methanol as eluents of increasing

polarity, to obtain around 30 fractions which were combined into 7 fractions based on the similarities of the appearance of spots on TLC (F-I to F-VII) (Figure 1.6). F-III (ethyl acetate:hexane 6:4) was further subjected to column chromatography over silica gel which delivered a beige powder, and appeared as a single spot on TLC (ethyl acetate:hexane 6:4). The ^{1}H NMR was recorded to obtain preliminary information. However, the data indicated the presence of a trace amount of impurity with an identical Rf value (indicated by TLC). Thus, this partially purified F-III was subjected to repetitive silica column chromatographic purification to obtain F-A. Multiple developments of F-A in ethyl acetate:hexane 3:7 as the mobile phase, helped to increase the resolution. Finally, purification of F-A using preparative TLC led to the isolation of 10 mg of beige powder (F-A-06).

Next, the ethyl acetate fraction was subjected to successive column chromatography over silica gel using mixtures of hexane, ethyl acetate, chloroform and methanol as eluents of increasing polarity, to obtain around 35 fractions which were combined into 7 fractions based on the similarities of the appearance of spots on TLC (F-I to F-VII) (Figure 1.6). The TLC analysis of F-II (ethyl acetate:hexane 3:7) showed an intense coloured spot when the TLC plate was sprayed with a 5% methanolic H_2SO_4 staining reagent. We targeted the purification of this spot on the silica gel column (ethyl acetate:hexane 3:7). For the preliminary investigation, we recorded ^{1}H & ^{13}C NMR of the partially purified F-II (brown sticky liquid). The NMR spectrum revealed the presence of impurity. Therefore, the obtained F-II was subjected to further purification by column chromatography over Sephadex LH-20 gel to obtain F-B (methanol:chloroform 1:1). F-B was then further purified on silica gel column chromatography to obtain two fractions, F-B-04 as a brown powder and F-B-05 as a white powder (ethyl acetate:hexane 4:6). The other fractions did not yield enough quantity of metabolites to characterize the structures completely.

1.5.3. Structure elucidation of metabolites

Instrumental techniques used to determine the structure of the purified metabolites from hexane and ethyl acetate fractions of *Enteromorpha* sp. included IR, ^{1}H NMR, ^{13}C NMR, DEPT, LCMS and Single-crystal X-ray Diffraction. ^{1}H NMR of F-A-06 purified from hexane fraction gave three ^{1}H signals in the aromatic region of the spectrum δH 7.81-7.83 (m, 1H), 7.52-7.57 (m, 1H), 7.24-7.28 (m, 2H). ^{13}C NMR of F-A-06 showed two aromatic

quaternary ^{13}C signals δC 155.2, 117.4 (confirmed by DEPT data). Combining the above ^{1}H and ^{13}C NMR results it can be inferred that F-A-06 contains 1,2-disubstituted aromatic ring. The appearance of 3377, 2885, 2719, 2576, 1612, 1550 cm^{-1} bands in IR analysis provide information about the presence of hydroxyl, carbonyl and aromatic skeleton. The presence of carbonyl (-C=O) is also indicated by the appearance of ^{13}C signal at δC 166.3. ^{13}C NMR of F-A-06 also shows the presence of enol carbons (-(OH)C=CH-) signals at δC 168.7 & 91.6. LC-ESI-MS data of F-A-06 showed [M + H]$^{+}$ peak at 163.0386. The molecular formula of F-A-06 was assigned as $C_9H_7O_3$ from LC-ESI-MS data and NMR data. The calculated double bond equivalence (DBE) is seven. The presence of an aromatic ring accounts for four DBE, carbonyl group accounts for one DBE. That leaves two out of seven unaccounted DBE. The remaining two DBE can be accounted for the presence of a double bond and a ring. Based on the above observations, a coumarin scaffold was assigned for the isolated compound F-A-06 (Figure 1.7). From the above structural information, four probable structures arise 4-hydroxycoumarin **20**, 3-hydroxycoumarin **20a**, 2-hydroxychromone **20b** and 3-hydroxychromone **20c**.

4-Hydroxycoumarin **20**   3-Hydroxycoumarin **20a**   2-Hydroxychromone **20b**   3-Hydroxychromone **20c**
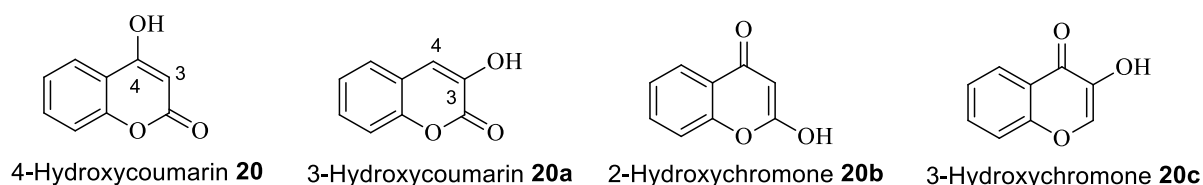
Figure 1.7: Probable structures of F-A-06.

The spectral data of F-A-06 matched with the reported spectral data of 4-hydroxycoumarin **20** (Table 1.1).[23–25]

Table 1.1: Comparison of NMR data of 4-hydroxycoumarin **20** with that of the literature.

20
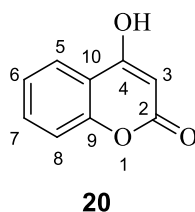
...continuation of table 1.1

Carbon number	^{1}H NMR (This work[a])	^{1}H NMR (Reported[a])[26]	^{13}C NMR (This work[a])	^{13}C NMR (Reported[a])[26]
1				
2			166.3	166.1
3	5.52(s, 1H)	5.61 (s, 1H)	91.6	91.7
4			168.7	168.4
5	7.81-7.83 (m, 1H)	7.84 (d, 1H)	124.6	124.6
6	7.24-7.28 (m, 1H)	7.36 (t, 1H)	125.4	125.3
7	7.52-7.54 (m, 1H)	7.66 (t, 1H)	134.0	134.0
8	7.24-7.28 (m, 1H)	7.39 (d, 1H)	117.6	117.6
9			155.2	155.2
10			117.4	117.3

[a]NMR solvent is MeOH-d$_4$

Additionally, we crystallized this beige powder F-A-06 from aqueous ethanol to obtain a transparent needle-shaped crystal which was subjected to Single-crystal X-ray Diffraction studies to give the crystal structure of the F-A-06 (Figure 1.8). The crystal structure of F-A-06 was revealed to be 4-hydroxycoumarin **20**. This further confirms the structure of F-A-06 to be 4-hydroxycoumarin **20**. To the best of our knowledge, the crystal structure of 4-hydroxycoumarin **20** has not been reported previously. *Enteromorpha* sp. is a new source for 4-hydroxycoumarin **20**.
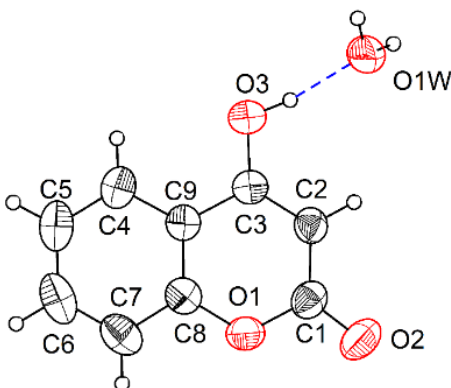
Figure 1.8: Crystal structure of 4-hydroxycoumarin **20**. Thermal ellipsoids are drawn at the 50% probability level and H atoms are shown as spheres of arbitrary radii. Intramolecular H-bond is shown in the broken line.

Chapter 1

The ^{13}C NMR spectrum of F-B-04 purified from ethyl acetate fraction of *Enteromorpha* sp. revealed 28 ^{13}C signals. The presence of 28 carbon signals could be attributed to a sterol moiety. NMR spectrum of F-B-04 showed a ^{1}H signal at δH 3.60-3.70 (m, 1H) and ^{13}C δC 70.4 which was attributed to the oxygenated methane (>CH-OH). F-B-04 showed the presence of a conjugated diene (>C=CH-CH=C<) by the appearance of NMR signals at δH 5.57-5.60 (m, 1H), δH 5.39-5.41 (m, 1H) and δC 141.3, 139.8, 119.6, 116.3. The side chain of sterol F-B-04 showed the presence of a double bond (-CH=CH-) by the appearance of NMR signals at δH 5.21 (t, J = 6.3 Hz, 2H) & δC 135.6, 132.0. Finally, combining the above data and comparing it with the reported data, ergosterol (ergosta-5,7,22-trien-3β-ol) **21** structure was assigned to F-B-04 (Figure 1.9, Table 1.2).[27] Captivatingly, the ^{1}H NMR spectrum of F-B-05 purified from ethyl acetate fraction appeared almost similar to that of sterol F-B-04, except the double bond proton signals shifted from δH 5.57-5.60 (m, 1H) and δH 5.39-5.41 (m, 1H) to δH 6.51 (d, J = 8.4 Hz, 1H) and δH 6.25 (d, J = 8.4 Hz, 1H). These proton shifts indicated the addition of oxygen molecules across the conjugated diene (>C=CH-CH=C<) of F-B-04 i.e. ergosterol **21**. F-B-05 was thus proved to be ergosterol peroxide **22**. The data matched with that of the reported literature (Figure 1.9, Table 1.3).[28]
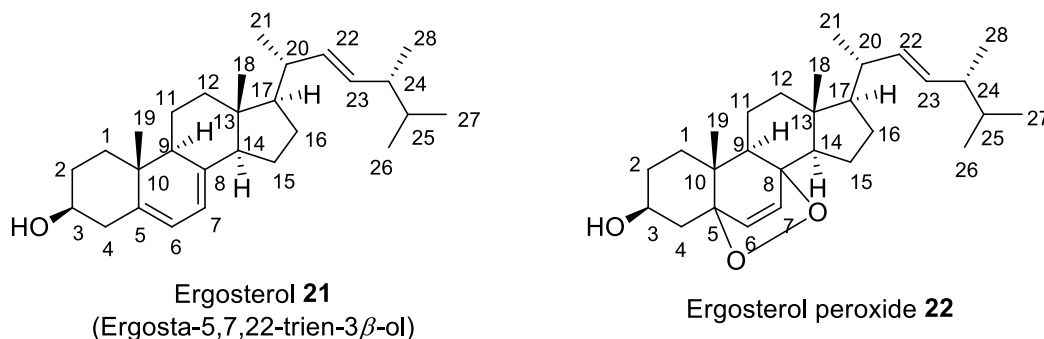
Figure 1.9: Structures of ergosterol **21** and ergosterol peroxide **22**.

Enteromorpha sp. was identified as a new source of these two sterols: ergosterol **21** and ergosterol peroxide **22**.

Table1.2: Comparison of NMR data of ergosterol **21** with that of the literature.
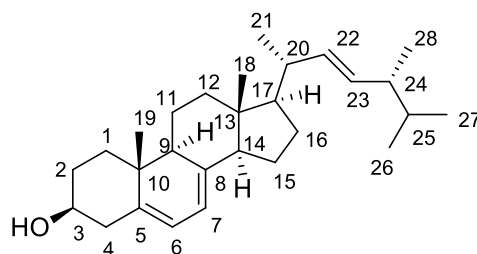
Ergosterol **21**
(Ergosta-5,7,22-trien-3β-ol)

Carbon number	^{1}H NMR (This work^{a})	^{1}H NMR (Reported^{a})[27]	^{13}C NMR (This work^{a})	^{13}C NMR (Reported^{a})[27]
1	1.23-1.37 (m, 1H) 1.45-1.53 (m, 1H)	1.2-2.50 (m, 2H)	38.4	38.4
2	1.23-1.37 (m, 1H) 1.45-1.53 (m, 1H)	1.2-2.50 (m, 2H)	32.0	32.0
3	3.60-3.70 (m, 1H)	3.58-3.75 (m, 1H)	70.4	70.4
4	1.99-2.09 (m, 2H)	1.2-2.50 (m, 2H)	40.8	40.8
5			139.8	139.8
6	5.39-5.41 (m, 1H)	5.37-5.39 (ddd, 1H)	119.6	119.6
7	5.57-5.60 (m, 1H)	5.56-5.58 (dd, 1H)	116.3	116.3
8			141.3	141.3
9	1.99-2.09 (m, 1H)	1.2-2.50 (m, 1H)	46.2	46.3
10			37.0	37.0
11	1.23-1.37 (m, 1H) 1.45-1.53 (m, 1H)	1.2-2.50 (m, 2H)	21.1	21.1
12	1.23-1.37 (m, 1H) 1.45-1.53 (m, 1H)	1.2-2.50 (m, 2H)	39.1	39.1
13			42.8	42.8
14	1.99-2.09 (m, 1H)	1.2-2.50 (m, 1H)	54.8	54.6
15	1.23-1.37 (m, 1H) 1.84-1.92 (m, 1H)	1.2-2.50 (m, 2H)	23.0	23.0
16	1.23-1.37 (m, 1H) 1.84-1.92 (m, 1H)	1.2-2.50 (m, 2H)	28.3	28.3

...continuation of table 1.2

17	1.45-1.53 (m, 1H)	1.2-2.50 (m, 1H)	55.7	55.8
18	0.64 (s, 3H)	0.63 (s, 3H)	12.0	12.0
19	1.05 (d, 3H)	1.05 (d, 3H)	17.6	17.6
20	2.44-2.52 (m, 1H)	1.2-2.50 (m, 1H)	40.4	40.4
21	0.93 (d, 3H)	0.93 (d, 3H)	21.1	21.1
22	5.21 (t, 1H)	5.20-5.27 (dd, 1H)	135.7	135.6
23	5.21 (t, 1H)	5.13-5.20 (dd, 1H)	132.0	132.0
24	2.22-2.36 (m, 1H)	1.2-2.50 (m, 1H)	42.8	42.8
25	1.84-1.92 (m, 1H)	1.2-2.50 (m, 1H)	33.1	33.1
26	0.81-0.86 (m, 6H)	0.83 (d, 3H)	19.9	19.9
27		0.84 (d, 3H)	19.6	19.6
28	0.96 (s, 3H)	0.95 (s, 3H)	16.3	16.3

[a]NMR solvent is $CDCl_3$

Table 1.3: Comparison of NMR data of ergosterol peroxide **22** with that of the literature.
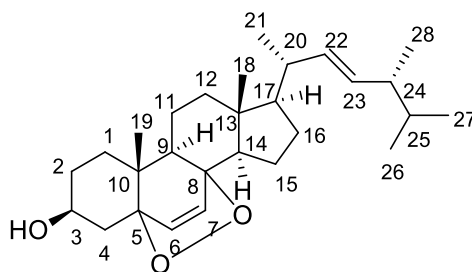
Ergosterol peroxide **22**

Carbon number	¹H NMR (This work[a])	¹H NMR (Reported[a])[28]	¹³C NMR (This work[a])	¹³C NMR (Reported[a])[28]
1			34.7	34.7
2			30.1	30.1
3	3.94-4.02 (m, 1H)	3.98 (m, 1H)	66.4	66.5
4			36.9	36.9
5			82.1	82.2
6	6.25 (d, 1H)	6.25 (d, 1H)	135.4	135.4
7	6.51 (d, 1H)	6.52 (d, 1H)	130.1	130.8

...continuation of table 1.3

8			79.4	79.4
9			51.1	51.1
10			36.9	37.0
11			20.6	20.6
12			39.3	39.4
13			44.6	44.6
14			51.8	51.7
15			23.4	23.4
16			28.6	28.4
17			56.2	56.2
18			12.9	12.9
19			18.2	18.2
20			39.7	39.7
21			20.9	20.9
22	5.10-5.27 (2H, m)	5.16 (dd, 1H)	135.2	135.2
23		5.14 (dd, 1H)	132.1	132.3
24			42.8	42.8
25			33.0	33.0
26			19.9	19.6
27			19.6	20.0
28			17.5	17.6

[a]NMR solvent is $CDCl_3$

A brief outline of the isolation protocol of secondary metabolites from methanol extract of *Enteromorpha* sp is depicted in figure 1.10.
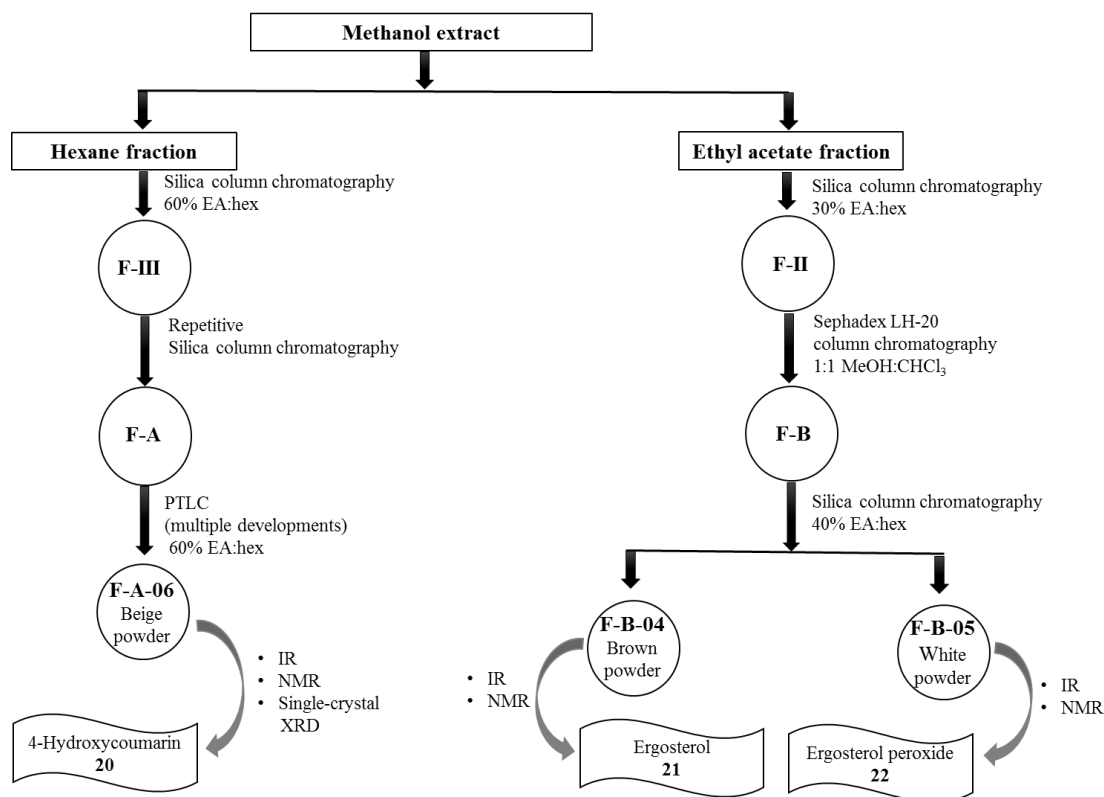
Figure 1.10: Isolation protocol of metabolites from methanol extract of *Enteromorpha* sp.

4-Hydroxycoumarin **20** and related compounds have been isolated from many plant species.[29] Recent studies documented that, 4-hydroxycoumarin **20** and its derivatives exhibit a wide spectrum of pharmacological activities such as anti-arthritis, anti-inflammatory, anti-viral, anti-bacterial, antipyretic, anti-cancer, etc. and have been resourcefully used in certain cardiac conditions, pulmonary embolism and as anti-coagulants, etc.[30–33] However, the ecological significance of the same remains to be a subject of further studies. Although 4-hydroxycoumarin do not possess tyrosinase inhibitory activity as reported by Asthana, S. *et al.*,[34] the presence of 4-hydroxycoumarin in algae is ecologically significant as coumarins aid in scavenging the harmful radicals generated during oxidative stress, protection from phytopathogens[35] and may also prevent herbivores from feeding on these algae in the ocean.

Ergosterol **21** and ergosterol peroxide **22** have been isolated from plentiful fungi, yeast, lichens, sponges,and algae.[36–41] Ergosterol **21** and its analogues have been studied to possess anti-fungal activity, anti-tumor activity, immunosuppressive activities, etc.[42–44] On the other hand, ergosterol peroxide **22** is well-known to inhibit breast cancer,[45] cervical cancer,[45] colon

cancer,[28] lung cancer,[46] etc. According to Taofiq, O. *et al.* cosmeceutical formulation of ergosterol **21** inhibited the tyrosinase enzyme however, its activity decreased gradually with time, giving it a short shelf-life.[47] Whereas Mukaiyama, T. revealed that ergosterol **21** did not remarkably suppress the melanogenesis in mouse melanoma cell line (B16 10F7), ergosterol peroxide **22** could significantly lower the melanin formation in B16 10F7.[48] Ergosterol **21** is a vitamin D_2 precursor and an essential part of the cell structure, therefore, is a biologically significant molecule. Ergosterol peroxide **22** has been reported as a natural product from various natural sources.[38–41] It is known to be an oxidation product of ergosterol **21** formed by ergosterol **21** scavenging the reactive oxygen species in the stressed cells. It's still a puzzle whether ergosterol peroxide **22** is really a metabolite or just an artefact formed during the isolation process.[38,39]

Thus, we believe that these bioactive metabolites (**20**-**22**) produced by algae are responsible for their chemical defense and play ecological roles in their protection. Overall, our results indicate that methanol extract of *Enteromorpha* sp. finds a remarkable opportunity in the development of an alternative edible source of tyrosinase inhibitors, which can be incorporated into the diet of humans and animals.[12]

1.6. Conclusion

1. Three compounds 4-hydroxycoumarin **20**, ergosterol **21** and ergosterol peroxide **22** were isolated, purified and characterized from methanolic extract of a marine algae *Enteromorpha* sp.

2. The structure of 4-hydroxycoumarin **20** was confirmed by Single-crystal X-ray Diffraction technique

3. *Enteromorpha* sp. is a new source of these isolated natural products **20**-**22**.

4. 4-Hydroxycoumarin **20** is known to exhibit activities such as anti-viral, anti-microbial, anti-cancer, etc.

5. Ergosterol **21** and ergosterol peroxide **22** are known anti-tyrosinase inhibitors and possess various bioactivities such as anti-cancer, immunosuppressive activities, etc.

Chapter 1

Section B: Isolation of secondary metabolites from marine sponge *Cinachyra cavernosa*

1.7.Introduction

Sponges are essential organisms of coral reef ecosystems and move very slowly during the period of reorganization of their bodies. Hence, they are observed to exist in various shapes, sizes and colours. They have adapted marvellous biochemical processes to compete for space, fight predators and survive the harsh environmental changes observed in the marine ecosystem. Thus, marine sponges bank a variety of interesting bioactive natural products.[49] In the 1950s, Bergmann and Feeney isolated anticancer drug leads arabinosyl nucleosides, spongothymidine **23** and spongouridine **24** from a Caribbean sponge *Cryptotethia crypta* for the very first time (Figure 1.11). This discovery led to the synthesis of the very first anti-cancer drug, cytosine arabinoside or ara-C**25** (a derivative of these nucleosides) derived from a marine source. Ara-C is widely employed in the treatment of Hodgkin's lymphoma and acute myelocytic leukaemia.[2,50] Since then, tremendous research is being carried out on marine sponges to identify drug prototypes. Over several years, a huge number of biologically active secondary metabolites have been isolated from marine sponges belonging to the natural product classes: sesquiterpene hydroquinones, cyclic depsipeptides, alkaloids, diterpenes, sulfated sterols, etc.[2,50,51] For instance, Cyanthiwigin B **26**, a diterpene from *Epipolasis reiswigi* portrayed anti-HIV activity ($EC_{50} = 42$ µM). Sesquiterpene phenols, curcuphenols **27a-d** from *Didiscus oxeata*, *Didiscus flavus*, *Myrmekioderma styx* and *Epipolasis* sp. are excellent anti-HIV-1 agents (EC_{50} = 31.2, 29.2, 18.4, 18.2 µM, respectively). Clathsterol **28**, a sulfated sterol from *Clathria* sp. possessed HIV-1 reverse transcriptase inhibition ($EC_{50} = 10$ µM) property. Halicyclamine A **29**, an alkaloid from *Haliclona* sp. proved to be an anti-TB agent. Dragmacidin F **30**, an alkaloid from genus *Halicortex* was shown to be anti-HIV-1 ($EC_{50} = 0.9$ µM) and anti-HSV-1 agents ($EC_{50} = 96$ µM).Callipeltin A **31**, acyclic depsipeptide from the genus *Callipelta* revealed HIV-1-induced cytopathic inhibition ($EC_{50} = 0.007$ µM) (Figure 1.11).[2,50,51]

Spongothymidine, **23**   Spongouridine, **24**   Ara-C, **25**   Cyanthiwigin B, **26**

Curcuphenols, **27**   Curcuphenol a, **a**   Curcuphenol c, **b**   Curcuphenol j, **c**   Curcuphenol r, **d**

R =

Clathsterol, **28**   Halicyclamine A, **29**   Dragmacidin F, **30**

Callipeltin A, **31**
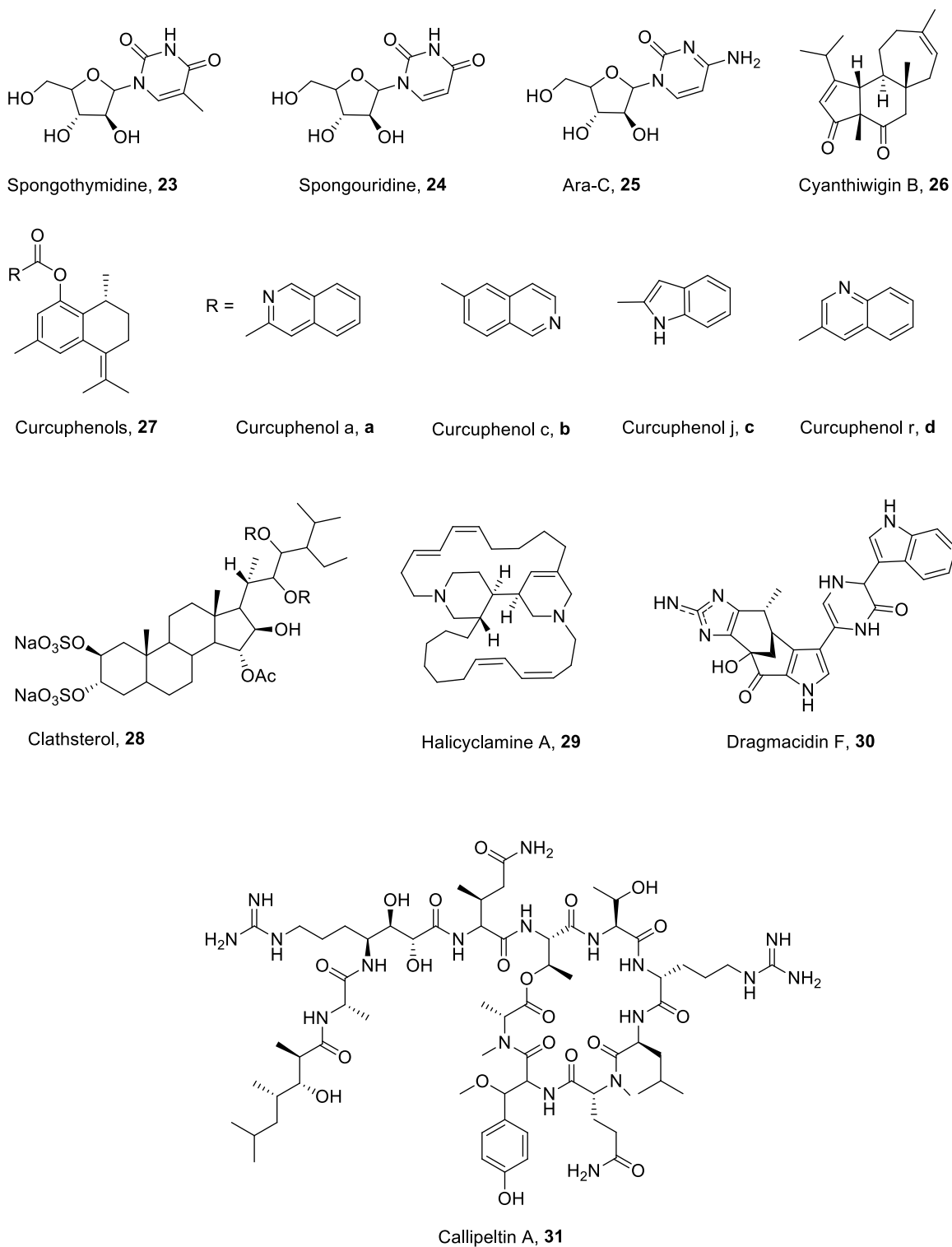
Figure 1.11: Structures of selective bioactive metabolites **23-31** from marine sponges in the literature.

Chapter 1

Scope of the present study

The sponge of genus *Cinachyra* (or *Cinachyrella*) and species *cavernosa* belongs to the family *Tetillidae*, order *Spirophorida* and class *Demospongia*.[52,53] The accurate classification of the sponges has been proved tedious just based on their morphology. Thus initially, *C. cavernosa* was recorded as *C. tarentina, C. australiensis* and also as *Chrotella cavernosa & Chrotella australiensis*. Bioactive natural products from sponges are not only medicinally important but also are very useful in biochemical taxonomic study.[54]

1.8. Objective

1. The objective of the present study is to isolate, purify and characterize the secondary metabolites from a marine sponge *Cinachyra cavernosa*.
2. To discover novel structures having exciting scaffolds which could be lead molecules in drug discovery.

1.9. Literature review of metabolites isolated from *Cinachyra* sp.

Cinachyra sp. are the bearers of unusual phospholipid fatty acids. Over 50 phospholipid fatty acids have been detected from *Cinachyra* sp. and especially from the chloroform:methanol (1:1 v/v) extracts of *C. alloclada* and *C. kükenthali*. The chief amongst these phospholipid fatty acids are hexadecanoic, 8-hexadecenoic, tetradecanoic, octadecenoic, 9-octadecenoic, 11-octadecenoic, 13-nonadecenoic, 10,13-octadecadienoic, 16-tricosenoic, 17-tetraracosenoic, 19-hexacosenoic and 5,9,23-tricontatrienoic acids from *C. alloclada. Cinachyra* sponges also house interesting and unusual methyl-branched long-chain fatty acids like 18-methyltetracosanoic, 18—methylpentacosanoic, 18—methylhexacosanoic, 23- methylpentacosanoic, 25-methyl-5,9-hexacosadienoic, 26-methyl-5,9-heptacosadienoic, 8,24-dimethylhexacosanoic, 6-bromo-5,9-nonacosadienoic, 5,9,13-trimethyltetradecanoic acids from *C. alloclada* and 17-methyltetracosanoic from *C. kükenthali*.[55,56]

There were several bioactive secondary metabolites isolated from *Cinachyra* sponges over the years. In the year 1983, Cardellina *et al.* isolated a long chain monoalkenyl glycerol ether, 17Z-tetracosenyl 1-glycerol ether **33** from dichloromethane extract of *C. alloclada* (Figure1.12).[57] In 1993, Fusetani *et al.* identified a cytotoxic macrolide, cinachyrolide A**32** (L1210 murine leukaemia cell line IC_{50} = < 0.6 ng/mL) from ether fraction of *Cinachyra* sp.[58]

Later in 2006, Shimogawa *et al.* recognized an alkaloid, cinachyramine **34** from the butanol fraction of *Cinachyra* sp. The trifluoroacetate salt of cinachyramine was found to be cytotoxic against the HeLa cell line (IC$_{50}$ = 6.8 μg/mL).[59] In 2008, Lakshmi *et al.* isolated two ceramides **35-36** and tetillapyrone **37** from the butanol fraction of *C. cavernosa*.[53] In 2015, Wahidullah *et al.* isolated phthalate esters (bis-(2-methyl propyl)phthalate **38a**, dibutyl phthalate **38b** and bis-(2-ethyl hexyl)phthalate **38c**) and a nucleoside, 9β-D-ribofuranosyl adenine **39** from butanol fraction of *C. cavernosa* (Figure 1.12).[54]

Cinachyrolide A, **32**

17*Z*-Tetracosenyl 1-glycerol ether, **33**

Cinachyramine, **34**

35

36

Tetillapyrone, **37**

Phthalate esters, **38**

R: **a** = bis-(2-Methyl propyl)phthalate

b = Dibutyl phthalate

c = bis-(2-Ethyl hexyl)phthalate

9β-D-Ribofuranosyl adenine, **39**
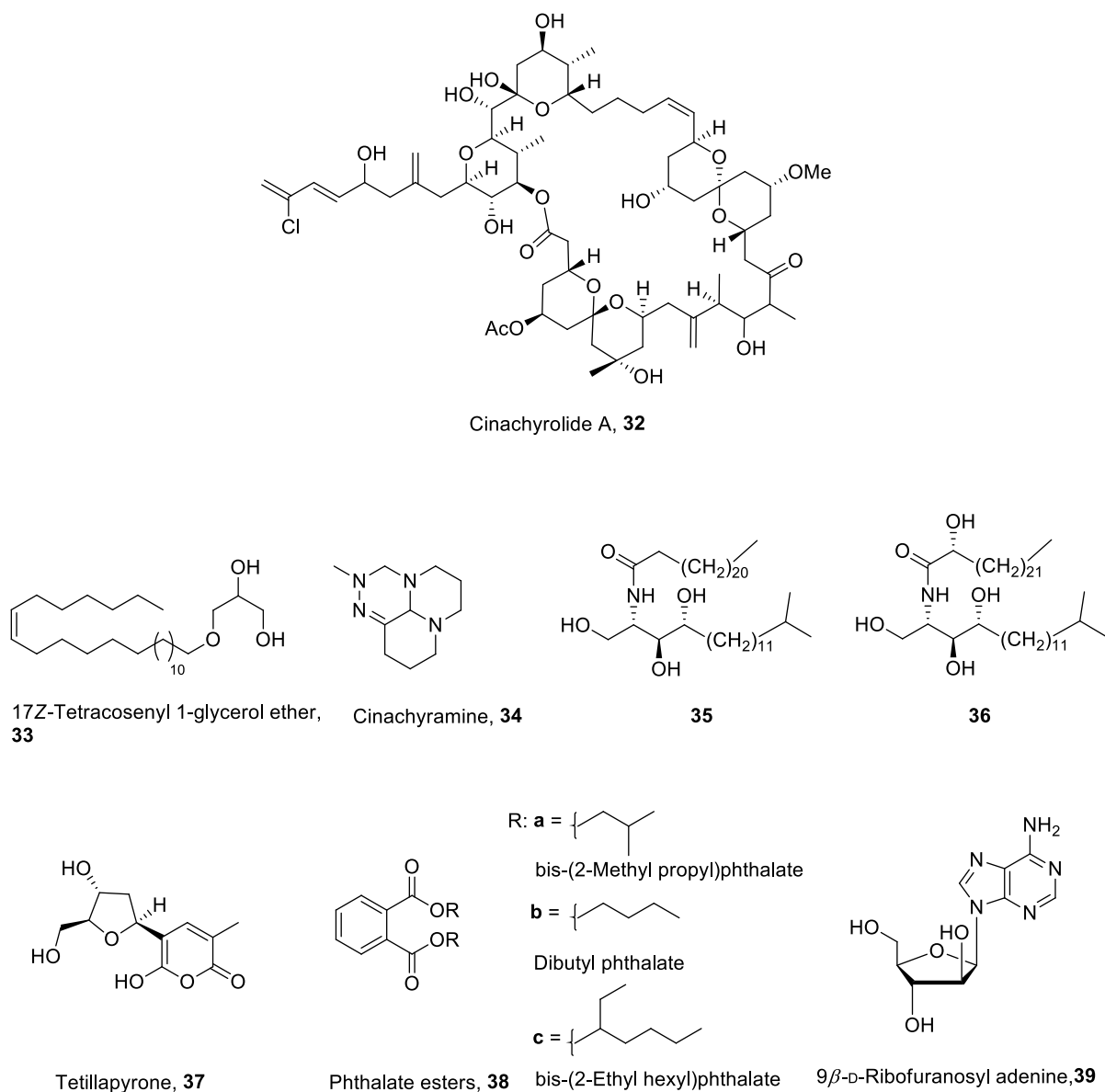
Figure 1.12: Structures of metabolites **32-39** isolated from *Cinachyra* sp. in the literature.

R: **17** =
Cholesterol

a =
24-Methylcholesterol

b =
22-*trans*-Cholesta-5,22-diene-3β-ol

c =
22-*trans*-24*S*-Ethylcholesta-5,22-diene-3β-ol

d =
24-Methylenecholesterol

e =
24-Methylcholest-5,22-diene-3β-ol

f =
24-Ethylcholesterol

g =
24-Oxocholesterol

R: **a** = $R_1 = R_2 = H$
Cholestanol

b = $R_1 = R_2 = H$
24-Methylcholestanol

c = $R_1 = OH, R_2 = H$
Cholestan-3β-5α-diol

d = $R_1 = H, R_2 = OH$
Cholestan-3β-6α-diol

R: **a** =
Cholest-4-ene-3-one

b =
24-Ethylcholest-4-ene-3-one

c =
24-Methylenecholest-4-ene-3-one

d =
24-Methylcholest-4,22-diene-3-one

R: **a** =
Cholest-4-ene-3,6-dione

b =
(24*R*)-24-Ethylcholest-4-ene-3,6-dione

R: **a** =
(6*E*)-Cholest-6-hydroximino-4-ene-3-one

b =
(24*R*, 6*E*)-24-Ethylcholest-6-hydroximino-4-ene-3-one

Clionasterol oleate, **44**

24-Methylcholest-7-ene-3β-ol, **45**

46

16-Dehydropregnenolone acetate, **47**

Gorgosterol, **48**

Figure 1.13: Structures of steroids **17**, **40-48** isolated from *Cinachyra* sp. in the literature.

Chapter 1

Several intriguing and unusual steroids were found to be inherited by *Cinachyra* sponges which could be a marker for this genus (Figure 1.13). The steroids identified from *Cinachyra* sponges are 3β-hydoxysterols **17a-g**, **40a-d**, ketosteroids **41a-d**, **42a-b**, hydroximino steroids **43a-b** and other steroids **44-48**. [52,54,60,61]

1.10. Results and discussion

The isolation of metabolites from the marine sponge *C. cavernosa* is broadly divided into three parts: extraction of the crude sample, purification of metabolites and structure elucidation of metabolites.

1.10.1. Extraction of the crude sample

To extract the metabolites from the sponge, the sponge solid material was soaked in 1:1 methanol:chloroform at room temperature. This is called solid-liquid extraction. The solvent was allowed to diffuse into the cells of the sponge and solubilize the metabolites. The solvent was filtered and concentrated under vacuum on a rotary evaporator at low temperature to give crude methanol:chloroform extract.[54,61]

1.10.2. Purification of metabolites

To further purify the crude methanol:chloroform extract, it was partitioned between two immiscible solvents. This is called liquid-liquid extraction. Primarily, crude methanol :chloroform (1:1 v/v) extract of *C. cavernosa* waspartitioned between hexane, ethyl acetate, *n*-butanol and water to obtain hexane fraction, ethyl acetate fraction, *n*-butanol fraction and aqueous fraction (Figure 1.14). In the present work, we directed our focus on the isolation of constituents from hexane fraction. The hexane fraction was subjected to successive column chromatography over silica gel using mixtures of hexane, ethyl acetate, chloroform and methanol as eluents of increasing polarity, to obtain around 38 fractions which were combined into 7 fractions based on the similarities of the appearance of spots on TLC (F-I to F-VII). F-III (ethyl acetate:hexane 6:4) was further subjected to column chromatography over silica gel to obtain F-C (ethyl acetate:hexane 4:6) and F-D (ethyl acetate:hexane 45:55). TLC analysis of the fraction F-C indicated a bright pink spot (ethyl acetate:hexane 3:7, $R_f = 0.3$) when sprayed with anisaldehyde-H_2SO_4 staining reagent with minor impurities. Thus, this partially purified fraction F-C was subjected to multiple developments in ethyl

acetate:hexane as the mobile phase to increase the resolution and finally, preparative TLC (ethyl acetate:hexane 2:8) purification led to the isolation of F-C-01 as white waxy solid.
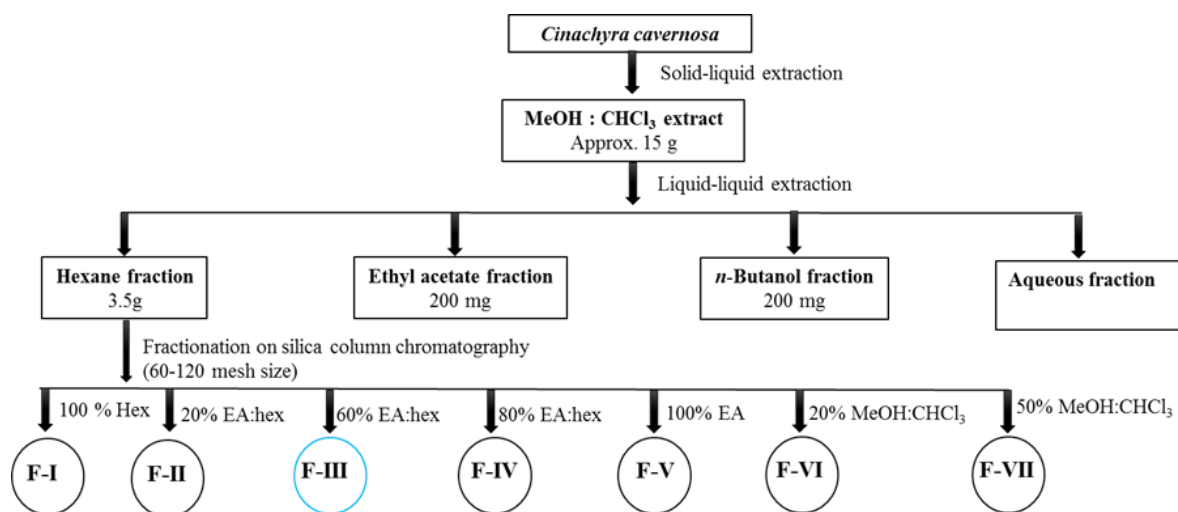
Figure 1.14: A brief outline of the extraction and fractionation process of secondary metabolites from *C. cavernosa* in the present work.

The TLC of fraction F-D revealed a dark blue spot (ethyl acetate:hexane 45:55, $R_f = 0.3$) when sprayed with anisaldehyde-H_2SO_4 staining reagent accompanied by minor impurities. Thus, F-D was subjected to multiple developments in ethyl acetate:hexane as the mobile phase to increase the resolution and finally, preparative TLC (ethyl acetate:hexane 25:75) purification led to the isolation of the F-D-01 white solid. The other fractions did not yield enough quantity of metabolites to characterize the structures completely.

1.10.3. Structure elucidation of metabolites

Instrumental techniques used to determine the structure of the purified metabolites from hexane fraction of *C. cavernosa* included IR, ^{1}H NMR, ^{13}C NMR, DEPT and HRMS. The IR analysis of F-C-01 purified from hexane fraction displayed bands 3387, 3305, 3225 cm^{-1} indicating the presence of hydroxyl groups (-OH). Interestingly, ^{13}C NMR of F-C-01 showed downfield ^{13}C signals at δC 64.3, 71.9, 72.5 which could be attributed to three methylene groups (-CH$_2$-) and δC 70.4 could be attributed to one methine group (>CH-) (confirmed by DEPT data). The ^{1}H NMR of F-C-01 gave four downfield ^{1}H peaks δH 3.47-3.57 (m, 4H), 3.67 (dd, $J = 11.4$ Hz, $J = 5.0$ Hz, 1H), 3.744 (dd, $J = 11.4$ Hz, $J = 4.0$ Hz, 1H), 3.88-3.89 (m,

1H) which could be attributed to three oxygenated methylene groups (-CH$_2$OH) and one oxygenated methine group (-OCH$_2$-). From the above structural data, F-C-01 is possibly a glycerol ether. Additionally, the NMR spectrum of F-C-01 showed the presence of long-chain methylene groups (–CH$_2$-) by the appearance of NMR signals at δH 1.27 (br, 32H), 1.59-1.61 (m, 2H), 2.04-2.11 (m, 4H) and δC 22.7, 26.1, 29.4-29.7, 31. NMR spectrum of F-C-01 also showed the presence of one methyl (-CH$_3$) NMR signal at δH 0.89 (bt, J = 5.8 Hz, 3H) and δC 14.2 (confirmed by DEPT data). The above structural assignments are in good agreement with those published for monoalkyl glycerol ethers.[57,62] Centred on this structural intel, a glycerol ether scaffold was assigned for F-C-01 and suggests F-C-01 to be a monoalkyl glycerol ether. HRMS (TOF MS ES+) measured of F-C-01 showed the appearance of peaks at m/z [M-H$_2$O] $^+$368.3210 (calculated for [M-H$_2$O] $^+$368.3649), m/z [M-O$_2$] $^+$354.3127 (calculated for [M-O$_2$] $^+$354.3862). Hence, F-C-01 is a monoalkyl glycerol ether **49** with C$_{21}$ hydrocarbon chain (Figure 1.15).

Monoalkyl glycerol ether, **49**
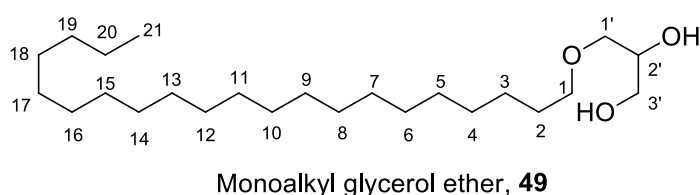
Figure 1.15: Structure of monoalkyl glycerol ether **49**.

In the year 1994, Quijano *et al.* reported a mixture of monoalkyl glycerol ethers (having hydrocarbon chain lengths C$_{14}$-C$_{21}$) from a marine sponge *Desmapsamma anchorata.*[62] The spectral data of monoalkyl glycerol ether **49** matched that of the literature data (Figure 1.15, Table 1.4).[57,62] To the best of our knowledge, a saturated monoalkyl glycerol ether with C$_{21}$ hydrocarbon chain has not been reported from *Cinachyra cavernosa*.

Table 1.4: Comparison of NMR data of monoalkylglycerol ether **49** with that of the literature.

49
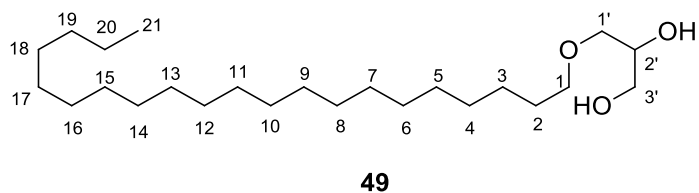
...continuation of table 1.4

Carbon number	^{1}H NMR (this work[a])	^{1}H NMR (reported[a])[57]	^{13}C NMR (this work[a])	^{13}C NMR (reported[a])[57]
1'	3.74 (dd,1H) 3.47-3.57 (m, 1H)	3.70 (dd, 1H) 3.45 (m, 1H)	71.9	71.7
2'	3.67 (dd,1H)	3.64 (dd, 1H)	70.4	70.5
3'	3.88-3.89 (m, 1H) 3.47-3.57 (m, 1H)	3.85 (m, 1H) 3.45 (overlapping m, 1H)	72.5	72.2
1	3.47-3.57 (m, 2H)	3.45 (overlapping m, 2H)	64.3	64.1
2	2.04-2.11 (4H, m)	2.03 (m, 4H)	31.9	31.8
3				
4	1.59-1.61 (2H, m)	1.58 (m, 2H)		
5				
6				
7				
8				
3				
10				
11			29.4-29.7	29.2-29.5
12				
13	1.27 (brs, 32H)	1.25 (brs, 32H)		
14				
15				
16				
17				
18				
19			26.1	25.9
20			22.7	22.5
21	0.89 (brt, 3H)	0.88 (brt, 3H)	14.2	13.9

[a]NMR solvent is CDCl$_3$

Chapter 1

The IR analysis of F-D-01 purified from hexane fraction of *C. cavernosa* displayed bands at 3631, 3401, 2967, 2936, 2884, 2864, 1477, 1383,1259, 1042, 959, 794 cm^{-1}. ^{1}H NMR spectrum of F-D-01 showed the presence of an oxygenated methine group (>CH-OH) by the appearance of a^{1}H signal at δH 3.54-3.58 (m, 1H).^{1}H NMR spectrum of F-D-01 showed the presence of a tri-substituted double bond (>C=CH$_2$-) by the appearance of ^{1}H NMR signals at δH 5.38 (brs, 1H). ^{1}H NMR spectrum of F-D-01 also showed presence of three methyl singlets (-CH$_3$) at δH 0.69 (s, 3H), 0.93 (d, *J* = 6.3 Hz, 3H), 1.03 (s, 3H) and a ^{1}H signal corresponding to methyls of isopropyl group (-CH(CH$_3$)$_2$) at δH 0.88 (d, *J* = 6.5 Hz, 6H). Further, the ^{13}C NMR spectrum of F-D-01 revealed 27 ^{13}C signals. The presence of 27 carbon signals could be attributed to a sterol moiety. The presence of oxygenated methine group (>CH-OH) in F-D-01 was further indicated by the appearance of ^{13}C NMR signals at δC 71.8. Also, the presence of a tri-substituted double bond (>C=CH$_2$-) in F-D-01 was further indicated by the appearance of ^{13}C NMR signals at δC 121.7, 140.7 (a quaternary carbon, confirmed by DEPT). Combining this structural information, suggests the sterol F-D-01 to be cholesterol (3β-cholest-5-ene-3-ol) **17** (Figure 1.16).
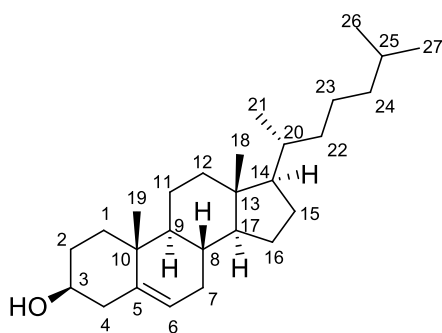
Cholesterol (3β-cholest-5-ene-3-ol), **17**

Figure 1.16: Structure of cholesterol **17**.

The observed spectral data matched that of the reported spectral data of cholesterol (3β-cholest-5-ene-3-ol) **17** (Figure 1.16, Table 1.5).[63,64] Thus, sterol F-D-01 is cholesterol **17**.

Table 1.5: Comparison of NMR data of cholesterol **17** with that of the literature.
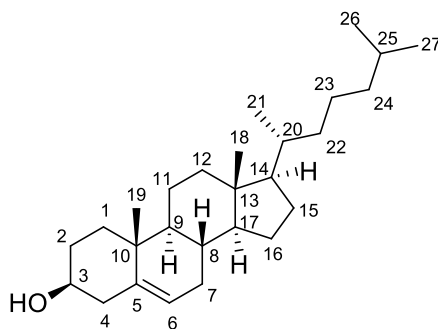
17

Carbon numbering	¹H NMR (This work^a)	¹H NMR (reported^a)[64]	¹³C NMR (This work^a)	¹³C NMR (reported^a)[63]
1	1.27-1.36 (m,2H)		37.2	37.5
2	1.85-1.88 (m, 1H) 1.45-1.66 (m, 1H)	1.90 (m, 1H) 1.58 (m, 1H)	31.6	31.6
3	3.54-3.58 (m, 1H)	3.47 (m, 1H)	71.8	71.3
4	2.26-2.31 (m, 2H)	2.30 (m, 2H)	42.3	42.4
5			140.7	141.2
6	5.38 (brs, 1H)	5.30 (brs, 1H)	121.7	121.3
7	1.97-2.05 (m, 2H)	2.05 (m, 2H)	31.9	32.0
8	1.85-1.88 (m, 1H)		31.9	32.0
9	1.85-1.88 (m, 1H)		50.1	50.5
10			36.5	36.5
11	1.45-.66 (m, 1H) 1.27-1.36 (m, 1H)		21.1	21.2
12	1.45-.66 (m, 1H) 1.27-1.36 (m, 1H)		28.2	28.3
13			42.3	42.4
14	1.45-1.66 (m, 1H)		56.8	56.9

...continuation of table 1.5

15	1.45-.66 (m, 1H) 1.27-1.36 (m, 1H)		23.8	24.3
16	1.45-.66 (m, 1H) 1.27-1.36 (m, 1H)		39.8	40.0
17	1.45-1.66 (m, 1H)		56.1	56.5
18	0.69 (s, 3H)	0.62 (s, 3H)	11.9	12.0
19	1.03 (s, 3H)	1.02 (s, 3H)	19.4	19.4
20	1.45-1.66 (m, 1H)		35.8	35.8
21	0.93 (d, 3H)		18.7	18.8
22			36.2	36.4
23	1.08-1.21 (m, 6H)		24.3	24.1
24			39.5	39.6
25	1.45-1.66 (m, 1H)		28.0	28.0
26	0.88 (d, J = 6.5 Hz, 6H)		22.6	22.6
27			22.8	22.9

[a]NMR solvent is $CDCl_3$

Cholesterol **17** is well known to be present in *Cinachyra cavernosa*. *C. cavernosa*was found to be a new source of monoalkyl glycerol ether **49**. An outline of the isolation protocol of secondary metabolites from methanol:chloroform extract of *Cinachyra cavernosa* is illustrated in figure 1.17.
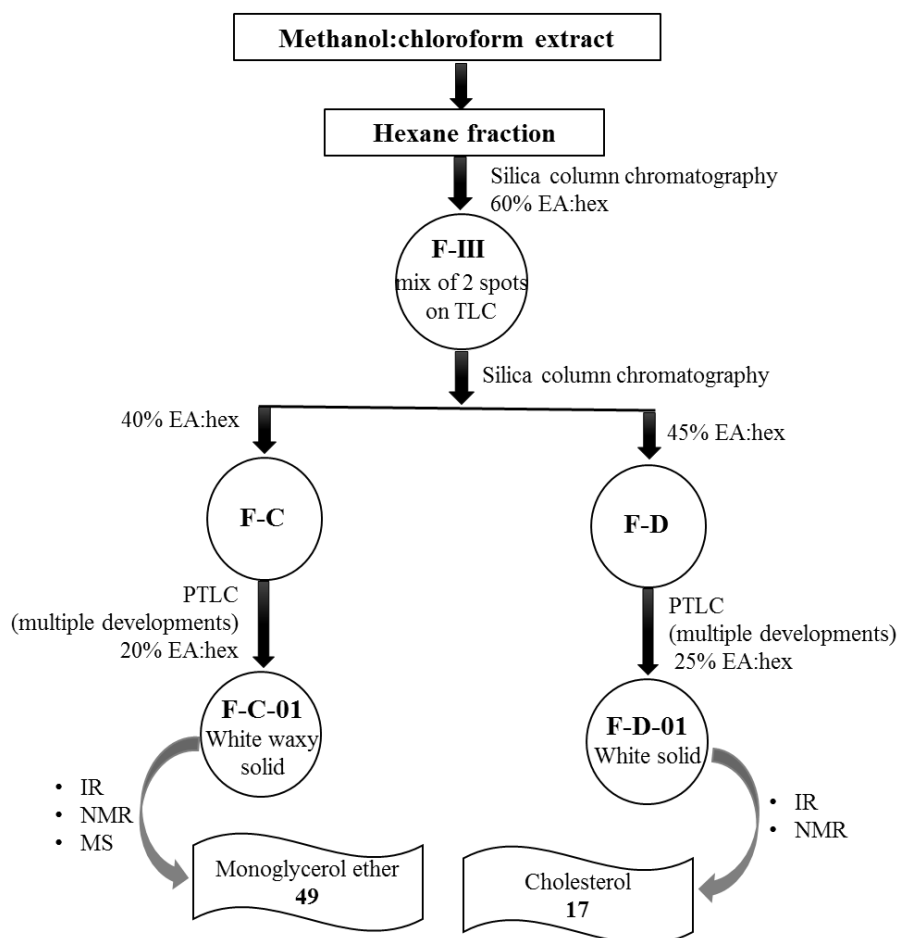
Figure 1.17: Isolation protocol of metabolites from methanol:chloroform extract of *Cinachyra cavernosa.*

Cholesterol and glycerol ethers are distributed widely in sponges. The main significance of cholesterol is the cell membrane fluidity and permeability by interacting with hydrophilic head groups and hydrophobic tails of phospholipids.[65] Monoalkyl glycerol ethers are known to possess antibacterial activities. Their significance in sponges is still not known, but it might have a role to play in the maintenance of sponge membranes, growth and may be essential in the defense mechanism of the sponge.[62] Thus, *Cinachyra* sponges are a treasure of fascinating bioactive secondary metabolites which could find a range of applications not only in the pharmaceuticals and related industries but also in studies about biochemical taxonomy.[54]

Chapter 1

1.11. Conclusion

1. Two compounds cholesterol **17** and monoalkyl glycerol ether **49** were isolated, purified and characterized from methanol:chloroform extract of a marine sponge *Cinachyra cavernosa.*

2. Monoalkyl glycerol ethers are known to be antibacterial agents. *C. cavernosa* is a new source of monoalkyl glycerol ether **49**.

3. Cholesterol **17** is an important metabolite that has a significant role to play in cell membrane structure and function to maintain cell membrane fluidity and permeability.

Chapter 1

1.12. Experimental part

1.12.1. Material and methods

Melting points (uncorrected) were determined in an open capillary using the Thiele melting point tube. Thin-layer chromatography was performed with Kieselgel 60 F254 (Merck aluminium support plates). TLC spots were developed in UV, 5% methanolic H_2SO_4 (heated at 110°C, 10 min), anisaldehyde-H_2SO_4 (heated at 110°C, 10 min). The absorbances at 475 nm were recorded on Shimadzu UV-2450 double beam spectrophotometer. Infrared data was recorded in the region between 4000 to 400 cm-1 on a Shimadzu IRPrestige-21 instrument. Column chromatography was performed with sephadex LH-20 and silica gel 60-200 mesh size as packing material. ^{1}H NMR, ^{13}C NMR and DEPT-135 spectra were recorded at room temperature on Bruker instrument (400 MHz for ^{1}H and 100 MHz for ^{13}C, chemical shifts are recorded in ppm relative to tetramethylsilane (TMS) as the internal standard. The mass spectra were recorded on liquid chromatography - electrospray ionisation - mass spectrometry (LC-ESI-MS) and high resolution mass spectrometry - time of flight - electrospray ionisation HRMS (TOF MS ES+). Crystal structure data was collected on Bruker D8 Quest Eco model diffractometer using graphite monochromated Mo-Kα radiation (λ = 0.71073 Å) at 293 K. The structural refinement was done by full-matrix least-square against F2 using all data (SHELXL). Crystallographic data for the structure of compound **20** reported herein have been deposited with the Cambridge Crystallographic Data Centre as Supplementary Publication No. 1919099. Copies of the data can be obtained free of charge, on application to CCDC. (e-mail:deposit@ccdc.cam.ac.uk; https://www.ccdc.cam.ac.uk). All the chemicals used in this study were of reagent grade and used as received without any further purification. Mushroom tyrosinase (Agaricus bisporus) (EC 1.14.18.1) was purchased from Sigma-Aldrich. L-tyrosine (purity ≥ 98%) was purchased from Sigma-Aldrich and kojic acid (purity ≥ 98%) was procured from Merck.

Experimental part of section A

1.12.2. Collection of algae and extraction

The algal species *Enteromorpha* sp. was collected from the coast of Anjuna Goa (India) and was identified by Dr PA Thomas (Central Marine Fisheries Research Institute, Trivandrum,

Chapter 1

India). They were frozen as soon as possible and transferred to the laboratory. The freshly collected organisms were initially freeze-dried. They were homogenized in a blender with little water and exhaustively extracted at room temperature with MeOH (1 L x 3). The combined extracts were filtered and concentrated under vacuum on a rotary evaporator at low temperature to give a crude methanolic extract. Methanolic extract (~15 g) of the algae *Enteromorpha* sp. was fractionated with hexane (100 ml x 3), ethyl acetate (100 ml x 3).

1.12.3. Isolation and purification

The hexane fraction (832 mg) was chromatographed initially on a silica gel column (60-200 mesh size, 2cm x 50cm) eluting with a series of mixtures consisting of hexane, ethyl acetate, chloroform and methanol in increasing polarity. The obtained fraction F-III (ethylacetate:hexane 6:4, 216 mg) was further purified by subjecting to repetitive column chromatography over silica gel to obtain fraction F-A (40 mg) and then final purification was carried out on preparative TLC (ethyl acetate:hexane 3:7, 10cm x 20cm) by multiple developments. This furnished 4-hydroxycoumarin **20** (F-A-06, beige powder, 10 mg). The ethyl acetate fraction (282 mg) was chromatographed initially on a silica gel column (60-200 mesh size, 2cm x 50cm) eluting with a series of mixtures consisting of hexane, ethyl acetate, chloroform and methanol in increasing polarity. The obtained fraction F-II (ethylacetate:hexane 3:7, 120 mg) was further subjected to column chromatography over Sephadex LH-20 (methanol:chloroform 1:1, 2cm x 50cm) to obtain F-B (98 mg). The fraction F-B was purified on a silica gel column (60-200 mesh size, 1cm x 30 cm) to furnish ergosterol **21**(ethyl acetate:hexane 4:6, F-B-04,brown powder, 11 mg) and ergosterol peroxide **22** (ethyl acetate:hexane 4:6, F-B-05, white powder, 6 mg).

4-Hydroxycoumarin 20

Beige solid; mp 215-216°C (reported 213-215°C) ;[23–25] IR v_{max} cm^{-1}: 3377, 2885, 2719, 2576, 1612, 1550; ^{1}H NMR (MeOH-d$_4$, 400 MHz): δH 5.55 (1H, s, H-D exchange), 7.24-7.28 (m, 2H), 7.52-7.57 (m, 1H), 7.81-7.83 (m, 1H);[26] ^{13}C NMR (MeOH-d$_4$,100 MHz): δC 91.6, 117.4, 117.6, 124.6, 125.4, 134.0, 155.2, 166.3, 168.7; LC-ESI-MS *m/z* calculated for $C_9H_7O_3$ [M + H]$^+$ 163.0395, found 163.0386.

Chapter 1

Ergosterol 21

Brown solid; mp 155-156°C (reported 160°C);[66] IR ν_{max} cm^{-1}: 3432, 2957, 2870; ^{1}H NMR (CDCl$_3$, 300 MHz): δH 0.64 (s, 3H), 0.81-0.86 (m, 6H), 0.93 (d, J = 6.9 Hz, 3H), 0.96 (s, 3H), 1.05 (d, J = 6.6 Hz, 3H), 1.23-1.37 (m, 6H), 1.45-1.53 (m, 5H), 1.84-1.92 (m, 3H), 1.99-2.09 (m, 4H), 2.22-2.36 (m, 1H), 2.44-2.52 (m, 1H), 3.60-3.70 (m, 1H), 5.21 (t, J = 6.3 Hz, 2H), 5.39-5.41 (m, 1H), 5.57-5.60 (m, 1H); ^{13}C NMR (CDCl$_3$, 75 MHz): δC 12.0, 16.3, 17.6, 19.6, 19.9, 21.1 (2C), 23.0, 28.3, 32.0, 33.1, 37.0, 38.4, 39.1, 40.4, 40.8, 42.8, 46.2 (2C), 54.8, 55.7, 70.4, 116.3, 119.6, 132.0, 135.6, 139.8, 141.3.

Ergosterol Peroxide 22

White solid; ^{1}H NMR (CDCl$_3$, 300 MHz): δH 3.94-4.02 (m, 1H), 5.10-5.27 (m, 2H), 6.25 (d, J = 8.4 Hz, 1H), 6.51 (d, J = 8.4 Hz, 1H);^{13}C NMR (CDCl$_3$, 75 MHz): δC 12.9, 17.5, 18.2, 19.6, 19.9, 20.6, 20.9, 23.4, 28.6, 30.1, 33.0, 34.7, 36.9, 37.0, 39.3, 39.7, 42.8, 44.6, 51.1, 51.8, 56.2, 66.4, 79.4, 82.1, 130.1, 132.1, 135.2, 135.4.

1.12.4. Method for anti-tyrosinase activity

Tyrosinase inhibition assay was performed as described by Ko *et al.*[67] with modifications. Crude methanol extract of *Enteromorpha* sp. was dissolved in DMSO to get a final concentration of 0.6 mg/mL. Kojic acid was used as a positive control. Briefly, 20 μL of mushroom tyrosinase (1000 U/mL) was pre-incubated with 120 μL of the test sample in 50 mM phosphate buffer (pH 6.9) for 5 minutes at 30°C. Then, 2 mM L-tyrosine (300 μL) was added to each reaction mixture and incubated at 30°C for 30 minutes. The enzyme reaction was monitored by measuring the absorbance at 475 nm. The percent inhibition of tyrosinase reaction was calculated as follows:

$$\text{Percent Inhibition} = [(A_{control} - A_{sample})/A_{control}] \times 100;$$

where $A_{control}$ is the absorbance without the test sample in the DMSO and A_{sample} is the absorbance with the test sample in DMSO.

Chapter 1

Experimental part section B

1.12.5. Collection of sponge and extraction

The sponge species *C. caversnosa* was collected fromAnjunaGoa (India) and was identified by Dr. PA Thomas (Central Marine Fisheries Research Institute, Trivandrum, India). They were frozen as soon as possible and transferred to the laboratory. The freshly collected organisms were initially freeze-dried. They were homogenized in a blender with little water and exhaustively extracted at room temperature with methanol:chloroform (1:1, v/v, 1 L x 3). The combined extracts were filtered and concentrated under vacuum on a rotary evaporator at low temperature to give a crude methanol/chloroform extract. Methanol:chloroform extract (~15 g) of the sponge *C. caversnosa* was fractionated between hexane (100 ml x 3) and water (100 ml x 3). The combined hexane layer was concentrated under vacuum on a rotary evaporator at low temperature to give a hexane fraction (~3.5 g).

1.12.6. Isolation and purification

The hexane fraction (~3.5 g) was chromatographed initially on a silica gel column (60-200 mesh size, 3cm x 60cm) eluting with a series of mixtures consisting of hexane, ethyl acetate, chloroform and methanol in increasing polarity. The obtained fraction F-III (ethyl acetate:hexane 6:4, 290 mg) was further purified by subjecting to repetitive column chromatography over silica gel (60-200 mesh size, 1cm x 60cm) to obtain fraction F-C (ethyl acetate:hexane 4:6, 28 mg) and fraction F-D (ethyl acetate:hexane 45:55, 60 mg). Preparative TLC of F-C (ethyl acetate:hexane 2:8, 12cm x 25cm) by multiple developments furnished monoalkyl glycerol ether **49** (F-C-01, white waxy solid, 8 mg). Preparative TLC of F-D (ethyl acetate:hexane 25:75, 10cm x 20cm) by multiple developments furnished 28 mg of cholesterol **17** (F-D-01, white solid, 28 mg).

Monoalkyl glycerol ether49

white solid; ethylacetate: hexane 3:7, R_f = 0.3; mp 65°C; IR ν_{max} cm^{-1}: 3387, 3305, 3225, 2981,2927,2833,1452, 1371, 1235, 1114, 1019, 818, 721; ^{1}H NMR (CDCl$_3$, 400 MHz): δH 0.89 (bt, *J* = 5.8 Hz, 3H), 1.27 (br, 32H), 1.59-1.61 (m, 2H), 2.04-2.11 (m, 4H), 3.47-3.57 (m, 4H), 3.67 (dd, *J* = 11.4 Hz, *J* = 5.0 Hz, 1H), 3.744 (dd, *J* = 11.4 Hz, *J* = 4.0 Hz, 1H),

Chapter 1

3.88-3.89 (m, 1H); ^{13}C NMR (CDCl$_3$, 100 MHz): δC 14.2, 22.7, 26.1, 29.4-29.7 (16C), 31.9, 64.3, 70.4, 71.9, 72.6; HRMS (TOF MS ES+) m/z calculated for [M-H$_2$O]$^+$ 368.3649, found 368.3210, m/z calculated for [M-O$_2$]$^+$ 354.3862, found 354.3127.

Cholesterol 17

White solid; ethyl acetate: hexane 45:55, R$_f$ = 0.3; mp 143°C;[63,64] IR v_{max} cm^{-1}: 3631, 3401, 2967, 2936, 2884, 2864, 1477, 1383, 1259, 1042, 959, 794; ^{1}H NMR (CDCl$_3$, 400 MHz): δH 0.69 (s, 3H), 0.88 (d, J = 6.5 Hz, 6H), 0.93 (d, J = 6.3 Hz, 3H), 1.03 (s, 3H), 1.08-1.21 (m, 6H), 1.27-1.36 (m, 6H), 1.45-1.66 (m, 9H), 1.85-1.88 (m, 3H), 1.97-2.05 (m, 2H), 2.26-2.31 (m, 2H), 3.54-3.58 (m, 1H), 5.38 (brs, 1H); ^{13}C NMR (CDCl$_3$, 100 MHz): δC 11.9, 18.7, 19.4, 21.1, 22.6, 22.8, 23.8, 24.3, 28.0, 28.2, 31.6, 31.9 (2C), 35.8, 36.2, 36.5, 37.2, 39.5, 39.8, 42.3, 42.3, 50.1, 56.1, 56.8, 71.8, 121.7, 140.7.

1.13. Spectra
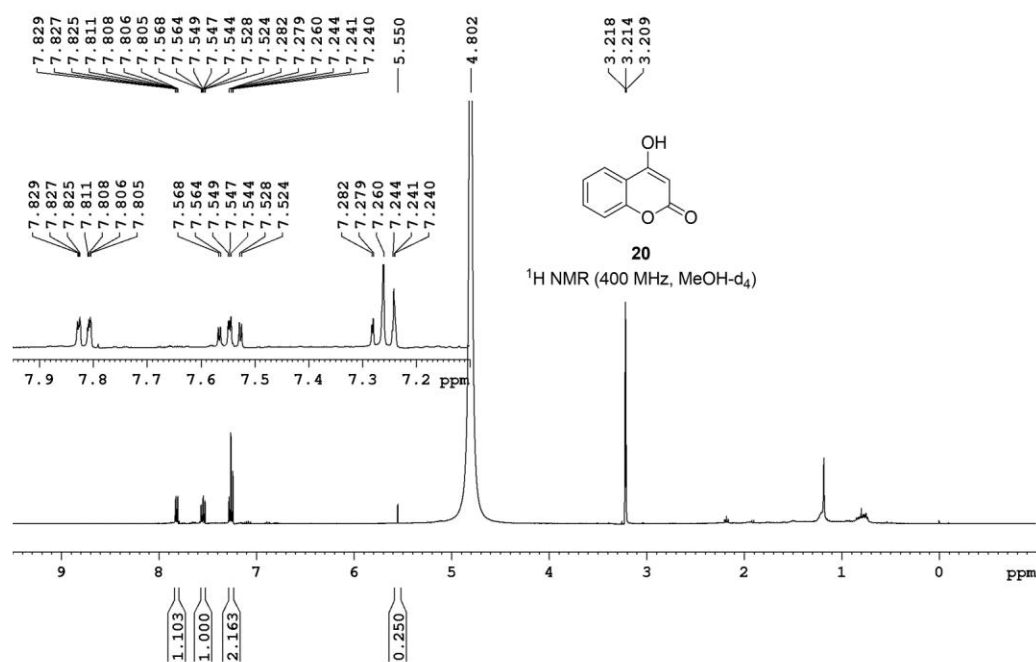
Figure 1.18: ^{1}H NMR spectrum of 4-hydroxycoumarin **20**.
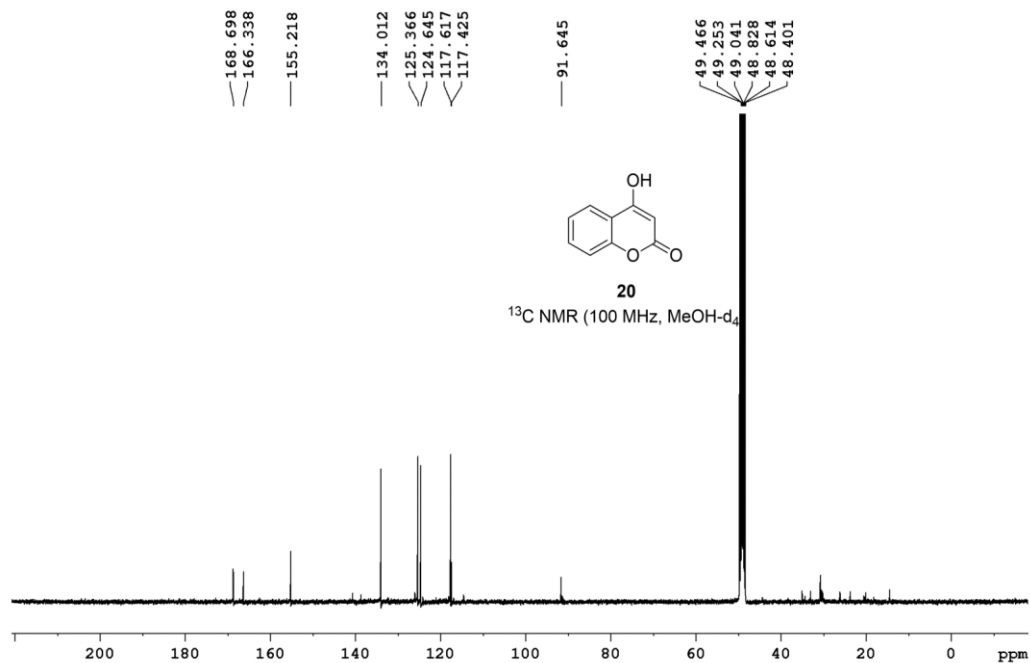
Figure 1.19: ^{13}C NMR spectrum of 4-hydroxycoumarin **20**.
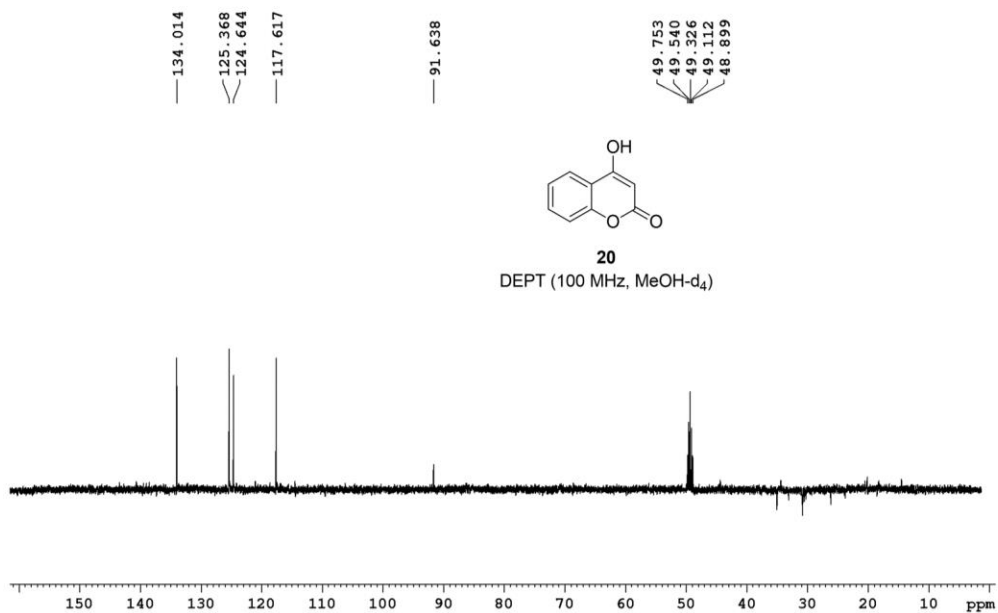
Figure 1.20: DEPT spectrum of 4-hydroxycoumarin **20**.
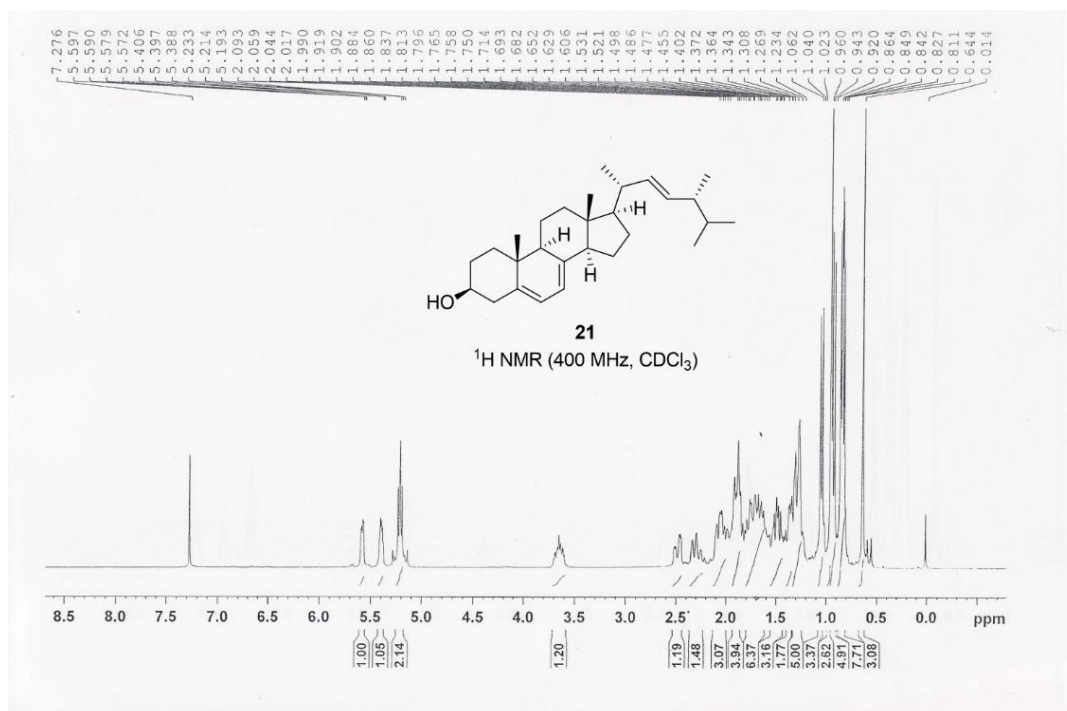
Figure 1.21: [^1]H NMR spectrum of ergosterol **21**.
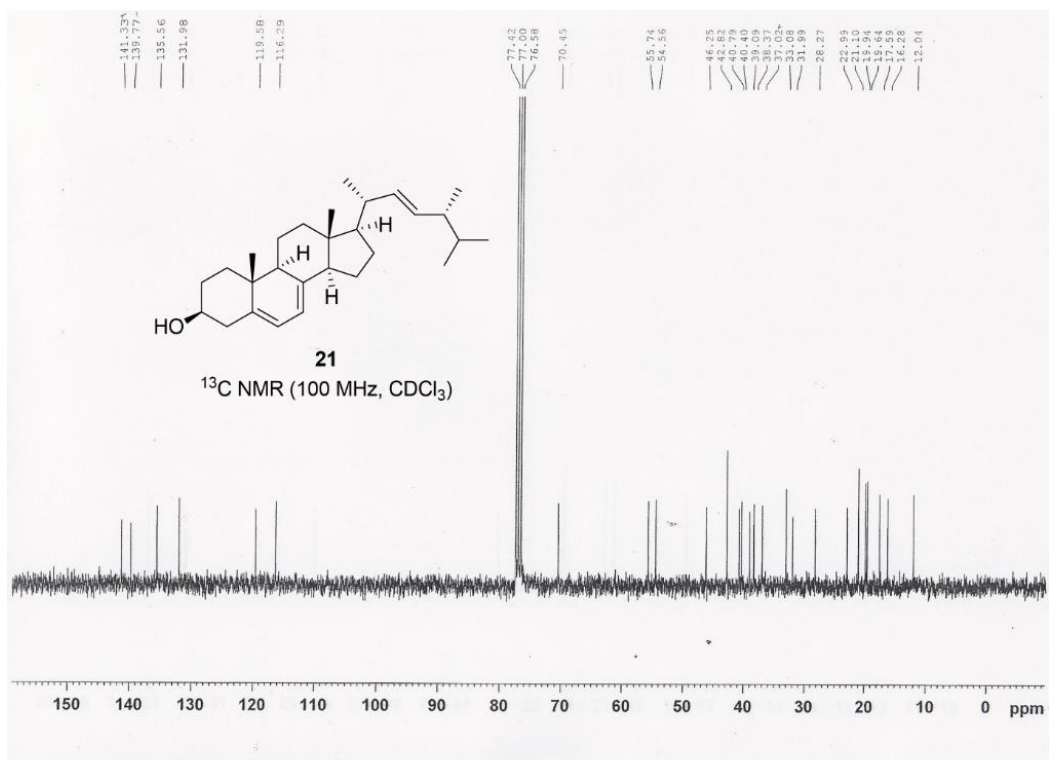
Figure 1.22: [^13]C NMR spectrum of ergosterol **21**.
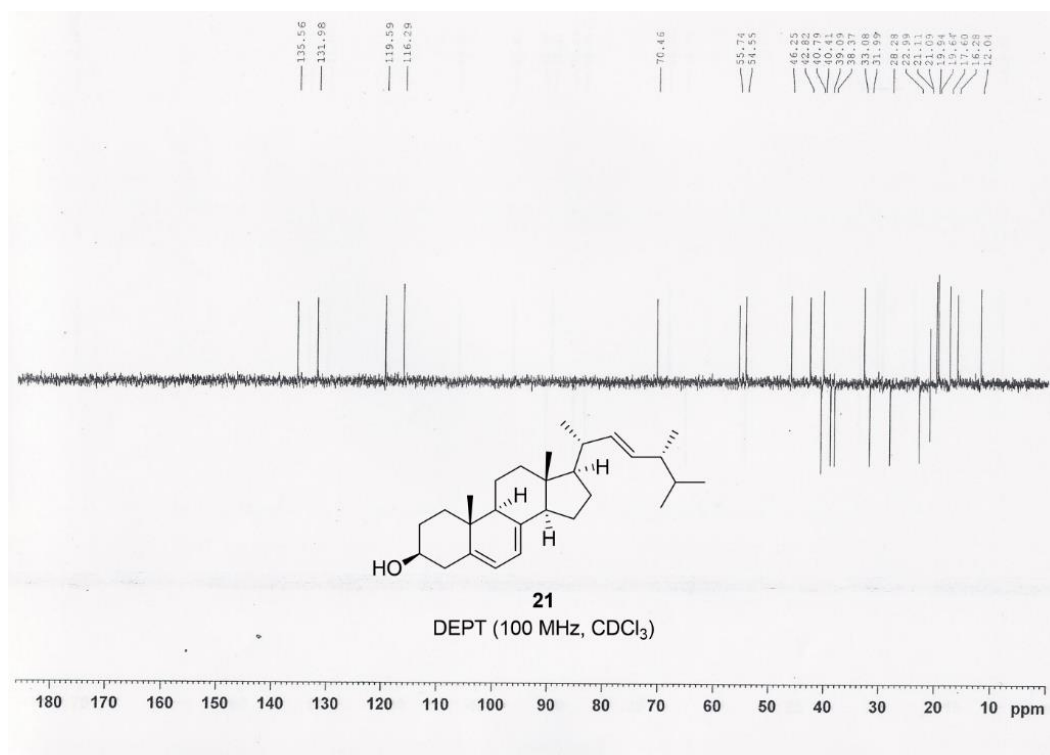
Figure 1.23: DEPT spectrum of ergosterol **21**.
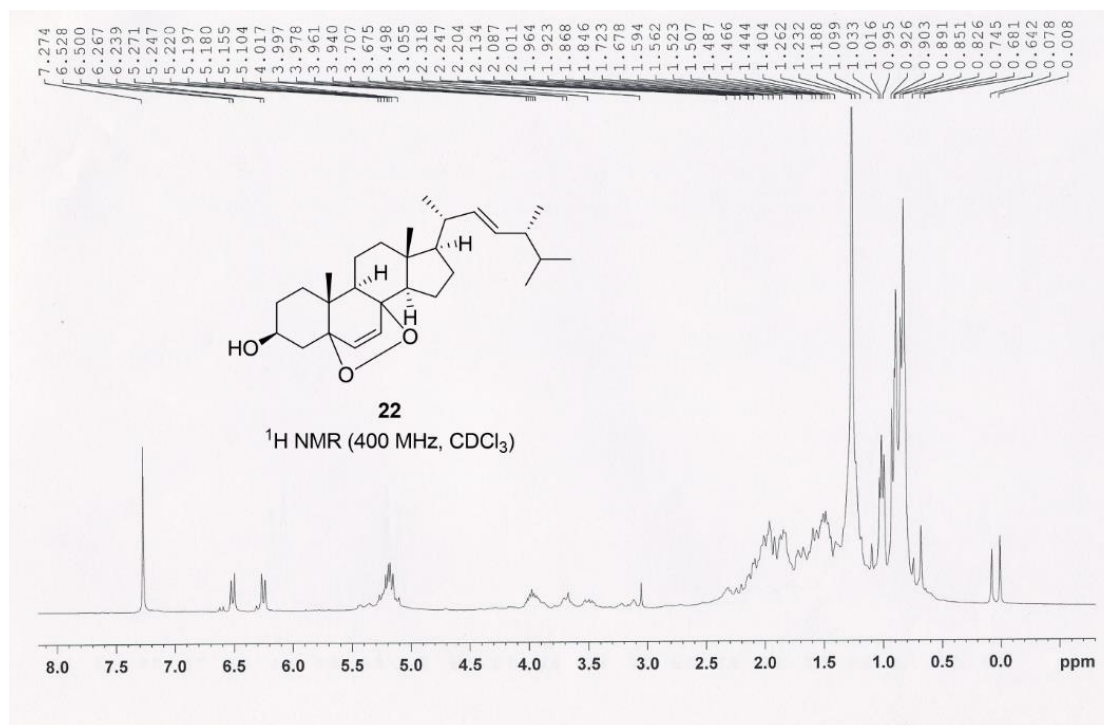
Figure 1.24: ^{1}H NMR spectrum of ergosterol peroxide **22**.
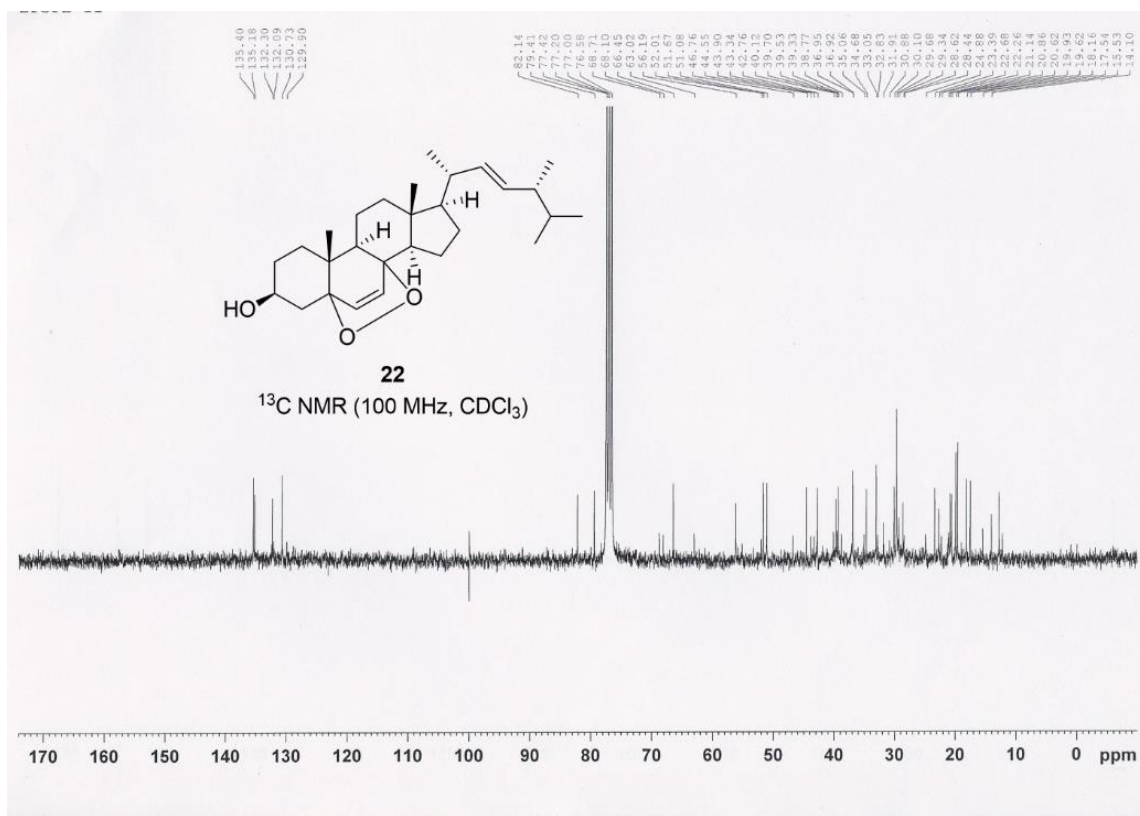
Figure 1.25: ^{13}C NMR spectrum of ergosterol peroxide **22**.
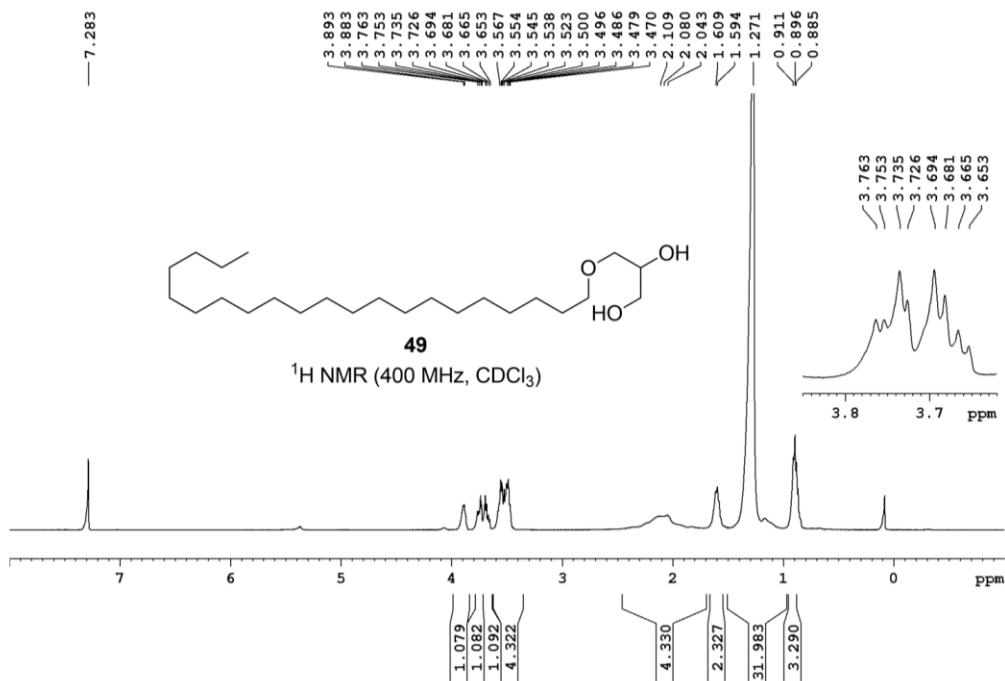
Figure 1.26: ^1H NMR spectrum of monoalkyl glycerol ether **49**.
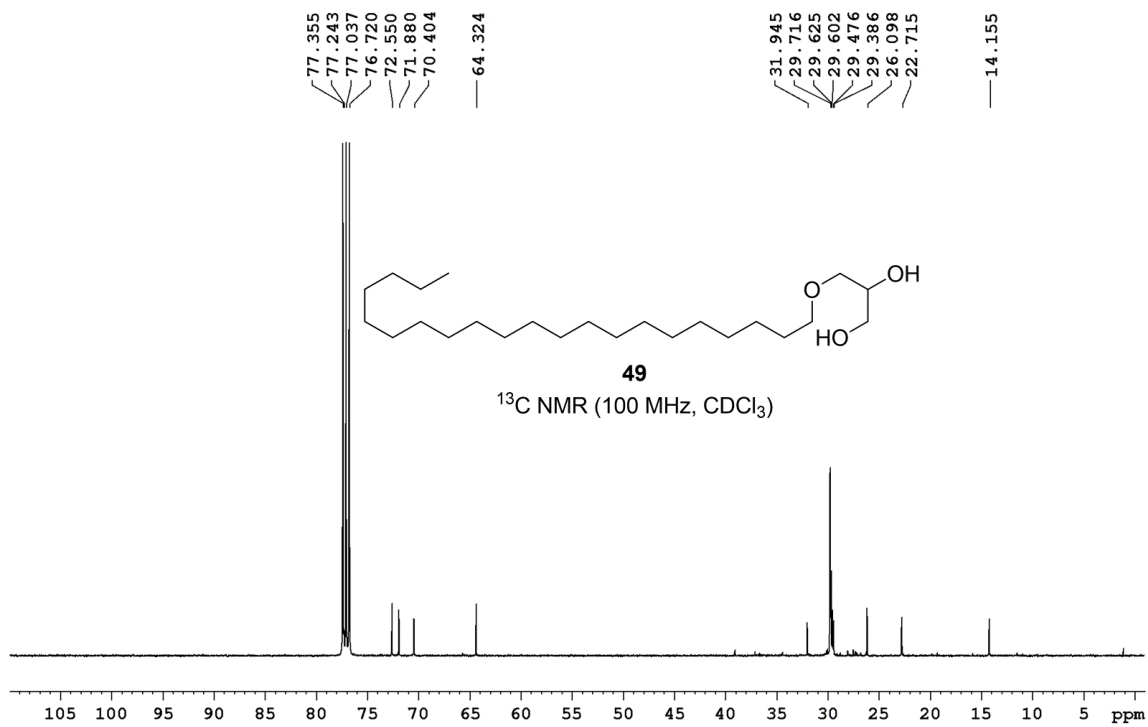
Figure 1.27: ^{13}C NMR spectrum of monoalkyl glycerol ether **49**.
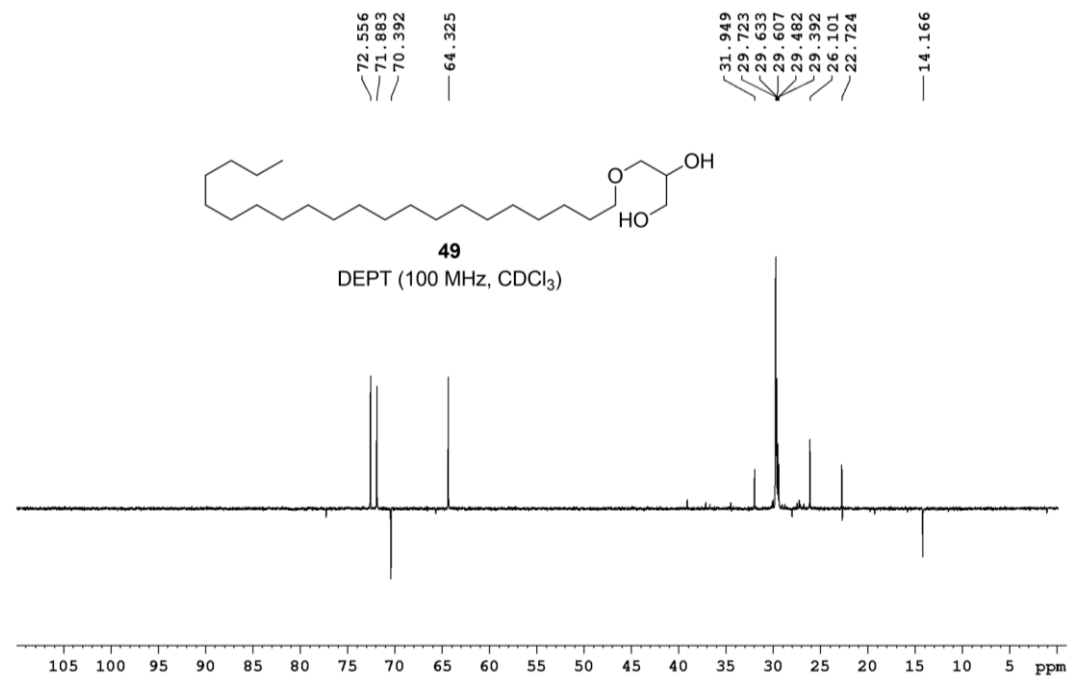
Figure 1.28: DEPT spectrum of compound **49**.
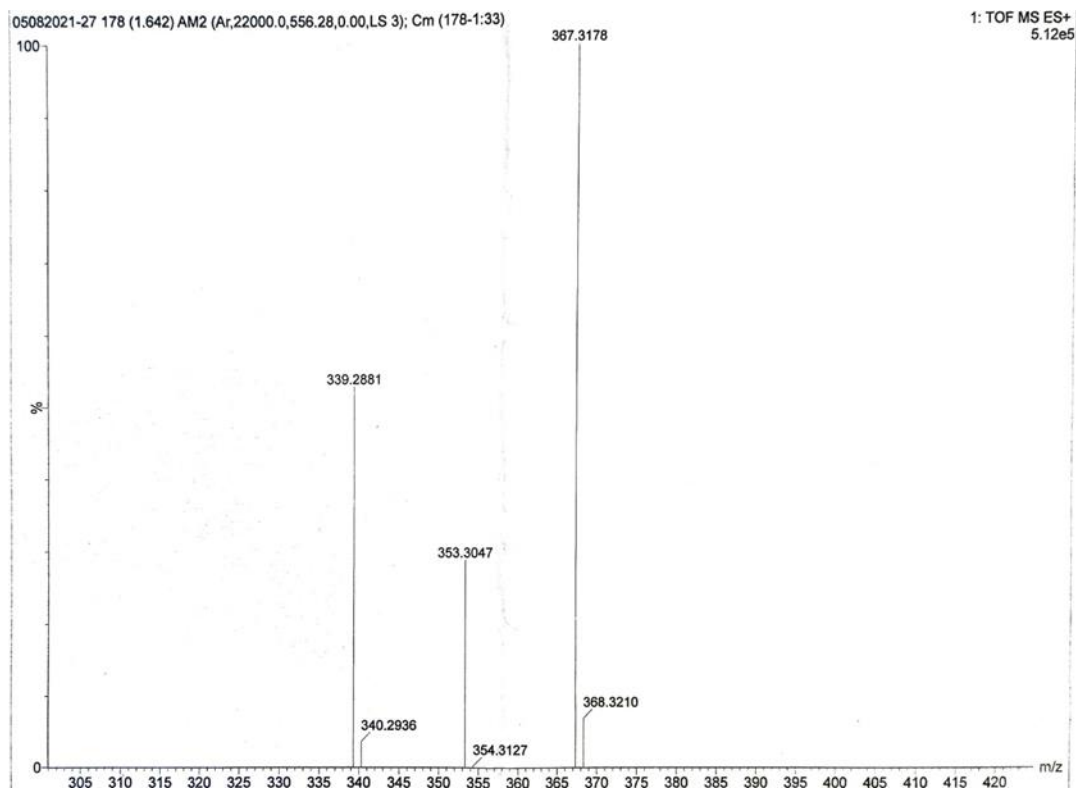
Figure 1.29: HRMS (TOF MS ES+) of monoalkyl glycerol ether **49**.
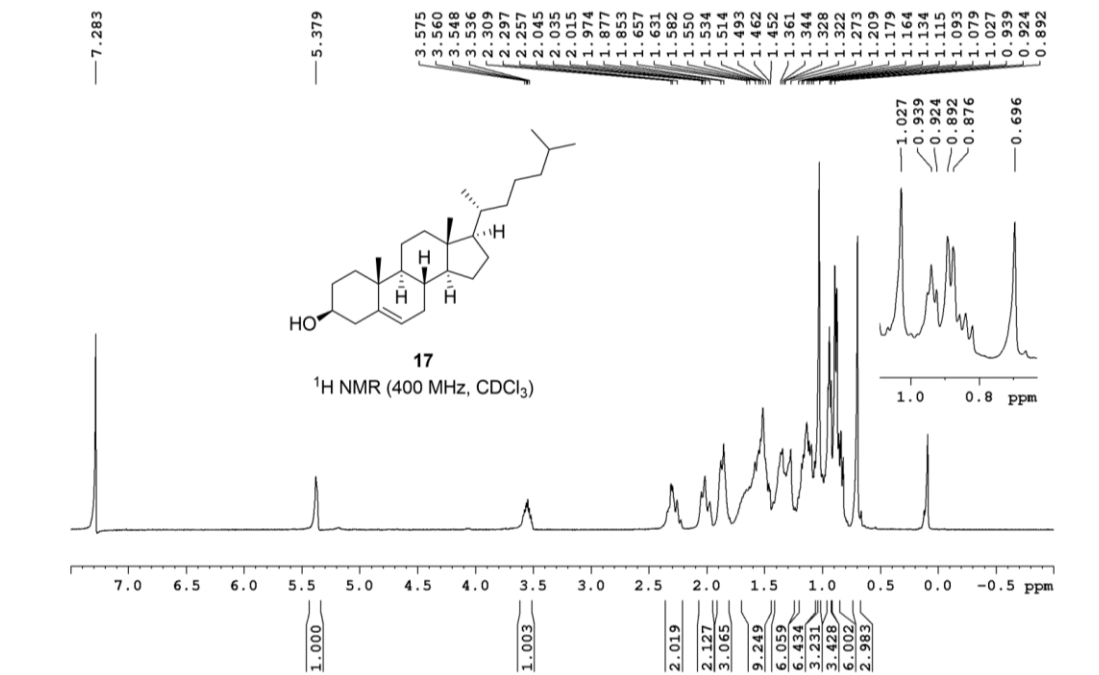
Figure 1.30: ^{1}H NMR spectrum of cholesterol **17**.
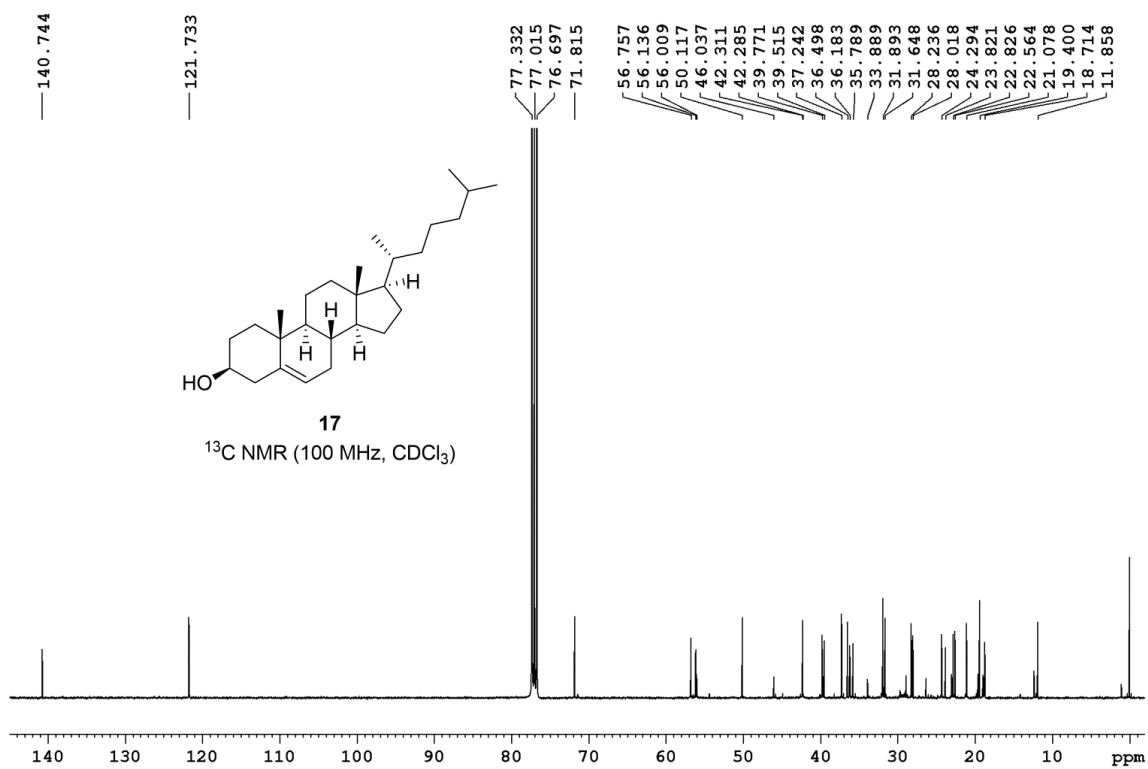
Figure 1.31: ^{13}C NMR spectrum of cholesterol **17**.
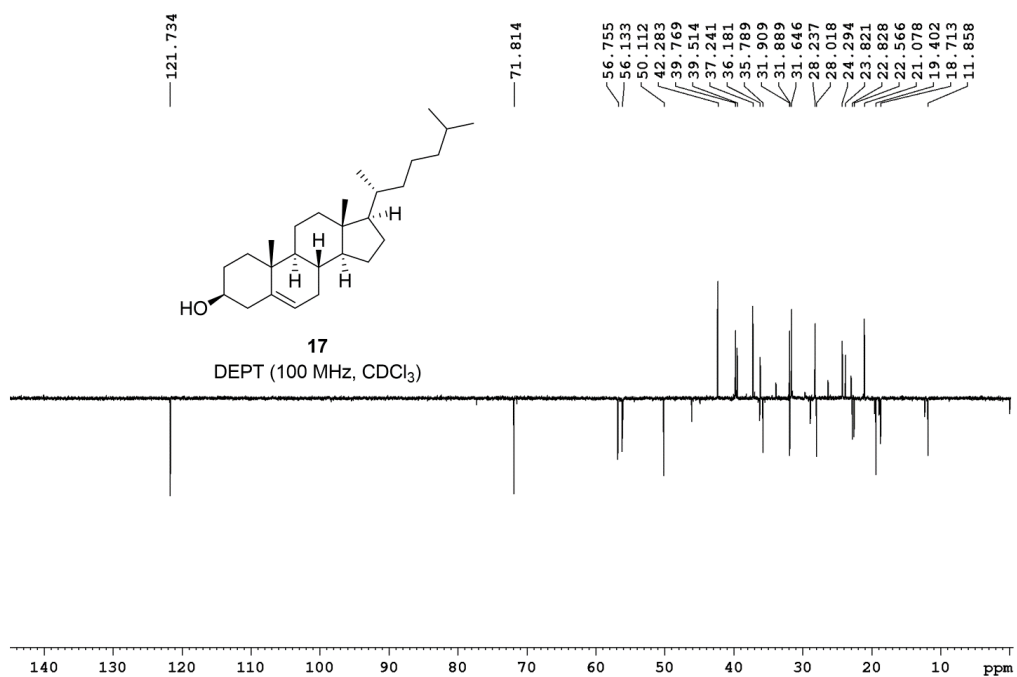
Figure 1.32: DEPT spectrum of cholesterol **17**.

1.14. Crystallographic data of 4-hydroxycoumarin 20

Table 1.6: Crystallographic data and structure refinement parameters for 4-hydroxycoumarin **20**.

	20
Chemical formula	$C_9 H_8 O_4$
M/g mol^{-1}	180.15
Temp./K	293
Crystal system	Orthorhombic
Space group	$P2_1 2_1 2_1$
a/Å	6.9209(3)
b/Å	10.0448(4)
c/Å	12.1384(5)
α/°	90
β/°	90
γ/°	90
V/Å^3	843.85(6)
Z	4
D_c/g cm^{-3}	1.418
μ/mm^{-1}	0.113
R	0.0380(1600)
wR	0.1032(2088)
F(000)	376.0

Table 1.7: Bond distances (Å) and angles (°) for 4-hydroxycoumarin **20**.

O1-C1	1.367(3)
O1-C8	1.378(3)
C1-O2	1.229(2)
C1-C2	1.405(3)
C2-C3	1.355(3)
O3-C3	1.324(2)
C3-C9	1.437(3)
C9-C8	1.381(3)
C9-C4	1.398(3)
C8-C7	1.383(3)
C7-C6	1.372(3)
C6-C5	1.376(4)
C5-C4	1.374(3)
C1-O1-C8	121.0(17)
O2-C1-O1	114.4(19)
O2-C1-C2	126.6(2)
O1-C1-C2	119.0(18)
C3-C2-C1	121.1(2)
O3-C3-C2	124.6(2)
O3-C3-C9	115.5(18)
C2-C3-C9	119.8(19)
C8-C9-C4	118.4(2)
C8-C9-C3	117.8(18)
C4-C9-C3	123.7(19)
O1-C8-C9	121.1(19)
O1-C8-C7	116.8(2)
C9-C8-C7	122.0(2)
C6-C7-C8	118.2(2)
C7-C6-C5	121.2(2)
C4-C5-C6	120.2(2)
C5-C4-C9	119.9(2)
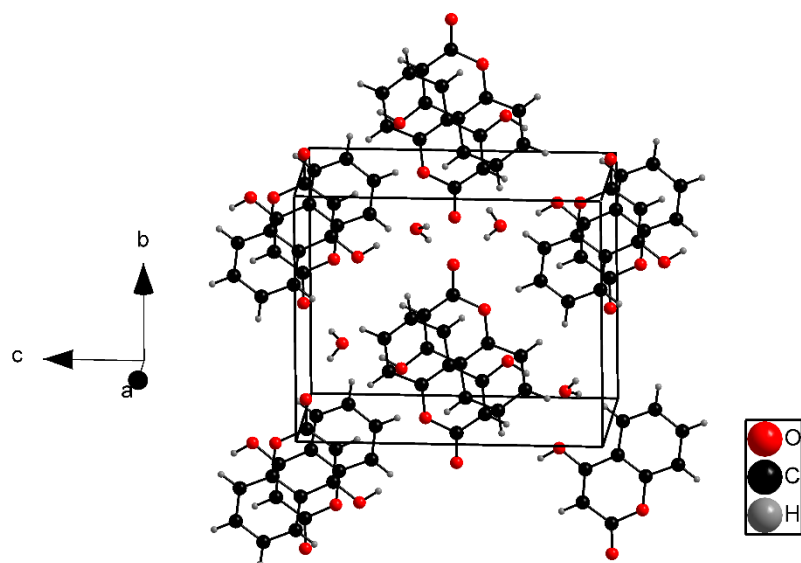
Figure 1.33: A view of the unit cell packing of 4-hydroxycoumarin **20**.
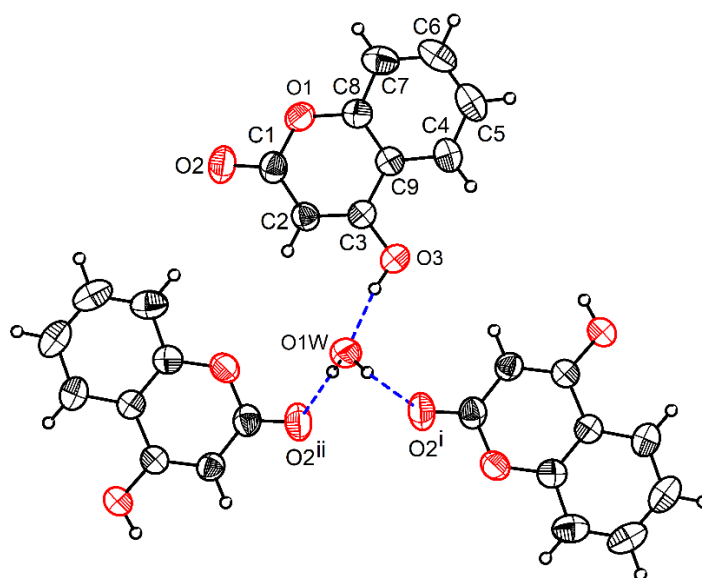
Figure 1.34: The H-bonding situation around the lattice water OW1. Each lattice water serves to link three molecules of the organic compound **20**with the aid of an intramolecular H-acceptor bond and two intermolecular H-donor bonds. Symmetry code: i) 1-x, -0.5+y, 1.5-z ii) 0.5-x, 1-y, 0.5+z.

Chapter 1

1.15. References

(1) Martins, M.; Silva, R.; M. M. Pinto, M.; Sousa, E. Marine Natural Products, Multitarget Therapy and Repurposed Agents in Alzheimer's Disease. *Pharmaceuticals* **2020**, *13*, 242. https://doi.org/10.3390/ph13090242.

(2) Gogineni, V.; Schinazi, R. F.; Hamann, M. T. Role of Marine Natural Products in the Genesis of Antiviral Agents. *Chem. Rev.* **2015**, *115*, 9655–9706. https://doi.org/10.1021/cr4006318.

(3) Jones, A.; Grkovic, T.; Sykes, M.; Avery, V. Trypanocidal Activity of Marine Natural Products. *Mar. Drugs* **2013**, *11*, 4058–4082. https://doi.org/10.3390/md11104058.

(4) Fukuda, T.; Ishibashi, F.; Iwao, M. Lamellarin Alkaloids: Isolation, Synthesis, and Biological Activity. In *Alkaloids: Chemistry and Biology*; Elsevier Inc., 2020; Vol. 83, pp 1–112. https://doi.org/10.1016/bs.alkal.2019.10.001.

(5) Piazza, V.; Roussis, V.; Garaventa, F.; Greco, G.; Smyrniotopoulos, V.; Vagias, C.; Faimali, M. Terpenes from the Red Alga Sphaerococcus Coronopifolius Inhibit the Settlement of Barnacles. *Mar. Biotechnol.* **2011**, *13*, 764–772. https://doi.org/10.1007/s10126-010-9337-4.

(6) Khan, M. T.; Kaushik, A. C.; Bhatti, A. I.; Zhang, Y.-J.; Zhang, S.; Wei, A. J.; Malik, S. I.; Wei, D. Q. Marine Natural Products and Drug Resistance in Latent Tuberculosis. *Mar. Drugs* **2019**, *17*, 549. https://doi.org/10.3390/md17100549.

(7) Venkateshwar Goud, T.; Srinivasa Reddy, N.; Raghavendra Swamy, N.; Siva Ram, T.; Venkateswarlu, Y. Anti-HIV Active Petrosins from the Marine Sponge Petrosia Similis. *Biol. Pharm. Bull.* **2003**, *26*, 1498–1501. https://doi.org/10.1248/bpb.26.1498.

(8) Bhadury, P.; Wright, P. Exploitation of Marine Algae: Biogenic Compounds for Potential Antifouling Applications. *Planta* **2004**, *219*, 561–578. https://doi.org/10.1007/s00425-004-1307-5.

(9) Vo, T.-S.; Ngo, D.-H.; Kim, S.-K. Marine Algae as a Potential Pharmaceutical Source for Anti-Allergic Therapeutics. *Process Biochem.* **2012**, *47*, 386–394. https://doi.org/10.1016/j.procbio.2011.12.014.

(10)   Lin, W.; Wang, W.; Liao, D.; Chen, D.; Zhu, P.; Cai, G.; Kiyoshi, A. Polysaccharides from *Enteromorpha Prolifera* Improve Glucose Metabolism in Diabetic Rats. *J. Diabetes Res.* **2015**, *2015*, 1–12. https://doi.org/10.1155/2015/675201.

(11)   Kumari, P.; Kumar, M.; Gupta, V.; Reddy, C. R. K.; Jha, B. Tropical Marine Macroalgae as Potential Sources of Nutritionally Important PUFAs. *Food Chem.* **2010**, *120*, 749–757. https://doi.org/10.1016/j.foodchem.2009.11.006.

(12)   Peña-Rodríguez, A.; Mawhinney, T. P.; Ricque-Marie, D.; Cruz-Suárez, L. E. Chemical Composition of Cultivated Seaweed *Ulva Clathrata* (Roth) C. Agardh. *Food Chem.* **2011**, *129*, 491–498. https://doi.org/10.1016/j.foodchem.2011.04.104.

(13)   Kuo, J.-M.; Hwang, A.; Hsu, H. H.; Pan, B. S. Preliminary Identification of Lipoxygenase in Algae (*Enteromorpha Intestinalis*) for Aroma Formation. *J. Agric. Food Chem.* **1996**, *44*, 2073–2077. https://doi.org/10.1021/jf950774c.

(14)   El-Shoubaky, G. A.; Youssef Moustafa, A. M.; Salem, E. A. E. Comparative Phytochemical Investigation of Beneficial Essential Fatty Acids on a Variety of Marine Seaweeds Algae. *Res. J. Phytochem.* **2008**, *2*, 18–26. https://doi.org/10.3923/rjphyto.2008.18.26.

(15)   Zhou, D.; Zhang, S.; Fu, H.; Chen, J. Liquefaction of Macroalgae *Enteromorpha Prolifera* in Sub-/Supercritical Alcohols: Direct Production of Ester Compounds. *Energy & Fuels* **2012**, *26*, 2342–2351. https://doi.org/10.1021/ef201966w.

(16)   Patra, J. K.; Kim, S. H.; Baek, K. H. Antioxidant and Free Radical-Scavenging Potential of Essential Oil from *Enteromorpha Linza* L. Prepared by Microwave-Assisted Hydrodistillation. *J. Food Biochem.* **2015**, *39*, 80–90. https://doi.org/10.1111/jfbc.12110.

(17)   Ray, B. Polysaccharides from *Enteromorpha Compressa*: Isolation, Purification and Structural Features. *Carbohydr. Polym.* **2006**, *66*, 408–416. https://doi.org/10.1016/j.carbpol.2006.03.027.

(18)   Cho, M.; Yang, C.; Kim, S. M.; You, S. Molecular Characterization and Biological Activities of Water-Soluble Sulfated Polysaccharides from *Enteromorpha Prolifera*.

Chapter 1

Food Sci. Biotechnol. **2010**, *19*, 525–533. https://doi.org/10.1007/s10068-010-0073-3.

(19) Guo, F.; Zhuang, X.; Han, M.; Lin, W. Polysaccharides from *Enteromorpha Prolifera* Protect against Carbon Tetrachloride-Induced Acute Liver Injury in Mice via Activation of Nrf2/HO-1 Signaling, and Suppression of Oxidative Stress, Inflammation and Apoptosis. *Food Funct.* **2020**, *11*, 4485–4498. https://doi.org/10.1039/D0FO00575D.

(20) Okai, Y.; Higashi-Okai, K. Potent Anti-Inflammatory Activity of Pheophytin A Derived from Edible Green Alga, *Enteromorpha Prolifera* (Sujiao-Nori). *Int. J. Immunopharmacol.* **1997**, *19*, 355–358. https://doi.org/10.1016/S0192-0561(97)00070-2.

(21) Agardh, J.; Okano, M.; Mizui, F.; Funaki, Y.; Aratani, T. Constituents in Marine Algae - VI. Seasonal Variation of Sterol, Hydrocarbon, Fatty Acid, and Phytol Fractions in *Enteromorpha Prolifera* (Mueller). *Bull. Japanese Soc. Sci. Fish.* **1983**, *49*, 621–626. https://doi.org/10.2331/suisan.49.621.

(22) Shanab, S. M. M.; Shalaby, E. A.; El-Fayoumy, E. A. *Enteromorpha Compressa* Exhibits Potent Antioxidant Activity. *J. Biomed. Biotechnol.* **2011**, *2011*, 1–11. https://doi.org/10.1155/2011/726405.

(23) Ogawa, A.; Kondo, K.; Murai, S.; Sonoda, N. Selenium-Assisted Carbonylation of o-Hydroxyacetophenone with Carbon Monoxide. *J. Chem. Soc. Chem. Commun.* **1982**, *2000*, 1283. https://doi.org/10.1039/c39820001283.

(24) Kasabe, A.; Mohite, V.; Ghodake, J.; Vidhate, J. Synthesis, Characterization and Primary Antimicrobial, Antifungal Activity Evaluation of Schiff Bases of 4-Chloro-(3-Substituted-Phenylimino)-Methyl-[2*H*]-Chromene-2-One. *E-Journal Chem.* **2010**, *7*, 377–382. https://doi.org/10.1155/2007/237645.

(25) Abdou, M. M.; El-Saeed, R. A.; Bondock, S. Recent Advances in 4-Hydroxycoumarin Chemistry. Part 1: Synthesis and Reactions. *Arab. J. Chem.* **2019**, *12*, 88–121. https://doi.org/10.1016/j.arabjc.2015.06.012.

(26) Traven, V. F.; Negrebetsky, V. V.; Vorobjeva, L. I.; Carberry, E. A. Keto–Enol

Tautomerism, NMR Spectra, and H–D Exchange of 4-Hydroxycoumarins. *Can. J. Chem.* **1997**, *75*, 377–383. https://doi.org/10.1139/v97-043.

(27)   Tao, R.; Wang, C.-Z.; Kong, Z.-W. Antibacterial/Antifungal Activity and Synergistic Interactions between Polyprenols and Other Lipids Isolated from Ginkgo Biloba L. Leaves. *Molecules* **2013**, *18*, 2166–2182. https://doi.org/10.3390/molecules18022166.

(28)   Nowak, R.; Drozd, M.; Mendyk, E.; Lemieszek, M.; Krakowiak, O.; Kisiel, W.; Rzeski, W.; Szewczyk, K. A New Method for the Isolation of Ergosterol and Peroxyergosterol as Active Compounds of Hygrophoropsis Aurantiaca and in Vitro Antiproliferative Activity of Isolated Ergosterol Peroxide. *Molecules* **2016**, *21*, 946. https://doi.org/10.3390/molecules21070946.

(29)   Wei, T.; Waqas, M.; Xiao, K.; Yang, B.; Luo, Y.; Luo, Q.; Zhang, J.; Wang, M.; Zhu, C.; He, T.; Lu, Z. Effective Degradation of Refractory Nitrobenzene in Water by the Natural 4-Hydroxycoumarin under Solar Illumination. *Chemosphere* **2019**, *215*, 199–205. https://doi.org/10.1016/j.chemosphere.2018.10.034.

(30)   Jung, J.-C.; Park, O.-S. Synthetic Approaches and Biological Activities of 4-Hydroxycoumarin Derivatives. *Molecules* **2009**, *14*, 4790–4803. https://doi.org/10.3390/molecules14114790.

(31)   Salinas-Jazmín, N.; de la Fuente, M.; Jaimez, R.; Pérez-Tapia, M.; Pérez-Torres, A.; Velasco-Velázquez, M. A. Antimetastatic, Antineoplastic, and Toxic Effects of 4-Hydroxycoumarin in a Preclinical Mouse Melanoma Model. *Cancer Chemother. Pharmacol.* **2010**, *65*, 931–940. https://doi.org/10.1007/s00280-009-1100-z.

(32)   Lin, Y.; Shen, X.; Yuan, Q.; Yan, Y. Microbial Biosynthesis of the Anticoagulant Precursor 4-Hydroxycoumarin. *Nat. Commun.* **2013**, *4*, 2603. https://doi.org/10.1038/ncomms3603.

(33)   Anees A. Pangal, Javed A. Shaikh, E. M. K. Current Developments of C3-Substituted Coumarin Hybrids as Anti-Cancer Agents. *Int. J. Phram. Sci. Rev. Res.* **2017**, *42*, 161–168.

(34)   Asthana, S.; Zucca, P.; Vargiu, A. V.; Sanjust, E.; Ruggerone, P.; Rescigno, A.

Structure–Activity Relationship Study of Hydroxycoumarins and Mushroom Tyrosinase. *J. Agric. Food Chem.* **2015**, *63*, 7236–7244. https://doi.org/10.1021/acs.jafc.5b02636.

(35) Bourgaud, F.; Hehn, A.; Larbat, R.; Doerper, S.; Gontier, E.; Kellner, S.; Matern, U. Biosynthesis of Coumarins in Plants: A Major Pathway Still to Be Unravelled for Cytochrome P450 Enzymes. *Phytochem. Rev.* **2006**, *5*, 293–308. https://doi.org/10.1007/s11101-006-9040-2.

(36) Mercer, E. I. The Biosynthesis of Ergosterol. *Pestic. Sci.* **1984**, *15*, 133–155. https://doi.org/10.1002/ps.2780150206.

(37) Brumfield, K. M.; Laborde, S. M.; Moroney, J. V. A Model for the Ergosterol Biosynthetic Pathway in *Chlamydomonas Reinhardtii*. *Eur. J. Phycol.* **2017**, *52*, 64–74. https://doi.org/10.1080/09670262.2016.1225318.

(38) Weete, J. D. Sterols of the Fungi: Distribution and Biosynthesis. *Phytochemistry* **1973**, *12*, 1843–1864. https://doi.org/10.1016/S0031-9422(00)91502-4.

(39) Da Graça Sgarbi, D. B.; Da Silva, A. J. R.; Carlos, I. Z.; Silva, C. L.; Angluster, J.; Alviano, C. S. Isolation of Ergosterol Peroxide and Its Reversion to Ergosterol in the Pathogenic Fungus *Sporothrix Schenckii*. *Mycopathologia* **1997**, *139*, 9–14. https://doi.org/10.1023/a:1006803832164.

(40) Luo, X.; Su, P.; Zhang, W. Advances in Microalgae-Derived Phytosterols for Functional Food and Pharmaceutical Applications. *Mar. Drugs* **2015**, *13*, 4231–4254. https://doi.org/10.3390/md13074231.

(41) Lin, Y.; Wen, B.; Zhang, Z.; Cai, J. Ergosterol Peroxide: An Effect-Directed Detecting Method from Anoectochilus Elwesii and Evaluation of Anticancer Activity. *Nat. Prod. Res.* **2021**, 1–6. https://doi.org/10.1080/14786419.2021.1949593.

(42) Kim, D. S.; Baek, N.-I.; Oh, S. R.; Jung, K. Y.; Lee, I. S.; Kim, J. H.; Lee, H.-K. Anticomplementary Activity of Ergosterol Peroxide from Naematoloma Fasciculare and Reassignment of NMR Data. *Arch. Pharm. Res.* **1997**, *20*, 201–205. https://doi.org/10.1007/BF02976145.

(43)   Yang, B.; Miller, P. A.; Möllmann, U.; Miller, M. J. Syntheses and Biological Activity Studies of Novel Sterol Analogs from Nitroso Diels−Alder Reactions of Ergosterol. *Org. Lett.* **2009**, *11*, 2828–2831. https://doi.org/10.1021/ol900997t.

(44)   Lin, M.; Li, H.; Zhao, Y.; Cai, E.; Zhu, H.; Gao, Y.; Liu, S.; Yang, H.; Zhang, L.; Tang, G. 2-Naphthoic Acid Ergosterol Ester, an Ergosterol Derivative, Exhibits Anti-Tumor Activity by Promoting Apoptosis and Inhibiting Angiogenesis. *Steroids* **2017**, *122*, 9–15. https://doi.org/10.1016/j.steroids.2017.03.007.

(45)   Prompiboon, P.; Bhumiratana, A.; Ruchirawat, S.; Boucias, D. G.; Wiwat, C. Isolation of Ergosterol Peroxide from Nomuraea Rileyi Infected Larvae of Tobacco Cutworm. *World J. Microbiol. Biotechnol.* **2008**, *24*, 2909–2917. https://doi.org/10.1007/s11274-008-9830-3.

(46)   Wu, H.-Y.; Yang, F.-L.; Li, L.-H.; Rao, Y. K.; Ju, T.-C.; Wong, W.-T.; Hsieh, C.-Y.; Pivkin, M. V.; Hua, K.-F.; Wu, S.-H. Ergosterol Peroxide from Marine Fungus Phoma Sp. Induces ROS-Dependent Apoptosis and Autophagy in Human Lung Adenocarcinoma Cells. *Sci. Rep.* **2018**, *8*, 17956. https://doi.org/10.1038/s41598-018-36411-2.

(47)   Taofiq, O.; Heleno, S. A.; Calhelha, R. C.; Fernandes, I. P.; Alves, M. J.; Barros, L.; González-Paramás, A. M.; Ferreira, I. C. F. R.; Barreiro, M. F. Phenolic Acids, Cinnamic Acid, and Ergosterol as Cosmeceutical Ingredients: Stabilization by Microencapsulation to Ensure Sustained Bioactivity. *Microchem. J.* **2019**, *147*, 469–477. https://doi.org/10.1016/j.microc.2019.03.059.

(48)   Mukaiyama, T.; Tsujimura, N.; Otaka, S.; Kosaka, Y.; Hata, K.; Hori, K.; Kenji, S. *Animal Cell Technology: Basic & Applied Aspects*; Shirahata, S., Ikura, K., Nagao, M., Ichikawa, A., Teruya, K., Eds.; Springer Netherlands: Dordrecht, 2008. https://doi.org/10.1007/978-1-4020-9646-4.

(49)   Faulkner, D. J. Marine Natural Products. *Nat. Prod. Rep.* **2002**, *19*, 1–48. https://doi.org/10.1039/b009029h.

(50)   Kumar, M. S.; Adki, K. M. Marine Natural Products for Multi-Targeted Cancer

Treatment: A Future Insight. *Biomed. Pharmacother* **2018**, *105*, 233–245. https://doi.org/10.1016/j.biopha.2018.05.142.

(51) Khan, M. T.; Kaushik, A. C.; Bhatti, A. I.; Zhang, Y.-J.; Zhang, S.; Wei, A. J.; Malik, S. I.; Wei, D. Q. Marine Natural Products and Drug Resistance in Latent Tuberculosis. *Mar. Drugs* **2019**, *17*, 549. https://doi.org/10.3390/md17100549.

(52) Rodríguez, J.; Nuñez, L.; Peixinho, S.; Jiménez, C. Isolation and Synthesis of the First Natural 6-Hydroximino 4-En-3-One- Steroids from the Sponges *Cinachyrella* Spp. *Tetrahedron Lett.* **1997**, *38*, 1833–1836. https://doi.org/10.1016/S0040-4039(97)00163-9.

(53) Lakshmi, V.; Raghubir, R.; Gupta, P. New Ceramides from the Sponge *Cinachyra Cavernosa*. *J. Asian Nat. Prod. Res.* **2008**, *10*, 747–751. https://doi.org/10.1080/10286020802030892.

(54) Wahidullah, S.; Naik, B. G.; Al-Fadhli, A. A. Chemotaxonomic Study of the Demosponge *Cinachyrella Cavernosa* (Lamarck). *Biochem. Syst. Ecol.* **2015**, *58*, 91–96. https://doi.org/10.1016/j.bse.2014.11.001.

(55) Barnathan, G.; Mirallès, J.; Gaydou, E. M.; Boury-Esnault, N.; Kornprobst, J.-M. New Phospholipid Fatty Acids from the Marine Sponge *Cinachyrella Alloclada* Uliczka. *Lipids* **1992**, *27*, 779–784. https://doi.org/10.1007/BF02535849.

(56) Barnathan, G.; Genin, E.; Velosaotsy, N. E.; Kornprobst, J.-M.; Al-Lihaibi, S.; Al-Sofyani, A.; Nongonierma, R. Phospholipid Fatty Acids and Sterols of Two *Cinachyrella Sponges* from the Saudi Arabian Red Sea: Comparison with *Cinachyrella* Species from Other Origins. *Comp. Biochem. Physiol. Part B Biochem. Mol. Biol.* **2003**, *135*, 297–308. https://doi.org/10.1016/S1096-4959(03)00085-X.

(57) Cardellina, J. H.; Graden, C. J.; Greer, B. J.; Kern, J. R. 17Z-Tetracosenyl 1-Glycerol Ether from the Sponges*Cinachyra Alloclada* And*Ulosa Ruetzleri*. *Lipids* **1983**, *18*, 107–110. https://doi.org/10.1007/BF02536103.

(58) Fusetani, N.; Shinoda, K.; Matsunaga, S. Bioactive Marine Metabolites. 48. Cinachyrolide A: A Potent Cytotoxic Macrolide Possessing Two Spiro Ketals from

Marine Sponge *Cinachyra* Sp. *J. Am. Chem. Soc.* **1993**, *115*, 3977–3981. https://doi.org/10.1021/ja00063a017.

(59)   Shimogawa, H.; Kuribayashi, S.; Teruya, T.; Suenaga, K.; Kigoshi, H. Cinachyramine, the Novel Alkaloid Possessing a Hydrazone and Two Aminals from *Cinachyrella* Sp. *Tetrahedron Lett.* **2006**, *47*, 1409–1411. https://doi.org/10.1016/j.tetlet.2005.12.087.

(60)   Aiello, A.; Fattorusso, E.; Magno, S.; Menna, M.; Pansini, M. Steroids of the Marine Sponge Cinachyra Tarentina: Isolation of Cholest-4-ene-3,6-dione and (24*R*)-24-ethylcholest-4-ene-3,6-dione. *J. Nat. Prod.* **1991**, *54*, 281–285. https://doi.org/10.1021/np50073a035.

(61)   Mishra, P. D.; Wahidullah, S.; D'souza, L. D.; Kamat, S. Y. Steroids from Marine Sponges Suberites Vestigium and Chrotella Australiensis. 1997, pp 719–721.

(62)   Quijano, L.; Cruz, F.; Navarrete, I.; Gómez, P.; Rios, T. Alkyl Glycerol Monoethers in the Marine Sponge*Desmapsamma Anchorata*. *Lipids* **1994**, *29*, 731–734. https://doi.org/10.1007/BF02538919.

(63)   Buchanan, H. J.; Cox, P. J.; Doidge-Harrison, S. M. S. V.; Howie, R. A.; Jaspars, M.; Wardell, J. L. Syntheses and Structures of 3-Stannylcholest-5-ene Species. *J. Chem. Soc. Perkin Trans. 1* **1997**, *623*, 3657–3664. https://doi.org/10.1039/a703596i.

(64)   Sawan, S. .; James, T. .; Gruenke, L. .; Craig, J. . Proton NMR Assignments for Cholesterol. Use of Deuterium NMR as an Assignment Aid. *J. Magn. Reson.* **1979**, *35*, 409–413. https://doi.org/10.1016/0022-2364(79)90063-5.

(65)   Albuquerque, H.; Santos, C.; Silva, A. Cholesterol-Based Compounds: Recent Advances in Synthesis and Applications. *Molecules* **2018**, *24*, 116. https://doi.org/10.3390/molecules24010116.

(66)   Toh Choon, R. L.; Sariah, M.; Siti Mariam, M. N. Ergosterol from the Soilborne Fungus Ganoderma Boninense. *J. Basic Microbiol.* **2012**, *52*, 608–612. https://doi.org/10.1002/jobm.201100308.

(67)   Ko, H.-H.; Chang, W.-L.; Lu, T.-M. Antityrosinase and Antioxidant Effects of Ent-Kaurane Diterpenes from Leaves of Broussonetia Papyrifera. *J. Nat. Prod.* **2008**, *71*, 1930–1933. https://doi.org/10.1021/np800564z.

Chapter 2

Chemical transformation of natural elemol to elemoxide and investigation of tyrosinase inhibition studies

2.1. Introduction

Over the years, natural product research has provided a wealth of compounds with wide applications in health science, medicine, pharmacy, biology, etc.[1] Though bioactive natural products serve as good lead compounds for the discovery of new drugs, most of them suffer from many shortcomings, such as complex structures, poor stability, solubility, etc. Therefore, chemical transformation of natural products is required to develop novel compounds with better physico-chemical, biochemical and pharmacokinetic properties, potency and selectivity.[1,2] For this purpose, generally, four synthetic approaches are applied (i) target-oriented synthesis (TOS);[3,4] (ii) diversity-oriented synthesis (DOS);[5] (iii) biology-oriented synthesis (BIOS);[6] and (iv) functional-oriented synthesis (FOS).[7]

Elemane, **1**   Elemol, **2**   Elemoxide, **3**

8-Hydroxyelemol, **4**   Phytuberin, **5**   R= Arabinose fucoside B, **6**
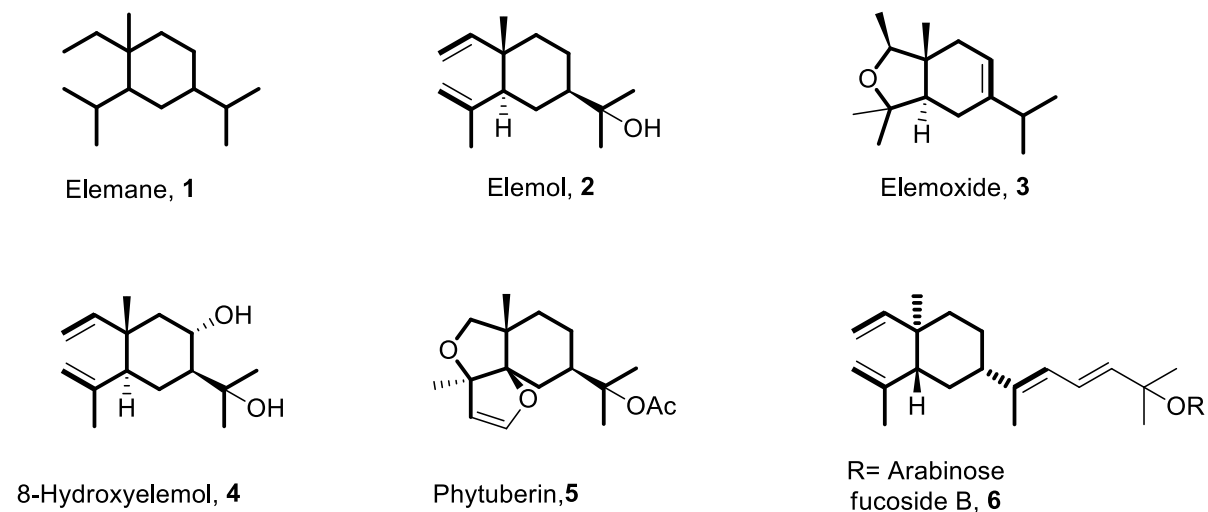
Figure 2.1: Bio-active compounds comprising of elemane scaffold.

Elemol **2** is an elemane **1** based sesquiterpene, which was isolated from *Manila elemi* oil and *Java Citronella* oil (Figure 2.1).[8,9] Several biologically active natural products such as; 8-hydroxyelemol **4** (an antifungal agent);[10] phytuberin **5** (an antifungal agent),[11] fuscoside B **6** (an anti-inflammatory agent and a leukotriene biosynthetic inhibitor) are also made up of elemane skeleton, some of which can be synthesized starting from elemol **2**.[12,13] Over the years, elemol **2** has been a model system for testing the methodologies in synthetic organic chemistry,

because of its easy availability.[8,11] Elemoxide **3**, a sesquiterpene oxide, also bears elemane **1** skeleton and is known to possess a pleasant odour hence, can be a perfumery agent.[9]

In the present study, we targeted the synthesis of elemoxide **3** from natural elemol **2** and investigation of their tyrosinase enzyme inhibition (Figure 2.2).

(-)-Elemol, **2**   (-)-Elemoxide, **3**
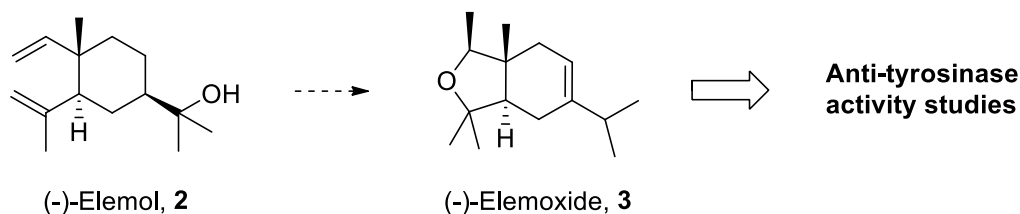
Figure 2.2: Outline of the present work.

Section A: Synthesis of (-)-elemoxide from commercially available natural elemol

2.2. Introduction

Fragrance or aroma compounds, traditionally used as perfumery, are volatile organic compounds of low molecular weight containing either aliphatic or aromatic structures found in flowers, plants, and trees. These odorant molecules are having direct application as flavouring and perfumery agents in the food and cosmetic industries. Therefore, there is a huge demand to explore fragrance chemistry through the design and synthesis of new odorants.[14] Elemoxide **3** possesses a pleasant odour which is a fusion of rhubarb, laurel, thyme and florex having commercial importance.[15] In search of novel compounds with fascinating medicinal properties we undertook the synthesis of elemoxide **3**, having a typical sesquiterpene skeleton and consisting of three chiral centres.

2.3. Objectives

1. To design and develop an efficient and facile route for the synthesis of (-)-elemoxide **3**
2. To provide experimental evidence of the mechanism of the transformation of (-)-elemol **2** to (-)-elemoxide **3**.

2.4. Literature review on the synthesis of elemoxide

The only report on elemoxide **3** appeared in 2006, by Wahidulla, S. *et al.* where dehydration and re-arrangement of (-)-elemol **2** with glacial acetic acid and perchloric acid produced a

complex mixture of compounds (elemoxide **3**, *β*-cyperone **7**, *α*-elemene **8**, *δ*-elemene **9**) and out of which elemoxide **3** was found in 8% yield only (Scheme 2.1).[15]
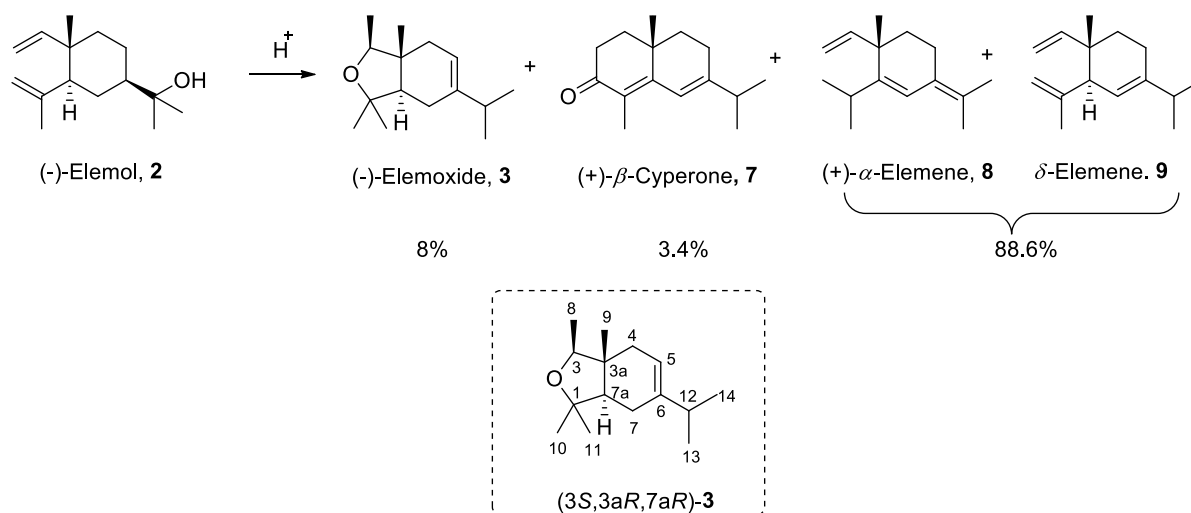
Scheme 2.1: Wahidulla's dehydration and re-arrangement reactions of elemol **2**.

"In 2016, Wahidulla, S. *et al.* demonstrated complete structural elucidation of elemoxide **3** using IR, EI-MS and extensive NMR spectroscopic techniques which included ¹H NMR, ¹³C NMR, ¹H-¹H COSY, ¹H-¹³C HSQC and HMBC.". The relative configuration of elemoxide **3** was assigned based on NOESY and NOE spectra. The absolute configuration of elemoxide **3** was established as (3*S*,3a*R*,7a*R*)-**3** based on its formation from elemol **2** (the absolute configuration of which is known) (Scheme 2.1). Wahidulla, S. *et al.* also proposed a plausible mechanistic pathway for the formation of elemoxide **3** from elemol **2**.

Scope of the present study

We thought to overcome the drawbacks of complex mixture formation in the transformation of elemol **2** to elemoxide **3** (by Wahidulla, S. *et al.*[15]) by designing and developing an efficient synthetic route for the synthesis of elemoxide **3**. The synthetic strategies are discussed in this section.

2.5. Results and discussion

Elemoxide **3** has a fascinating scaffold consisting of a tetrahydrofuran ring fused to a cyclohexene ring and has three chiral centres. Retrosynthetic analysis of elemoxide **3** starting from (-)-elemol **2** is depicted in scheme 2.2.
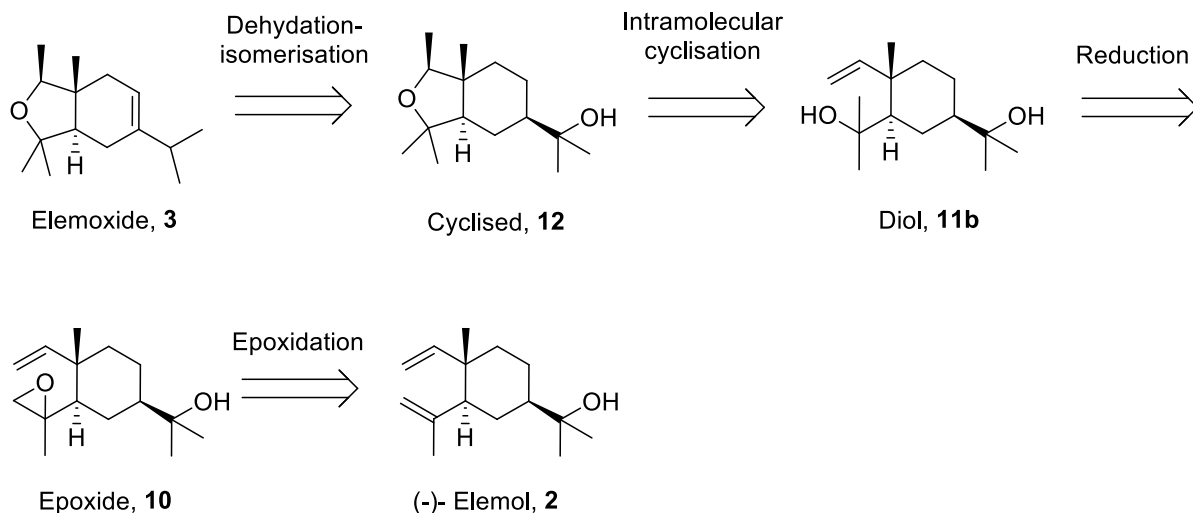
Scheme 2.2: Retrosynthesis of elemoxide **3**.

Elemoxide **3** could be obtained by dehydration-isomerisation of cyclised **12**. Cyclised **12** could be acquired by intramolecular cyclisation of diol **11b**. Diol **11b** could be in turn obtained by the reductive opening of epoxide **10**. Epoxide **10** could be achieved from commercially available (-)-elemol **2** by epoxidation reaction (Scheme 2.2).
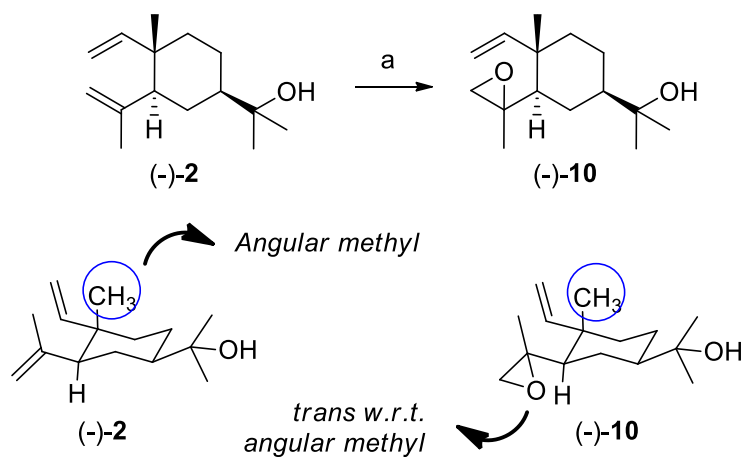
Reagents and conditions: (a) *m*-CPBA (1.20 equiv), CH$_2$Cl$_2$, 0°C (2h) then rt (1h), 80%

Scheme 2.3: Synthesis of epoxide **10**.

Epoxide **10** could be synthesised from commercially available (-)-elemol **2** via regioselective oxidation of the double bond (Scheme 2.3). It has been well documented in the literature that the regioselectivity of the epoxidation of diene is controlled by electronic factors, as with

peracid oxidants,[16] or by a directing group, as with Sharpless epoxidation. In the synthesis of liphagal,[17] Manzaneda *et al.* demonstrated the chemoselectivity of *m*-CPBA to oxidize the more hindered but also the more electron-rich alkene, regardless of the steric hindrance.[18] Pleasingly, oxidation of elemol **2** with *m*-CPBA at 0°C in CH_2Cl_2 was found to be chemoselective producing requisite epoxide **10** in 80% yield. The IR bands 1383, 1175, 910 cm^{-1} shows the presence of epoxide ring and the band 3363 cm^{-1} shows the presence of hydroxyl moiety. The NMR of epoxide **10** showed the presence of an epoxy ring by displaying signals at δH 2.68-2.58 (d, $J = 4.6$ Hz, 1H), 2.67 (dd, $J = 4.6$ Hz, $J = 0.6$ Hz, 1H); δC 53.2, δC 58.2 (a quaternary carbon confirmed by DEPT). In addition, the ^{1}H NMR of epoxide **10** showed the presence of monosubstituted alkene (-CH=CH$_2$) signals at δH 4.95 (dd, $J = 10.8$ Hz, $J = 1.2$ Hz, 1H), 4.99 (dd, $J = 17.5$ Hz, $J = 1.2$ Hz, 1H), 5.77 (dd, $J = 17.5$ Hz, $J = 10.8$ Hz, 1H). Thus, confirming the monoepoxidation of the elemol to give epoxide **10**. The stereochemistry of epoxy ring of **10** was not of consequence in the further manipulation and was assumed to be *trans* (to the angular methyl group) based on ^{1}H NMR shift (Scheme 2.3).

The reductive ring opening of epoxides, especially in enantiopure form, to the corresponding alcohols is a powerful tool in synthetic organic chemistry.[19] Reductive cleavage of oxiranes can be performed in the presence of various dissolving metals, and metal hydrides.[20] LiAlH$_4$ is commonly used in epoxide reductive ring opening.[21] The reaction and regioselectivity of the product depend highly on the substitution of the epoxide ring carbons. Generally, the opening of the epoxy ring occurs at the less substituted carbon. However, when the reaction of epoxide **10** was carried out using LiAlH$_4$ (~0.06 M in anhyd THF) gave reverse selectivity i.e. primary alcohol **11a** as the major product (Scheme 2.4).
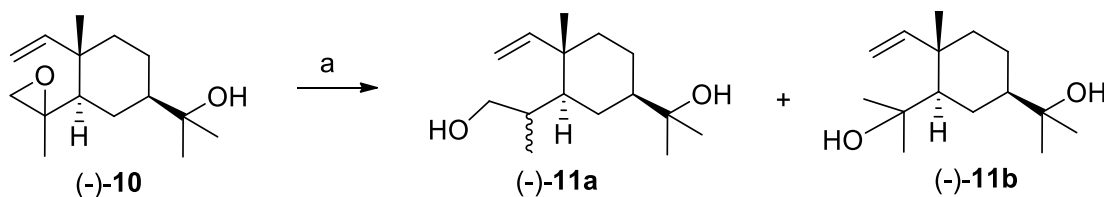
Reagents and conditions: (a) **10** (0.84 mmol), LiAlH$_4$ (~0.06 M in anhyd THF, 1.50 equiv), 0°C-rt, 82% of **11a** or **10** (4.20 mmol), LiAlH$_4$ (~0.9 M in anhyd THF, 1.50 equiv), 0°C-rt, 83% of **11b**

Scheme 2.4: Synthesis of diol **11a** and **11b**.

Table 2.1: Reductive ring opening of epoxide **10** by varying concentration of LiAlH$_4$ in anhyd THF.

Sr. No	Concentration of LiAlH$_4$ in anhyd THF (M)	Yield of **11a** (%)	Yield of **11b** (%)
1	~0.1	82	-
2	~0.3	80	-
3	~0.5	73	Minor quantity (detected on TLC)
4	~0.9	10	83

IR spectrum of **11a** displayed a hydroxyl band at 3447 cm^{-1}. Even though the NMR of **11a** witnesses the disappearance of the peaks corresponding to the epoxy ring at δH 2.68-2.58 (d, J = 4.6 Hz, 1H), 2.67 (dd, J = 4.6 Hz, J = 0.6 Hz, 1H) & δC 53.20, but its ^{1}H NMR spectrum doesn't indicate the appearance of the tertiary alcohol moiety (-C(CH$_3$)$_2$OH) expected in the diol **11b**. Further, the NMR of **11a** displayed signal corresponding to the methylene protons (>CH$_2$) at δH 3.91 (dt, J = 14.1 Hz, J = 1.3 Hz, 1H), 3.99 (dt, J = 14.1 Hz, J = 1.2 Hz, 1H) and δC 66.47 (confirmed by DEPT) confirming the formation of primary alcohol **11a**. Repetition of the reaction by changing the temperature of the reaction gave similar results. Interestingly, we found that the solvent volume used in the reaction could lead to the expected regioselectivity. We then repeated the reaction with ~0.1, ~0.3 M and ~0.5 M LiAlH$_4$ in anhyd THF. We still observed similar results (Table 2.1). However, the formation of some amount of **11b** (detected on TLC) was observed when ~0.5 M LiAlH$_4$ concentration was employed. Diol **11b** was obtained as the major product (83% yield) with ~0.9 M LiAlH$_4$ solution in anhyd THF. The IR spectrum of diol **11b** displayed hydroxyl bands at 3364, 3080 cm^{-1}. ^{1}H NMR of diol **11b** showed the presence of four methyl (-CH$_3$) peaks at δH 1.11 (s, 6H), 1.14 (s, 6H). These methyl (-CH$_3$) peaks were attributed to the methyls of tertiary alcohol moieties (-C(-CH$_3$)$_2$OH) of diol **11b**. The NMR of diol **11b** did not show the presence of epoxide signals. Thus, confirming the formation of diol **11b** from epoxide **10**.

Chapter 2

The reduction of an unsymmetrical epoxide with $LiAlH_4$ occurs at the less substituted carbon producing more substituted alcohol. However, it is known in the literature that with 'mixed hydrides' obtained by mixing $LiAlH_4$ & $AlCl_3$ in the 3: 1 ratio, the reduction occurred at more substituted carbon of an unsymmetrical epoxide producing less substituted alcohol.[22] Also, organoaluminium reagents such as diisobutylaluminium 2,6-di-*tert*-butyl-4 methylphenoxide and diisobutylaluminium 4-bromo-2,6-di-*tert*-butylphenoxide produces less substituted alcohols from functionalized epoxides.[23]

A
Solvent separated ion pair

B
Contact ion pair
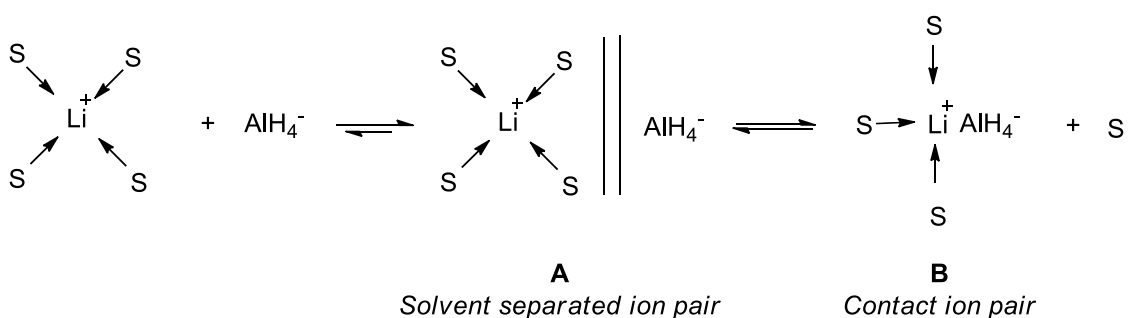
Scheme 2.5: Representation of the existence of $LiAlH_4$ in ethereal solvents. S = solvent molecule.

$LiAlH_4$ in tetrahydrofuran (or any ethereal solvent) can be present as free ions, solvent separated ions (**A**) or contact ion pair (**B**) in dilute solutions (0.1 M - 0.00001 M) and triple ions in more concentrated solution (>1M) at ambient temperatures (Scheme 2.5).[24,25] The coordination number of lithium in contact ion pair (**B**) is 3. $LiAlH_4$ dissociates considerably, as more solvent molecules tend to get closer to lithium cation and lithium coordination number 4 was seen.[24,25]

a) Dissociative pathway: LiAlH₄ (~0.06 M in anhyd THF)
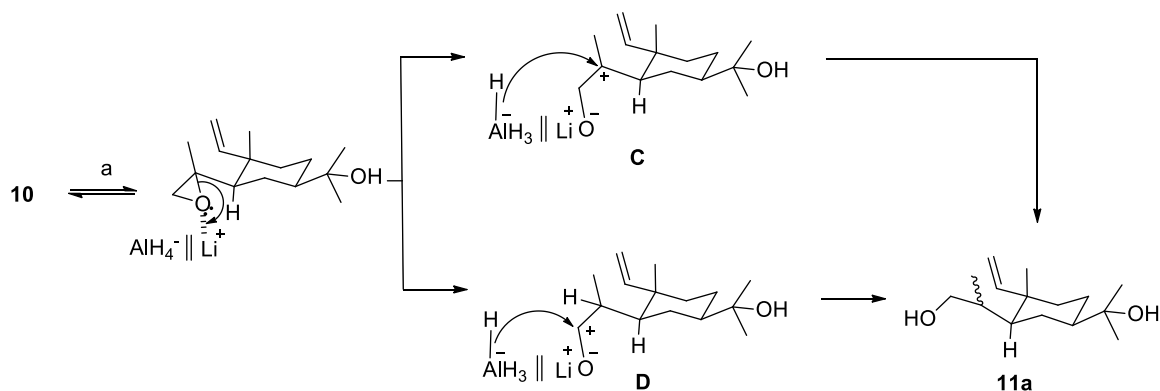
b) Concerted pathway: LiAlH₄ (~0.9 M in anhyd THF)
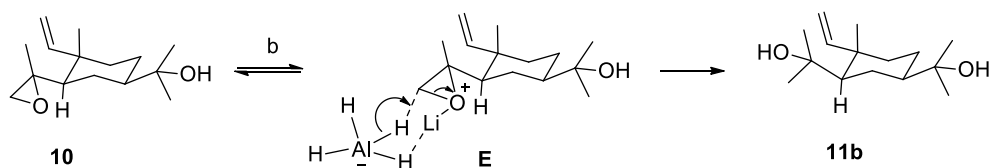
Scheme 2.6: Rationalisation of the formation of diols **11a** and **11b**. a) Possible dissociative pathway leading to the formation of **11a** in diluted solution (~0.06 M LiAlH₄ in anhyd THF) (b) Possible concerted pathway leading to the formation of **11b** in comparatively concentrated solution (~0.9 M LiAlH₄ in anhyd THF).

Based on prior elegant work of reductions involving LiAlH₄[22,24,25] we rationalized the formation of diols **11a** and **11b** via two possible mechanistic pathways: dissociative and concerted mechanism (Scheme 2.6).[25] In diluted solution, LiAlH₄ can dissociate considerably and the reduction can undergo a dissociative mechanism pathway (Scheme 2.6a). In this pathway, the epoxide oxygen can be activated by solvated lithium cation. The complexation of lithium to epoxide oxygen polarizes the carbon-oxygen bond involving ring-opening of the epoxide to form predominantly the more stable carbonium ion. This is followed by either direct reduction by AlH₄⁻ (Scheme 2.6a, **C**) or hydride migration and subsequent reduction by AlH₄⁻ (Scheme 2.6a, **D**) providing diol **11a**. A similar pathway was observed in the reduction of unsymmetrical epoxides with mixed hydride reagents.[22] In comparatively concentrated solution, a concerted mechanism might occur via a six membered cyclic transition state (Scheme 2.6b, **E**) which leads to the formation of **11b** (Scheme 2.6b).
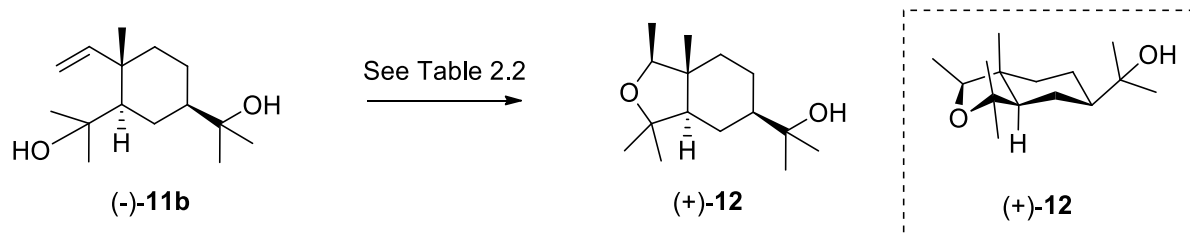
Scheme 2.7: Synthesis of cyclized product **12**.

Table 2.2: Optimisation of cyclisation step for the synthesis of **12**.

Sr. No.	Reagents and conditions	Yield (%)
1	Hg(OAc)$_2$, anhyd THF, reflux, 24h; NaBH$_4$, NaOH[26]	31
2	Hg(OAc)$_2$, anhyd THF, Cs$_2$CO$_3$, reflux, 24h; NaBH$_4$, NaOH	55
3	I$_2$ (10 mol %), PhSiH$_3$ (20 mol %), CH$_2$Cl$_2$, rt, 1h[27]	70
4	5 mol % PdCl$_2$(PPh$_3$), CuCl, O$_2$ balloon, DCE, rt.,48h[28]	Complex mixture
5	1 mol % RuCl$_2$(p-cymene)$_2$, CuOAc, DCE, reflux, 48h[29]	Complex mixture
6	2.00 equiv KO^{t}Bu, 2.00 equiv n-BuLi, hexane, 0°C-rt, 24h[30]	Complex mixture

After successfully yielding the diol **11b**, our efforts were focused on the construction of a bicyclic skeleton of elemoxide through intramolecular cyclization methods (Scheme 2.7). After a brief survey of reaction conditions, we found that the intramolecular oxymercuration followed by demercuration of diol **11b** shall provide us with the required product **12**. Hence, diol **11b** was subjected to oxymercuration reaction under anhydrous condition wherein mercurial intermediate was generated in situ, which on reduction using standard conditions (NaBH$_4$ in the presence of aqueous NaOH in THF)[26] afforded the desired cyclized product **12** along with unreacted starting material (Table 2.2). Low conversion yields (31%) were obtained using standard mercuration condition. The reason attributed to this low conversion could be the less nucleophilicity of the hydroxyl group of diol **11b**. In the next attempt, the yield of intramolecular cyclization was improved (55%) by employing a modified condition using a stoichiometric amount of Cs$_2$CO$_3$ during the oxymercuration step. Additionally, to increase the efficiency of constructing the cyclic ether skeleton of elemoxide, various reagents such as PdCl$_2$(PPh$_3$)$_2$/CuCl,[31,32] RuCl$_2$(p-cymene)$_2$/CuOAc[29,33] and KO^{t}Bu/n-BuLi[34,35] were attempted

without any success (Table 2.2). In 2015, M. Shibuya and co-workers demonstrated the applicability of the silane-iodine catalytic system for the intramolecular hydroalkoxylation of unactivated alkenes.[27] Using the same strategy, we treated diol **11b** with I_2 and $PhSiH_3$ in CH_2Cl_2 to deliver the expected cyclised product **12** in 70% yield. IR of cyclised alcohol **12** displayed a band at 3420 cm^{-1} due to the presence of the hydroxyl group. The disappearance of the NMR peaks corresponding to the olefin (-CH=CH$_2$) δH 4.88 (dd, J = 10.4 Hz, J = 1.1 Hz, 1H), 4.96 (dd, J = 17.7 Hz, J = 1.1 Hz, 1H), 6.00 (dd, J = 17.6 Hz, 10.8 Hz, 1H), & δC 109.5, 153.0 and the appearance of the newly generated methyl (-CH$_3$) peak δH 1.04 (d, J = 6.4 Hz, 3H); δC 13.0 along with the methine (-CH-) signal δH 3.42 (q, J = 6.4 Hz, 1H); δC 77.8 confirmed the conversion of diol **11b** to the cyclised alcohol **12**. It is rationalized that cyclized product **12** attains envelop-chair conformation with the newly generated methyl group (in the cyclic ether skeleton) arranging itself above the plane (Scheme 2.7).[36,37]

(+)-**12**   (-)-**3**
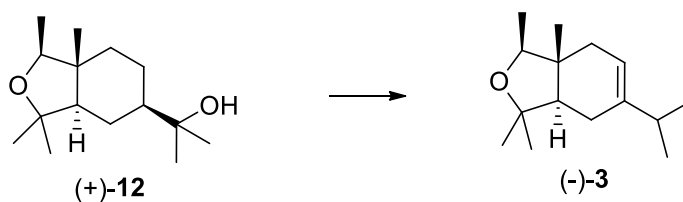
Reagents and conditions: CH$_3$COOH/HClO$_4$, rt, 72h, 70%

Scheme 2.8: Synthesis of elemoxide **3**.

To this end, we subjected cyclised product **12** to dehydration and double-bond isomerization using acetic acid/perchloric acid conditions (Scheme 2.8).[15] This reaction yielded 70% elemoxide **3**. The appearance of the NMR signals corresponding to the internal tri-substituted olefin (>C=CH-) signals at δH 5.29 (t, J = 4.4, 1H); δC 116.7, 142.3 (quaternary signal, confirmed by DEPT) confirms the formation of elemoxide **3**. The LCMS (ESI, positive) m/z calculated for $C_{15}H_{26}O$ [M + H]$^+$ 223.20, found 223.24, further confirms the formation of elemoxide **3**. This completed the efficient synthesis of elemoxide **3** a fragrant compound in 4 steps in 32% overall yield.

A) Wahidulla's hypothesis in the conversion of elemol **2** to elemoxide **3**

(-)-Elemol, **2**   **Diol**   (-)-Elemoxide, **3**
                Proposed intermediate   8%
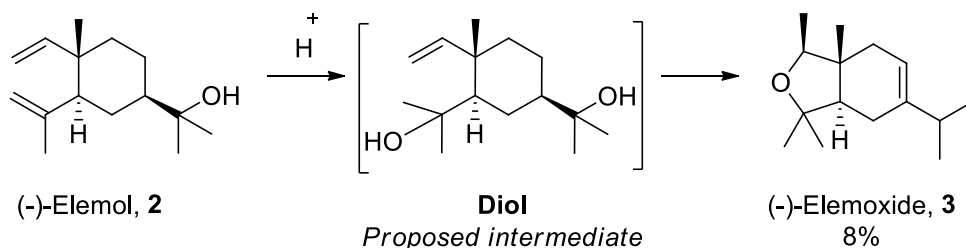
B) Present work: Experimnetal proof for Wahidulla's hypothesis

(-)-Diol, **11b**   (-)-Elemoxide, **3**   (+)-α-Elemene, **8**
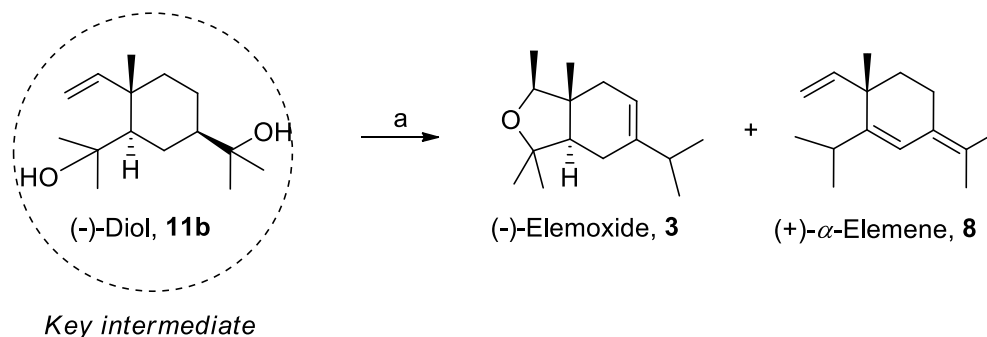
Key intermediate

Reagents and conditions: (a) $CH_3COOH/HClO_4$, rt, 48h, 26% of elemoxide **3** & 47% of α-elemene **8**

Scheme 2.9: Conversion of the key intermediate diol **11b** to elemoxide **3** (one step protocol). A) Wahidulla's hypothesis in the conversion of elemol **2** to elemoxide **3**. B) Experimental proof for the Wahidulla's hypothesis in the present work.

Wahidulla *et al.* hypothesised that the diol is one of the intermediate products in the conversion of elemol **2** to elemoxide **3** (Scheme 2.9A).[15] We subjected the synthesized diol **11b** to acetic acid/perchloric acid condition. This experiment yielded 26% elemoxide **3** along with 47% of natural product α-elemene **8** (Scheme 2.9B). The NMR peaks corresponding to the three double bonds i.e a monosubstituted olefin (-CH=CH$_2$) at δH 4.89 (dd, J = 17.4 Hz, J = 1.6 Hz, 1H), 4.94 (dd, J = 10.4 Hz, J = 1.6 Hz, 1H) & 5.69 (dd, J = 17.2 Hz, J = 10.4 Hz, 1H); δC 112.4, 146.1, a tri-substituted endocyclic double (-CH=CH-) bond at δH 6.29 (s, 1H); δC 119.5, 149.6 and a tera-substituted exocyclic double bond (>C=C<) δC 124.5, 127.9 confirms the formation of α-elemene **8**. Consequently, our experiment gives experimental proof for the previously proposed mechanism for the formation of elemoxide **3** from elemol **2** (Scheme 2.9). Thus, diol **11b** served as the key intermediate in the conversion of elemol **2** to elemoxide **3**.
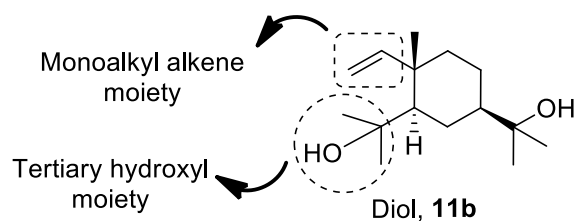
Figure 2.3: Structure of diol **11b**.

To rationalize the formation of elemoxide **3** (as a minor product) and α-elemene **8** (as the major product) from diol **11b** we will have to look at the structure of diol (Figure 2.3). The intramolecular hydroxyl attack on monoalkyl (-CH=CH$_2$) and 1,2-dialkyl (-CH=CH-) substituted alkenes is a difficult challenge compared with phenyl (-C$_6$H$_5$), trialky (>CH=C-) and 1,1-dialkyl (>C=CH$_2$) substituted alkenes due to the difficulty in the electrophilic activation.[27] As evident from the synthesis of cyclized **12** (Scheme 2.7, Table 2.2), facile intramolecular hydroxyl attack on the monoalkyl alkene of diol **11b** occurred after the activation of monoalkyl alkene and hydroxyl by reagent systems such as Hg(OAc)$_2$/Cs$_2$CO$_3$ and PhSiH$_3$/I$_2$. Owing to the difficulty of the electrophilic activation of monoalkyl alkene explains the formation of elemoxide **3** as the minor product from diol **11b**. On the other hand, acids are good dehydrating agents because they have a high affinity to water and therefore absorbs water rapidly. Further, it is reported in the literature that mixture of acids such as perchloric acid/acetic acid is an efficient acid system for dehydration and isomerization reaction because it induces little or negligible quantity of polymerization of alkene.[38] This explains the formation of α-elemene **8** as the major product from diol **11b**.

2.6. Conclusion

1. An efficient and facile synthetic route for the transformation of elemol **2** to elemoxide **3** was developed with an overall yield of 32%.
2. Feasible regioselective epoxidation, reduction, oxymercuration-demercuration, silane-iodine catalyzed cyclisation and dehydration-isomerisation reactions were employed.
3. All the reaction conditions were modified and tuned carefully to obtain the optimum yields of the desired products.

4.   Our work confirms that the proposed intermediate diol **11b** is indeed an intermediate involved in the transformation of elemol **2** to elemoxide **3**.

Chapter 2

Section B: Tyrosinase inhibition studies of elemane-based sesquiterpenes

2.7. Introduction

Tyrosinase, also known as polyphenol oxidase is a sophisticated copper-carrying enzyme, which bio-catalyzes the biosynthesis of melanins from L-tyrosine through a chain of oxidative reactions. Melanin plays an essential role in protecting the skin from getting damaged upon exposure to harmful UV radiation.[39] The mechanism of monophenolase and diphenolse activity of tyrosinase is illustrated in Scheme 2.10.[40]
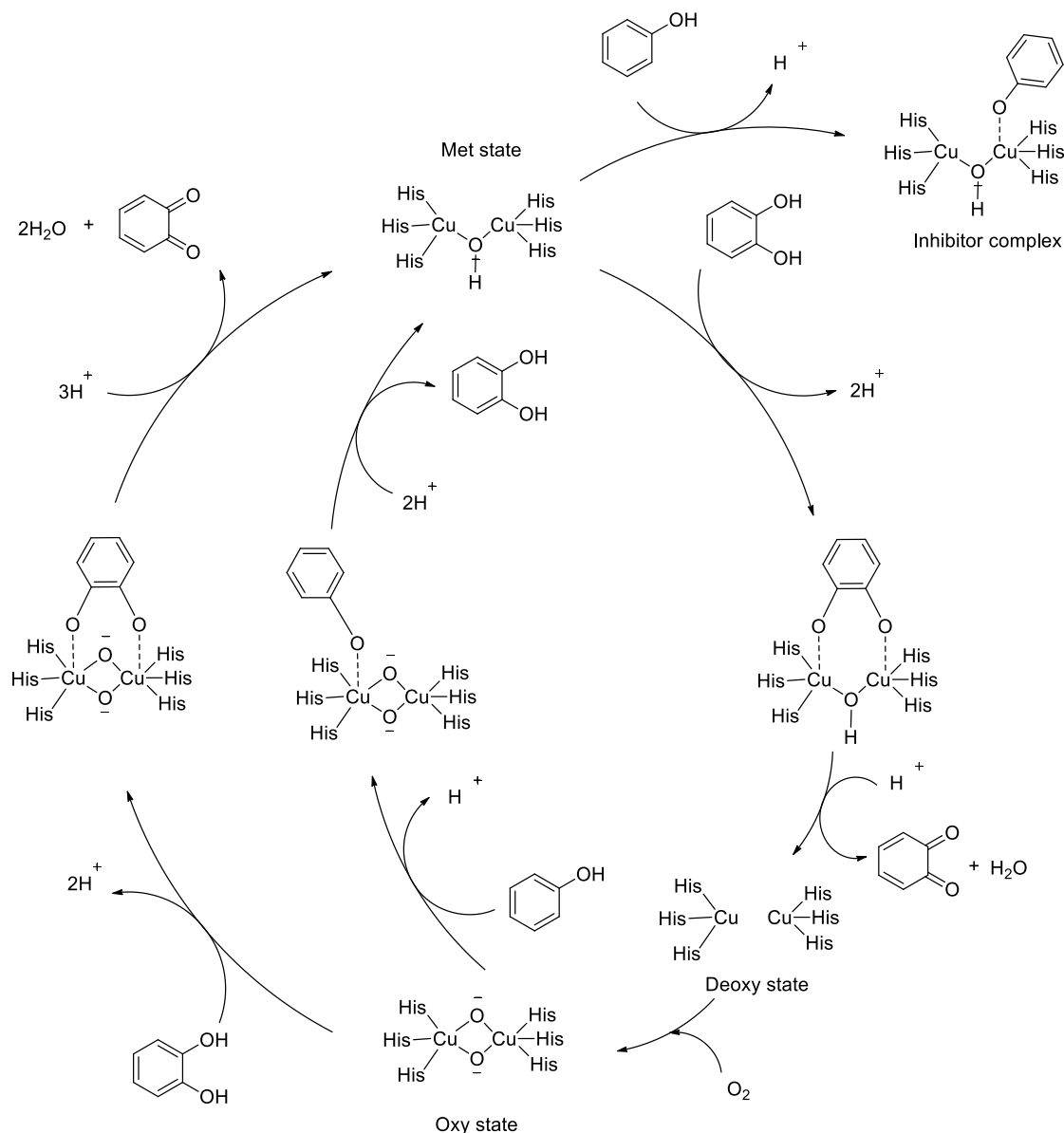
Scheme 2.10: Mechanism of monophenolase and diphenolase activity of tyrosinase enzyme.

Chapter 2

However, excessive melanin production can cause melanoma in humans and undesirable enzymatic browning in commercially important fungi, fruits and vegetables which lowers the commercial grade of fungi, fruits and vegetables.[41,42] Numerous conventional techniques (for example: autoclaving & blanching, microwave food blanching, application of chemicals, etc.) are being put in use to minimize or eliminate undesirable enzymatic browning in commercial fungi, fruits and vegetable products. However, these methods are found to make alterations in the texture, quality and also in the nutrient content of the food products in a significant way.[42] Most of the commercial tyrosinase inhibitors (kojic acid, arbutin, aloesin, etc.) suffer from various drawbacks such as toxicity, carcinogenicity, etc.[43] Thus, tyrosinase inhibitors find a wide spectrum of applications in cosmetic, agriculture and food industries.[42,44,45] Not only this, there is a huge demand for tyrosinase inhibitors in pest control as well, because tyrosinase is also concerned with the defensive and development processes in insects.[39] There are several synthetic, semi-synthetic and natural tyrosinase inhibitors derived from countless natural sources (plants,[46] fungi,[47] bacteria,[48] etc.) reported in the literature.[44] However, only a few of these tyrosinase inhibitors are categorized in a safe zone.[44,45] Therefore, it is required to continue the search for new and safer tyrosinase inhibitors.

Terpenes play an important role in the defense mechanism of the species against abiotic and biotic ecological stresses and are primarily accountable for the natural pleasant aroma.[49,50] Terpenes are receiving a great deal of demand in food industries,[51] pharmaceuticals,[52] perfumery and cosmetic industries,[51] as well as pesticide industries[53] because of the prominent bio-activities that it acquires; such as anti-fungal,[54] anti-oxidant, anti-cancer,[55] anti-microbial,[56] insecticidal activities,[53] etc. The volatile property of most terpenes is the principal reason for its use in cosmetics, as well as in aromatherapy.[49] Elemoxide **3**, a sesquiterpene oxide, is a prospective perfumery agent. It is a volatile colourless liquid having a pleasant smell and was patented to be a sturdy odorant amidst the sesquiterpenes.[15] In search of new safer tyrosinase inhibitors and to understand the SAR, we have screened elemoxide **3**, elemol **2** and the rest of the synthetic intermediates (**8**, **10-12**) containing elemane skeleton, for their ability to inhibit the tyrosinase enzyme *in vitro*.

Chapter 2

2.8. Objective

To investigate the tyrosinase enzyme inhibition properties of the synthesized elemane-based sesquiterpenes.

2.9. Results and discussion
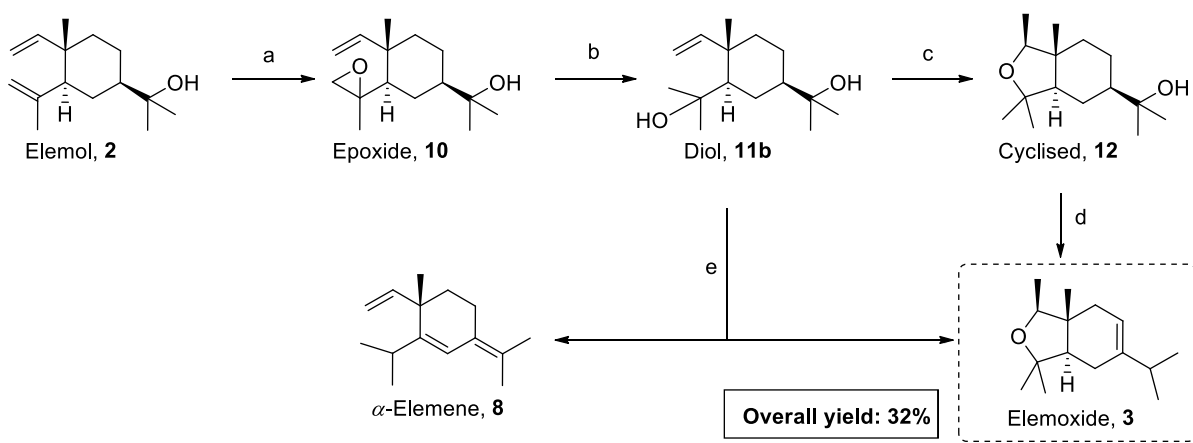
Reagents and conditions: (a) *m*-CPBA(1.20 equiv), CH$_2$Cl$_2$, 0°C (2h) then rt (1h), 80%; (b) **10** (4.2 mmol), LiAlH$_4$ (~0.06 M in anhyd THF, 1.50 equiv), 0°C-rt, 83%; (c) I$_2$ (10 mol%), CH$_2$Cl$_2$, PhSiH$_3$ (20 mol%), rt, 1h, 70%; (d) CH$_3$COOH/HClO$_4$, 72h, 70%; (e) CH$_3$COOH/HClO$_4$, 48h, 26% elemoxide **3** and 47% of α-elemene **8**.

Scheme 2.11: Outline of the synthesis of elemoxide **3** and the other elemane-based sesquiterpenes (**8**, **10**-**12**) from naturally occurring elemol **2**.

Terpenes have been widely used in medicine because of their biological values.[57] Plant leaves accumulate sesquiterpenes which, safeguards them from direct exposure to harmful ultraviolet radiations from the sun besides serving as vaccines for various pathogenic fungi, microbes, and so on.[50] Elemol **2**, a natural sesquiterpene, is known to be an insecticidal and ani-ulcer agent.[58] In 1986, Asakawa *et al.* claimed that elemol **2** does not undergo any structural transformation when administered orally in rabbits and it is predicted that it cannot induce skin sensitization or irritation.[59,60] The mushroom tyrosinase inhibition of elemoxide **3**, α-elemene **8**, epoxide **10**, diol **11b**, and cyclised product **12** were studied and compared with that of starting elemol **2** and the reference kojic acid (Scheme 2.11).

Chapter 2

Table 2.3: *In vitro* anti-tyrosinase studies of sesquiterpenes elemol **2**, epoxide **10**, diol **11b**, cyclised product **12**, elemoxide **3**, α-elemene **8** and reference kojic acid.

Sr No.	Conc. (µM)	% Anti-tyrosinase activity ± SEM[a]						
		Elemol **2**	Epoxide **10**	Diol **11b**	Cyclised **12**	Elemoxide **3**	α-Elemene **8**	kojic acid[b]
1	2	14.00 ± 1.00	04.30 ± 1.00	03.50 ± 1.00	04.00 ± 0.95	10.00 ± 1.86	12.00 ± 1.00	05.00 ± 1.50
2	20	14.39 ± 3.10	20.66 ± 2.01	19.00 ± 1.02	18.00 ± 1.00	38.89 ± 2.10	22.00 ± 1.50	21.96 ± 2.50
3	60	25.68 ± 2.00	39.74 ± 6.41	20.00 ± 2.30	27.54 ± 1.64	68.96 ± 3.52	27.5 ± 0.50	44.70 ± 5.30
7	100	47.50 ± 1.50	45.41 ± 2.44	23.00 ± 1.05	36.36 ± 3.20	68.99 ± 1.50	45.88 ± 0.70	69.00 ± 0.90
5	200	47.50 ± 1.00	55.56 ± 2.00	29.00 ± 2.50	53.50 ± 0.50	80.00 ± 2.38	63.52 ± 0.30	88.63 ± 0.70
6	400	48.00 ± 1.00	58.00 ± 1.50	40.00 ± 1.38	66.00 ± 4.95	85.00 ± 1.15	68.00 ± 1.70	90.00 ± 0.50
7	600	58.34 ± 8.33	61.54 ± 3.00	65.00 ± 0.60	70.00 ± 2.00	88.00 ± 1.25	73.00 ± 0.20	94.50 ± 2.00
8	800	60.00 ± 3.00	65.00 ± 2.00	75.00 ± 2.00	73.00 ± 1.50	98.00 ± 1.40	85.00 ± 0.10	99.00 ± 0.20

[a] Standard error from the mean of the triplicates, [b] Reference compound

As evident from Table 2.3, all the sesquiterpenes (**2**-**3**, **8**, **10**-**12**) can subdue the activity of mushroom tyrosinase. It is observed that the anti-tyrosinase activity profile of epoxide **10** and cyclised product **12** is almost a-like. The tyrosinase inhibitory activity of diol **11b** is almost similar to that of the starting elemol **2**. The anti-tyrosinase activity profile of elemoxide **3** is similar to that of the reference kojic acid over a range of concentrations. Additionally, elemoxide **3** reaches its maximum activity of around 98% at the concentration level of 800 µM.

Table 2.4: IC_{50} of elemane based sesquiterpenes and reference kojic acid.

Sr No.	Sesquiterpenes	$IC_{50} \pm SEM^{a}$ (µM)
1	Elemol **2**	432.14 ± 03.17
2	Epoxide **10**	159.16 ± 08.90
3	Diol **11b**	467.64 ± 10.82
4	Cyclised **12**	176.61 ± 10.35
5	Elemoxide **3**	29.99 ± 02.48
6	α-Elemene **8**	102.19 ± 03.49
7	Kojic acid **13**	44.07 ± 02.71

^{a} standard error from the mean of the triplicates
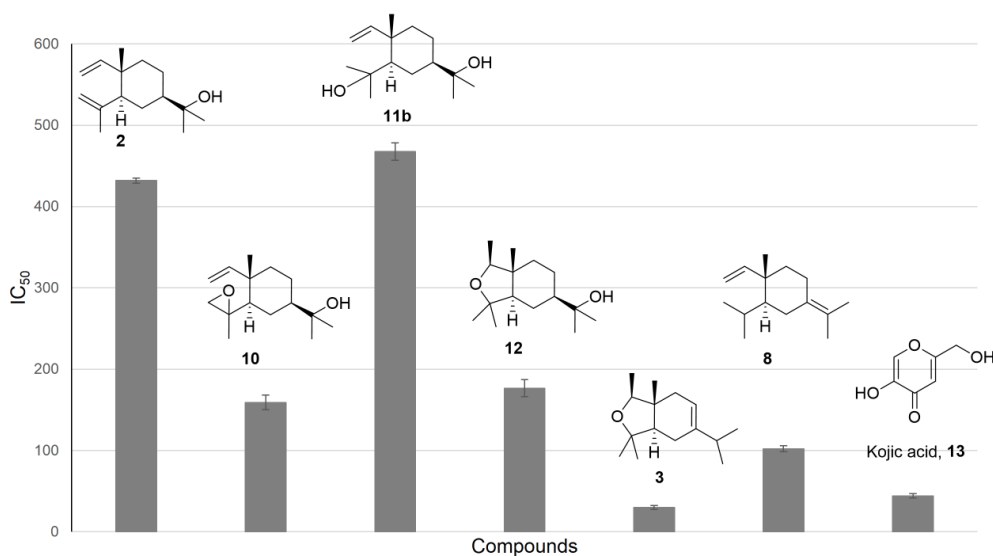
Figure 2.4: 50% tyrosinase inhibitory concentrations (IC_{50}) of elemane-based sesquiterpenes.

IC_{50} values of all tested elemane-based sesquiterpenes were calculated using Microsoft Excel 2013 (Microsoft Corporation, India). As shown in (Table 2.4, Figure 2.4), IC_{50} values of all the synthesized sesquiterpenes, studied for their *in vitro* anti-tyrosinase activities against mushroom tyrosinase fall in the range of   29.99 -467.64 µM. It can be inferred that diol **11b**

(IC$_{50}$ = 467.64 ± 10.82 µM) has almost similar anti-tyrosinase activity compared to that of the starting elemol **2** (IC$_{50}$ = 432.14 ± 03.17 µM). Epoxide **10** (IC$_{50}$ = 159.16 ± 08.90 µM) and cyclised product **12** (IC$_{50}$ = 176.61 ± 10.35 µM) showed almost two times more anti-tyrosinase activity than that of the starting elemol **2**. α- Elemene **8** (IC$_{50}$ = 102.19 ± 3.49 µM) showed around four times more activity than that of the starting elemol **2**. Elemoxide **3** revealed almost 14 times more anti-tyrosinase activity than that of the starting elemol **2**. Additionally, elemoxide **3** showed comparable IC$_{50}$ to that of the positive control kojic acid **13** (IC$_{50}$ = 44.07 ± 02.71 µM). The other compounds (**8**, **10-12**) showed lower tyrosinase inhibition than kojic acid. Amongst the elemane-based sesquiterpenes (**3**, **8**, **10**-**12**), elemoxide **3** was found to be the best mushroom tyrosinase inhibitor (Table 2.4, Figure 2.4).

Elemoxide, **3** α-Pinene, **14** α-Terpineol, **15**

Mulberrofuran G, **16**   Kuwanon G, **17**
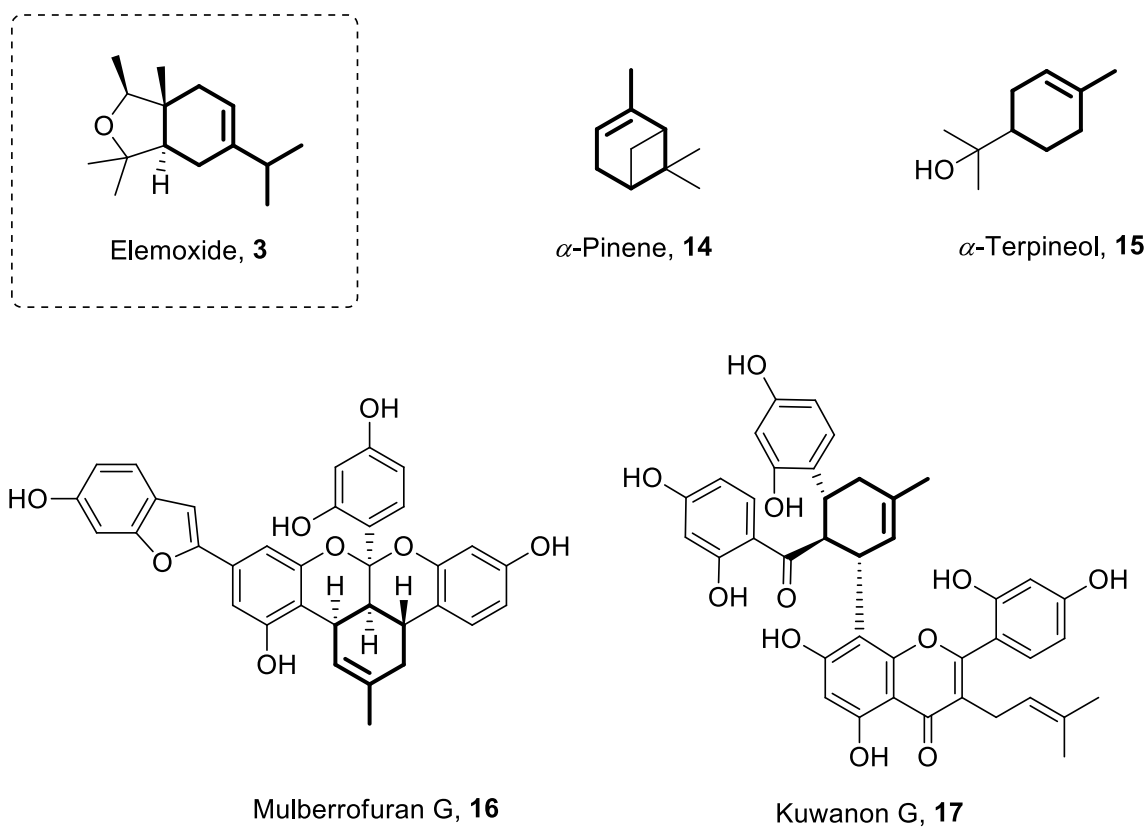
Figure 2.5: Natural tyrosinase inhibitors **14**-**17** containing methyl cyclohexene functionality.

In 2017, Chao and coworkers conducted *in vivo* tyrosinase and melanogenesis inhibitory studies of essential oil, consisting of methyl cyclohexene containing terpenes (α-pinene **14**, α-terpineol **15**, etc) and declared the results to be satisfactory (Figure 2.5).[61] Likewise, in 2018,

Koirala *et al.* demonstrated that the methyl cyclohexene portion of the natural products kuwanon G **17** and mulberrofuran G **16** is one of the key influences of their tyrosinase inhibition property (Figure 2.5). The computational simulation studies revealed that the methyl cyclohexene fraction contained in these compounds can hydrophobically interact with the enzyme, at its active site, readily and effectively.[62] Fascinatingly, elemoxide **3** also is made up of *iso*-propyl cyclohexene moiety (homologated methyl cyclohexene moiety). The presence of oxygen heterocyclic ring along with cyclohexene core may be an important requirement for inhibitory activity of such sesquiterpene skeleton, as it is expected to bind the enzyme through oxygen and inhibit its activity.

Skin ailments such as freckles (lentigo simplex), age spots (solar lentigo), melasma, etc. are results of excessive pigmentation and can inevitably lead to psychological anxiety.[45] Amongst the tyrosinase inhibitors used in cosmeceutical formulations have certain shortcomings. For instance, the possibility of degradation of ascorbic acid,[63] minimal bio-availability of ellagic acid,[64] inadequate dermal permeation and less stability in the formulation of kojic acid & arbutin, skin sensitization and exogenous ochronosis by hydroquinones,[65] and so on. Elemoxide **3**, a volatile liquid sesquiterpene oxide, derived from natural elemol **2** can be an alternative safer tyrosinase inhibitor. This result finds elemoxide **3** to be a potential tyrosinase inhibitor that can also be useful to impart fragrance to a cosmetic formulation. Further, there is a wide scope for conducting advanced studies concerning mammalian tyrosinase assay, *in vivo* cell-based assay, toxicity and elucidation of the detailed mechanism of action.

2.10. Conclusion

1. All the synthesized elemane-based sesquiterpenes **3**, **8**, **10**-**12** were tested for mushroom tyrosinase enzyme inhibition.
2. Elemoxide **3** revealed almost 14 times more anti-tyrosinase activity than that of the starting elemol **2**.
3. Elemoxide **3** was identified as a novel tyrosinase inhibitor, which showed comparable anti-tyrosinase activity to that of the commercially well-known tyrosinase inhibitor kojic acid.

Chapter 2

2.11. Experimental part

2.11.1. Material and methods

Thin-layer chromatography was performed with Kieselgel 60 F254 (Merck aluminium support plates). TLC spots were visualised by staining the TLC plate with iodine, KMnO$_4$ -acetone (1.5g of KMnO$_4$, 10g K$_2$CO$_3$, and 1.25mL 10% NaOH in 200mL water). The absorbances at 475 nm were recorded on Shimadzu UV-2450 double beam spectrophotometer. Infrared data was recorded in the region between 4000 to 400 cm-1 on a Shimadzu IRPrestige-21 instrument. Column chromatography was performed with sephadex LH-20 and silica gel 60-200 mesh size as packing material. ^{1}H NMR, ^{13}C NMR and DEPT-135 spectra were recorded at room temperature on Bruker instrument (400 MHz for ^{1}H and 100 MHz for ^{13}C), chemical shifts are recorded in ppm relative to tetramethylsilane (TMS) as the internal standard. Optical rotations (concentration in grams/ 100 mL solvent) were measured using sodium D line on Rudolph Research Analytical Polarimeter. The mass spectra were recorded on liquid chromatography - electrospray ionisation - mass spectrometry (LC-ESI-MS). Mushroom tyrosinase (Agaricus bisporus) (EC 1.14.18.1) was purchased from Sigma-Aldrich. L-tyrosine (purity ≥ 98%) was purchased from Sigma-Aldrich and kojic acid (purity ≥ 98%) was procured from Merck.

Experimental part of section A

2.11.2. Procedure for synthesis of epoxide 10
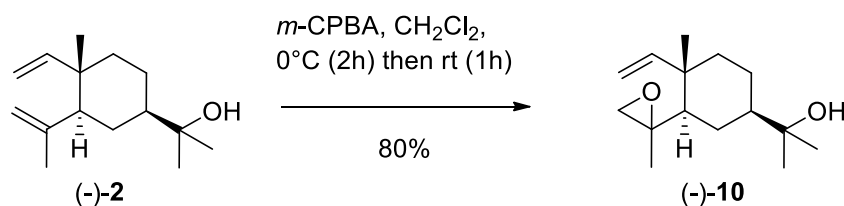
In a single neck round bottom flask equipped with a guard tube filled with calcium chloride and the magnetic bar was placed 70% *m*-CPBA (1.20 equiv). To this 2/3rd of CH$_2$Cl$_2$ (27 mL) was added by gently stirring the solution mechanically and the solution was cooled to 0 °C. Meanwhile, a solution of elemol **2** (8.99 mmol) was prepared with the remaining 1/3rd of CH$_2$Cl$_2$ (13 mL) and this solution was added dropwise to the solution in a round bottom flask.

The reaction mass was stirred at 0°C for 2h and then at rt for 1h. The progress of the reaction was monitored using TLC. The reaction mixture was decanted into a separating funnel. The residue was rinsed with an additional 5 mL CH_2Cl_2 and transferred to the same separating funnel. The organic layer was washed with 10% aqueous sodium sulphite (20 mL × 3), to destroy all the perbenzoic acid. Then, the organic layer was washed with 10% aqueous $NaHCO_3$ (20 mL × 2), to remove benzoic acid. The organic layer was dried over Na_2SO_4 and the volatile solvent was distilled under reduced pressure. The residue was purified by column chromatography (ethyl acetate:hexane 3:7) to afford pure **10** as a pale yellow viscous liquid (1.7 g, 80%). R_f (ethyl acetate:hexane 2:8) = 0.63; $[\alpha]^{23.6}_D$ = -3.02 (c 0.45, $CHCl_3$); IR (thin film, cm^{-1}): 3397, 2970, 2941, 2870, 1711, 1632, 1454, 1383, 1175, 910; ^{1}H NMR (400 MHz, $CDCl_3$) δ 1.01 (s, 3H), 1.20 (s, 3H), 1.23 (s, 6H), 1.29-1.42 (m, 7H), 1.84-1.88 (m, 1H), 2.58 (d, J = 4.6, 1H), 2.67 (dd, J = 4.6 Hz, J = 0.6, 1H), 4.95 (dd, J = 10.8 Hz, J = 1.2 Hz, 1H), 4.99 (dd, J = 17.5 Hz, J = 1.2 Hz, 1H); 5.77 (dd, J = 17.5 Hz, J = 10.8 Hz, 1H); ^{13}C NMR (100 MHz, $CDCl_3$) δ 17.4, 19.7, 22.2, 24.9, 27.1, 27.4, 39.1, 41.0, 48.7, 53.2, 56.2, 58.2, 72.6, 110.6, 149.2.

2.11.3. Procedure for synthesis of diol 11b
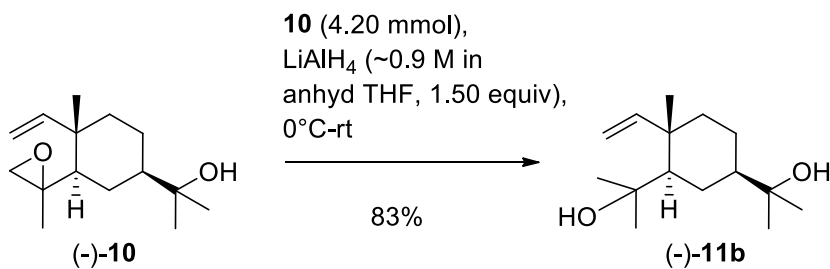
In a two neck round bottom flask, suspension of $LiAlH_4$ (~0.9 M in anhyd THF, 1.50 equiv) was prepared under N_2 atmosphere. To this suspension, a solution of epoxide **10** (4.20 mmol) was added with the help of a syringe in one lot at -3°C to 0°C. Hydrogen evolution was observed. The temperature of the reaction mixture was gradually increased from 0°C to rt. The reaction mass was magnetically stirred for 1 h. After complete consumption of **10** as followed by TLC (1h), the reaction was quenched with approx. 2N KOH (20 mL) under vigorous stirring and N_2 atmosphere. THF was distilled completely on rota-vap under reduced pressure. The

aqueous layer was extracted in ethyl acetate (20 mL × 3). The organic layer was washed with brine. The combined organic layer was dried over Na_2SO_4 and the volatile solvent was distilled under reduced pressure to obtain **11b** as white low-melting waxy solid (836 mg, 83% yield). R_f (ethyl acetate:hexane 55:45) = 0.7; $[\alpha]^{26.2}_D$ = -9.99 (c 0.16, $CHCl_3$); IR (KBr, cm^{-1}): 3364, 3080, 2971, 2934, 2864, 1630, 1468, 1371, 1198, 1126, 1057, 1011, 901, 822; ^{1}H NMR (400 MHz, $CDCl_3$) δ 1.11 (s, 6H), 1.13 (s, 3H), 1.14 (s, 6H), 1.17-1.18 (m, 2H), 1.24-1.33 (m, 3H), 1.51-1.56 (m, 2H), 1.71-1.74 (m, 1H), 2.37 (bs, 1H), 4.88 (dd, J = 10.8 Hz, J = 1.1 Hz, 1H), 4.96 (dd, J = 17.7 Hz, J = 1.1 Hz, 1H), 6.00 (dd, J = 17.6 Hz, J = 10.8 Hz, 1H); ^{13}C NMR (100 MHz, $CDCl_3$) δ 17.1, 23.1, 25.4, 26.5, 27.5, 28.3, 31.2, 40.3, 43.8, 49.4, 55.6, 72.9, 75.6, 109.5, 153.0.

2.11.4. Procedure for synthesis of diol 11a
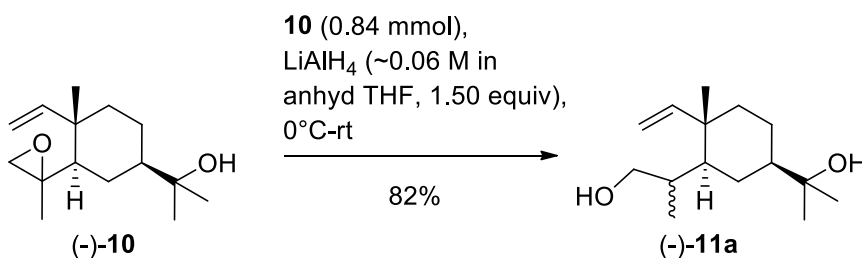
In a two neck round bottom flask, suspension of LiAlH₄ (~0.06 M in anhyd THF, 1.50 equiv) was prepared under N_2 atmosphere. To this suspension, a solution of epoxide **10** (0.84 mmol) was added with the help of a syringe in one lot at -3°C to 0°C. Hydrogen evolution was observed. The temperature of the reaction mixture was gradually increased from 0°C to rt. The reaction mass was magnetically stirred for 1 h. After complete consumption of **10** as followed by TLC (1h), the reaction was quenched with approx. 2N KOH (20 mL) under vigorous stirring and N_2 atmosphere. THF was distilled completely on rota-vap under reduced pressure. The aqueous layer was extracted in ethyl acetate (20 mL × 3). The organic layer was washed with brine. The combined organic layer was dried over Na_2SO_4 and the volatile solvent was distilled under reduced pressure to obtain **11a** as a colourless viscous liquid (170 mg, 82% yield). R_f (ethyl acetate:hexane 55:45) = 0.6; IR (thin film, cm^{-1}): 3447, 3080, 3036, 2972, 2938, 2870, 1638, 1466, 1443, 1379, 1175, 1124, 1055, 1009, 910; ^{1}H NMR (400 MHz, $CDCl_3$) δ 0.92 (s, 3H), 1.14 (s, 9H), 1.24-1.32 (m, 3H), 1.39-1.40 (m, 3H), 1.53 (m, 3H), 3.91 (dt, J = 14.1 Hz,

$J = 1.3$ Hz, 1H), 3.99 (dt, $J = 14.1$ Hz, $J = 1.4$ Hz, 1H), 4.78 (s, 1H), 4.85 (dddd, $J = 19.1$ Hz, $J = 12.0$ Hz, $J = 3.7$ Hz, $J = 1.3$ Hz, 2H), 5.10 (d, $J = 1.3$, 1H), 5.69 (dd, $J = 10.5$ Hz, $J = 17.8$ Hz, 1H); ^{13}C NMR (100 MHz, CDCl$_3$) δ 14.9, 21.4, 26.0, 26.2 (2C), 27.9, 38.5, 38.6, 46.9 (2C), 48.3, 66.5, 71.7, 109.7, 148.6.

2.11.5. Procedure for synthesis of 12 via oxymercuration demercuration
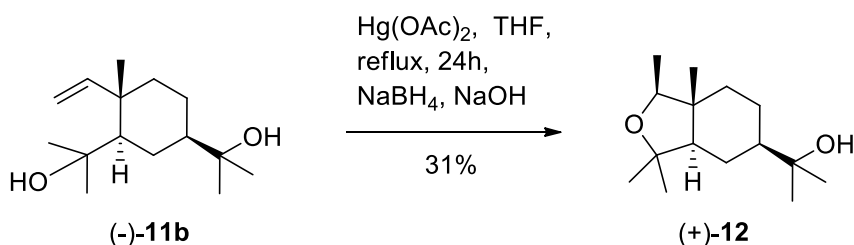
In a two neck 50 mL round bottom flask, equipped with a water circulation condenser and a guard tube filled with calcium chloride; was placed a solution of **11b** (2.09 mmol) in anhyd THF (3 mL) under magnetical stirring. To this solution, Hg(OAc)$_2$ (1.50 equiv) was added at rt. This reaction mass was refluxed (60-63 °C) for 24h. Progress of the reaction was monitored by TLC. The reaction was quenched with approx. 5 N NaOH (10 mL), followed by dropwise addition of a solution of NaBH$_4$ (1.70 equiv) in approx. 5 N NaOH to break the mercury acetate complex. The reaction mass was stirred for an additional 1 h at rt. The reaction mass was transferred to the separating funnel and grey matter was allowed to settle, which was then separated. THF was completely distilled using rota-vap under reduced pressure. The aqueous layer was extracted with ethyl acetate (15 mL × 3). The organic layer was washed with brine. The combined organic layer was dried over Na$_2$SO$_4$ and the volatile solvent was distilled under reduced pressure. The residue was purified by column chromatography (ethyl acetate:hexane = 3:7) to afford pure **12** as a colourless volatile low-melting solid (154 mg, 31% yield).

2.11.6. Procedure for synthesis of 12 via oxymercuration demercuration employing Cs₂CO₃
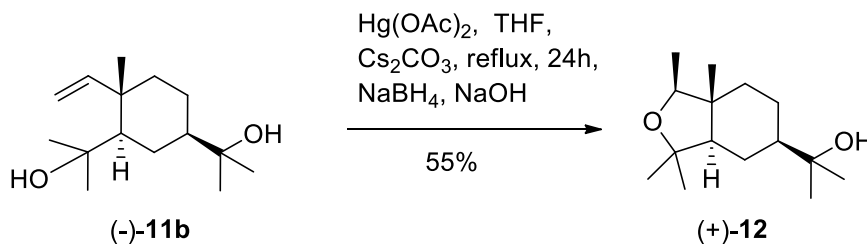
Hg(OAc)₂, THF,
Cs₂CO₃, reflux, 24h,
NaBH₄, NaOH

55%

(-)-11b   (+)-12

In a two neck 50 mL round bottom flask, equipped with a water circulation condenser and a guard tube filled with calcium chloride; was placed a solution of **11b** (2.20 mmol) in anhyd THF (3 mL) under magnetical stirring. To this solution, Hg(OAc)₂ (1.50 equiv) was added at rt. This reaction mass was refluxed (60-63 °C) for 17h. To the reaction mixture Cs₂CO₃ (1.20 equiv) was added and refluxed for another 7h. Progress of the reaction was monitored by TLC. The reaction mass was transferred to the separating funnel and grey matter was allowed to settle, which was then separated. THF was completely distilled using rota-vap under reduced pressure. The aqueous layer was extracted with ethyl acetate (15 mL × 3). The organic layer was washed with brine. The combined organic layer was dried over Na₂SO₄ and the volatile solvent was distilled under reduced pressure. The residue was purified by column chromatography (ethyl acetate:hexane = 3:7) to afford pure **10a** as colourless volatile low-melting solid (294 mg, 55% yield).

2.11.7. Procedure for synthesis of 12 via intramolecular cyclisation using silane−iodine catalytic system

I₂ (10 mol %),
PhSiH₃ (20 mol %),
CH₂Cl₂, rt, 1h

70%

(-)-11b   (+)-12
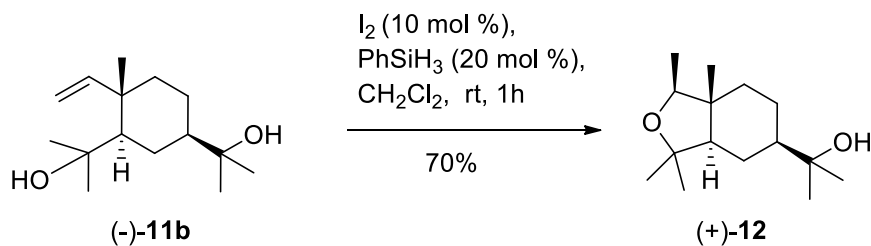
In a 50 mL two neck round bottom flask was placed a solution of iodine (10 mol%, 0.10 equiv) and CH₂Cl₂ (2 mL) under N₂ atmosphere. To this solution, PhSiH₃ (20 mol%, 0.20 equiv) was added dropwise using syringe under mechanical stirring. Solution of **11b** (0.42 mmol) in

CH$_2$Cl$_2$ (2 mL) was then added in a lot to the above solution. The reaction mass was stirred for 1h at rt. Progress of the reaction was monitored using TLC. Reaction was quenched with approx. 3 N NaOH (10 mL). Extra 10 mL CH$_2$Cl$_2$ was added and aqueous layer was separated. Organic layer was then washed with saturated aqueous solution of Na$_2$S$_2$O$_3$. Organic layer was dried over Na$_2$SO$_4$ and volatile solvent was distilled under reduced pressure. The residue was purified by column chromatography (ethyl acetate:hexane = 3:7) to afford pure **12** as colorless volatile low-melting solid (70 mg, 70% yield). R$_f$ (ethyl acetate:hexane 2:8) = 0.2; [α] $^{22.6}$ D = 4.21 (c 0.380, CHCl$_3$); IR (KBr, cm^{-1}): 3420, 2966, 2930, 2864, 1722, 1468, 1373, 1261, 1088, 1051, 1024, 920, 802; ^{1}H NMR (400 MHz, CDCl$_3$) δ 0.78 (s, 3H), 1.04 (d, J = 6.2 Hz, 3H), 1.15 (s, 6H), 1.17 (s, 6H), 1.24-1.36 (m, 3H), 1.42-1.48 (m, 3H), 1.51-1.63 (m, 2H), 3.42 (q, J = 6.4 Hz, 1H); ^{13}C NMR (100 MHz, CDCl$_3$) δ 12.5, 13.0, 20.8, 21.0, 23.0, 26.1, 26.8, 29.4, 35.0, 42.5, 48.5, 57.1, 71.9, 77.8, 80.6.

2.11.8. Procedure for synthesis of (-)-elemoxide 3 from cyclized product 12
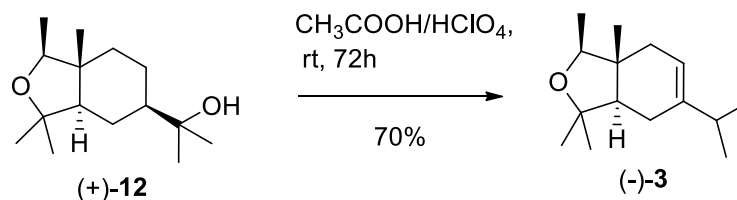
In a 25 mL single neck round bottom flask, **12** (0.27 mmol) was dissolved in a solution of 60% perchloric acid (1.50 equiv) and glacial acetic acid (1.50 equiv). This solution was mechanically stirred at rt for 72h. Progress of the reaction was monitored using TLC. To this reaction mass, 5 mL water was added and aqueous layer was extracted in diethyl ether (10 mL × 3). The organic layer was washed with brine. The combined organic layer was dried over Na$_2$SO$_4$ and the volatile solvent was distilled under reduced pressure. The residue was purified by column chromatography (ethyl acetate:hexane = 3:97) to afford pure **3**[15] as a colourless volatile viscous liquid (42 mg, 70% yield). R$_f$ (ethyl acetate:hexane 1:9) = 0.6; [α] $^{25.6}$ D = -33.07 (c 0.302, EtOH); IR (thin film, cm^{-1}): 2968, 1711, 1462, 1383, 606; ^{1}H NMR (400 MHz, CDCl$_3$) δ 0.70 (s, 3H), 0.95 (dd, J = 6.8 Hz, J = 2.1 Hz, 6H), 1.06 (d, J = 6.3 Hz, 3H), 1.09 (s, 3H), 1.17 (s, 3H), 1.63-1.70 (m, 2H), 1.18-1.85 (m, 3H), 2.19 (p, J = 6.8, 1H), 3.48 (q, J = 6.4

Hz, 1H), 5.29 (t, J = 4.4 Hz, 1H); ^{13}C NMR (100 MHz, CDCl$_3$) δ 11.6, 13.4, 20.3, 20.9, 22.8, 23.8, 29.6, 34.2, 36.7, 41.7, 53.3, 77.7, 80.2, 116.7, 142.3; LCMS (ESI, positive) m/z calculated for C$_{15}$H$_{26}$O [M + H]$^+$ 223.20, found 223.24.

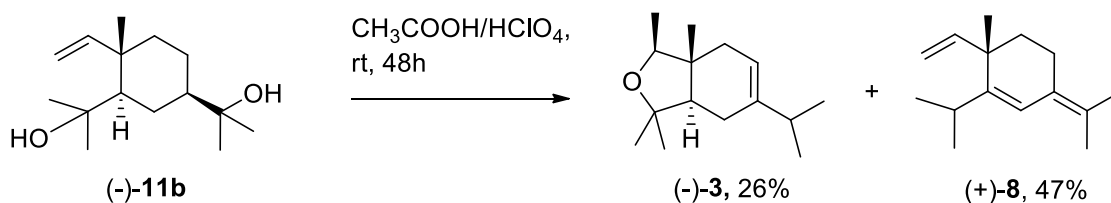### 2.11.9. Procedure for synthesis of elemoxide 3 & α-elemene 8 from diol 11b

In a 50 mL single neck round bottom flask, **11b** (2.16 mmol) was dissolved in a solution of 60% perchloric acid (0.06 mL) and glacial acetic acid (6.2 mL) this solution was mechanically stirred at rt for 48h. Progress of the reaction was monitored using TLC. To this reaction mass, 10 mL water was added and the aqueous layer was extracted in diethyl ether (15 mL × 3). The organic layer was washed with brine. The combined organic layer was dried over Na$_2$SO$_4$ and the volatile solvent was distilled under reduced pressure. The residue was purified by column chromatography (petroleum ether) to afford pure **8**[15] as a colourless volatile viscous liquid (244 mg, 47% yield) and (ethyl acetate:hexane = 3:97) to afford pure **3**[15] as a colourless volatile viscous liquid (135 mg, 26% yield) respectively, as major products.

α-elemene **8:** R$_f$ (ethyl acetate:hexane 1:9) = 0.2; [α] $^{28.4}$$_D$= 27.46 ($c$ 0.43, CHCl$_3$); IR (thin film, cm^{-1}): 2968, 1838, 665, 646, 552, 511; ^{1}H NMR (400 MHz, CDCl$_3$) δ 0.97 (dd, J = 5.2 Hz, J = 1.6 Hz, 6H), 1.10 (s, 3H), 1.151.18 (m, 2H), 1.65 (s, 3H), 1.73 (s, 3H), 2.19-2.26 (m, 3H), 4.89 (dd, J = 17.4 Hz, J = 1.6 Hz, 1H), 4.94 (dd, J = 10.6 Hz, J = 1.5 Hz, 1H), 5.69 (dd, J = 17.4 Hz, J =10.6 Hz, 1H), 6.29 (s, 1H); ^{13}C NMR (100 MHz, CDCl$_3$) δ 19.6, 20.6, 22.9, 23.6, 24.6, 25.2, 29.3, 37.6, 42.1, 112.4, 119.5, 124.5, 127.9, 146.1, 149.6.

Chapter 2

Experimental part of section B

2.11.10. Method for *in vitro* mushroom tyrosinase inhibition activity

Tyrosinase inhibition assay was performed as described by Ko *et al.*[66] with modifications. The sesquiterpenes: elemol **2**, elemoxide **3,** α- elemene **8**, epoxide **10**, diol **11b**, cyclised product **12**, were dissolved in DMSO to get the final concentrations of: 2, 20, 60, 100, 200, 400, 600 and 800 μM. Kojic acid was used as the positive control. Briefly, 20 μL of mushroom tyrosinase (1000 U/mL) and 120 μL of the test sample in 50 mM phosphate buffer (pH 6.9) was kept for 5 minutes at 32 ± 2 ˚C. Then, 2 mM L-tyrosine (300 μL) was added to each reaction mixture and kept at 32 ± 2 ˚C for 30 minutes. The enzyme reaction was monitored by measuring the absorbance at 475 nm. The percent inhibition of tyrosinase reaction was calculated as follows:

$$\text{Percent Inhibition} = [(A_{control} - A_{sample})/A_{control}] \times 100$$

where, $A_{control}$ is the absorbance without the test sample in the methanol and A_{sample} is the absorbance with the test sample in DMSO.

2.12.   Spectra
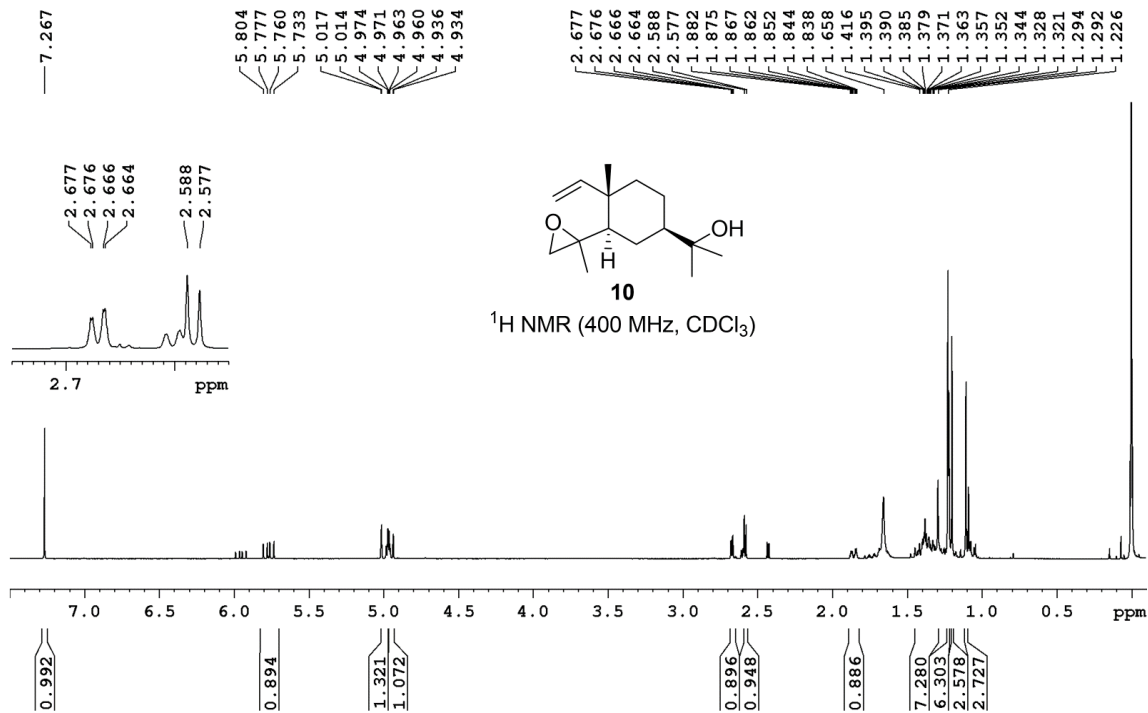
Figure 2.6: ^{1}H NMR Spectrum of **10**.
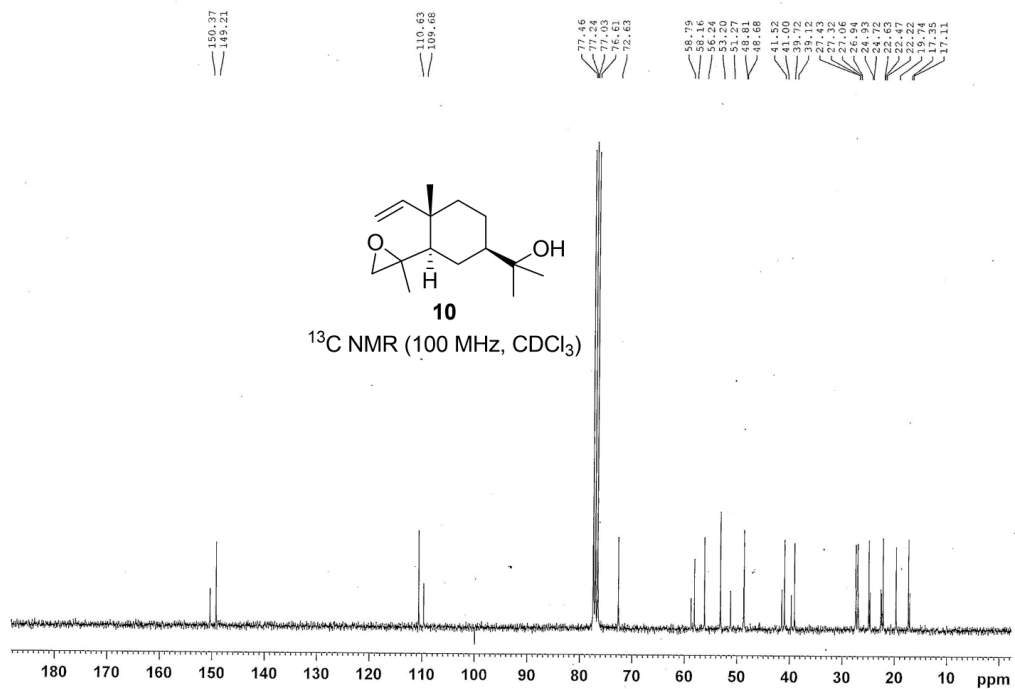
Figure 2.7: ^{13}C NMR Spectrum of **10**.
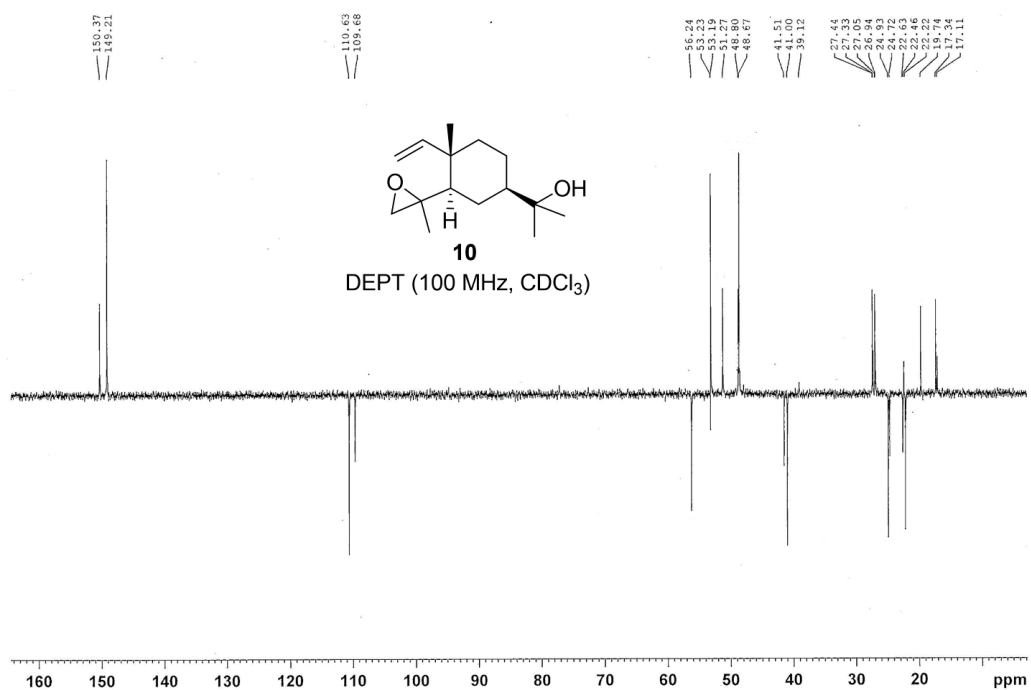
Figure 2.8: DEPT Spectrum of **10**.
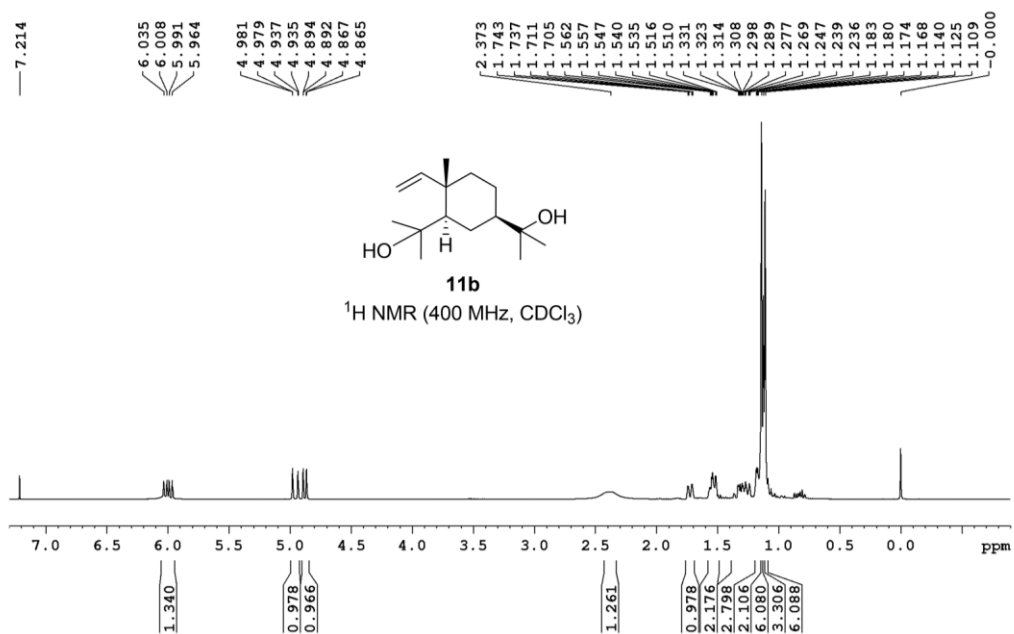
Figure 2.9: ^{1}H NMR Spectrum of **11b**.
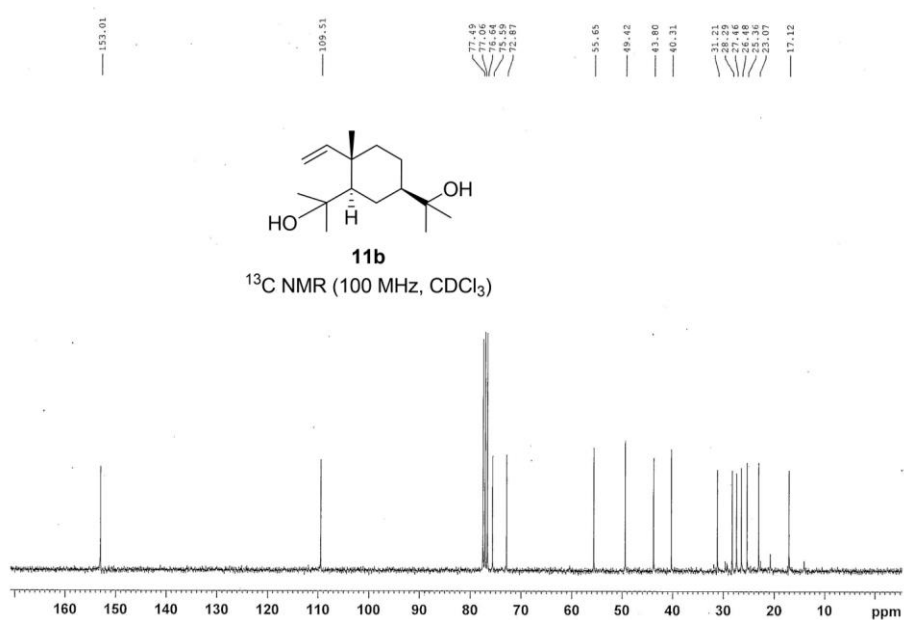
Figure 2.10: ^{13}C NMR Spectrum of **11b**.
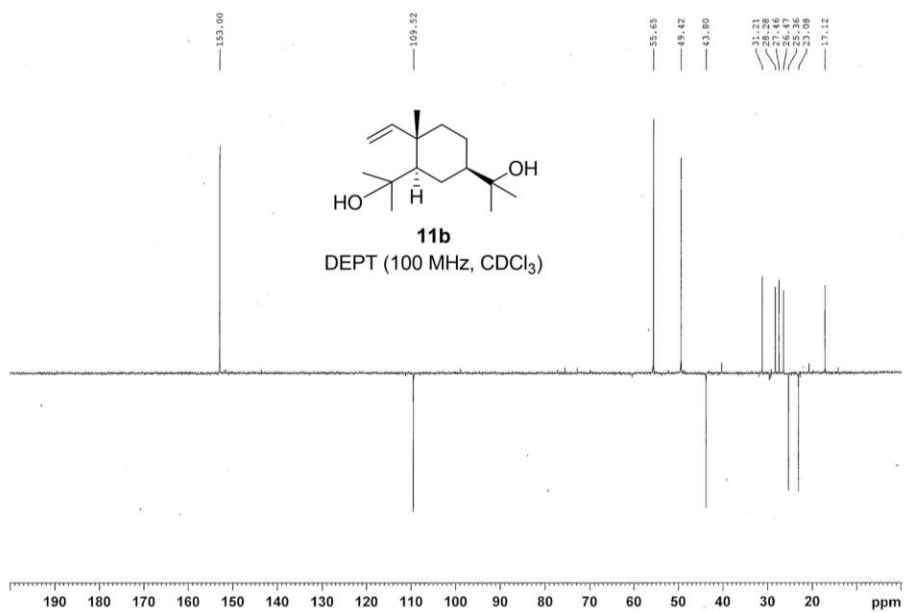
Figure 2.11: DEPT Spectrum of **11b**.
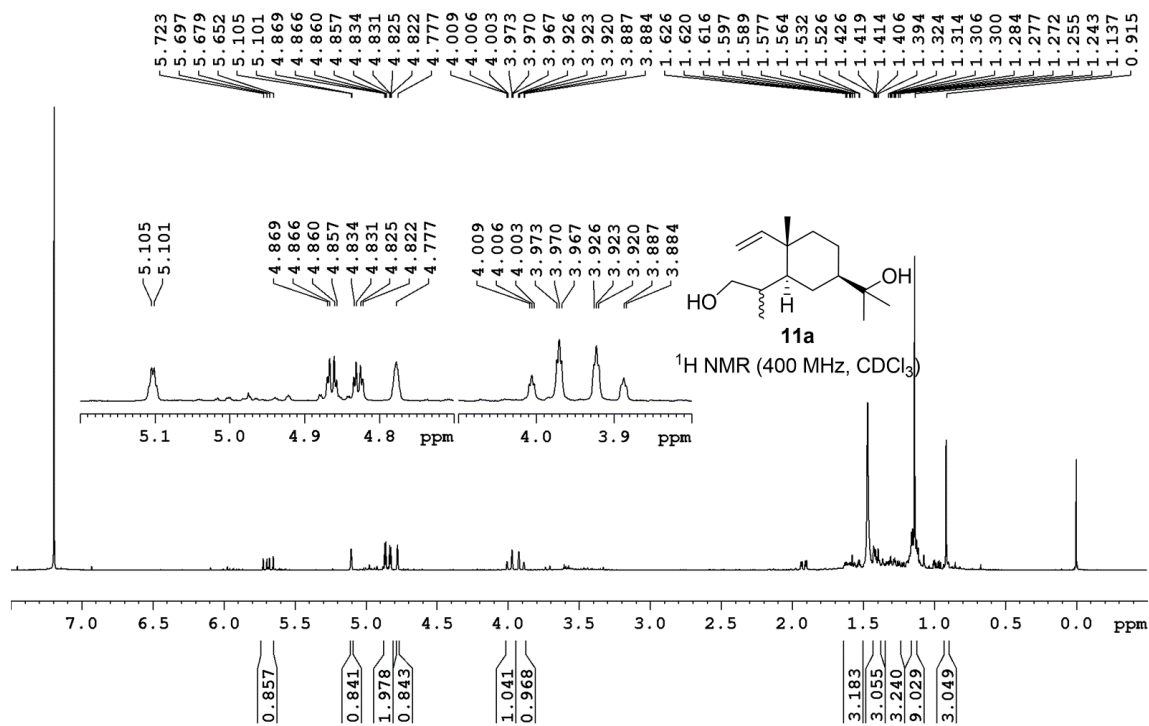
Figure 2.12: ^{1}H NMR Spectrum of **11a**.
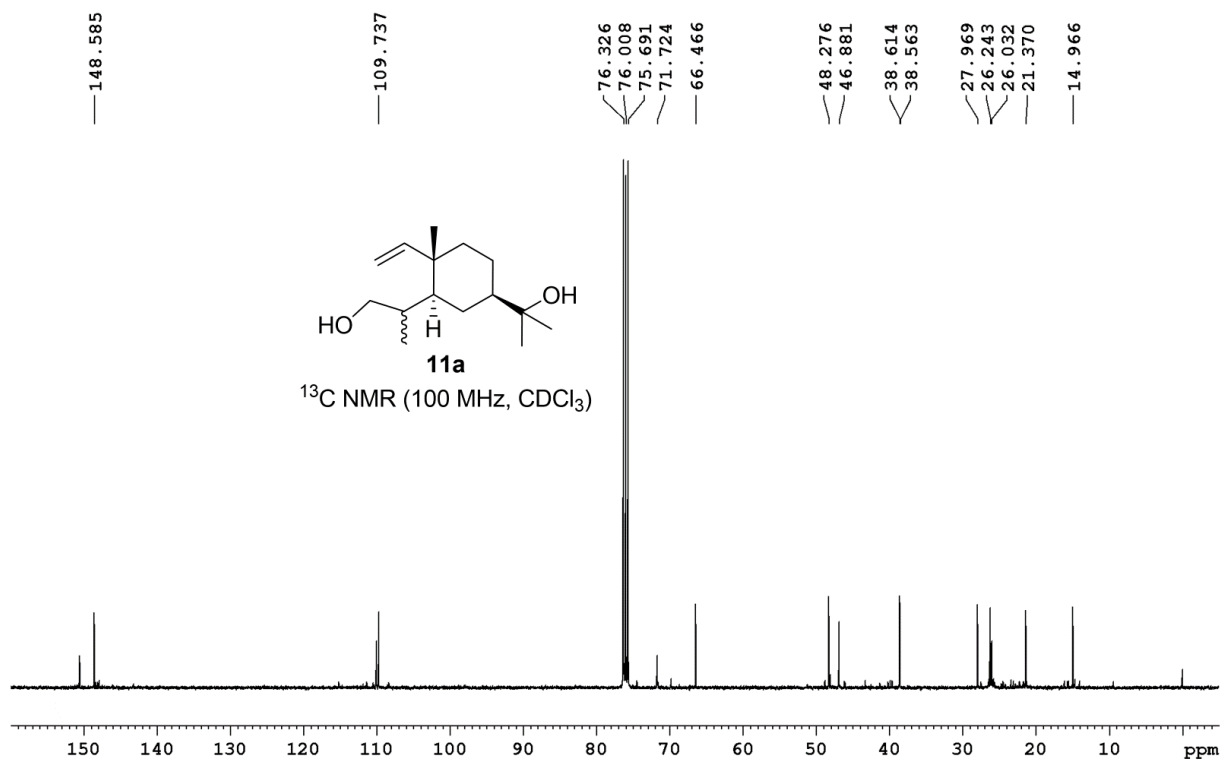
Figure 2.13: ^{13}C NMR Spectrum of **11a**.
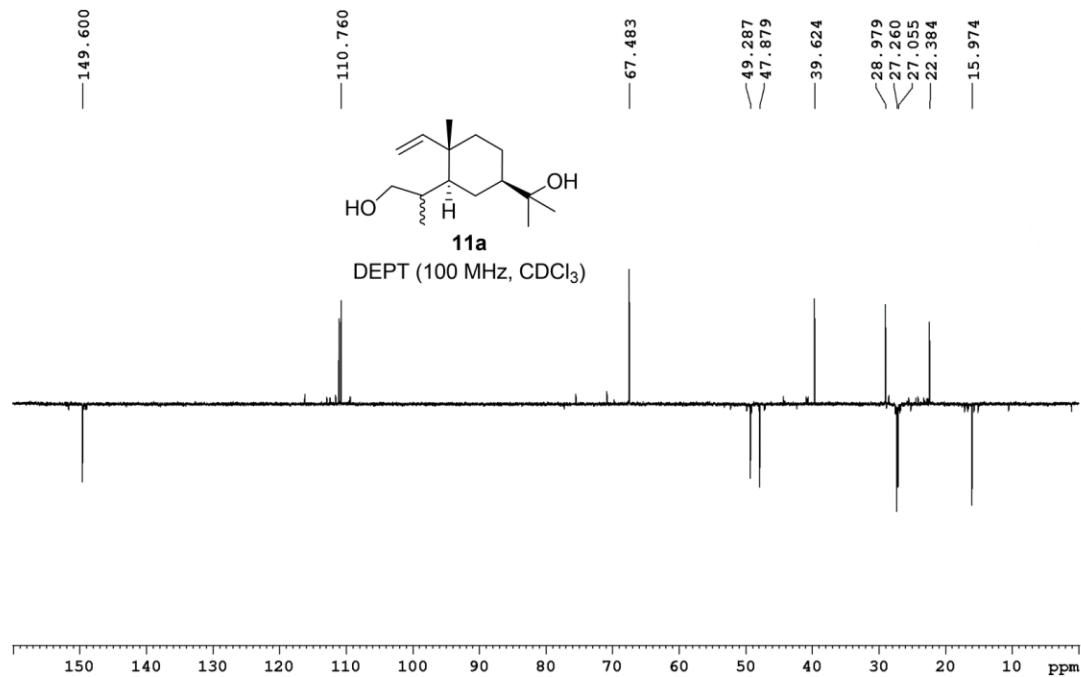
Figure 2.14: DEPT Spectrum of **11a**.
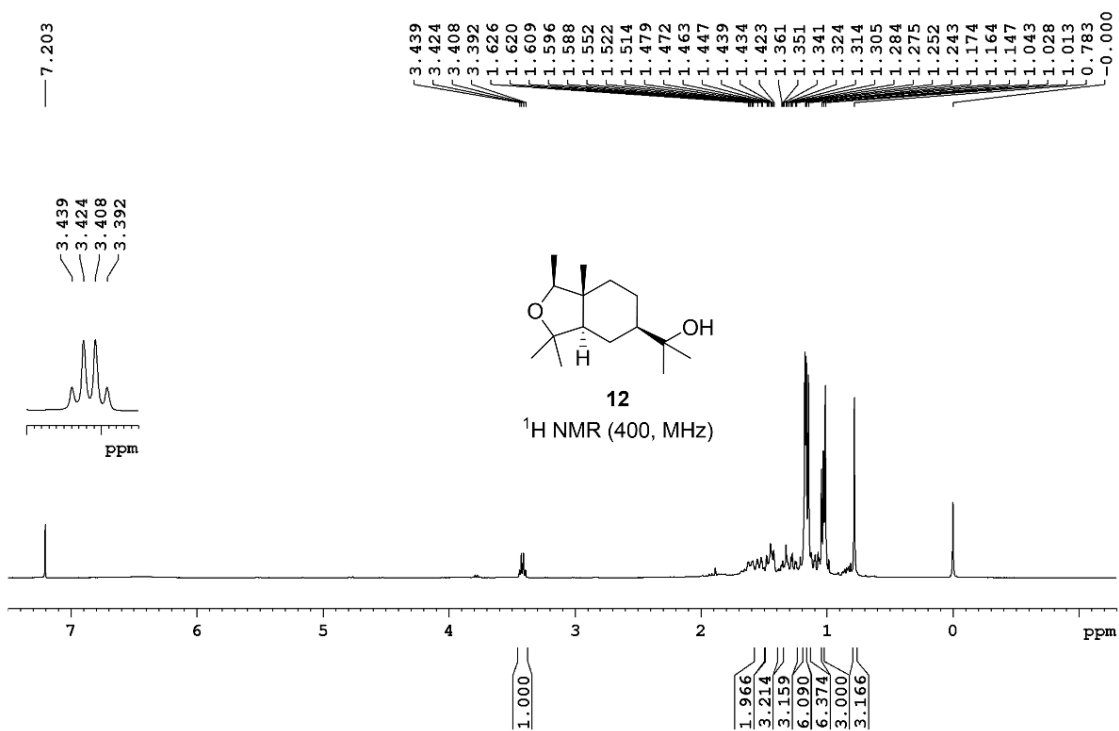
Figure 2.15: ^{1}H NMR Spectrum of **12**.
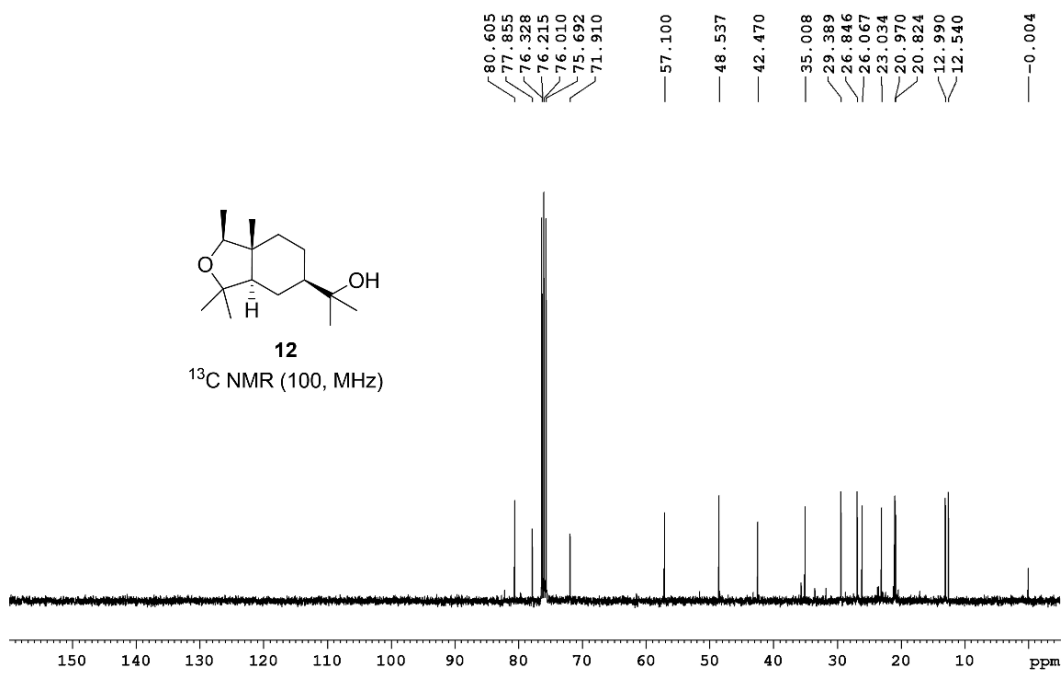
Figure 2.16: ^{13}C NMR Spectrum of **12**.
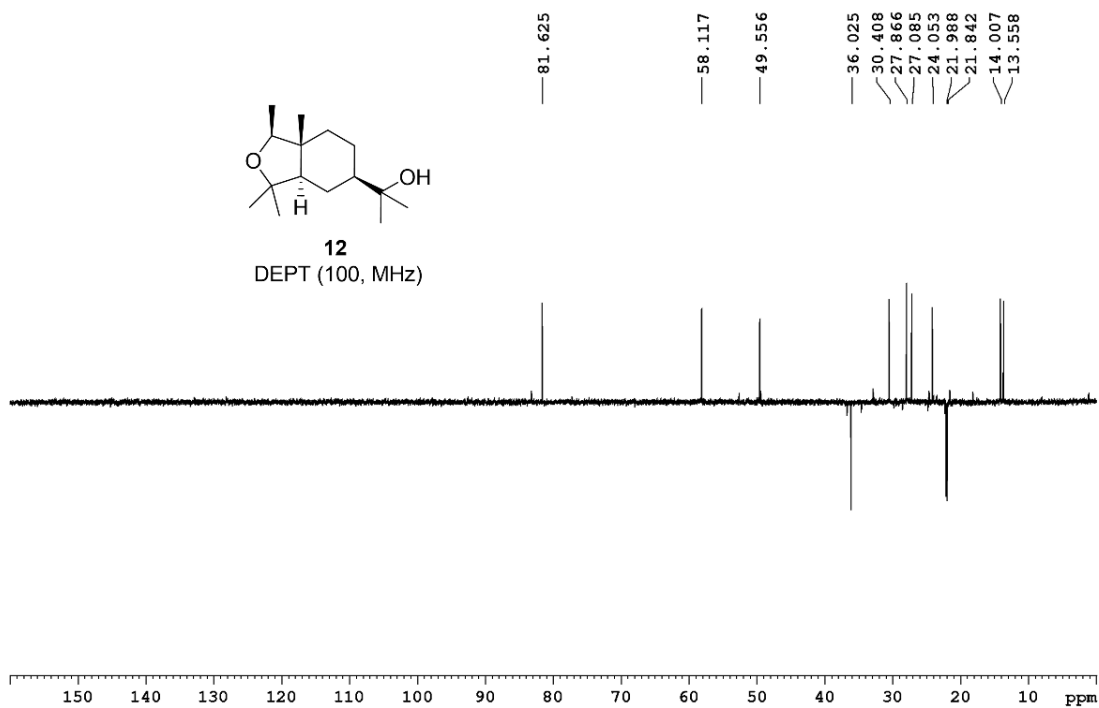
Figure 2.17: DEPT Spectrum of **12**.
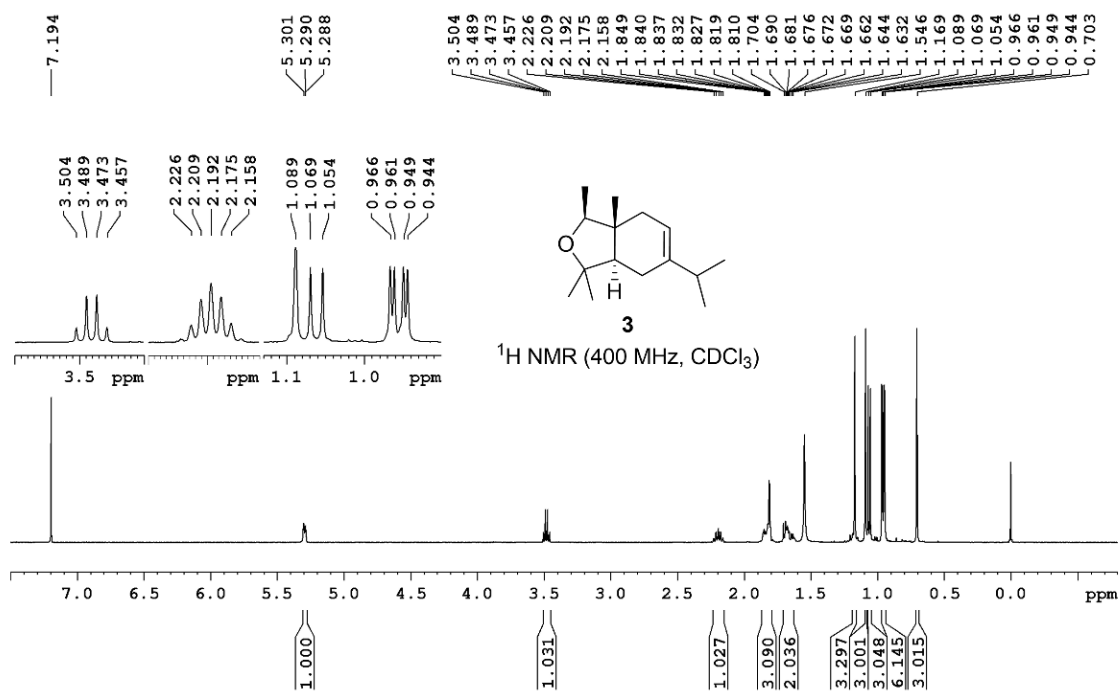
Figure 2.18: ^{1}H NMR Spectrum of **3**.
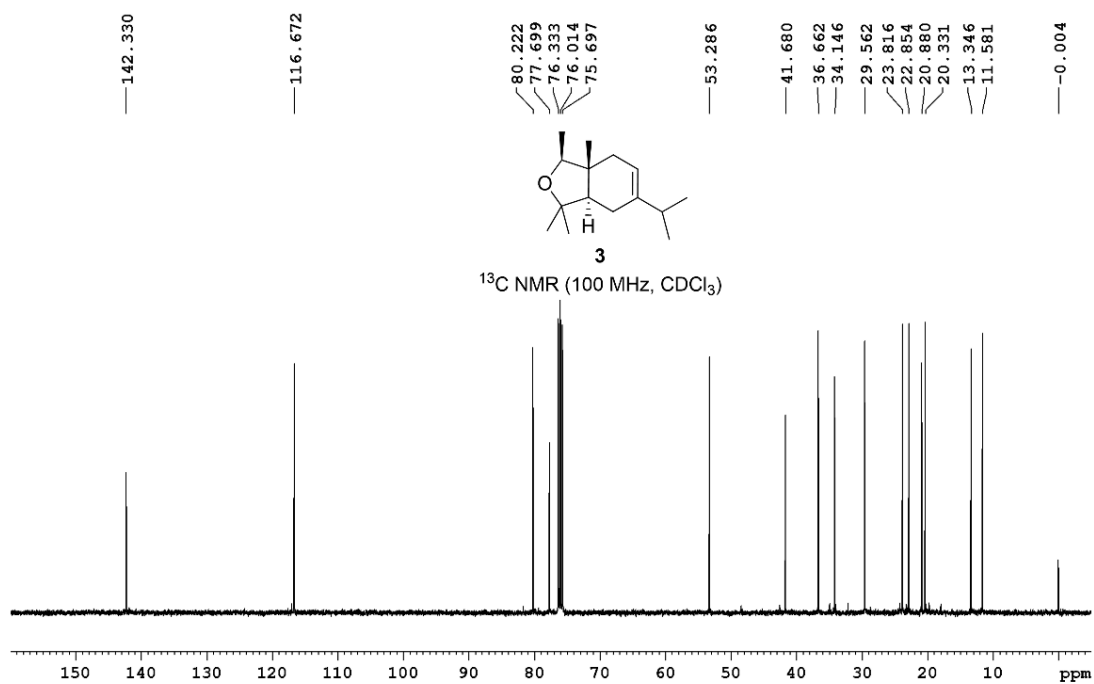
Figure 2.19: ^{13}C NMR Spectrum of **3**.
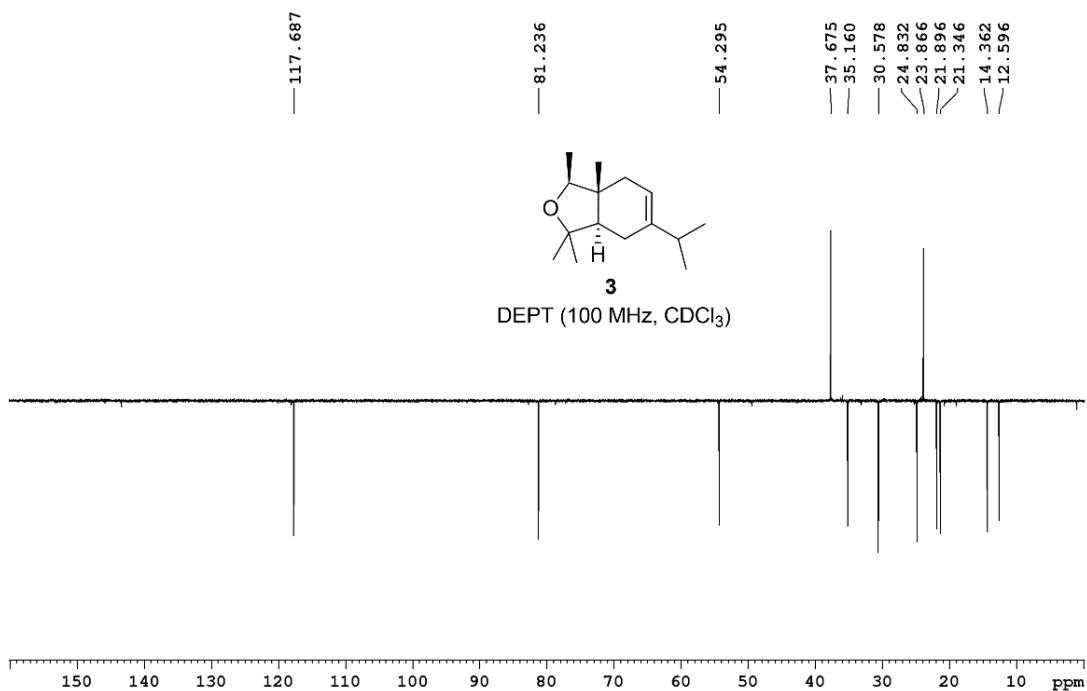
Figure 2.20: DEPT Spectrum of **3**.
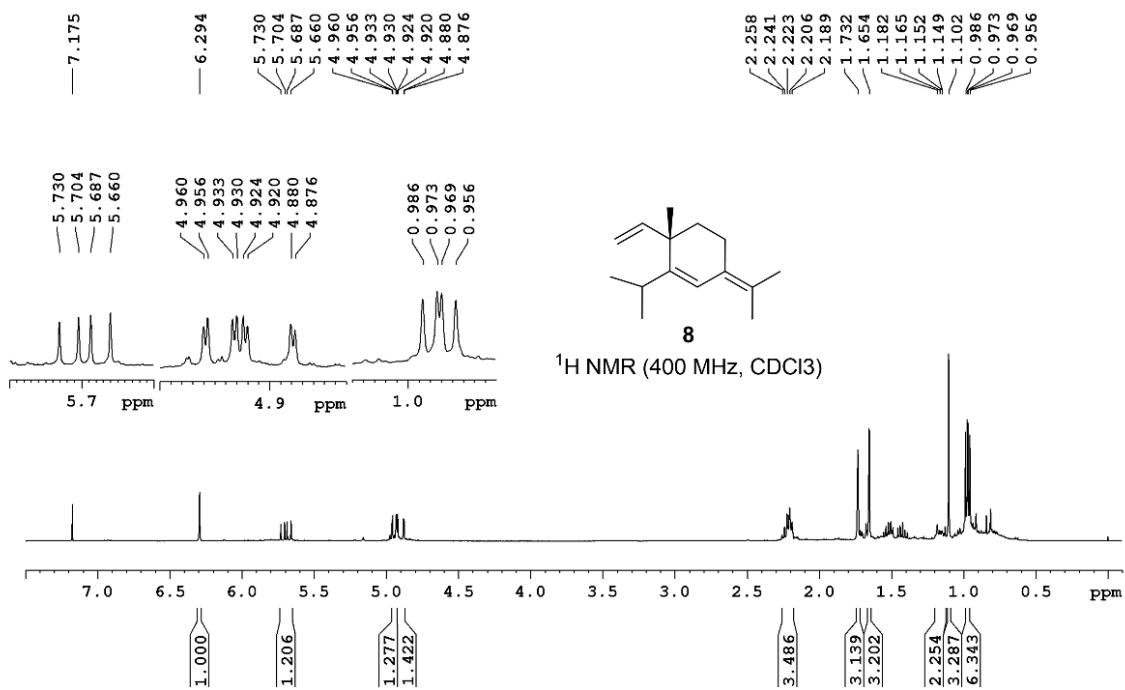
Figure 2.21: ^{1}H NMR Spectrum of **8**.

Figure 2.22: ^{13}C NMR Spectrum of **8**.
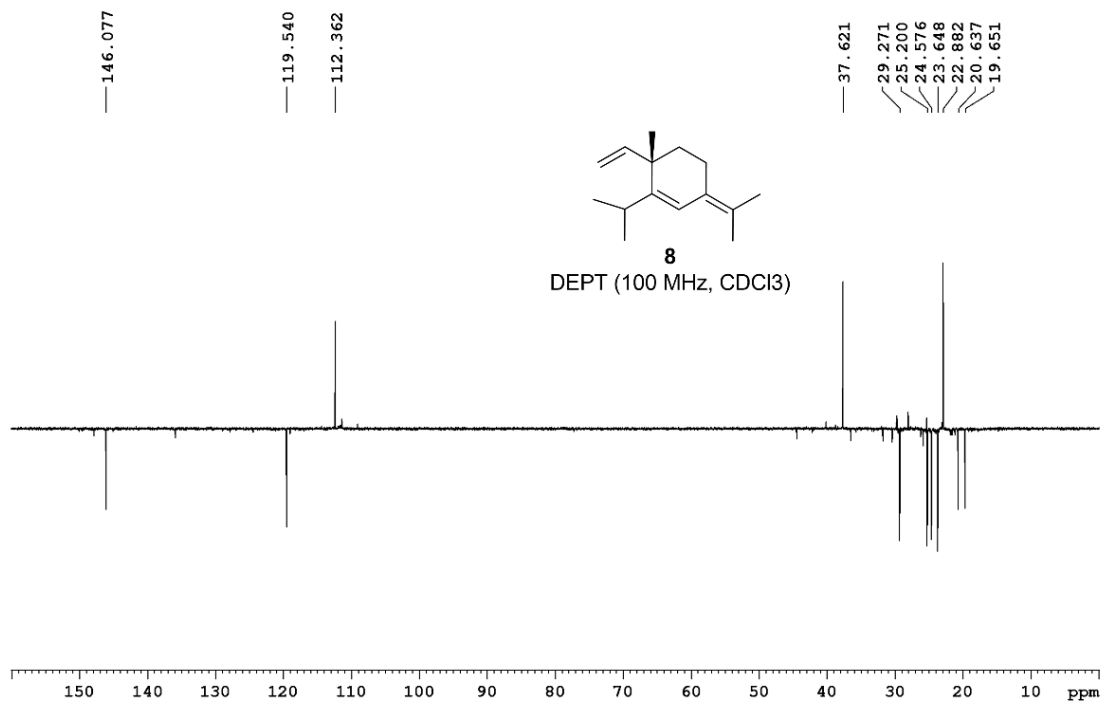
Figure 2.23: DEPT Spectrum of **8**.

Chapter 2

2.13. References

(1)   Guo, Z. The Modification of Natural Products for Medical Use. *Acta Pharm. Sin. B* **2017**, *7*, 119–136. https://doi.org/10.1016/j.apsb.2016.06.003.

(2)   Yao, H.; Liu, J.; Xu, S.; Zhu, Z.; Xu, J. The Structural Modification of Natural Products for Novel Drug Discovery. *Expert Opin. Drug Discov.* **2017**, *12*, 121–140. https://doi.org/10.1080/17460441.2016.1272757.

(3)   Schreiber, S. L. Target-Oriented and Diversity-Oriented Organic Synthesis in Drug Discovery. *Science..* **2000**, *287*, 1964–1969. https://doi.org/10.1126/science.287.5460.1964.

(4)   Burke, M. D.; Lalic, G. Teaching Target-Oriented and Diversity-Oriented Organic Synthesis at Harvard University. *Chem. Biol.* **2002**, *9*, 535–541. https://doi.org/10.1016/S1074-5521(02)00143-6.

(5)   Tan, D. S. Diversity-Oriented Synthesis: Exploring the Intersections between Chemistry and Biology. *Nat. Chem. Biol.* **2005**, *1*, 74–84. https://doi.org/10.1038/nchembio0705-74.

(6)   Wetzel, S.; Bon, R. S.; Kumar, K.; Waldmann, H. Biology-Oriented Synthesis. *Angew. Chemie Int. Ed.* **2011**, *50*, 10800–10826. https://doi.org/10.1002/anie.201007004.

(7)   Wender, P. A.; Verma, V. A.; Paxton, T. J.; Pillow, T. H. Function-Oriented Synthesis, Step Economy, and Drug Design. *Acc. Chem. Res.* **2008**, *41*, 40–49. https://doi.org/10.1021/ar700155p.

(8)   Kim, D.; Lim, J. I.; Shin, K. J.; Kim, H. S. A Stereoselective Synthesis of (±)-Elemol via an Intramolecular S$_N$2′ Ester Enolate Alkylation. *Tetrahedron Lett.* **1993**, *34*, 6557–6558. https://doi.org/10.1016/0040-4039(93)88103-P.

(9)   Halsall, T. G.; Theobald, D. W.; Walshaw, K. B. 199. Studies in the Synthesis of Terpenes. Part VIII. The Absolute Configuration of Elemol. *J. Chem. Soc.* **1964**, No. V, 1029. https://doi.org/10.1039/jr9640001029.

(10)   Taber, D. F.; Wang, Y. Kinetic vs. Thermodynamic Control in Intramolecular Diene Cyclozirconation: Synthesis of Elemol. *Tetrahedron Lett.* **1995**, *36*, 6639–6642.

https://doi.org/10.1016/00404-0399(50)1392-U.

(11) Kido, F.; Kitahara, H.; Yoshikoshi, A. Study on the Synthesis of Phytuberin from Elemol. *J. Org. Chem.* **1986**, *51*, 1478–1481. https://doi.org/10.1021/jo00359a017.

(12) Shin, J.; Fenical, W. Fuscosides A-D: Anti-Inflammatory Diterpenoid Glycosides of New Structural Classes from the Caribbean Gorgonian Eunicea Fusca. *J. Org. Chem.* **1991**, *56*, 3153–3158. https://doi.org/10.1021/jo00009a042.

(13) Iwashima, M.; Nagaoka, H.; Kobayashi, K.; Yamada, Y. Total Synthesis of Marine Diterpene Fuscol. *Tetrahedron Lett.* **1992**, *33*, 81–82. https://doi.org/10.1016/S0040-4039(00)77678-7.

(14) Stepanyuk, A.; Kirschning, A. Synthetic Terpenoids in the World of Fragrances: Iso E Super ® Is the Showcase. *Beilstein J. Org. Chem.* **2019**, *15*, 2590–2602. https://doi.org/10.3762/bjoc.15.252.

(15) Wahidulla, S.; Govenkar, M. B.; Paknikar, S. K. Reaction of Elemol with Acetic Acid/Perchloric Acid: Characterization of a Novel Oxide and (+)-*β*-Cyperone. *Helv. Chim. Acta* **2006**, *89*, 496–501. https://doi.org/10.1002/hlca.200690050.

(16) Boyer, F.-D.; Hanna, I.; Ricard, L. Formal Synthesis of (±)-Guanacastepene A: A Tandem Ring-Closing Metathesis Approach. *Org. Lett.* **2004**, *6*, 1817–1820. https://doi.org/10.1021/ol049452x.

(17) He, J.; Ling, J.; Chiu, P. Vinyl Epoxides in Organic Synthesis. *Chem. Rev.* **2014**, *114*, 8037–8128. https://doi.org/10.1021/cr400709j.

(18) Alvarez-Manzaneda, E.; Chahboun, R.; Alvarez, E.; José Cano, M.; Haidour, A.; Alvarez-Manzaneda, R. Enantioselective Total Synthesis of the Selective PI3 Kinase Inhibitor Liphagal. *Org. Lett.* **2010**, *12*, 4450–4453. https://doi.org/10.1021/ol101173w.

(19) Moschona, F.; Savvopoulou, I.; Tsitopoulou, M.; Tataraki, D.; Rassias, G. Epoxide Syntheses and Ring-Opening Reactions in Drug Development. *Catalysts* **2020**, *10*, 1117. https://doi.org/10.3390/catal10101117.

(20) Flaherty, T. M.; Gervay, J. Hydride Addition to 1,2-Anhydrosugars: A Highly

Stereoselective Route to Anhydroalditols. *Tetrahedron Lett.* **1996**, *37*, 961–964. https://doi.org/10.1016/0040-4039(95)02339-9.

(21)   Andrejevi, V.; Bjelakovi, M.; Mihailovi, M. M.; Mihailovi, M. L. The Reductive Conversion of Some Cyclic and Acyclicvic-Epoxides to Alcohols by Means of Lithium Aluminium Hydride/Aluminium Trichloride. *Helv. Chim. Acta* **1985**, *68*, 2030–2032. https://doi.org/10.1002/hlca.19850680727.

(22)   Ashby, E. C.; Cooke, B. The Mechanism of Mixed Hydride Reductions. Effects of Reagent Composition, Nature of Halogen, and Solvating Ligand on the Mechanism of Epoxide Reduction. *J. Am. Chem. Soc.* **1968**, *90*, 1625–1630. https://doi.org/10.1021/ja01008a037.

(23)   Maruoka, K.; Saito, S.; Ooi, T.; Yamamoto, H. Selective Reduction of Methylenecycloalkane Oxides with 4-Substituted Diisobutylaluminum 2,6-di-Tert-Butylphenoxides. *Synlett* **1991**, *23*, 255. https://doi.org/10.1002/chin.199201108.

(24)   Ashby, E. C.; Boone, J. R. Mechanism of Lithium Aluminum Hydride Reduction of Ketones. Kinetics of Reduction of Mesityl Phenyl Ketone. *J. Am. Chem. Soc.* **1976**, *98*, 5524–5531. https://doi.org/10.1021/ja00434a020.

(25)   Bikiel, D. E.; Di Salvo, F.; González Lebrero, M. C.; Doctorovich, F.; Estrin, D. A. Solvation and Structure of LiAlH 4 in Ethereal Solvents. *Inorg. Chem.* **2005**, *44*, 5286–5292. https://doi.org/10.1021/ic050330q.

(26)   Brown, H. C.; Geoghegan, P. J. Solvomercuration-Demercuration. I. Oxymercuration-Demercuration of Representative Olefins in an Aqueous System. Mild Procedure for the Markovnikov Hydration of the Carbon-Carbon Double Bond. *J. Org. Chem.* **1970**, *35*, 1844–1850. https://doi.org/10.1021/jo00831a028.

(27)   Fujita, S.; Abe, M.; Shibuya, M.; Yamamoto, Y. Intramolecular Hydroalkoxylation of Unactivated Alkenes Using Silane–Iodine Catalytic System. *Org. Lett.* **2015**, *17*, 3822–3825. https://doi.org/10.1021/acs.orglett.5b01797.

(28)   Semmelhack, M. F.; Bodurow, C. Intramolecular Alkoxypalladation/Carbonylation of Alkenes. *J. Am. Chem. Soc.* **1984**, *106*, 1496–1498.

https://doi.org/10.1021/ja00317a059.

(29) Li, Y.; Xie, F.; Liu, Y.; Yang, X.; Li, X. Regio- and Diastereoselective Access to Fused Isoxazolidines via Ru(II)-Catalyzed C–H Activation of Nitrones and Coupling with Perfluoroalkylolefins. *Org. Lett.* **2018**, *20*, 437–440. https://doi.org/10.1021/acs.orglett.7b03775.

(30) Schlosser, M.; Zellner, A.; Leroux, F. Pentadienyl Type Lithium and Potassium Species: The Regioselectivity of Their Reactions with Electrophiles. *Synthesis.* **2001**, *2001*, 1830–1836. https://doi.org/10.1055/s-2001-17521.

(31) Messina, F.; Botta, M.; Corelli, F.; Villani, C. Stereoselective Synthesis of *α*-Aryl-2-Benzofuranmethanamines and *α*-Aryl-1H-Indole-2-Methanamines through Palladium-Mediated Annulation of Chiral *α*-Arylpropargylamines. *Tetrahedron: Asymmetry* **2000**, *11*, 1681–1685. https://doi.org/10.1016/S0957-4166(00)00131-2.

(32) He, A.; Sutivisedsak, N.; Spilling, C. D. Stereoselective Synthesis of Cyclic Ethers via the Palladium-Catalyzed Intramolecular Addition of Alcohols to Phosphono Allylic Carbonates. *Org. Lett.* **2009**, *11*, 3124–3127. https://doi.org/10.1021/ol900980s.

(33) Shankar, M.; Guntreddi, T.; Ramesh, E.; Sahoo, A. K. Transformable Sulfoximine Assisted One-Pot Double Annulation of Vinylic C–H Bonds with Unactivated Alkynes. *Org. Lett.* **2017**, *19*, 5665–5668. https://doi.org/10.1021/acs.orglett.7b02824.

(34) Schlosser, M. Superbases for Organic Synthesis. *Pure Appl. Chem.* **1988**, *60*, 1627–1634. https://doi.org/10.1351/pac198860111627.

(35) Lochmann, L.; Janata, M. 50 Years of Superbases Made from Organolithium Compounds and Heavier Alkali Metal Alkoxides. *Cent. Eur. J. Chem.* **2014**, *12*, 537–548. https://doi.org/10.2478/s11532-014-0528-0.

(36) Fülöp, F.; Bernáth, G.; Pihlaja, K. Synthesis, Stereochemistry and Transformations of Cyclopentane-, Cyclohexane-, Cycloheptane-, and Cyclooctane-Fused 1,3-Oxazines, 1,3-Thiazines, and Pyrimidines. In *Advances in Heterocyclic Chemistry*; 1997; Vol. 69, pp 349–477. https://doi.org/10.1016/S0065-2725(08)60085-9.

(37) Smith, M. B. Retrosynthesis, Stereochemistry, and Conformations. In *Organic*

Synthesis; Elsevier, 2017; pp 1–60. https://doi.org/10.1016/B978-0-12-800720-4.00001-5.

(38) Hubert, A. J.; Reimlinger, H. The Isomerization of Olefins Part II. Thermal and Catalytic Lsomerization of Olefins Using Acids, Metals, Metal Complexes, or Boron Compounds as Catalysts. *Synthesis.* **1970**, *1970*, 405–430. https://doi.org/10.1055/s-1970-21620.

(39) Fernandes, M. S.; Kerkar, S. Microorganisms as a Source of Tyrosinase Inhibitors: A Review. *Ann. Microbiol.* **2017**, *67*, 343–358. https://doi.org/10.1007/s13213-017-1261-7.

(40) Messerschmidt, A. Copper Metalloenzymes. In *Comprehensive Natural Products II*; Elsevier, 2010; Vol. 2, pp 489–545. https://doi.org/10.1016/B978-008045382-8.00180-5.

(41) Zubair, R.; Lyons, A. B.; Vellaichamy, G.; Peacock, A.; Hamzavi, I. What's New in Pigmentary Disorders. *Dermatol. Clin.* **2019**, *37*, 175–181. https://doi.org/10.1016/j.det.2018.12.008.

(42) Parvez, S.; Kang, M.; Chung, H.-S.; Bae, H. Naturally Occurring Tyrosinase Inhibitors: Mechanism and Applications in Skin Health, Cosmetics and Agriculture Industries. *Phyther. Res.* **2007**, *21*, 805–816. https://doi.org/10.1002/ptr.2184.

(43) Pillaiyar, T.; Namasivayam, V.; Manickam, M.; Jung, S.-H. Inhibitors of Melanogenesis: An Updated Review. *J. Med. Chem.* **2018**, *61*, 7395–7418. https://doi.org/10.1021/acs.jmedchem.7b00967.

(44) Zolghadri, S.; Bahrami, A.; Hassan Khan, M. T.; Munoz-Munoz, J.; Garcia-Molina, F.; Garcia-Canovas, F.; Saboury, A. A. A Comprehensive Review on Tyrosinase Inhibitors. *J. Enzyme Inhib. Med. Chem.* **2019**, *34*, 279–309. https://doi.org/10.1080/14756366.2018.1545767.

(45) Panzella, L.; Napolitano, A. Natural and Bioinspired Phenolic Compounds as Tyrosinase Inhibitors for the Treatment of Skin Hyperpigmentation: Recent Advances. *Cosmetics* **2019**, *6*, 57. https://doi.org/10.3390/cosmetics6040057.

(46)   Seo, B.; Yun, J.; Lee, S.; Kim, M.; Hwang, K.; Kim, J.; Min, K. R.; Kim, Y.; Moon, D. Barbarin as a New Tyrosinase Inhibitor from Barbarea Orthocerus. *Planta Med.* **1999**, *65*, 683–686. https://doi.org/10.1055/s-1999-14092.

(47)   Lu, R.; Liu, X.; Gao, S.; Zhang, W.; Peng, F.; Hu, F.; Huang, B.; Chen, L.; Bao, G.; Li, C.; Li, Z. New Tyrosinase Inhibitors from Paecilomyces Gunnii. *J. Agric. Food Chem.* **2014**, *62*, 11917–11923. https://doi.org/10.1021/jf504128c.

(48)   Takahashi, S.; Iwai, H.; Kosaka, K.; Miyazaki, T.; Osanai, Y.; Arao, N.; Tanaka, K.; Nagai, K.; Nakagawa, A. Byelyankacin: A Novel Melanogenesis Inhibitor Produced by *Enterobacter* Sp. B20. *J. Antibio.* **2007**, *60*, 717–720. https://doi.org/10.1038/ja.2007.93.

(49)   Dhifi, W.; Bellili, S.; Jazi, S.; Bahloul, N.; Mnif, W. Essential Oils' Chemical Characterization and Investigation of Some Biological Activities: A Critical Review. *Medicines* **2016**, *3*, 25. https://doi.org/10.3390/medicines3040025.

(50)   Singh, B.; Sharma, R. A. Plant Terpenes: Defense Responses, Phylogenetic Analysis, Regulation and Clinical Applications. *3 Biotech* **2015**, *5*, 129–151. https://doi.org/10.1007/s13205-014-0220-2.

(51)   Burt, S. Essential Oils: Their Antibacterial Properties and Potential Applications in Foods—a Review. *Int. J. Food Microbiol.* **2004**, *94*, 223–253. https://doi.org/10.1016/j.ijfoodmicro.2004.03.022.

(52)   Tajkarimi, M. M.; Ibrahim, S. A.; Cliver, D. O. Antimicrobial Herb and Spice Compounds in Food. *Food Control* **2010**, *21*, 1199–1218. https://doi.org/10.1016/j.foodcont.2010.02.003.

(53)   Kim, S.-I.; Park, C.; Ohh, M.-H.; Cho, H.-C.; Ahn, Y.-J. Contact and Fumigant Activities of Aromatic Plant Extracts and Essential Oils against Lasioderma Serricorne (Coleoptera: Anobiidae). *J. Stored Prod. Res.* **2003**, *39*, 11–19. https://doi.org/10.1016/S0022-474X(02)00013-9.

(54)   Fitzgerald, D. Analysis of the Inhibition of Food Spoilage Yeasts by Vanillin. *Int. J. Food Microbiol.* **2003**, *86*, 113–122. https://doi.org/10.1016/S0168-1605(03)00059-X.

(55)   Modzelewska, A.; Sur, S.; Kumar, S.; Khan, S. Sesquiterpenes: Natural Products That Decrease Cancer Growth. *Curr. Med. Chem. Agents* **2005**, *5*, 477–499. https://doi.org/10.2174/1568011054866973.

(56)   Schnitzler, P.; Koch, C.; Reichling, J. Susceptibility of Drug-Resistant Clinical Herpes Simplex Virus Type 1 Strains to Essential Oils of Ginger, Thyme, Hyssop, and Sandalwood. *Antimicrob. Agents Chemother.* **2007**, *51*, 1859–1862. https://doi.org/10.1128/AAC.00426-06.

(57)   Bhavaniramya, S.; Vishnupriya, S.; Al-Aboody, M. S.; Vijayakumar, R.; Baskaran, D. Role of Essential Oils in Food Safety: Antimicrobial and Antioxidant Applications. *Grain Oil Sci. Technol.* **2019**, *2*, 49–55. https://doi.org/10.1016/j.gaost.2019.03.001.

(58)   Chu, S. S.; Jiang, G. H.; Liu, Z. L. Insecticidal Compounds from the Essential Oil of Chinese Medicinal Herb Atractylodes Chinensis. *Pest Manag. Sci.* **2011**, *67*, 1253–1257. https://doi.org/10.1002/ps.2180.

(59)   Asakawa, Y.; Ishida, T.; Toyota, M.; Takemoto, T. Terpenoid Biotransformation in Mammals IV Biotransformation of (+)-Longifolene, (-)-Caryophyllene, (-)-Caryophyllene Oxide, (-)-Cyclocolorenone, (+)-Nootkatone, (-)-Elemol, (-)-Abietic Acid and (+)-Dehydroabietic Acid in Rabbits. *Xenobiotica* **1986**, *16*, 753–767. https://doi.org/10.3109/00498258609043566.

(60)   Bhatia, S. P.; Letizia, C. S.; Api, A. M. Fragrance Material Review on Elemol. *Food Chem. Toxicol.* **2008**, *46*, S147–S148. https://doi.org/10.1016/j.fct.2008.06.045.

(61)   Chao, W.-W.; Su, C.-C.; Peng, H.-Y.; Chou, S.-T. Melaleuca Quinquenervia Essential Oil Inhibits α-Melanocyte-Stimulating Hormone-Induced Melanin Production and Oxidative Stress in B16 Melanoma Cells. *Phytomedicine* **2017**, *34*, 191–201. https://doi.org/10.1016/j.phymed.2017.08.024.

(62)   Koirala, P.; Seong, S.; Zhou, Y.; Shrestha, S.; Jung, H.; Choi, J. Structure–Activity Relationship of the Tyrosinase Inhibitors Kuwanon G, Mulberrofuran G, and Albanol B from Morus Species: A Kinetics and Molecular Docking Study. *Molecules* **2018**, *23*, 1413. https://doi.org/10.3390/molecules23061413.

(63)   Spínola, V.; Mendes, B.; Câmara, J. S.; Castilho, P. C. Effect of Time and Temperature on Vitamin C Stability in Horticultural Extracts. UHPLC-PDA vs Iodometric Titration as Analytical Methods. *LWT - Food Sci. Technol.* **2013**, *50*, 489–495. https://doi.org/10.1016/j.lwt.2012.08.020.

(64)   Arulmozhi, V.; Pandian, K.; Mirunalini, S. Ellagic Acid Encapsulated Chitosan Nanoparticles for Drug Delivery System in Human Oral Cancer Cell Line (KB). *Colloids Surfaces B Biointerfaces* **2013**, *110*, 313–320. https://doi.org/10.1016/j.colsurfb.2013.03.039.

(65)   Parvez, S.; Kang, M.; Chung, H.-S.; Cho, C.; Hong, M.-C.; Shin, M.-K.; Bae, H. Survey and Mechanism of Skin Depigmenting and Lightening Agents. *Phyther. Res.* **2006**, *20*, 921–934. https://doi.org/10.1002/ptr.1954.

(66)   Ko, H.-H.; Chang, W.-L.; Lu, T.-M. Antityrosinase and Antioxidant Effects of Ent - Kaurane Diterpenes from Leaves of Broussonetia Papyrifera. *J. Nat. Prod.* **2008**, *71*, 1930–1933. https://doi.org/10.1021/np800564z.

Chapter 3

SARS-CoV-2 molecular docking studies of thio-analogue of marine natural product varitriol and its synthetic studies

3.1.Introduction

The cause of deadly COVID-19 (coronavirus disease 2019) is SARS CoV-2 (severe acute respiratory syndrome coronavirus-2).[1] Amongst the coronaviruses, SARS-CoV-2 is highly pathogenic with a higher fatality rate in humans and is believed to have originally appeared in animals like civets, camels, pangolins and bats.[2] In 2019, SARS-CoV-2 spread to the entire world after its outbreak in the Hubei province of Wuhan, China. The whole world grappled with various challenges due to this global pandemic because the important sectors such as pharmaceutical, health, education, social, economic, etc. were extensively affected. This ultimately caused event cancellations, unemployment, prohibition to gather in public places, declined foreign and domestic trades and led to the downfall of the global economy and loss of livelihood.[1]

Humans become infected with viruses such as SARS-CoV-2 by indirect or direct exposure to respiratory secretions. Coronavirus-infected patients may exhibit a variety of symptoms, ranging from moderate to severe symptomatic to asymptomatic features. There may be symptoms such as headaches, coughs, colds, fatigue, aches, fever, loss of taste, loss of smell, diarrhoea, discolouration of fingers or toes, breathing difficulties, or organ dysfunction.[1] These viruses are regarded as recurring health risks because of their widespread distribution, their wide genetic diversity, frequent recombination of their genomes, and their increasing activity at the human-animal interface. Currently, COVID-19 is still spreading throughout the world. People are hoping for specific treatments in addition to vaccinations.[3] It is, therefore, necessary to continue the search for effective therapy for SARS-CoV-2.

In the present study, we designed a new anti-viral agent inspired by a marine natural product and took up its synthesis.

Chapter 3

Section A: SARS-CoV-2 molecular docking studies of thiovaritriol to evaluate its potential for COVID-19 treatment

3.2. Introduction

SARS-CoV-2 is spreading at an alarming rate globally. To combat SARS-CoV-2, antiviral medicines need to be developed urgently. Conventional drug design and development may require a lot of money, time and manpower, but there is no guarantee that the desired candidates will be effective and potent. As a result, computer assisted drug design (CADD) has emerged over the past few years as a feasible and effective alternative to traditional approaches, since they decrease the cost burden while improving the results after bridging the gap between chemical and biological science. As one of these CADD tools, molecular-docking should not be overlooked because it provides a comprehensive understanding of how the identified hits interact with biological targets to explain their mode of action. This method concentrates scientists' attention on the most promising chemicals, thereby eliminating the need to conduct tests of all the candidates in synthetic and biological laboratories to test their potency.[1,3]

The marine ecosystem is known to be an important source of potential drugs. Varitriol **1** was first isolated by Barrero *et al.* from the marine fungus *Emericella variecolor* in the year 2002.[4] This fungus was isolated from a sponge collected in Venezuelan waters of the Caribbean Sea. The structure of varitriol **1** is made up of a furanose block and an aromatic block and it displays excellent anti-tumour properties (Figure 3.1).[4,5] It does not inhibit the growth of bacteria and yeast at 100 μg/mL and also, it has not been explored for antiviral properties to date. [4,5]

- Renal cancer GI_{50} = 4.63 x 10^{-7} M
- Breast cancer GI_{50} = 2.10 x 10^{-7} M
- CNS cancer GI_{50} = 2.44 x 10^{-7} M
- Prostate cancer GI_{50} = 1.10 x 10^{-6} M
- Leukemia GI_{50} = 2.52 x 10^{-5} M
- Ovarian cancer GI_{50} = 6.82 x 10^{-5} M
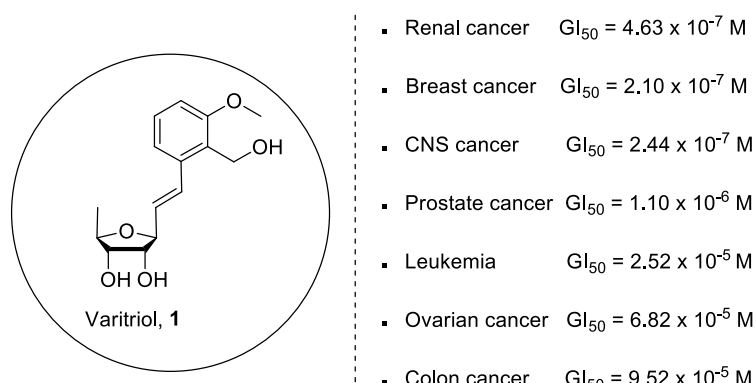- Colon cancer GI_{50} = 9.52 x 10^{-5} M

Varitriol, **1**

Figure 3.1: Biological activities of varitriol **1**. GI_{50} = concentration of a drug that reduces total cell growth by 50%.

Chapter 3

This section discusses SARS-CoV-2 molecular docking studies of the marine natural product varitriol **1** along with thiovaritriol **2** and 3'-*epi*- thiovaritriol **3** (Figure 3.2) in search of novel drug-like molecules for COVID-19 treatment.

Varitriol, **1**   Thiovaritriol, **2**   3'-*epi*-Thiovaritriol, **3**
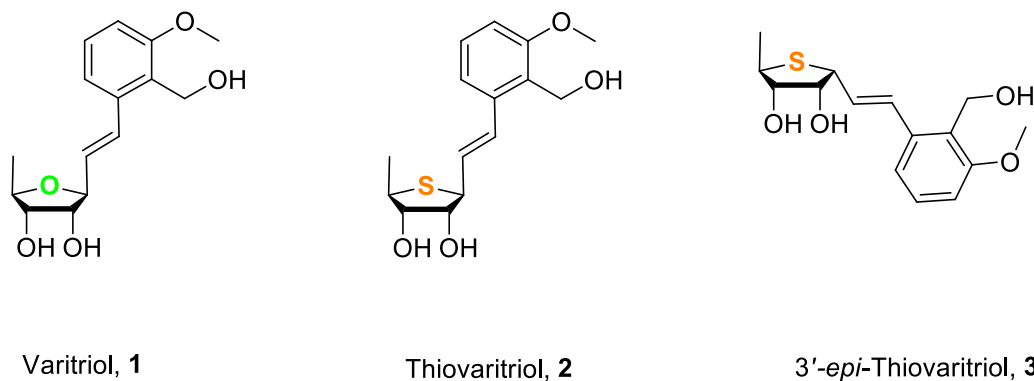
Figure 3.2: Structures of varitriol **1**, thiovaritriol **2** and 3'-*epi*-thiovaritriol **3**.

3.3. Objectives

1. To design a novel antiviral agent inspired by the bioactive marine natural product varitriol **1**.

2. To evaluate the antiviral potential of varitriol **1**, thiovaritriol **2** and 3'-*epi*-thiovaritriol **3** against SARS-CoV-2 using molecular docking studies.

3.4. Literature review on selected antiviral drugs against SARS-CoV-2: Molecular docking studies and its use in COVID-19 treatment

Different studies have been conducted on natural and synthesized compounds against SARS-CoV-2 by targeting different viral enzymes and proteins.[3,6] The U.S. Food and Drug Administration (FDA) has authorized convalescent plasma therapy with high antibody levels to treat COVID-19 during an emergency.[7,8] Inhibitors of different RNA viruses are also being repurposed for the treatment of COVID 19.[3] The backbone of current antiviral medication isnucleoside analogues including remdesivir, molnupiravir and favipiravir.[6]
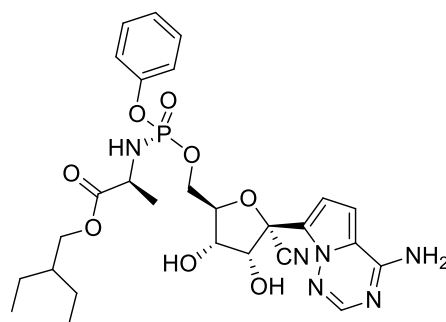
Remdesivir, **4**

Figure 3.3: Structure of remdesivir **4**.

Molecular docking of remdesivir **4** (Figure 3.3) with SARS-CoV-2 basically formed interactions such as conventional hydrogen bonds, electrostatic bonds, hydrophobic interactions (pi-alkyl interactions) and also unfavourable hydrogen bonds.[1,6] The binding energies of the **4** with different selected proteins of SARS-CoV-2 (PDB ID: 7BV2, 6M71, 6LU7, 6Y2E) were in the range of -6.5 to -9.2 kcal/mol.[1,6,9] Remdesivir **4** is the FDA-approved antiviral in hospitalized COVID-19 patients.[2,6] Bio-activity studies have demonstrated that **4** acts by inhibiting the viral RNA replication inside the host body.[1] Viral RNA replication is controlled by RNA-dependent RNA polymerase (RdRp). The host lacks a functional equivalent to this protein RdRp. Due to the absence of a counterpart to RdRp in mammalian cells, its inhibition is not expected to cause target-related side effects. Therefore, RdRp is considered an important therapeutic target.[1,3,6] The intravenous administration of remdesivir suffers limitations, especially for unhospitalized patients. Although it is effective, its impotency in patients with immunodeficiency, heart failure, hypotension, respiratory dysfunction, and renal impairment has prevented it from being a solution in the fight against the deadly virus. It has been found that remdesivir also has a few adverse effects, including cognitive delirium, kidney damage, nausea, vomiting, and rectal bleeding.[1,2]
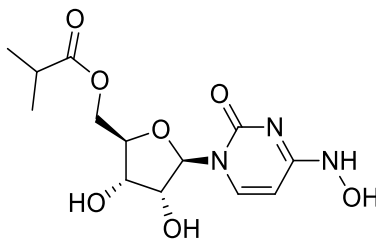
Molnupiravir, **5**

Figure 3.4. Structure of molnupiravir **5**.

Molecular docking of molnupiravir **5** (Figure 3.4) with SARS-CoV-2 mainly formed interactions such as conventional hydrogen bonds, covalent bonds (carbon hydrogen bonds), non-covalent bonds (van der Waals, pi-cation, pi-anion, pi-sigma) and hydrophobic interactions (pi-alkyl interactions).[2,6] The binding energies of the **5** with different selected proteins of SARS-CoV-2 (PDB ID: 6M71, 7C2K, 7BV2) were in the range of -7.3 to -10 kcal/mol.[1,2,6] One possible antiviral mechanism of molnupiravir is inhibition of viral RNA replication by targeting SARS-CoV-2 (RdRp).[2,3,6,10] **5** is currently in phase II/III clinical studies.[2] Fortunately, recent studies of a phase II trial have revealed that by administrating **5** orally, nasopharyngeal SARS-CoV-2 infection can be highly reduced. **5** fascinatingly has a favourable safety and tolerability profile.[3] Interestingly, studies revealed that **5** is active against the drug resistance viral variants, for instance, the variants resistant to remdesivir.[2] Additionally, **5** was able to inhibit the SARS-CoV-227.5 times more as compared to remdesivir. Hence, molnupiravir could fight the present and future viral mutations.[6]
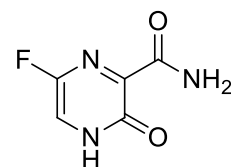
Favipiravir, **6**

Figure 3.5: Structure of favipiravir**6**.

Molecular docking of favipiravir **6** (Figure 3.5) with SARS-CoV-2 showed conventional hydrogen bonding, halogen (fluorine) interactions and pi-anion interactions.[3,11] The binding energies of **6** with different selected proteins of SARS-CoV-2 (PDB ID:6LVN, 6M3M,

6W37, 6VXS, 6LXT, 6WJI, 6W75·B, 6W4B, 6VSB, 6Y2E, 6VWW, 6W9C, 6VYB, 6M71.A, 6M71.C, 6W75.A, 6VXX) were in the range of -4.0 to -6.7 kcal/mol.[1,9,12] In vitro studies of favipiravir **6** showed that it can effectively inhibit SARS-CoV-2 by inhibiting the activity of RNA dependent RNA polymerase (RdRp) of RNA viruses.[12,13] The outcomes of phase III clinical trials of **6** have demonstrated that it can quicken the recovery of patients suffering from COVID-19. Especially, the patients with non-severe novel coronavirus recovered faster than the control group (group without favipiravir **6** treatment).[14] The 7-day clinical recovery rate of the common COVID-19 patients treated with favipiravir **6** was 71.43%, compared to that of the control group which was 55.68%. Also, treatment of patients with hypertension/diabetes with favipiravir **6** felt faster relief from symptoms like fever and cough.[13] In addition, the CT scan of the chest showed significant improvement in the patients treated with favipiravir **6**.[3] Furthermore, COVID-19 patients treated with favipiravir **6** were observed with good tolerance and lesser side effects.[14] Large-scale clinical trials are pending which can further confirm the effectiveness and safety of favipiravir **6** in the treatment of COVID-19.[3]

As described above, the drugs used for the treatment of SARS-CoV-2 infection are effective but suffer from different drawbacks. Also, these drugs are gradually developing resistance to viral variants. To fight the viral variants and to prevent viruses with similar genomic and pathological characteristics from returning a few years later, safe and effective drugs need to be developed.

Scope of the present study

As part of the ongoing global efforts to prevent the spread of SARS-CoV-2 we directed our focus to design and develop novel anti-viral agents inspired by a bioactive marine natural product varitriol.

3.5.Results and discussion

To fight SARS-CoV-2 we designed a thio-version of varitriol **1**. Varitriol **1** consists of a furanose ring. The furanose ring can be metabolically and chemically unstableand therefore associated with clinical toxicity.[15]
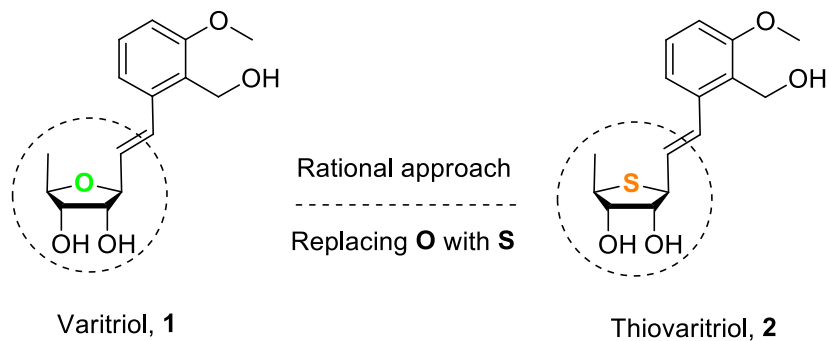
Figure 3.6: Rational design for thiovaritriol inspired from marine natural product varitriol.

To design a novel candidate for SARS-CoV-2, we thought to replace the furanose ring of varitriol **1** with a thiosugar ring to form thiovaritriol **2** (Figure 3.6). So, the thio-version of varitriol contains a thiolane unit (thiosugar block) and an aromatic block.

In search of potent inhibitors of SARS-CoV-2, we performed *in silico* screening of ligands against the selected protein (PDB ID: 6VWW) of SARS-CoV-2 using molecular docking.[16] The free software AutoDock 4.2 was used for this study.[17,18] To begin with blind docking was carried out to understand the binding mode of the ligands into the protein site.
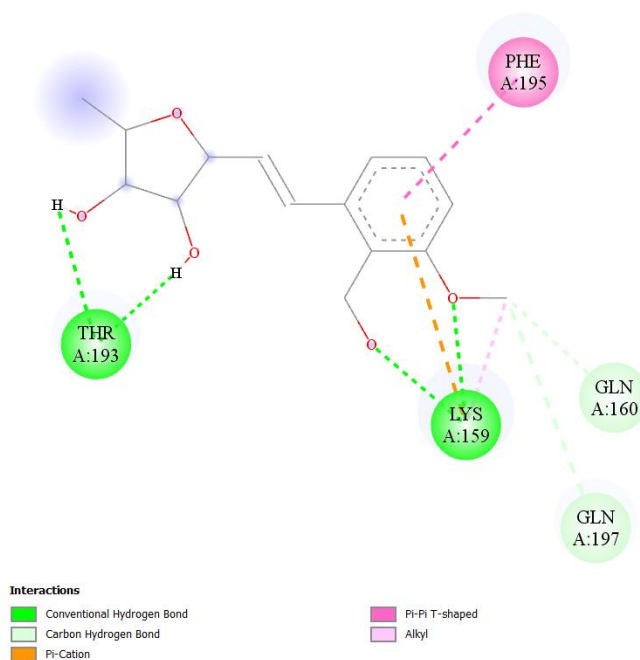

Figure 3.7: 2D binding conformation ofvaritriol **1** to SARS CoV-2 (Blind Docking).

Varitriol showed four conventional hydrogen-bonding interactions with the amino acid residues Thr193 and Lys159. It formed two carbon-hydrogen bonds with the protein residues Gln160 and Gln197. Further, it exhibited π-cation interaction with the amino acid residue Lys159. Additionally, it also formed π-π-T-shaped interaction with the protein residue Phe195 and alkyl interaction with the amino acid residue Lys159 (Figure 3.7). Figure 3.8 represents 3D binding conformations of varitriol **1** to SARS CoV-2 obtained as a result of blind docking.

Figure 3.8: 3D binding conformation of varitriol **1** to SARS CoV-2 (Blind Docking). A) Ribbon structure of protein. B) Surface structure of protein.

Figure 3.9: 2D binding conformation of thiovaritriol**2**to SARS CoV-2 (Blind docking).

Thiovaritriol **2** showed four conventional hydrogen-bonding interactions with the binding site residues Ser294, His250, Thr341 and His235. It formed a carbon-hydrogen bond with the protein amino acid residue Val292 and a π-donor hydrogen bond with the amino acid residue

His250. Additionally, it exhibited alkyl & pi-alkyl interactions with the protein amino acid residues Leu346, Lys345, Tyr343 and Val292 (Figure 3.9). Figure 3.10 represents 3D binding conformations of thiovaritriol **2** to SARS CoV-2 obtained as a result of blind docking.
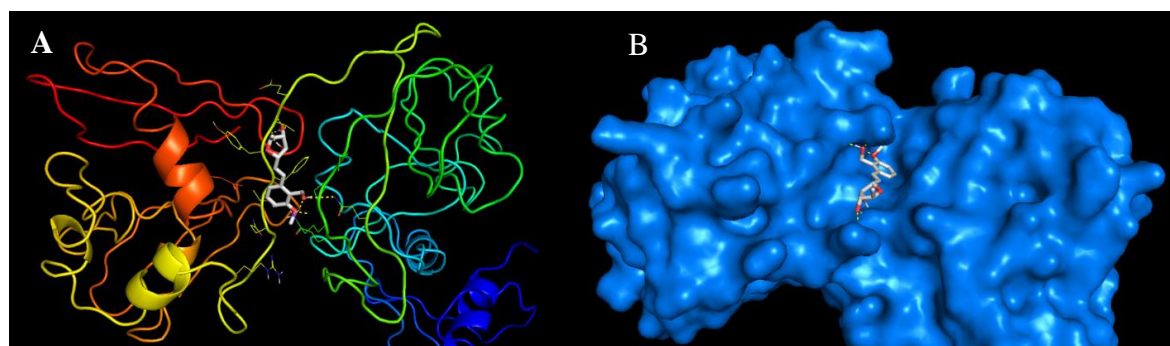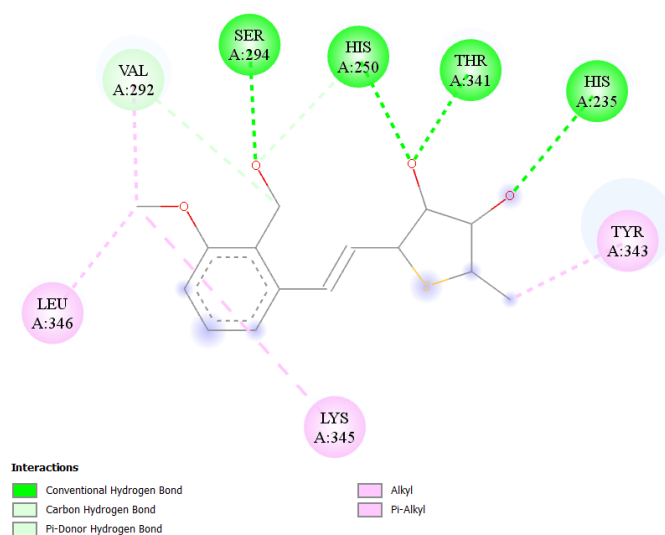

Figure3.10: 3D binding conformation of thiovaritriol **2** to SARS CoV-2 (Blind Docking). A) Ribbon structure of protein. B) Surface structure of protein.

Figure 3.11: 2D binding conformation of 3'-*epi*-thiovaritriol **3** to SARS CoV-2 (Blind docking).

Hoping for the possibility to enhance the activity of thiovaritriol **2**, we envisioned to dock the 3'-epimer of thiovaritiol **3** with SARS-CoV-2. It is well known in the literature that

diastereomers of drug candidates can have a significant difference in their activities.[3] Blind docking results of the 3'-*epi*-thiovaritriol **3** showed several interactions with SARS-CoV-2. It showed four conventional hydrogen bonds with the protein amino acid residues Thr193 and Lys159. It formed a carbon-hydrogen bond with Gln160. Further it exhibited π-cation interaction with amino acid residue Lys159. Additionally it showed sulphur interaction with protein residue Phe195 and alkyl interaction with the amino acid residue Lys159 (Figure 3.11). Figure 3.12 represents 3D binding conformations of 3'-*epi*-thiovaritiol **3** to SARS CoV-2 obtained as a result of blind docking.
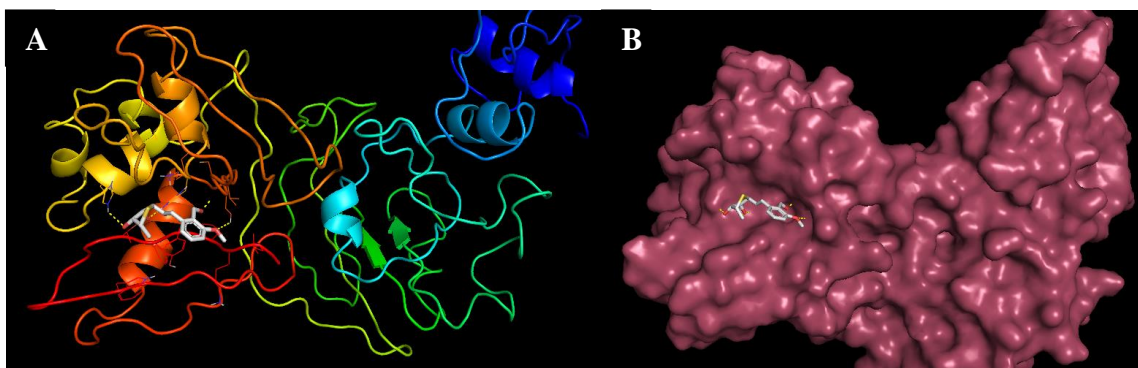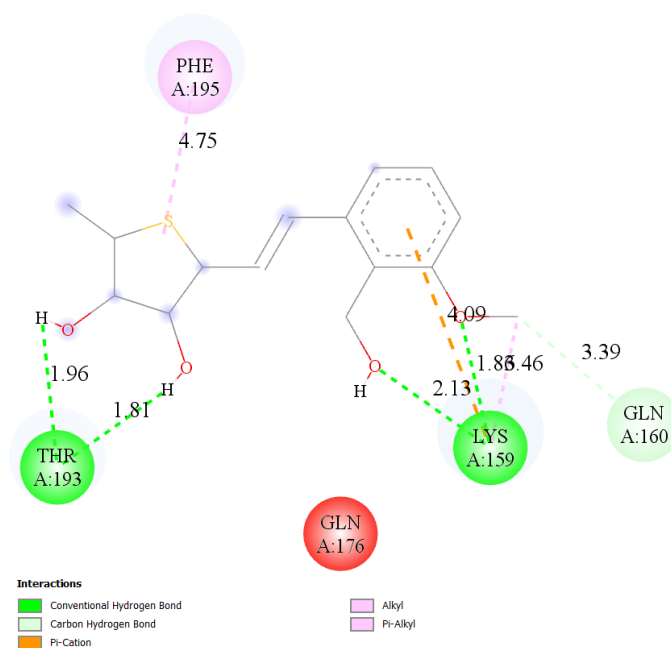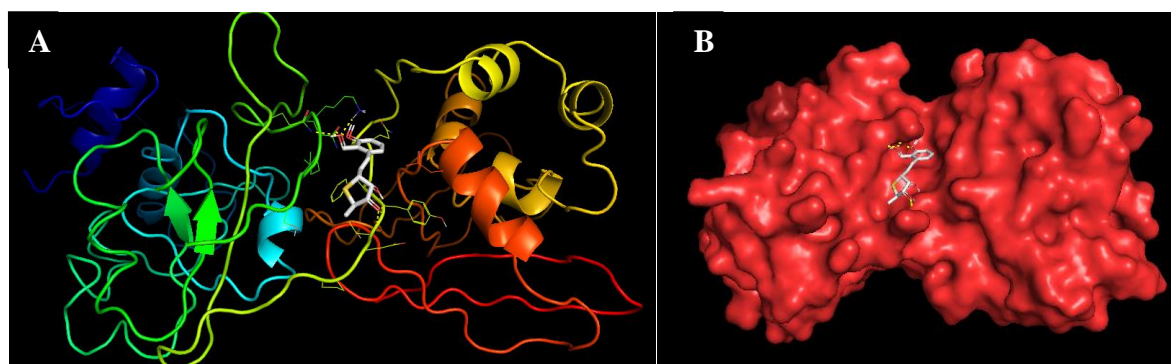

Figure 3.12: 3D binding conformation of 3'-*epi*-thiovaritiol **3** to SARS CoV-2 (Blind Docking). A) Ribbon structure of protein. B) Surface structure of protein.
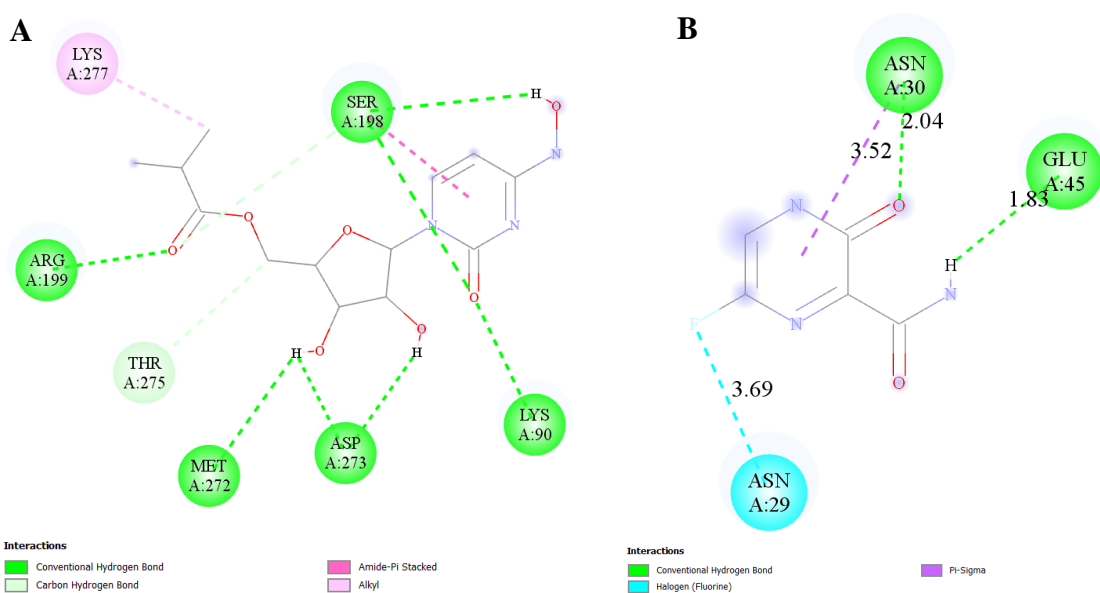

Figure 3.13: 2D binding conformations of A) Molnupiravir **5** and B) Favipiravir **6** to SARS CoV-2 (Blind docking).

The protein-ligand interactions were compared with the standard drugs molnupiravir **5** and favipiravir **6**. Molnupiravir **5** formed seven conventional hydrogen bonds with protein residues Arg199, Met272, Asp273, Lys90 and Ser198. Further, it showed two carbon-hydrogen bonds with amino acid residues Th275 and Ser198. Additionally, it exhibited an amide pi-stacked interaction with the amino acid residue Ser198 and an alkyl interaction with the amino acid residue Lys277 (Figure 3.13). Favipiravir **6** formed two conventional hydrogen bonds with protein residues Asn30 and Glu45. It showed pi-sigma interaction with protein residue Asn30. Further, it exhibited a halogen interaction with protein residue Asn29 (Figure 3.13). Figure 3.14 represents 3D binding conformations of molnupiravir **5** to SARS CoV-2 and Figure 3.15 represents 3D binding conformations of favipiravir **6** to SARS CoV-2 obtained as a result of blind docking.
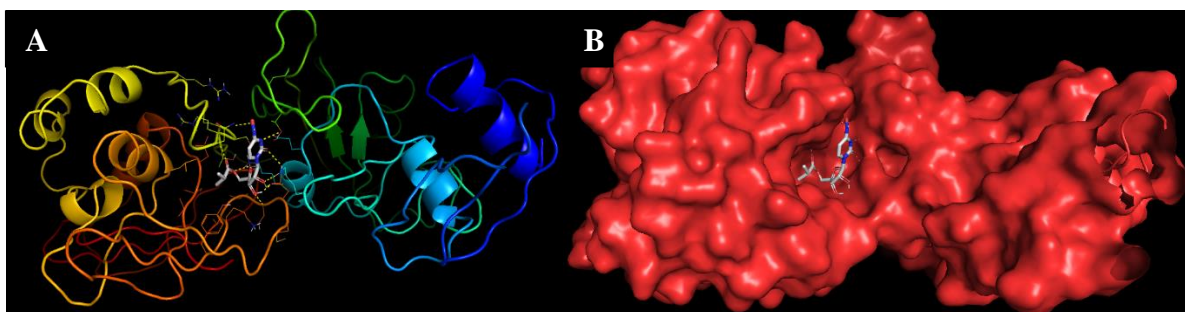
Figure 3.14: 3D binding conformation of molnupiravir **5** to SARS CoV-2 (Blind Docking). A) Ribbon structure of protein. B) Surface structure of protein.
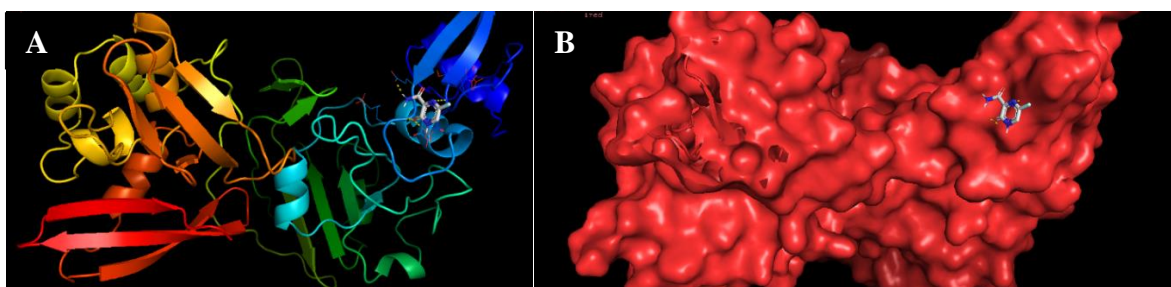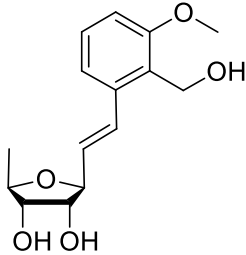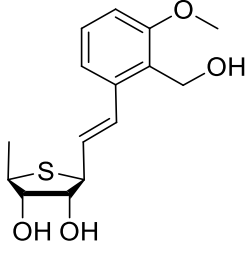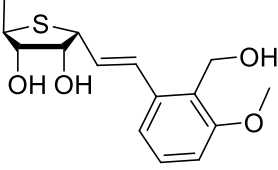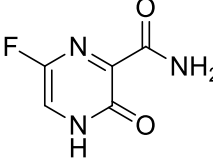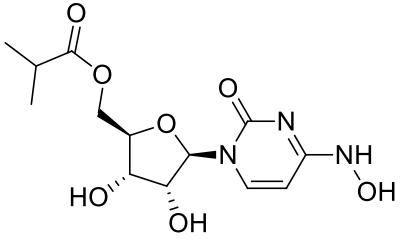
Figure 3.15: 3D binding conformation of favipiravir **6** to SARS CoV-2 (Blind Docking). A) Ribbon structure of protein. B) Surface structure of protein.

Table 3.1: Binding energies of various ligands to the selected protein (6VWW) of SARS CoV-2 obtained by blind docking.

Sr No.	Ligands	B.E (Kcal/mol)	Ki values (µM)
1	Varitriol, **1**	-6.20	28.43
2	Thiovaritriol, **2**	-6.61	14.29
3	3′-*epi*-Thiovaritriol, **3**	-7.37	3.96
4	Favipiravir, **6**	-4.14	924.35

5	Molnupiravir, **5**	-7.18	5.44

B. E = binding energy Ki = inhibition constant

To understand the amount of binding exhibited by the ligands to the protein, the binding energy was evaluated. In the process of complex formation between the protein and its ligand, the extent of energy released is determined by binding energy. A more negative value of binding energy more stable is the protein-ligand complex and hence, better will be the activity.[19] A summary of the binding energies of all the ligands with the target protein of SARS-CoV-2 using blind docking has been given in Table 3.1. Interestingly, thiovaritriol **2** (-6.61 Kcal/mol) and 3'-*epi*-thiovaritriol **3** (-7.37 Kcal/mol) portrayed better binding efficiency than the parent varitriol **1** (-6.20 Kcal/mol). Both thiovaritriol **2** and 3'-*epi*-thiovaritriol **3** showed higher affinity to SARS-CoV-2 than the standard drug favipiravir **6** (-4.14 Kcal/mol). The thiovaritriol–enzyme complex and 3'-*epi*-thiovaritriol–enzyme complex is stabilized mainly by hydrogen bonds, covalent bonds, non-covalent bonds and hydrophobic interactions. Both these ligands form more interactions with the protein than the reference drug favipiravir **6** in their respective pockets. Further, 3'-*epi*-thiovaritriol **3** showed higher potency than the reference drug candidate molnupiravir **5** (-7.18 Kcal/mol). The interaction of sulphur from the thiolane unit of 3'-*epi*-thiovaritriol **3** with the amino acid residue Phe195 may explain the apparent higher potency of **3** to SARS-CoV-2. Additionally, 3'-*epi*-thiovaritriol **3** portrayed a better affinity to SARS-CoV-2 than its diastereomer thiovaritriol **2** as seen by their docking scores. This difference in binding affinities might be due to the different binding orientations of thiovaritriol **2** and 3'-*epi*-thiovaritriol **3** to their respective binding pocket of the enzyme. Inhibition constant (Ki) is asign of how potential an inhibitor can be. It is the concentration required to produce half-maximum inhibition.[20] From Inhibition constants (Ki) (Table 3.1) it can be inferred that thiovaritriol **2** (14.29 μM) and 3'-*epi*-thiovaritriol **3** (3.96 μM)) are better inhibitors of SARS CoV-2 than parent varitriol

(28.43 µM) and the reference favipiravir **6** (924.35 µM). *3'-epi*-Thiovaritriol **3** could bind to SARS-CoV-2 even better than the reference molnupiravir **5** (5.44 µM).

In literature, **5** and **6** have been docked with different proteins of SARS-CoV-2 to understand the stable complex formation with the least binding energies. As discussed in section 3.4, molecular docking of molnupiravir **5** with SARS-CoV-2 (PDB ID: 6M71) has binding energy -7.3 kcal/mol in the literature.[6] This result is comparable with the binding energy of **5** (-7.18 kcal/mol) with SARS-CoV-2 (PDB ID: 6VWW) in the present study. Similarly, the binding energy (-4.14 kcal/mol) of favipiravir **6** complex with SARS-CoV-2 (PDB ID: 6VWW) in the present study is comparable with that of thereported result which is -4.7 kcal/mol (PDB ID: 6VWW).[12]

To check the consistency, site-specific docking was performed of all the ligands with the selected protein (PDB ID: 6VWW) of SARS-CoV-2 using the free software AutoDock 4.2. The several interactions between ligand and protein helped to understand their binding mode into the active site of the protein.

Figure 3.16: 2D binding conformations of varitriol **1** to SARS CoV-2 (Site-specific docking).

Varitriol **1** showed three conventional hydrogen bonding with the amino acid residues

Thr275, Leu346. It formed one carbon-hydrogen bond with the protein residue Asn75. Further it exhibited two alkyl interactions with amino acid residues Met272, Ile270 (Figure 3.16). Figure 3.17 represents 3D binding conformations of varitriol **1** to SARS CoV-2 obtained as a result of site-specific docking.

Figure 3.17: 3D binding conformation of varitriol **1** to SARS CoV-2 (Site-specific docking). A) Ribbon structure of protein. B) Surface structure of protein.
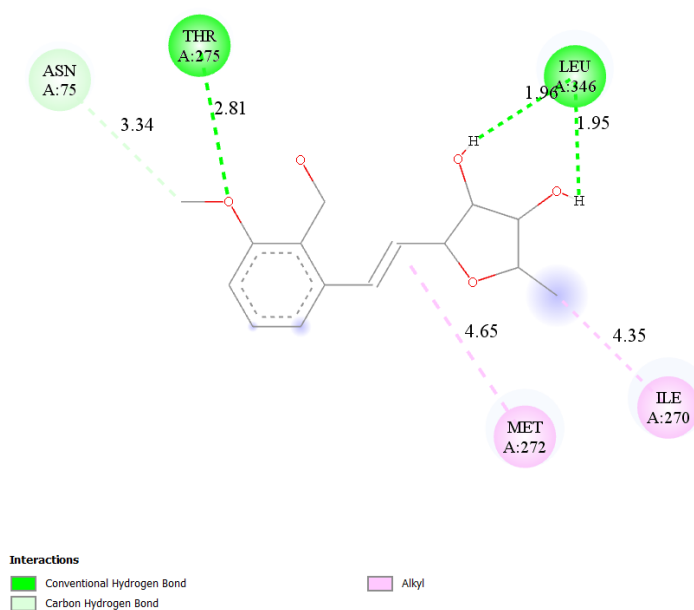

Figure 3.18: 2D binding conformations of thiovaritriol **2** to SARS CoV-2 (Site-specific docking).

Thiovaritriol **2** formed three conventional hydrogen bonds with the amino acid residues Val276, Thr275, Asn75. It showed Van der Waals interactions with the protein residue Asp324. Further, it exhibited pi-donor hydrogen-bond with the amino acid residue Ser274.

Additionally, Thiovaritriol **2** was found to have three alkyl interactions with the amino acid residues Met272, Lys277, Ile270 and pi-alkyl interaction with the amino acid residue Met272 (Figure 3.18). Figure 3.19 represents 3D binding conformations of thiovaritriol **2** to SARS CoV-2 obtained as a result of site-specific docking.

Figure 3.19: 3D binding conformation of thiovaritriol **2** to SARS CoV-2 (Site-specific docking). A) Ribbon structure of protein. B) Surface structure of protein.
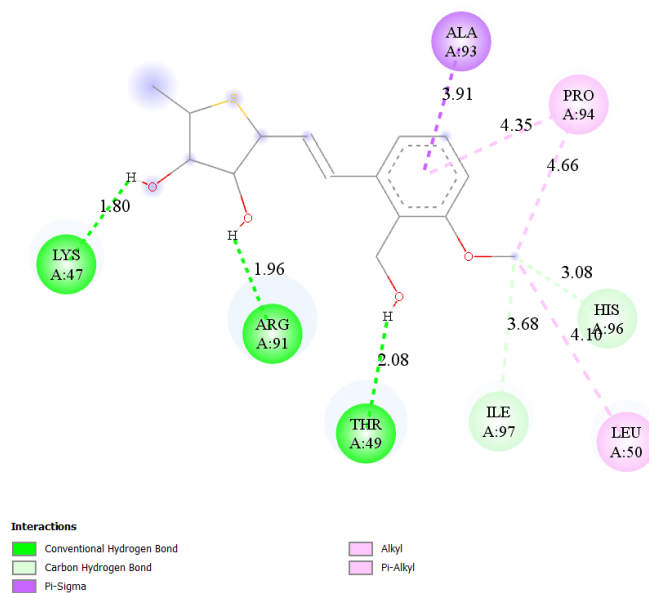
Figure 3.20: 2D binding conformations of 3'-*epi*-thiovaritriol **3** to SARS CoV-2 (Site-specific docking).

3'-*epi*-Thiovaritriol **3** formed three conventional hydrogen bonds with the amino acid residues Lys47, Arg91, Thr49. It showed two carbon-hydrogen bonds with the amino acid residues Ile97, His96. Further, it was found to have pi-sigma interaction with the amino acid

residue Ala93. Additionally, it exhibited two alkyl interactions with the protein residues Pro94, Leu50 and pi-alkyl interaction with the amino acid residues Pro94 (Figure 3.20). Figure 3.21 represents 3D binding conformations of 3'-*epi*-thiovaritriol **3** to SARS CoV-2 obtained as a result of site-specific docking.
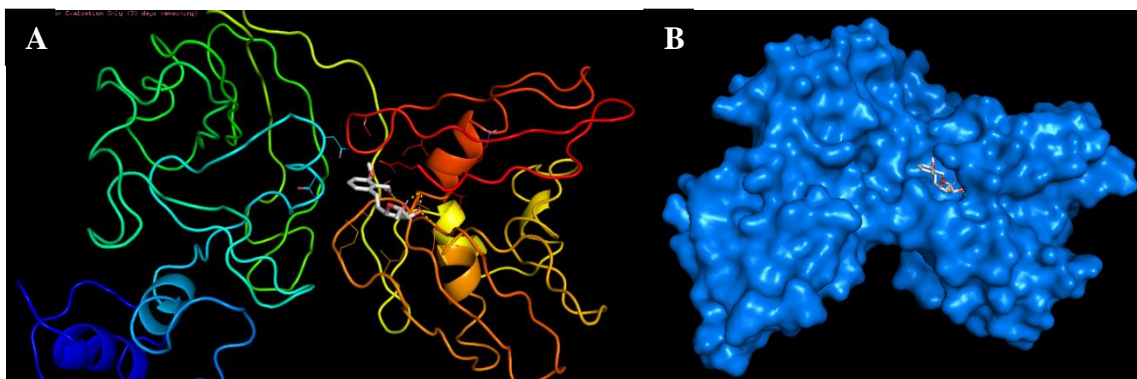

Figure 3.21: 3D binding conformation of 3'-*epi*-thiovaritriol **3** to SARS CoV-2 (Site-specific docking). A) Ribbon structure of protein. B) Surface structure of protein.
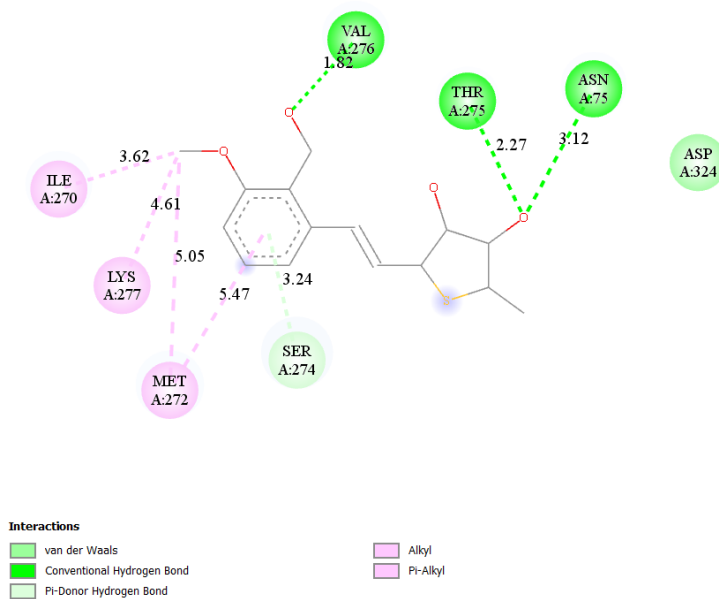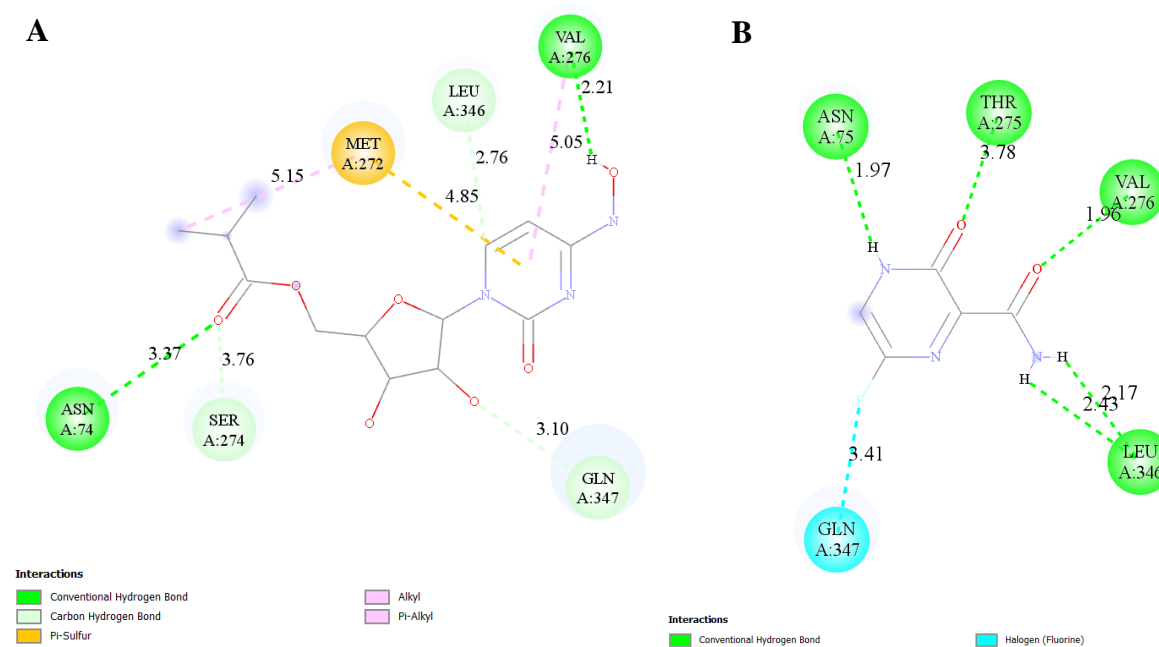

Figure 3.22: 2D binding conformations of A) molnupiravir **5** and B) favipiravir **6** to SARS CoV-2 (Site-specific docking).

The site-specific protein-ligand interactions were compared with standard drugs molnupiravir **5** and favipiravir**6**. Molnupiravir **5** showed two conventional hydrogen bonds with the protein

residues Asn74, Val276. It also formed three carbon-hydrogen bonds with the amino acid residues Ser274, Gln347, Leu346. Further it showed pi-sulfur ineraction with the protein residue Met272. Additionally, it exhibited alkyl interaction with the amino acid residue Met272 and pi-alkyl interaction with the amino acid residue Val276 (Figure 3.22). Favipiravir **6** showed five conventional hydrogen bond interactions with protein residues Asn75, Thr275, Val276, Leu346. Additionally, it was found to have a halogen interaction with the amino acid residue Gln347 (Figure 3.22). Figure 3.23 represents 3D binding conformations of molnupiravir **5** to SARS CoV-2 obtained as a result of site-specific docking. Figure 3.24 represents 3D binding conformations of favipiravir **6** to SARS CoV-2 obtained as a result of site-specific docking.
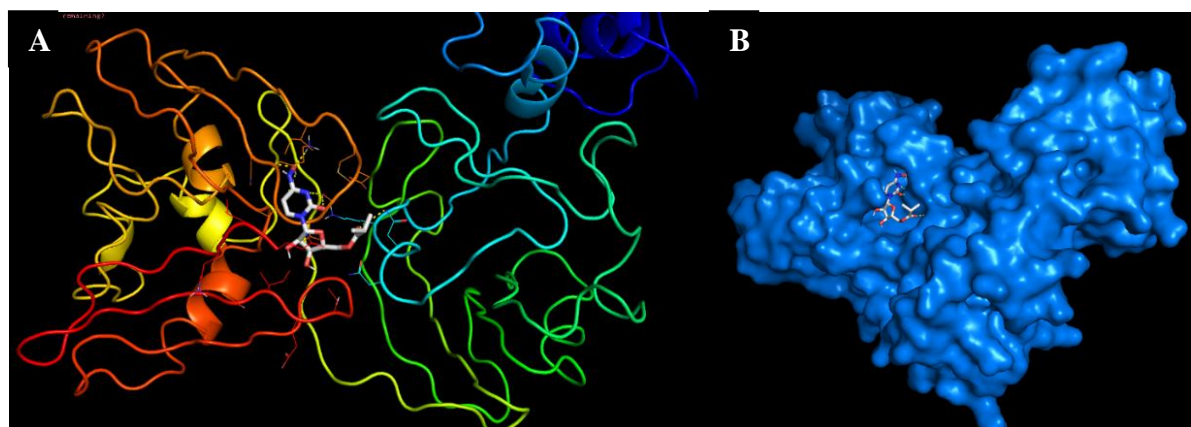
Figure 3.23: 3D binding conformation of molnupiravir **5** to SARS CoV-2 (Site-specific docking). A) Ribbon structure of protein. B) Surface structure of protein.
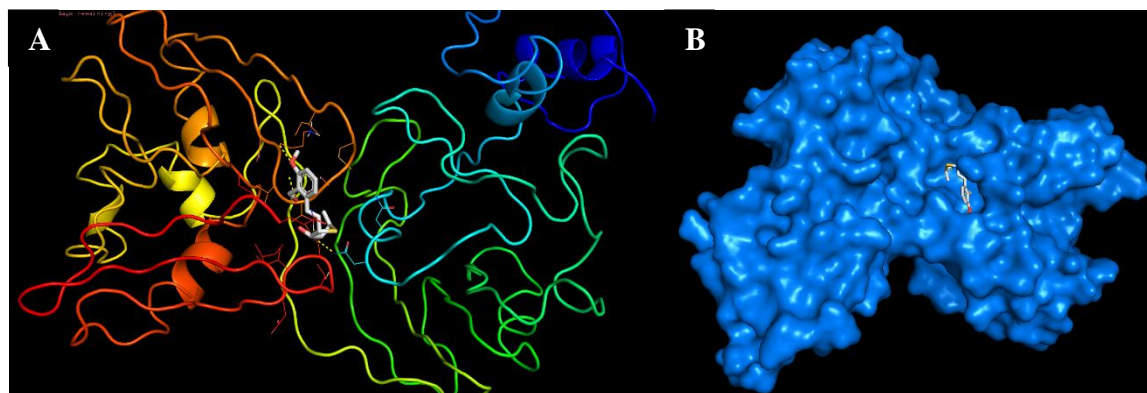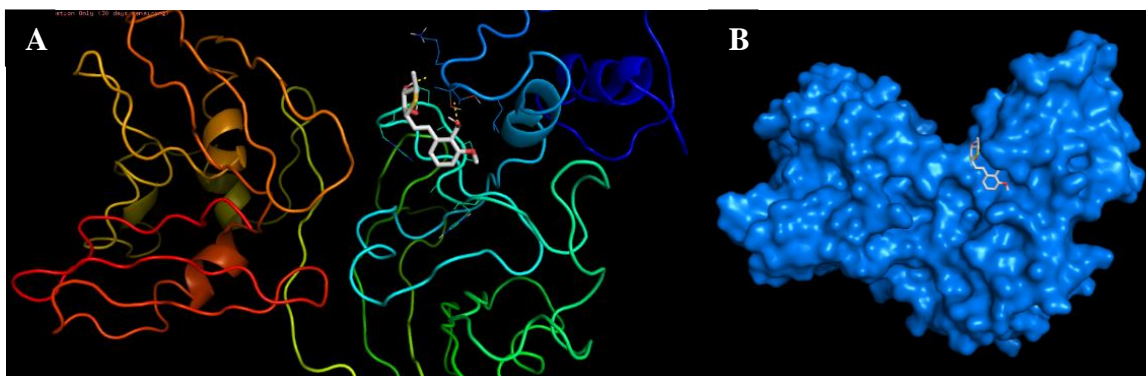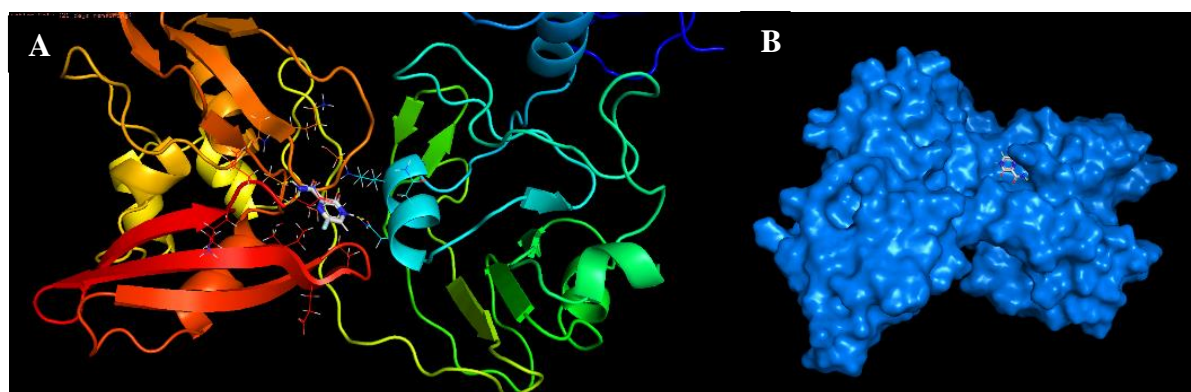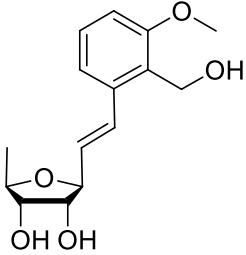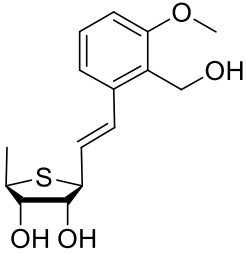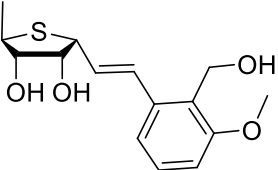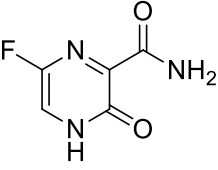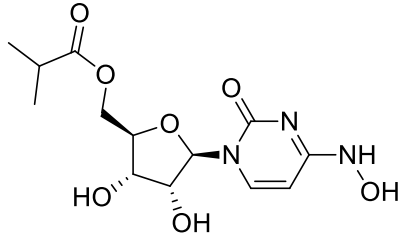

Figure 3.24: 3D binding conformation of favipiravir **6** to SARS CoV-2 (Site-specific docking). A) Ribbon structure of protein. B) Surface structure of protein.

Chapter 3

Table 3.2: Binding energies of various ligands to the selected protein (6VWW) of SARS CoV-2 obtained as a result of site-specific docking.

Sr No.	Ligands	B.E (Kcal/mol)	Ki values
1	Varitriol, **1**	-5.01	212.41 µM
2	Thiovaritriol, **2**	-6.26	30.97 µM
3	3′-*epi*-Thiovaritriol, **3**	-6.45	18.62 µM
4	Favipiravir, **6**	-3.29	3.85 mM

5	Molnupiravir, **5**	-4.77	316.93 µM

B.E = binding energy Ki = inhibition constant

During the molecular docking process, it was observed that even though all the ligands bound to the same binding pocket, thiovaritriol **2** (-6.26 Kcal/mol) and 3'-*epi*-Thiovaritriol **3** (-6.45 Kcal/mol) had the most negative binding energies, hence more efficient binding interaction in comparison with the parent varitriol **1** (-5.01 Kcal/mol) (Table 3.2). Also, thiovaritriol **2** and 3'-*epi*-thiovaritriol **3** showed better binding affinity and interaction compared to the standard drugs molnupiravir **5** (-4.77 Kcal/mol) and favipiravir **6** (-3.29 Kcal/mol). As seen in 2D conformation images of the interaction of thiovaritriol **2** and 3'-*epi*-thiovaritriol **3** with the specific protein site, both these ligands form a total of nine stable interactions with the protein site. These interactions mainly include stable hydrogen bonds, covalent bonds, non-covalent bonds and hydrophobic interactions. The calculated lower binding energies of thiovaritriol **2** and 3'-*epi*-thiovaritriol **3** is possibly due to the stable & more number of interactions of these ligands with the protein site as compared to varitriol **1** and the reference drugs molnupiravir **5** & favipiravir **6**. Additionally, 3'-*epi*-thiovaritriol **3** was predicted with the most negative binding affinity compared to thiovaritriol **2**. As discussed earlier, this difference in binding affinities might be due to the different binding orientations of thiovaritriol **2** and 3'-*epi*-thiovaritriol **3** to the binding pocket of the enzyme. As seen in table 3.2, the inhibition constant (Ki) of thiovaritriol **2** (30.97 µM) and 3'-*epi*-thiovaritriol **3** (18.62 µM)) are lower than the parent varitriol (212.41 µM) and the reference drugs molnupiravir **5** (316.93 µM) & favipiravir **6** (3.85 mM). In addition, 3'-*epi*-thiovaritriol **3** bears lower inhibition constant than its diastereomer of thiovaritriol **2**.

In a nutshell, thiovaritriol **2** forms conventional hydrogen bonds, carbon hydrogen bonds, pi-donor hydrogen bonds, and alkyl and pi-alkyl interactions with the SARS-CoV-2 protein. 3'-*epi*-Thiovaritriol **3** forms conventional hydrogen bonds, carbon hydrogen bonds, pi-cation/pi-

sigma, alkyl and pi-alkyl interactions with the SARS-CoV-2 protein. From the molecular docking studies, we can infer that thiovaritriol **2** and 3*'-epi*-thiovaritriol **3** portrayed better binding affinitiesto SARS-CoV-2 than the parent varitriol **1**. This is evident from the more negative values of binding energies of thiovaritriol **2** (-6.26 kcal/mol) and 3*'-epi*-thiovaritriol **3** (-6.45 kcal/mol) compared to that of varitriol **1** (-5.01 kcal/mol). Also, it can be inferred that 3*'-epi*-thiovaritriol **3**have a stronger binding affinity towards the binding site of the SARS-CoV-2 protein than its diastereomer thiovaritriol **2** (as evident from the binding energy values). Hence, thiovaritriol **2** and 3*'-epi*-thiovaritriol **3** can be a lead in the search for potential antiviral agents. In addition, we disclose the method towards the synthesis of these molecules which is discussed in the next section of this chapter.

3.6. Conclusion

1. Varitriol **1** , thiovaritriol **2** and 3*'-epi*-thiovaritriol **3** are evaluated for their use in the treatment of SARS CoV-2 infection using molecular docking studies for the first time.
2. Both the thio-analogues of varitriol i.e. thiovaritriol **2** and3*'-epi*-thiovaritriol **3** portrayed better binding affinity to SARS CoV-2 better than varitriol **1**.
3. Thiovaritriol **2** and 3*'-epi*-thiovaritriol **3** were found to have good binding interaction with SARS-CoV-2 protein (PDB ID: 6VWW) than the reference drugs.
4. 3*'-epi*-Thiovaritriol **3** displayed more affinity to the SARS CoV-2 than thiovaritriol **2**. This difference in binding affinities could be due to the different binding orientations of thiovaritriol **2** and 3*'-epi*-thiovaritriol **3** to the binding pocket of the SARS-CoV-2 protein.

Chapter 3

Section B: Synthetic studies towards thiovaritriol

3.7. Introduction

Thiolane containing organic compounds are a large class of functional molecules with a variety of important applications. Modern drug discovery is one of these major applications.[21] Molecules bearing thiolane scaffold have been widely explored for their medicinal potential over several decades. Many of these compounds exhibit effective biological activities and pharmacological properties. In fact, some of them have been developed into important drugs..[21,22] It is a well-known fact that 50% of commercial medicines have taken inspiration from natural products and that natural products serve as lead templates in the discovery of modern medicines.[23] In the present study, we directed our focus towards the synthesis of thio-version of the marine natural product varitriol **1** i.e thiovaritriol **2** and 3*'-epi*-thiovaritriol **3**. The docking study in section A of this chapter revealed that thiovaritriol **2** and 3*'-epi*-thiovaritriol **3**, shows better binding affinity for SAR-CoV-2 than the parent varitriol **1** (Figure 3.25). Thiovaritriol **2** and 3*'-epi*-thiovaritriol **3** could find potential in the treatment of COVID-19. In this study, we have designed a concise route towards the synthesis of thiovaritriol **2** and 3*'-epi*-thiovaritriol **3**.

Varitriol, **1**

B.E = −5.01 Kcal/mol
Ki = 212.41 μM

Thiovaritriol, **2**

B.E = −6.26 Kcal/mol
Ki = 30.97 μM

3*'-epi*-Thiovaritriol, **3**

B.E = −6.45 Kcal/mol
Ki = 18.62 μM
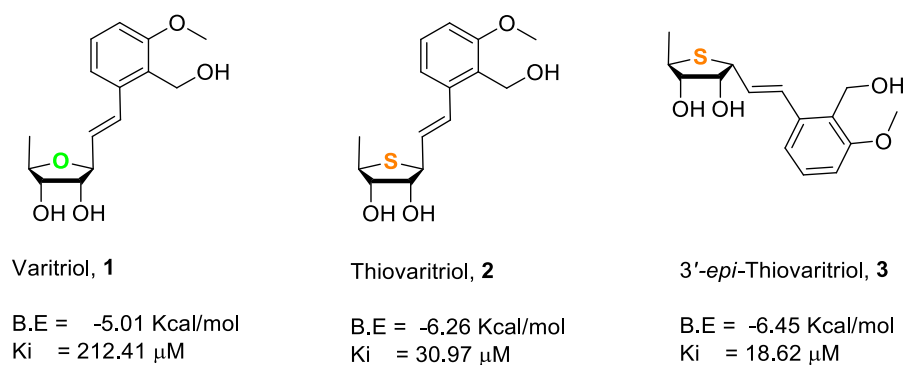
Figure 3.25: Thiovaritriol **2** and 3*'-epi*-thiovaritriol **3** as potent SARS-CoV-2 inhibitors than parent varitriol **1**. B.E = binding energy. Ki = inhibition constant.

3.8. Objective

To design an efficient synthetic route for the synthesis of thio-analogues of marine natural product varitriol **1**.

Chapter 3

3.9. Literature review on varitriol synthesis and synthesis of thiolane unit in selected bioactive organic compounds

Varitriol synthesis

There are quite a few chemical reaction routes reported for the synthesis of vartriol in the literature.[5,24] It can be prepared from various functionalized furanose units and aromatic units. A summary of different building units used in the synthesis of varitriol is depicted in figure 3.26.
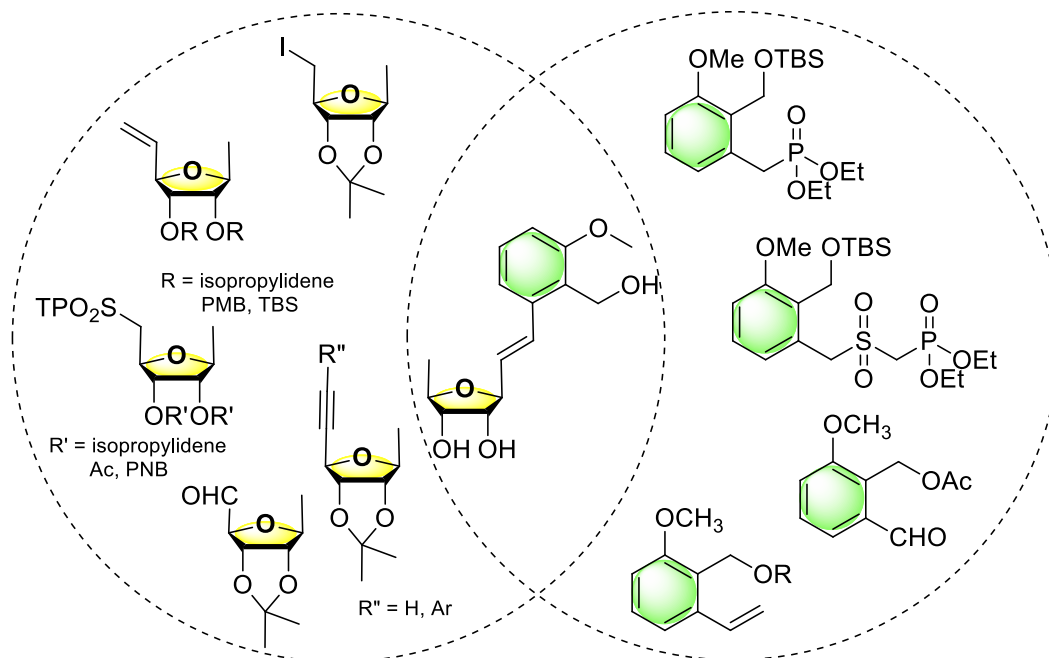
Figure 3.26: Building unitsusedfor the synthesis of varitriol **1**.

Synthesis of thiolane unitin selected bioactive organic compounds

There are no reports on thiovaritriol **2** and *3'-epi*-thiovaritriol **3** in the literature. The construction of thiolane moiety has gained interest in organic chemistry owing to its biological, pharmacological and other applications. A well-established method to assemble thiolane units (tetrahydrothiophenes) is chiral pool techniques which employ chiral synthons to import stereogenic centres and functionalities suitable for further transformation of the required targets.[21,25] For instance, thiolane unit can be synthesised from chiral α-amino acids (L-cysteine[26] and L-aspartic acid[27]), α-hydroxy acid esters ((*S*)-dimethyl malonate[28] and (*S*)-ethyl lactate[29]), (*S*)- and (*R*)-glycidols,[30,31] terpenes ((+)-pulegone)[32] and sugars (D-ribose,[33]

D-glucose,[34] D-/L-xylose,[34] D-/L-arabinose,[35] D-galactose,[36] D-lyxose,[36] D-mannose,[37] D-erythrose,[38] D-mannitol,[39] D-sorbitol[40] and L-iditol[41]) (Figure 3.27).
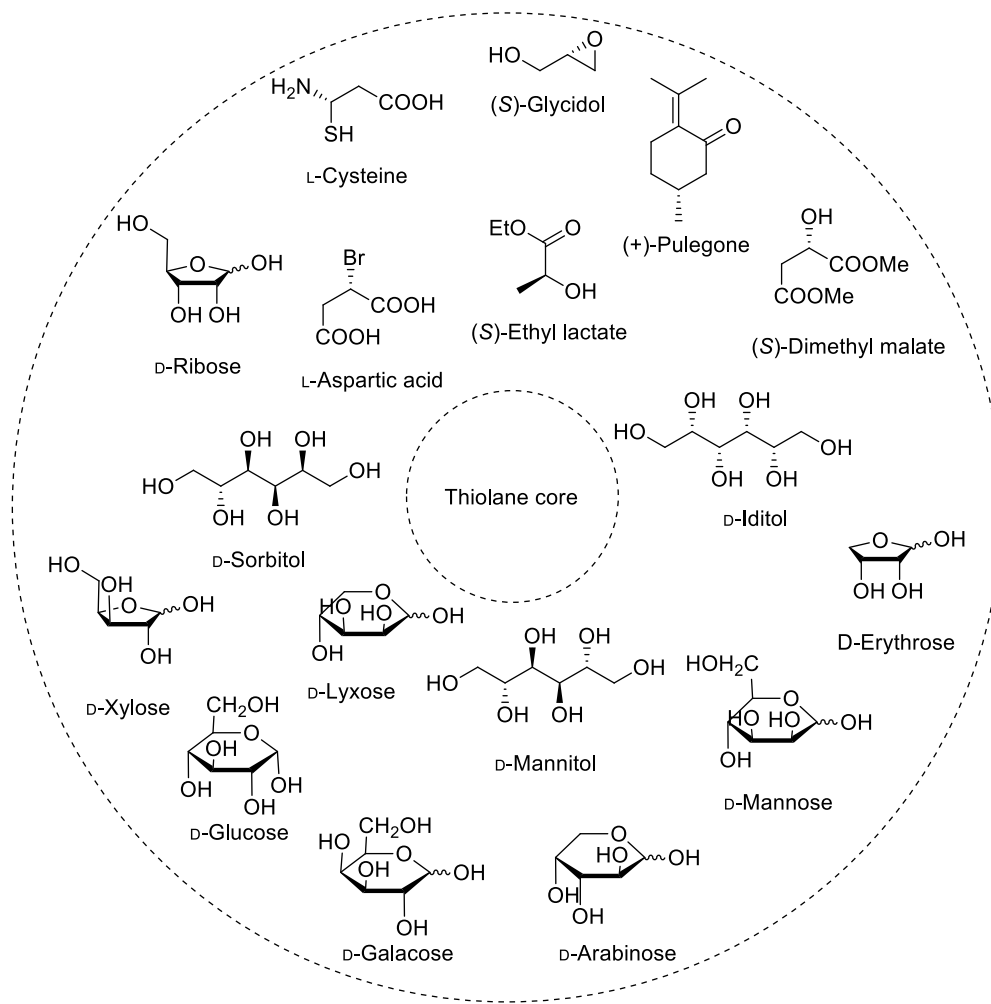
Figure 3.27: Chiral synthons used in constructing the thiolane core.

For the purpose of construction of thiolane unit sulphur has been introduced into molecules by sulfurization agents such as sodium sulfide (Na_2S), disodium tetrasulfide (Na_2S_4), sodium hydrosulfide (NaSH), carbon disulfide (CS_2), thiourea (($NH_2)_2CS$), Thioacetic acid (AcSH), potassium thioacetate (KSAc), benzyl mercaptan (BnSH), etc.[21,22] Numerous chemical methods for constructing thiolane unit has been employed which includes rearrangement reactions, nucleophilic displacement reactions, late-stage sulfurization, intramolecular cyclisation of sulfides, etc. We have also comprehensively reviewed recent synthetic strategies, biological activities and structure-activity relationship studies of thiolane-based molecules in a review article entitled "Synthetic access to thiolane-based therapeutics and

biological activity studies".[22] Some selected recent approaches involving the building of thiolane backbone have been assembled in the schemes below (Scheme 3.1-3.5).
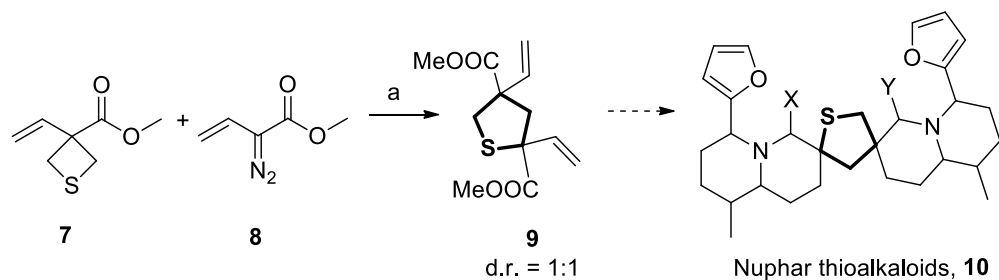
Reagents and conditions: (a) 2% $Rh_2(OAc)_4$, PhH, 80°C, 20 h, 71% yield.

Scheme 3.1: Synthetic access to *Nuphar* sesquiterpene thioalkaloids **8**

Nuphar sesquiterpene thioalkaloids: In the year 2015, Zakarian and co-workers assembled thiolane unit **9** with the aid of highly efficient rhodium-catalysed Stevens-type re-arrangement. This approach was applied in the formal synthesis of *Nuphar* sesquiterpene thioalkaloids **10** possessing antimetastatic, antifungal, and antibacterial properties (Scheme 3.1).[22]
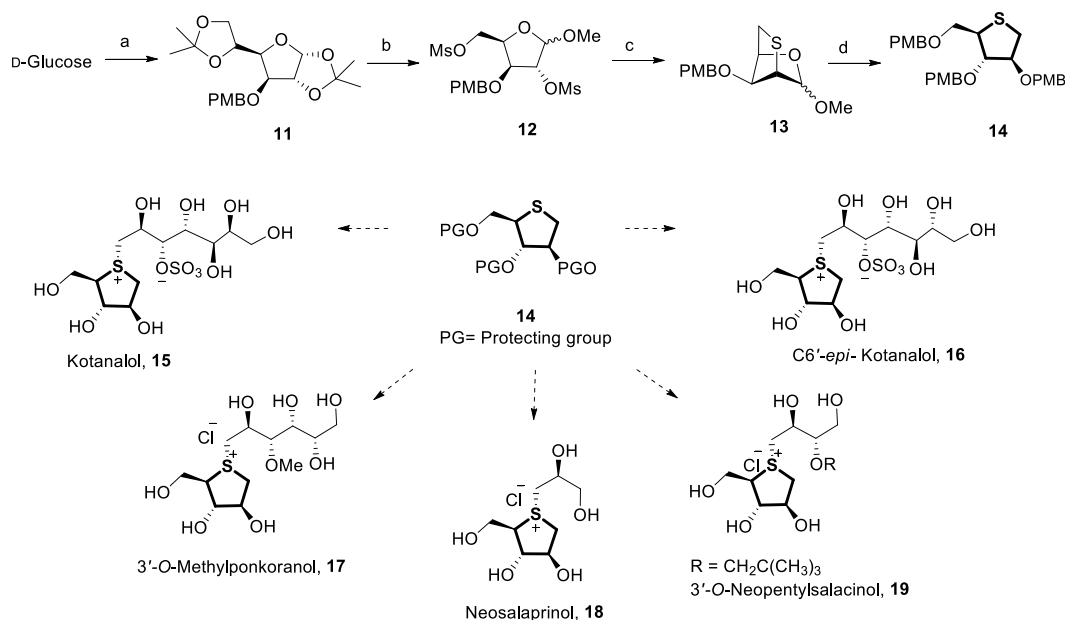
Reagents and conditions: (a) *i*. acetone, conc. H_2SO_4, 0 °C *ii*. PMB-Cl; (b) *i*. 2M HCl, THF *ii*. $NaIO_4$, H_2O, MeOH *iii*. $NaBH_4$, MeOH, 84% (over 6 steps) *iv*. 5% HCl/MeOH, 91% *v*. MsCl, Py; (c) $Na_2S \cdot DMF$, 100 °C, 78% (α-anomer), 73% (β-anomer) (over 2 steps); (d) *i*. 4M HCl, THF *ii*. $NaBH_4$, MeOH, 90% (over 2 steps) *iii*. PMB-Cl.

Scheme 3.2: Synthetic access to thiosugar sulphonium salts from *Salacia* sp.

*Thiosugar sulphonium salts:*In the past decade, several syntheses of thiosugar sulphonium salts and analogues (**15-19**) displaying α-glucosidase inhibitory activity from *Salacia* sp. were reported using D-glucose derived thiosugar **14** as the key precursor (Scheme 3.2).[22]
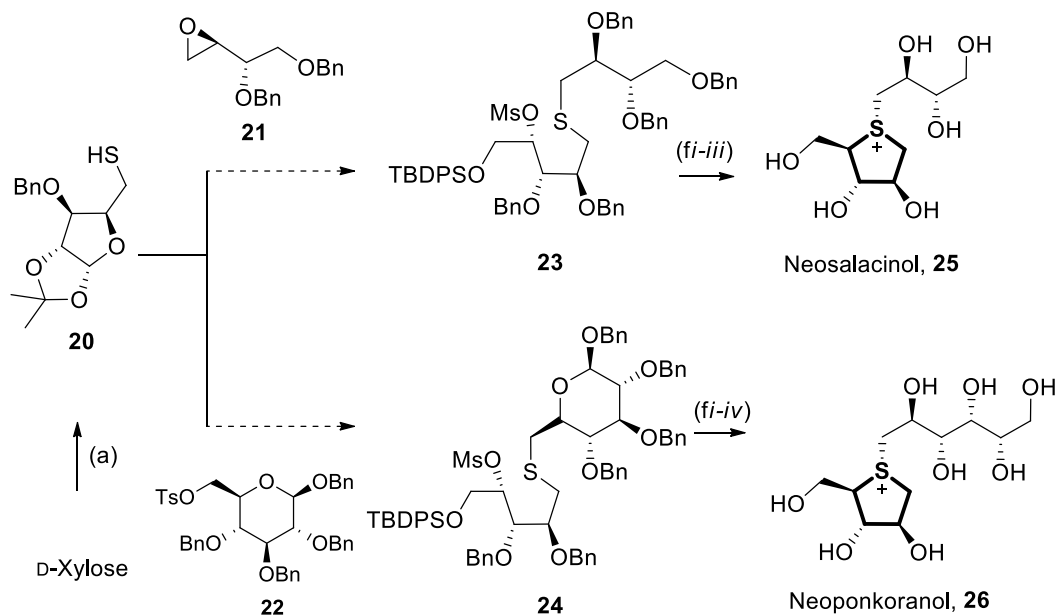
Reagents and conditons: (a) *i*. Acetone, H_2SO_4, $CuSO_4$, rt *ii*. 0.2% aq. HCl, rt, 95% (over 2 steps) *iii*. TsCl, Py, $CHCl_3$, 0°C-rt, 90% *iv*. BnBr, NaH, DMF, 0°C, 1h, 95%; *v*. KSAc, DMF, 80°C, 2h, 93% *vi*. LiAlH₄, THF, 0°C, 30min, 96%; (f) *i*. EtOH, reflux, 90/94% ($\alpha{:}\beta$ = 23:1 & 20:1) *ii*. H_2, Pd-C, 20% aq. TFA, 90% *iii*. IRA400J(Cl⁻ form), MeOH, H_2O, rt, 12h, 89% *iv*. NaBH₄, H_2O, 0°C, 2h, 52% (over 3 steps).

Scheme 3.3. Synthetic access to thiosugar de-sulphonates (neo-compounds) from *Salacia* sp.

Thiosugar de-sulphonates: In the year 2016, Muraoka and co-workers developed a high diastereoselective route for the synthesis of naturally occurring de-sulphonates of thiosugar sulphonium salts i.e. neo-compounds neosalacinol **25** and neoponkoranol **26**. This route employed diastereoselective intramolecular cyclisation of desirably alkylated sulphides **23** & **24** obtained from key thioether **20** to access neosalacinol **25** and neoponkoranol **26** (Scheme 3.3).[22]

Albomycins: In the year 2018, He and coworkers designed and developed a synthesis of albomycins **31** belonging to the sideromycins (antibiotics) which were first isolated in 1947 from the soil microbe *Streptomyces grideus*. The pathway for tailoring the thiolane unit **30** from a chiral sugar precursor **27** is depicted in scheme 3.4.[22]
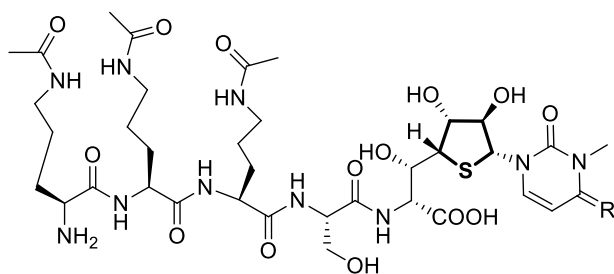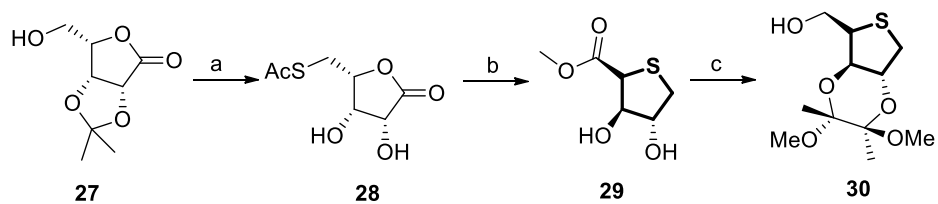
Reagents and conditions: (a) *i*. AcSH, diisopropyl azodiformate, PPh₃, 89% *ii*. TFA, 90%; (b) *i*. TsCl, DABCO *ii*. K₂CO₃, MeOH, 81%; (c) *i*. 2,3-butanedione, CSA, CH(OMe)₃, MeOH, 86% *ii*. (ⁱBu₂AlH)₂, 98%.

Scheme 3.4: Synthetic access to albomycins **31**.
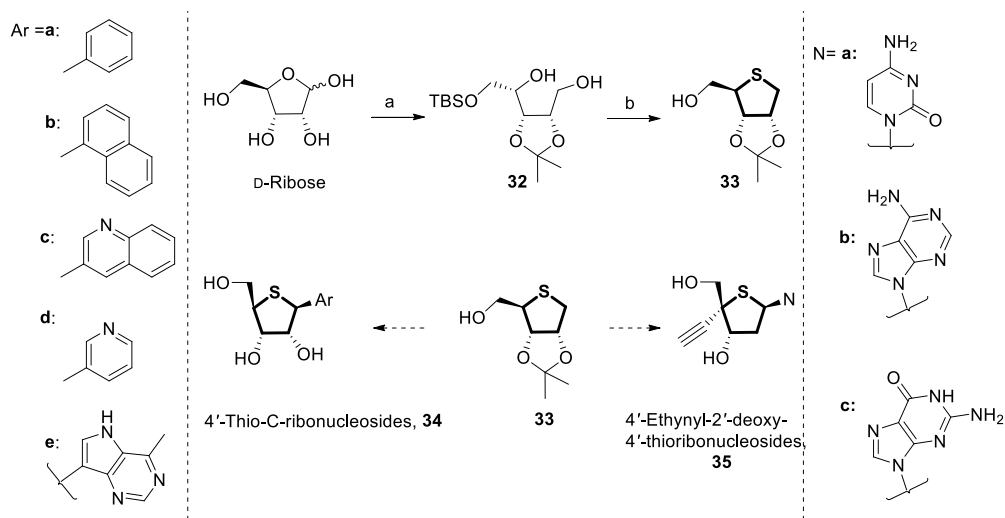
Reagents and conditions: (a) *i*. Br₂, H₂O, K₂CO₃ ii. Acetone, H₂SO₄ (cat.) (65% over 2 steps) *iii*. MsCl, NEt₃, CH₂Cl₂ *iv*. KOH, H₂O (59% over 2 steps) *v*. TBDPSCl, imidazole *vi*. NaBH₄, THF/MeOH (b)*i*. MSCl, Py *ii*. Na₂S.9H₂O, DMF, 80°C (66% over 4 steps) *iii*. TBAF (81%).

Scheme 3.5: Synthetic access to 4'-thionucleosides **34a-e** and **35a-c**.

4'-Thionucleosides: Thiosugar **33** formed from D-ribose was used as the key intermediate to synthesis 4'-thionucleosides **34a-e** and **35a-c** (Scheme 3.5).[22]

Chapter 3

Thiolane-based therapeutics have many advantages-For instance,
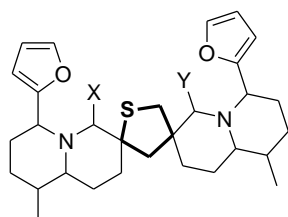
Nuphar thioalkaloids, **10**

1.The sulfur atom in the thiolane unit of Nuphar sesquiterpene thioalkaloids **10** is responsible for its anti-cancer activities.[22]

Kotanalol, **15**

2.The thiosugar sulphonium salts e.g. kotanalol **15** from *Salacia* sp.displayed were excellent *α*-glucosidase inhibitory agents.

Albomycin, **30**

3.The sulphur atom in albomycin **31** is of utmost importance for its anti-bacterial activity. Replacing sulphur with oxygen results in the loss of complete anti-bacterial activity of albomycin.[22]

4'-ethynyl 2'-deoxy-4'-thioguanosine,**35**

4.4'-thionucleosides exhibit better activity compared to their oxo-counterparts. 4'-Ethyl 2'-deoxy-4'-thioguanosine**35** exhibited tremendous inhibitory action against Herpes Simplex Virus (HSV-1) and displayed less toxicity to the host cells in comparison to its 'oxo' counterpart.[22]

All these interesting observations portray the pharmacological importance of thiolane functionality in a pharmacore.

Chapter 3

3.10. Results and discussion
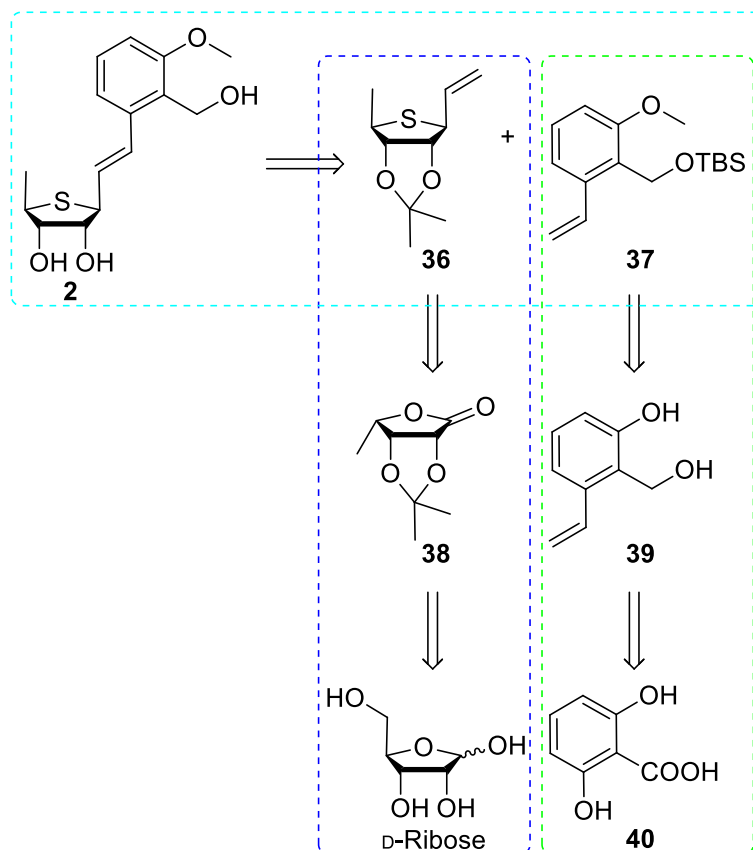
Scheme 3.6: Retrosynthetic analysis of thiovaritrol.

Retrosynthetically, the entire thiovaritriol **2** molecule can be built from two main building blocks: the thiosugar building block **36** and the aromatic building block **37**. Chiral sugar precursor- D-ribose would be the perfect precursor for installing the required stereogenic centres in the thiosugar building block **36**. Hence, thiosugar building block **36** would be obtained from D-ribose via a key intermediate lactone **38**. Next, the aromatic building block **37** could be synthesized starting from 2,6-dihydroxybenzoic acid **40** via a substituted styrene intermediate **39**.[42] Finally, the two building blocks: the thiosugar building block **36** and the aromatic building block **37** would be coupled together to construct the target thiovaritriol **2**. The synthesis of thiovaritriol is divided into three parts: (a) synthesis of thiosugar **36**, as an advanced intermediate, (b) synthesis of aromatic building block **37** and (c) coupling of thiosugar **36** with aromatic building block **37** (Scheme 3.6).

Chapter 3

3.10.1. Synthesis of thiosugar intermediate from D-ribose
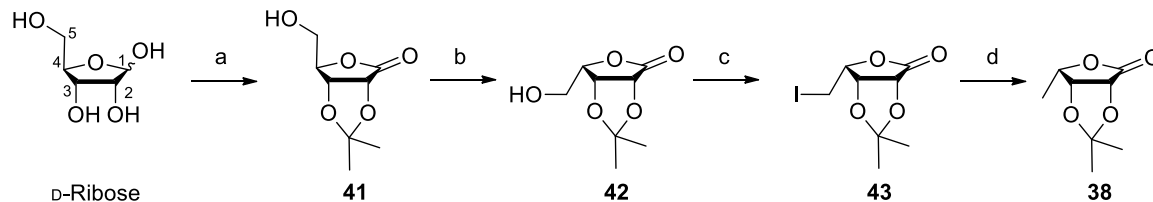
Reagents and conditions: (a) *i*.Br$_2$, NaHCO$_3$ (2.00 equiv), H$_2$O, 0°-rt, 24 h *ii*.anhyd. Acetone, 2,2-dimethoxypropane, conc. H$_2$SO$_4$ (cat.), rt, 4h, 88% yield (2 steps); (b) *i*.MsCl (2.50 equiv), anhyd. pyridine, 0°C-rt, 2 h *ii*.Aqueous KOH, rt, 6h, 70% yield (2 steps); (c) I$_2$ (2.20 equiv), triphenyl phosphine (3.00 equiv), imidazole (3.00 equiv), anhyd. PhCH$_3$, reflux, 1 h, 91% yield; (d) AIBN (0.008 equiv) and Bu$_3$SnH (1.10 equiv), anhyd.PhCH$_3$, reflux, 3 h, 94% yield.

Scheme 3.7: Synthesis of the key intermediate lactone **38**.

The first part consists of the synthesis of thiosugar **50** from D-ribose.The key intermediate lactone **38** was synthesized starting from readily available chiral pool precursor, D-ribose (Scheme 3.7). This synthesis aims at the anomeric (C1) oxidation and C4 epimerisation of D-ribose. The oxidation of the anomeric (C1) centre of D-ribose to deliver D-ribonolactone is of utmost importance at this stage because the chiral natural sugars can coexist as several isomers as well as open-chain structures in the solution. Therefore, D-ribonolactone was targeted to be the "chiral cornerstone" in the synthesis of the key intermediate lactone **38**.[33] For this purpose, we inclined towards a convenient multigram-scale synthesis of D-ribonolactone by aqueous bromine oxidation of D-riboseaccompanied by a one-pot 2,3-isopropylidene formation by the treatment of anhydrous acetone catalyzed by concentrated sulfuric acid to yield D-ribonolactone acetonide **41**.[33] The IR band of **41** 3469 cm^{-1} depicts the presence of hydroxyl functionality. The NMR peaks appearing at δH 1.32 (s, 3H), 1.41 (s, 3H) & δC 24.4, 25.7 due to the methyl groups (-CH$_3$) and a quaternary carbon δC 112.1 (confirmed by DEPT) of isopropylidene functionality confirms the acetonide formation. The IR band appearing at 1750cm^{-1} and the quaternary ^{13}C peak appearing at δC 174.01 (confirmed by DEPT) due to C1 carbonyl (-C=O) confirms the success of anomeric (C1) oxidation.

Next, the C4 epimerisation was attained via the formation of mesylateof **41** and the immediate action of aqueous KOH on the crude mesylate to form L-lyxonolactone acetonide **42**.[33] The IR spectrum of **42** displayed hydroxyl band at 3204 cm^{-1} and lactone carbonyl band at 1771 cm^{-1}. The R$_f$ (ethyl acetate: hexane 6:4) changed from 0.60 to 0.79. At the same

time, the ^{1}H NMR signalof C5 methylene group (-CH$_2$-) shifted from 4.57 (t, J = 1.6 Hz, 1H) to δH 4.63 (dq, J = 5.4 Hz, J = 3.0 Hz, 1H). This revealed the epimerization at C4. Further, an Appel-type iodination reaction of L-lyxonolactone acetonide **42** by employing a heterocyclic baseyielded iodate **43**.[43–47] The hydroxyl band at 3204 cm^{-1} was absent in the IR spectrum of iodate **43**. The NMR of iodate **43** shows peaks at δH 3.35 (dq, J = 6.0 Hz, J = 3.6 Hz, 2H) and δC-0.004 due to the C5 methylene group (-CH$_2$-). This confirms the formation of iodate **43**. With iodate **43** in hand, the key intermediate lactone **38** was successfully prepared by subjecting iodate **43** to a de-iodination reaction with tributyltin hydride and AIBN in hot toluene (Scheme 3.7).[44,47] The NMR of lactone **38** showed peaks at δH1.43 (d, J = 6.8 Hz, 3H)& δC 13.6 due to the C5 methyl group (-CH$_3$). This indicates the formation of lactone **38**. This category of carbohydrate derived lactones can serve as essential intermediates in the total synthesis of numerous natural products and therapeutics.[47–50]
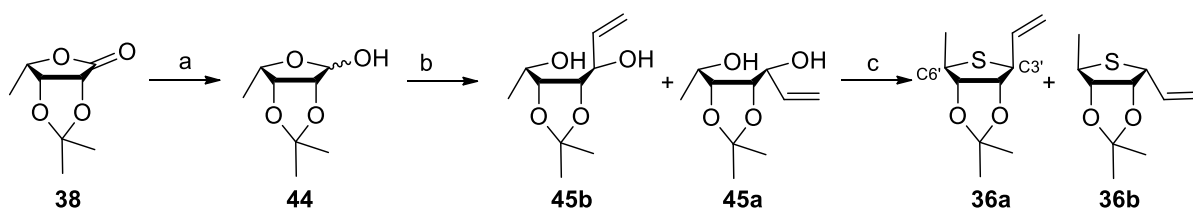
Reagents and conditions: (a) (^{i}Bu$_2$AlH)$_2$ (2.20 equiv), anhyd. THF, -70°C, 2h, 90% yield (α:β = 1:0.25); (b) vinylmagnesium bromide (5.00 equiv), anhyd. THF, 0°C-rt, 6 h, 87% yield (**45a:45b** = 0.95:1); (c) *i*. MsCl (2.50 equiv) , NEt$_3$(3.00 equiv) , CH$_2$Cl$_2$, 0°C-rt, 4 h *ii*.Na$_2$S·xH$_2$O (1.20 equiv), TBAI (0.20 equiv), anhyd. DMF, 50°C, 12 h, 50% yield (**36a:36b** = 1:0.95).

Scheme 3.8: Synthesis of thiosugar building block.

The success of yielding the key intermediate in sufficient quantity led to the synthesis of thiosugar **36** (Scheme 3.8). For the same purpose, lactone **38** was subjected to controlled hydride reduction by (^{i}Bu$_2$AlH)$_2$ at -70°C to obtain an inseparable diastereomeric mixture of lactol **44** (α:β = 1:0.25, determined by ^{1}H NMR).[51] The appearance of hydroxyl IR band at 3435 cm^{-1}, the disappearance of C1 carbonyl (-C=O) IR band at 1776 cm^{-1} and the presence of downfield NMR signals at δH 5.35 (s, 1H, major), δH 4.53 (qd, J = 10.8 Hz, J = 3.2 Hz, 1H, minor); δC 100.7 (major), 96.6 (minor) confirms the lactol **44** formation. It is a pre-requisite to cleave the furanose ring of lactol **44** with an appropriate nucleophile to replace the oxygen atom from the furanose ring with a sulphur atom. Hence, vinylmagnesium

bromide was selected as a suitable nucleophile. Thus, exposing lactol **44** to a solution of 1M vinylmagnesium bromide in dry tetrahydrofuran astonishingly yielded both the diastereomers of diol **45** in 87% yield ($\alpha{:}\beta$ = 0.95:1, determined by ^{1}H NMR) despite the presence of the bulky acetonide protecting group (Scheme 3.8).[52,53] The IR spectra of diol **45a** and **45b** displayed hydroxyl bands at 3319, 3088 cm^{-1} and 3341, 3080 cm^{-1}, respectively. The appearance of terminal monosubstituted olefinic NMR signals at δH 5.28 (dt, J = 10.6 Hz, J = 1.5 Hz, 1H), 5.43 (dt, J = 17.3 Hz, J = 1.6 Hz, 1H), 6.01 (dddd, J = 15.8 Hz, J = 10.4 Hz, J = 5.2 Hz, J = 1.6 Hz, 1H); δC 108.0, 116.4 in case of **45a** and δH 5.27 (dt, J = 10.4 Hz, J = 1.2 Hz, 1H), 5.40 (dt, J = 17.2 Hz, J = 1.2 Hz, 1H), 5.94 (dddd, J = 17.2 Hz, J = 10.4 Hz, J = 6.4 Hz, J = 5.6 Hz, 1H); δC 108.3, 117.1 in case of **45b** proves the success of vinyl nucleophilic addition and formation of diastereomeric diol **45a** & **5b**. The relative configurations of diols **459a** and **45b** were assigned by carrying out backward synthetic analysis of diastereomeric thiosugar formation **36a** & **36b**. This is discussed in detail at the end of this sub-section in scheme 3.9. The formation of both the diastereomers of diol (**45a** & **45b**) is essential to access both the diastereomers of thiosugar **36a** & **36b**. Thus, the key intermediate lactone **38** served as a versatile intermediate for the synthesis of both diastereomers of thiosugar.

The diol diastereomers (**45a** & **45b**) were not separated at this stage and the crude diastereomeric mixture was directly converted to the corresponding di-mesylates. The obtained di-mesylates were then immediately engaged in the cyclisation step using $Na_2S{\cdot}xH_2O$ to yield both the diastereomers of thiosugar **36a** & **36b** ($\alpha{:}\beta$ = 1:0.9, determined by ^{1}H NMR) (Scheme 3.8).[54] Thiosugar diastereomeric separation by chromatography proved easy at this step. The IR spectrum of **36a** & **36b** witnessed the disappearance of 3319, 3088 cm^{-1} and 3341, 3080 cm^{-1} hydroxyl bands, respectively. The appearance of upfield NMR shifts δH 3.33 (qd, J = 7.6 Hz, J = 1.6 Hz, 1H), 4.05 (dd, J = 8.8 Hz, 4.4 Hz, 1H); δC 48.1, 53.5 in the case of **36a** and δH 3.34 (sx, J = 6.8 Hz, J = 1.6 Hz, 1H), 3.85 (dd, J = 8.4 Hz, J = 5.6 Hz, 1H); δC 45.97, 54.30 in the case of **36b** due to C6' and C3'(–CH-) in the thiolane ring proves the success of the cyclisation step.

Table 3.3: Comparative analysis of vicinal coupling constants.

(3′S,4′R,5′S, 6′R)-**36a**   (3′R,4′R,5′S, 6′R)-**36b**
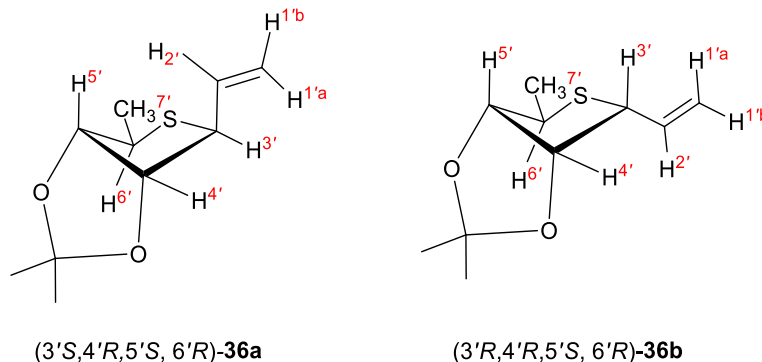
Thiosugar	$^3J_{2',1'a}$	$^3J_{2',1'b}$	$^3J_{2',3'}$	$^3J_{3',4'}$	$^3J_{4',5'}$	$^3J_{5',6'}$	$^3J_{6',7'}$
36a	17.0	10.0	8.8	4.8	5.4	1.6	7.6
36b	16.8	10.4	8.4	6.0	5.6	1.6	6.8

All the values are measured in Hz.

^{1}H NMR vicinal coupling constants were compared of thiosugars **36a** & **36b**.[55] As evident in Table 3.3, $^3J_{2',1'a}$, $^3J_{2',1'b}$, $^3J_{2',3'}$, $^3J_{4',5'}$ and $^3J_{5',6'}$ of both **36a** & **36b** are similar. Interestingly, $^3J_{3',4'}$ of thiosugar **36a** (4.8 Hz) and **36b** (6.0 Hz) differ. This suggests 3′,4′-*anti* configuration in **36b** ($^3J_{3',4'}$ = 6.0 Hz). On account of this, the relative configurations of thiosugar were assigned: (3′S,4′R,5′S, 6′R)-**36a** and (3′R,4′R,5′S, 6′R)-**36b**.
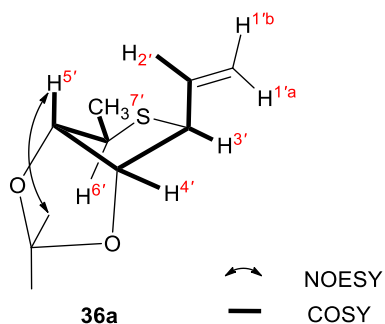
Figure 3.28: Selected 2D NMR correlations for thiosugar **36a**.

The ^{1}H-^{1}H COSY spectrum of **36a** revealed C2'to C3', C3' to C4', C4'to C5', C5' to C6' and C6' to C7'connections (Figure 3.28)**.** The NOESY spectrum of **36a** showed no correlation of H7'/H3' suggesting that H7' and H3'to be in different planes. These observations further confirmed the relative stereochemistry of thiosugar as (3′S,4′R,5′S, 6′R)-**36a** and (3′R,4′R,5′S,6′R)-**36b**.
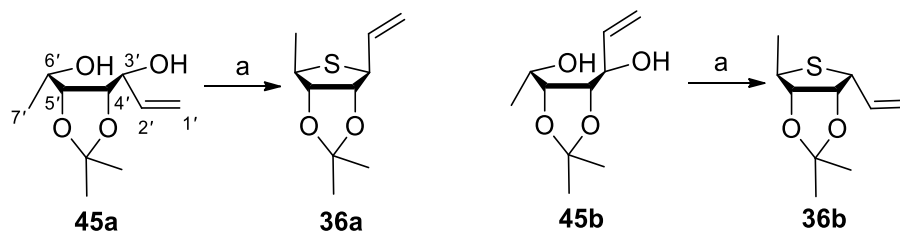
Reagents and conditions: (a) *i*.MsCl (2.50 equiv) , NEt₃(3.00 equiv), anhyd. CH₂Cl₂, 0°C-rt, 4 h *ii*.Na₂S·xH₂O (1.20 equiv), TBAI (0.20 equiv), anhyd. DMF, 50°C, 12 h, 50% yield.

Scheme 3.9: Backward analysis of diastereomeric thiosugar formation.

Further, to carry out the back analysis of the diastereomeric formation of thiosugar **36** from diol **45**, the diastereomeric mixture of diols **45a** & **45b** were separated by chromatography. Each diol diastereomer was converted to its corresponding di-mesylate in different pots and the di-mesylate was then immediately reacted with Na₂S.xH₂O. The di-mesylate of diol **45a** formed (3′*R*,4′*R*,5′*S*, 6′*R*)-**36a** whereas, the di-mesylate of diol **45b** formed (3′*R*,4′*R*,5′*S*, 6′*R*)-**36b** (Scheme 3.9). The explanation of these stereochemical outcomes can be endorsed by the fact that the ring closure by double sulphide displacement is accompanied by strain, which leads to the inversion of configurations at C3′ and C6′. Based on this, the relative configurations of diols were assigned: (3′*R*,4′*S*,5′*R*,6′*R*)-**45a** and (3′*S*,4′*S*,5′*R*,6′*R*)-**45b**.

3.10.2. Synthesis of aromatic building block from 2,6-dihydroxybenzoic acid

For the synthesis of aromatic building block **37**, we inclined towards the transformations reported in the literature beginning from easily accessible and cheap starting material 2,6-dihydroxybenzoic acid **40** with minor adaptations (Scheme 3.10). Monoacetonide protection of 2,6-dihydroxybenzoic acid **40** gave protected phenol **46** and then the free hydroxyl in the protected phenol **46** was reacted with triflic anhydride to form triflate **47**.[56] The ^{1}H NMR spectrum of phenol **46** displayed a peak at δH 1.75 (s, 6H) due to two methyl (-CH₃) groups, peaks at δH 6.45 (dd, J = 8.4 Hz, J = 0.8 Hz, 1H), 6.64 (dd, J = 8.4 Hz, J = 0.8 Hz, 1H) & 7.42 (t, J = 8.4, 1H) due to the aromatic protons and peak at δH 10.34 (s, 1H) due to phenolic hydroxyl (-OH). ^{13}C NMR spectrum of phenol **46** showed peaks at δC 107.2 (a quaternary carbon, confirmed by DEPT) which was attributed to the isopropylidene group (>C(CH₃)₂).

This verifies the formation of protected phenol **46**. The phenolic hydroxyl band at 3204 cm^{-1} was absent in the IR spectrum of triflate **47.** The appearance of quaternary^{13}C signals at
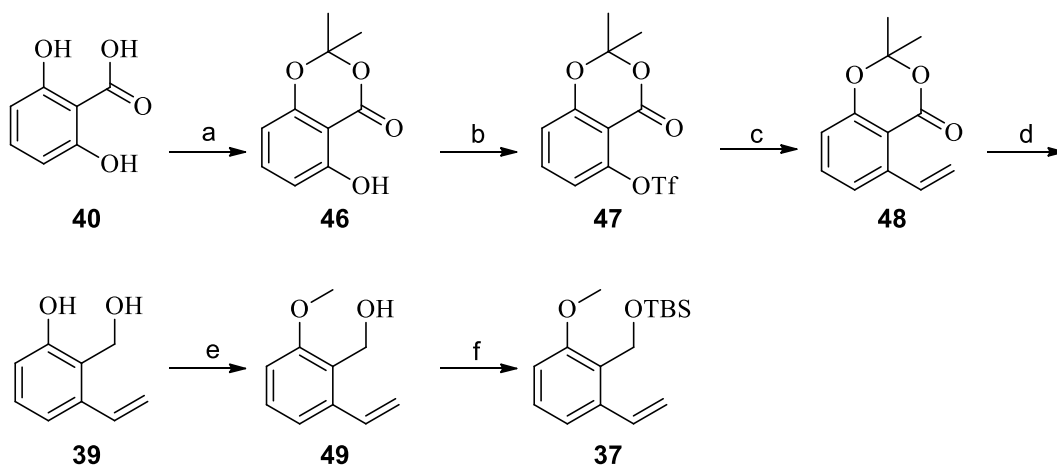
Reagents and conditions: (a) SOCl$_2$ (1.30 equiv), DMAP (0.05 equiv), anhyd. acetone (1.25 equiv),0°C-rt, 24h, 80% yield; (b)Triflic anhydride (1.20 equiv), anhyd. pyridine (3.70 equiv), anhyd. CH$_2$Cl$_2$, 0°C-rt, 1h, 88% yield; (c) PdCl$_2$(dppf)$_2$ (5 mol%), NEt$_3$ (1.30 equiv), potassium vinyltrifluoroborate (1.10 equiv), EtOH, reflux, 4.5h, 94% yield; (d) LiAlH$_4$ (1.50 equiv), anhd. THF, 0°C-rt, 1h, 91% yield; (e) Methyl iodide (2.00 equiv), K$_2$CO$_3$ (2.00 equiv), anhd. acetone, rt, 4h, 70% yield; (f)TBS-Cl (1.20 equiv), imidazole (3.05 equiv), anhd. CH$_2$Cl$_2$, rt, 1h, 85% yield.

Scheme 3.10: Synthesis of aromatic building block **37**.

δC 108.3 (due to -CF$_3$, confirmed by DEPT) and quaternary ^{13}C signals at δC 157.1 (due to carbonyl –C=O, confirmed by DEPT) verifies the formation of triflate **47**.

Triflate **47** was subjected to Suzuki cross-coupling to gain protected styrene **48**,[57] which was followed by LiAlH$_4$ reduction to obtain substituted styrene intermediate **39** (Scheme 3.10). The NMR spectra of the protected styrene **48** portrayed the presence of monosubstituted olefinic functionality at δH 5.43 (dd, $J = 11.2$ Hz, $J = 1.2$ Hz, 1H), 5.72 (dd, $J = 17.2$ Hz, 1.2 Hz, 1H), 6.89 (dd, $J = 8.0$ Hz, $J = 0.8$ Hz, 1H) & δC 117.9, 135.4 thus, confirming the formation of protected styrene **48**. The IR spectrum of substituted styrene intermediate **39** observed the disappearance of carbonyl band 1732 cm^{-1} and the appearance of hydroxyl bands 3280, 3183 cm^{-1}. Proton peaks due to the isopropylidene methyl groups ($>$C(CH$_3$)$_2$) at δH 1.72 (s, 6H) were absent in the ^{1}H NMR spectrum of **39**. The ^{1}H NMR spectrum of **39** showed the presence of a methylene (–CH$_2$-) group at δH 4.87 (s, 2H). ^{13}C peak due to

carbonyl carbon (-C=O) at δC 160.4 (a quaternary carbon, confirmed by DEPT) was absent in the ^{13}C NMR spectrum of **39**. This confirms the formation ofsubstituted styrene intermediate **39**. It is worthy to note that substituted styrene intermediate **39** would decompose over time and cannot be stored for long.

Eventually, mono-methylation and TBS-Cl protection of **39** in the same sequence, efficiently yielded the aromatic building block **37** (Scheme 3.10).[58] The NMR spectra of mono-methylated alkene **49** exhibited the appearance of δH 3.87 (s, 3H) and δC 55.6 due to the methoxymethyl (-OCH$_3$) group thus, confirming the formation of methylated styrene **49**. The band due to the hydroxyl moiety 3327 cm^{-1} disappeared in the IR spectrum of aromatic building block **37**. The NMR spectra of aromatic building block **37** revealed the presence of δH -0.0001 (s, 6H), 0.84 (s, 9H) & δC -5.2 (2C), 18.5 (quaternary carbon, confirmed by DEPT), 25.99 (3C) due to the presence of *tert*-butyldimethyl silyl (-(CH$_3$)$_2$SiC(CH$_3$)$_3$) group. Thus, verifying the formation of **37**.

3.10.3. Synthesis of thiovaritriol via coupling of thiosugar and styrene derivative

Reagents and conditions: (a)**36a/36b**, **37** (1.00 equiv), Grubbs II (5 mole%), anhd. CH$_2$Cl$_2$, rt, 40 h, 42% yield
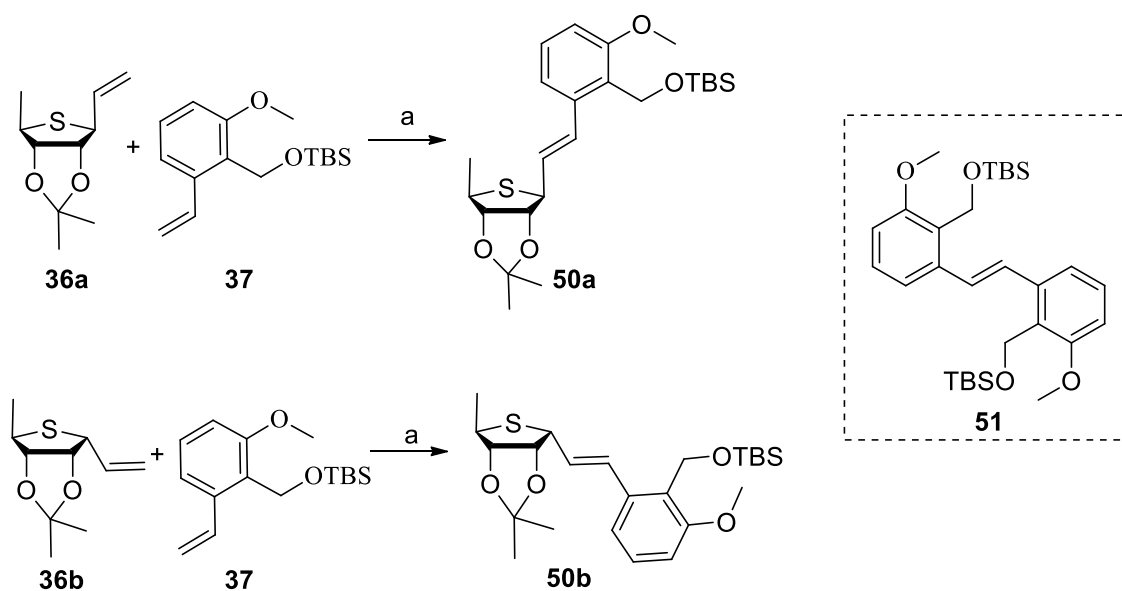
Scheme 3.11: Synthesis of protected thiovaritriol **50a** and **50b** via metathesis.

Towards this end, thiosugar building block (**36a** & **36b**) was joined to the aromatic building block **37** via the key metathesis step with the aid of the famous Grubb's IInd generation catalyst (Scheme 3.11).[58] Delightfully, in both the cases we accomplished the cross-coupled products (**50a** & **50b**), in 42 % yield (based on 20% recovered thiosugar). The NMR spectra of **50a/50b** showed both signals pertaining to thiosugar building block (in the aliphatic region) and aromatic building block signals (in the aromatic region). In addition, the vicinal di-substituted olefin NMR signals of **50a** were observed at δH 6.20 (dd, J = 16.0 Hz, J = 9.2 Hz, 1H), 6.91 (d, J = 15.6 Hz, 1H); δC 108.8, 118.0 and that of **50b** were observed at δH 6.07 (dd, J = 15.6 Hz, J = 8.4 Hz, 1H), 7.00 (d, J = 15.6 Hz, 1H); δC 108.9, 117.8. Hence, proving the formation of protected thiovaritriol **50a/50b**. In addition, self-coupled product **51** (26% yield) was observed (Scheme 3.11). The NMR spectra of **51** executed chemical shifts corresponding to only aromatic building block and the vicinal di-substituted olefin signals δH 6.75 (dd, J = 8.0 Hz, J = 1.2 Hz, 1H); δC 128.6 thus, verifying the formation of self-coupled product **51**.
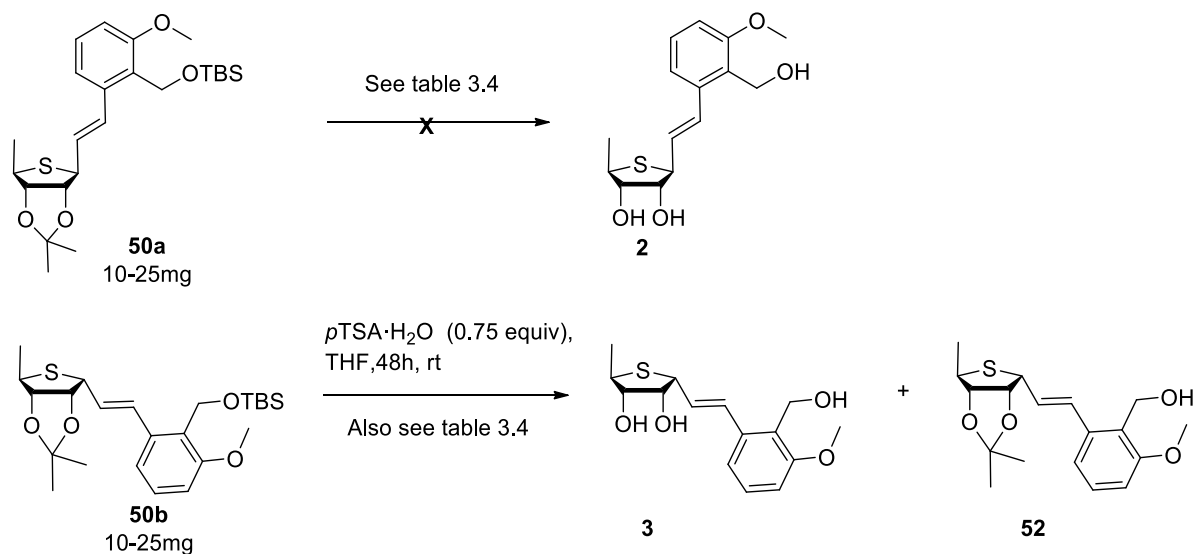
Scheme 3.12: Synthesis of thiovaritriol.

Table 3.4: Optimization of deprotection of **50a** and **50b**.

| Sr. No.	Reaction condition*	Yield (%)
1	2M aq. HCl, rt	Complex mixture
2	80% aq. acetic acid, rt	Complex mixture
3	85% aqueous formic acid	Complex mixture
4	1M TBAF in THF, 0°C to rt	Complex mixture
5	*p*TSA (1.13) equiv),THF, 48h, rt	Complex mixture
6	*p*TSA·H$_2$O (0.75equiv), THF, 48h, rt	61% of 3*'-epi*-thiovaritriol **3** 16% of **52**

*These reactions were carried out on milligram scale (starting from 10-25 mg of **50a** and **50b**)

To complete the synthesis of thiovaritriol, the **50a**/**50b** were then subjected to deprotection (Scheme 3.12, Table 3.4). Several one-pot acidic deprotection reaction conditions (2M aqueous HCl,[53] 80% aqueous acetic acid,[48] 85% aqueous formic acid,[55,56] and 1M TBAF in THF)[57] failed to provide us with the desired target molecule. But instead, we obtained an unexpected complex mixture of products. We then thought to use a comparatively weaker acidic deprotection condition by employing *p*TSA.[58] When 1.13 equiv *p*TSA·H$_2$O was used we ended up with a complex mixture (Scheme 3.12, Table 3.4, entry 5). Fortifyingly, we obtained the desired 3*'-epi*-thiovaritriol **3** when *p*TSA·H$_2$O (0.75 equiv) was added portion wise. Along with 3*'-epi*-thiovaritriol **3**, **52** was also obtained (Scheme 3.12). IR spectrum of 3*'-epi*-thiovaritriol **3** showed the presence of hydroxyl band at 3339 cm^{-1}. ^{1}H NMR spectrum of 3*'-epi*-thiovaritriol **3** did not have peaks corresponding to *tert*-butyldimethylsilyl protecting group (-(CH$_3$)$_2$SiC(CH$_3$)$_3$) at δH -0.02 (6H), 0.82 (s, 9H). Also, proton peaks due to isopropyledene group (>C(CH$_3$)$_2$) at δH 1.26 (s, 3H) and 1.49 (s, 3H) were absent ^{1}H NMR spectrum of 3*'-epi*-thiovaritriol **3**. ^{1}H NMR spectrum of 3*'-epi*-thiovaritriol **3** showed both signals pertaining to thiosugar building block (in the aliphatic region) and aromatic

building block signals (in the aromatic region). In addition, the vicinal di-substituted olefin ^{1}H signals of **3** were observed at δH 5.96 (dd, J = 8.4 Hz, J = 15.6 Hz, 1H) and 6.84 (d, J = 15.2 Hz, 1H,). This spectral information reveals the formation of 3'-*epi*-thiovaritriol **3**.

^{1}H NMR spectrum of **52** showed the appearance of peaks due to isopropylidene group (>C(CH$_3$)$_2$) at δH 1.26 (s, 3H) and 1.49 (s, 3H). But, the proton peaks due to *tert*-butyldimethylsilyl protecting group (-(CH$_3$)$_2$SiC(CH$_3$)$_3$) at δH-0.02 (6H) and 0.82 (s, 9H) were absent in the ^{1}H NMR spectrum of **52**. ^{1}H NMR spectrum of **52** showed both signals pertaining to the thiosugar building block (in the aliphatic region) and aromatic building block signals (in the aromatic region). In addition, the vicinal di-substituted olefin ^{1}H signals of **52** were observed at δH 6.75 (d, J = 16.0 Hz, 1H) and 7.15 (d, J = 8.0 Hz, 1H). This spectral information shows the formation of **52**.
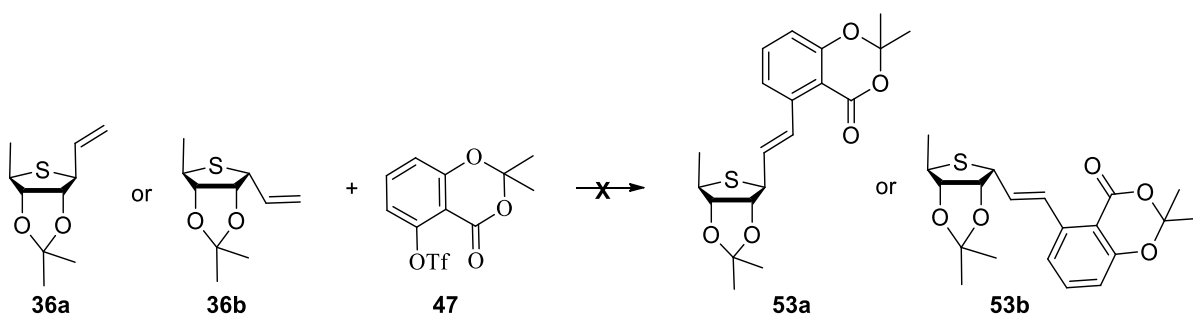
Reagents and condition: **36a/36b**, **47** (1.70 equiv), Pd(PPh$_3$)$_2$Cl$_2$ (20 mole%), NEt$_3$, LiCl, anhd. DMF, 120°C, 4 h, MW irradiation.

Scheme 3.13: Synthetic attempt to form **53a** and **53b**.

Another synthetic attempt was the Heck-coupling between thiosugar building block **36a/b** and triflate **47** desiring to obtain **53a/53b** (Scheme 3.13). However, we failed to obtain the desired targetsinstead, we ended up with an unwanted complex reaction mixture.

In a nutshell, we successfully achieved the synthesis of 3'-*epi*-thiovaritriol **3** by joining thiosugar **36b** and aromatic building block **37** via metathesis reaction. Further optimization of the reaction conditions of the deprotection step was not possible at this stage as the deprotection was carried out on a very less scale (milligram scale). This gave rise to challenges such as difficulty in the detection of products by TLC and yields in trace amounts of the compounds. There is scope for further optimization of the deprotection reaction conditions.

Chapter 3

3.11. Conclusion

1. Marine natural product varitriol **1** was modified to generate novel thiovaritriol derivatives which could further find potential as antiviral agents against SARS-CoV-2 infections.

2. The synthesis of vinylated thiosugar **36** was achieved for the first time which could be explored as an advanced intermediate in the synthesis of modified nucleosides.

Chapter 3

3.12. Experimental part

3.12.1. Material and methods

Melting points (uncorrected) were determined in an open capillary using the Thiele melting point tube. Thin-layer chromatography was performed with Kieselgel 60 F254 (Merck aluminium support plates). TLC spots were visualised in UV and by staining the TLC plate with iodine, $KMnO_4$ -acetone (1.5g of $KMnO_4$, 10g K_2CO_3, and 1.25mL 10% NaOH in 200mL water), anisaldehyde- H_2SO_4 (10 mL of 5% anisaldehyde in acetic acid, 5% methanolic H_2SO_4, heated at 110°C, 10 min). Infrared data was recorded in the region between 4000 to 400 cm-1 on a Shimadzu IRPrestige-21 instrument. Column chromatography was performed with silica gel 60-200 mesh size as packing material. ^{1}H, ^{13}C, DEPT-135, ^{1}H-^{1}H COSY and NOESY NMR spectra were recorded at room temperature on Bruker instrument (400 MHz for ^{1}H and 100 MHz for ^{13}C), chemical shifts are recorded in ppm relative to tetramethylsilane (TMS) as the internal standard. Optical rotations (concentration in grams/ 100 mL solvent) were measured using sodium D line on Bellingham + Stanley Ltd. ADP220 Polarimeter. The mass spectra were recorded on high resolution mass spectrometry - time of flight - electrospray ionisation HRMS (TOF MS ES+). All the chemicals used in this study were of reagent grade and used as received without any further purification.

Experimental part of section A

3.12.2. Molecular docking

Blind docking

The molecular docking has been performed against the selected protein (PDB ID: 6VWW)[16] using AutoDock 4.2 to evaluate the binding mode of ligand and interactions in the active site.[17] The required ligand structures were drawn using Chem Draw version 12.0 and then converted to .pdb format in OpenBabel (ver 2.4.1).[64] Whereas, 3D structures of molnupiravir **5** and favipiravir **6** were obtained from PubChem database.[65] The target protein and ligands were processed in PDBQT format using AutoDock Tools for further use in the molecular docking process.[18,19] AutoGrid was used for the preparation of the grid map using a grid box. The grid size was set to $126 \times 126 \times 126$ xyz points with grid spacing of 0.513 Å and grid

Chapter 3

center was designated at dimensions (x, y, and z): -73.809, 28.700 and -24.197. A scoring grid is calculated from the ligand structure to minimize the computation time. AutoDock was employed for docking using protein and ligand information along with grid box properties in the configuration file. During the docking procedure, both the protein and ligands are considered rigid. The pose with the lowest energy of binding was extracted for further analysis. Out of 10 binding positions generated for each ligand, the position with the most negative binding energy, indicating stronger binding interaction was considered.[19] The inhibition constant (Ki) was obtained from the binding energy (ΔG) using the formula: Ki = exp(ΔG/RT), where R is the universal gas constant (1.985×10^{-3} kcal mol^{-1} K^{-1}) and T is the temperature (298.15 K).[20] The visualization of docking simulation poses was done using PyMOL and Discovery Studios Visualizer 2021.[19]

Site-specific docking

The protocol followed was similar to that of blind docking. The grid size was set to $50 \times 60 \times 60$ xyz points with grid spacing of 0.408 Å and grid center was designated at dimensions (x, y, and z): -75.060, 25.999 and -14.400. The specific protein binding site was recognised using Schrödinger suite with the help of SiteMap tool that consisted of a large binding area.[66]

Experimental part of section B

3.12.3. Procedure for synthesis of D-ribonolactone andD-ribonolactone acetonide 41
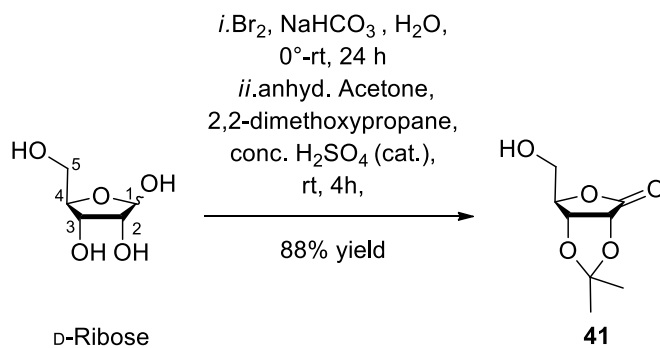
In a single neck round bottom flask equipped with a pressure-equalizing dropping funnel and magnetic bar D-ribose (0.266 mol) was stirred in distilled water (100 mL). To this sodium bicarbonate (2.00 equiv)was added while continuing the stirring. The reaction mixture was cooled to 0 °C through an ice-salt bath after 20 min of stirring at rt. Note that the reaction

mixture eventually turns homogenous in the course of the reaction. Bromine (1.10 equiv) was added dropwise to the cold reaction mixture in the round bottom flask throughout 3 h, while cautiously maintaining the internal temperature of the reaction mixture to less than 5°C. After the complete addition of bromine, the dropping funnel was replaced with a stopper and the homogenous reaction mass was stirred at rt overnight. The reaction mixture was then neutralized with approx. 88% formic acid (30 mL) and the acidic solution was concentrated under vacuum on rota-vap to obtain a dark grey solid residue. Around 10 mL of toluene was added to the residue and was concentrated again under vacuum on rota-vap. This was repeated twice to ensure the complete removal of moisture from the residue. The residue was used for the next reaction without any further purification. To obtain pure D-ribonolactone the residue was dissolved in hot ethanol and filtered. The residue was washed several times with hot ethanol. The filtrate was refrigerated overnight to obtain colourless crystals of D-ribonolactone. R_f (MeOH:CHCl$_3$ 2:8) = 0.57. $[\alpha]^{23.6}_D$ = -10.0 (c1.00, H$_2$O) (reported $[\alpha]^{25}_D$ = -11.9 (c 0.99, H$_2$O);[67] mp 95 ˚C (reported 85-87 °C);[67] IR (KBr) cm^{-1} 3500, 3375, 3188, 1750, 1594, 1375; ^{1}H NMR (400 MHz, DMSO-d_6) δ 3.57 (dd, J = 4.8 Hz, J = 3.6 Hz, 2H), 4.13 (t, J = 4.8, 1H), 4.24 (t, J = 3.6, 1H), 4.43 (dd, J = 7.6, J = 5.2, 1H), 5.17 (t, J = 5.2 Hz, 1H), 5.39 (d, J = 3.6 Hz, 1H), 5.76 (d, J = 7.6 Hz, 1H); ^{13}C NMR (100 MHz, DMSO-d_6) δ 61.0, 69.1, 69.8, 85.9, 177.0.

The above-obtained residue containing D-ribonolactonewas dissolved in dry acetone (802 mL) and transferred in two neck round bottom flask under nitrogen atmosphere and equipped with a mechanical stirrer. To this, around 5 g 4Å MS were added. Next, 2,2-dimethoxypropane (42.5 mL) and conc. H$_2$SO$_4$ (0.02 equiv) were added consecutively. After 2 h of stirring at rt, an extra 5 g 4Å MS was added. The reaction progress was monitored by TLC. The reaction was quenched with sodium bicarbonate after another 2 h and filtered under a vacuum. The residue was washed with acetone and the filtrate was concentrated on rota-vap under a vacuum. The solid residue obtained was then dissolved in hot ethyl acetate (500 mL) and filtered. The filtrate was then concentrated on rota-vap under vacuum to 1/4th of its original volume. The white crystals obtained of compound **41** were filtered and washed with cold ethyl acetate. The filtrate was then cooled to obtain the rest of compound **41** as colourless crystals (44 g, 88% yield over two steps). R_f (ethyl acetate:hexane 6:4) = 0.60; $[\alpha]^{26.2}_D$ = -59.0 (c 1.05, CHCl$_3$) (reported-$[\alpha]^{20}_D$ = -66.9 (c 1.00, CHCl$_3$);[68-69] mp 137 ˚C

(reported 133-137 °C);[68-69] IR (KBr) cm^{-1} 3469, 2978, 2906, 1750; ^{1}H NMR (400 MHz, CDCl$_3$) δ 1.32 (s, 3H), 1.41 (s, 3H), 2.62 (bs, 1H), 3.74 (d, J = 12.4 Hz, 1H), 3.93 (dd, J = 12.0 Hz, J = 1.6 Hz, 1H), 4.57 (t, J = 1.6 Hz, 1H), 4.72 (d, J = 5.6 Hz, 1H), 4.78 (d, J = 5.6 Hz, 1H); ^{13}C NMR (100 MHz, CDCl$_3$) δ 24.4, 25.7, 60.9, 74.6, 77.2, 81.8, 112.1, 174.0.

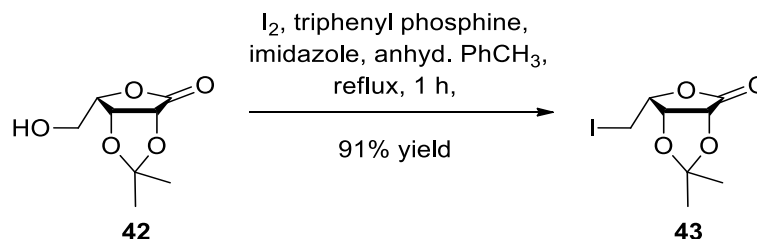### 3.12.4. Procedure for synthesis of ʟ-lyxonolactone acetonide 42
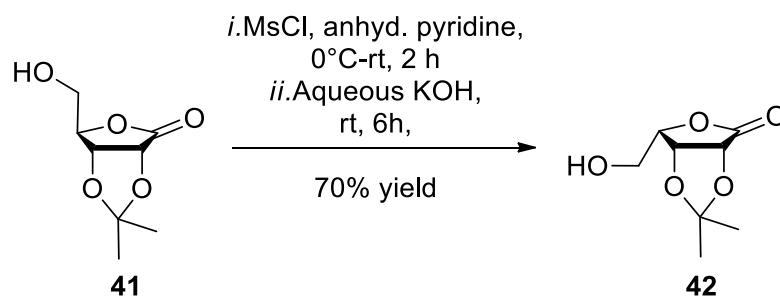
In a two neck round bottom flask, ᴅ-ribonolactone acetonide **41** (0.056 mol) dissolved in anhyd. pyridine (35 mL) was added under N$_2$ atmosphere. To this solution, mesyl chloride (2.50 equiv) was added at 0°C. The temperature of the reaction mixture was gradually increased from 0°C to rt. After complete consumption of **41** as followed by TLC (2 h), the reaction was quenched with cold water (100 mL). The compound was extracted with CH$_2$Cl$_2$ (100 mL × 3) thrice. The combined organic layers were washed with brine. The organic layer was dried over Na$_2$SO$_4$ and the volatile solvent was distilled under reduced pressure to obtain a light brown viscous liquid which was used for the next reaction without further purification.

To the above obtained residue, approx. 2.2 M aq. KOH (74 mL) was added by maintaining the reaction mass temperature below 25 °C. The resulting solution was stirred for 6 h at rt. Next, the reaction mass was neutralized with approx. 3N HCl and the acidic solution was concentrated under vacuum on rota-vap to obtain a colourless solid residue. This residue was triturated with acetone. The combined organic solvent was dried with MgSO$_4$ and distilled under reduced pressure to give colourless solid. The solid was purified by column chromatography (ethyl acetate:hexane 6:4) to afford pure **42** as colourless crystals (7.4 g, 70% yield over two steps). R$_f$ (ethyl acetate:hexane 6:4) = 0.79; [α] $^{26.2}$ $_D$ = -75.0 (c 0.20, acetone) (reported[α] ^{25} $_D$ = -85.6 (c 1.00, acetone);[68-69] mp 94 ˚C (reported 93-94 °C);[68-69] IR (KBr) cm^{-1} 3204, 2990, 2934,1771; ^{1}H NMR (400 MHz, CDCl$_3$) δ 1.42 (s, 3H), 1.50 (s, 3H),

2.03 (bs, 1H), 3.98 (dd, J = 5.2 Hz, J = 12.4 Hz, 2H), 4.06 (dd, J = 12.4 Hz, J = 6.8 Hz, 1H), 4.63 (dq, J = 5.4 Hz, J= 3.0 Hz, 1H), 4.88-4.92 (m, 2H); ^{13}C NMR (100 MHz, CDCl$_3$) δ 25.8, 26.7, 60.9, 76.1, 76.2, 78.9, 114.6, 173.2.

3.12.5. Procedure for synthesis of iodate 43

42 → **43**

Reagents/conditions above arrow: I$_2$, triphenyl phosphine, imidazole, anhyd. PhCH$_3$, reflux, 1 h, 91% yield

In a two neck round bottom flask, equipped with a water circulation condenser and continuous nitrogen flow; was placed a solution of **42** (0.018 mol) in anhyd Toluene (50 mL) under magnetical stirring. To this solution, triphenylphosphine (3 equiv) and imidazole (3.00 equiv) were added under constant stirring. The reaction mixture was heated to 60°C. Now, iodine (2.20 equiv) was added in portions. This reaction mass was refluxed for 1 h. Progress of the reaction was monitored by TLC. The reaction mass was allowed to cool at rt and ethyl acetate (100mL) was added to it. The organic layer was then washed with a saturated aqueous solution of Na$_2$S$_2$O$_3$ solution (100 mL). the aqueous layer was extracted with ethyl acetate (100mL × 3). The combined organic layers were dried over Na$_2$SO$_4$ and the volatile solvent was distilled under reduced pressure. The residue was purified by column chromatography (ethyl acetate:hexane 2:8) to afford pure **43** as a colourless crystalline solid (5 g, 91% yield). R$_f$ (ethyl acetate:hexane 2:8) = 0.50; [α] $^{26.2}$ $_D$ = -30.0 (*c* 0.25, acetone); mp 88 °C; IR (KBr) cm^{-1} 2990, 2936, 1769; ^{1}H NMR (400 MHz, CDCl$_3$) δ 1.36 (s, 3H), 1.41 (s, 3H), 3.35 (dq, J = 6.0 Hz, J = 3.6 Hz, 2H), 4.61 (dddd, J = 9.2 Hz, J = 6.0 Hz, J = 5.6 Hz, J = 3.2 Hz, 1H), 4.80 (d, J = 5.2 Hz, 1H), 4.86 (dd, J = 5.2 Hz, J = 3.2 Hz, 1H); ^{13}C NMR (100 MHz, CDCl$_3$) δ -0.004, 28.4, 29.3, 78.4, 79.2, 81.2, 116.8, 176.0. HRMS (TOF MS ES+) *m/z* calculated for C$_8$H$_{11}$IO$_4$Na [M + Na]$^+$ 320.9600, found 320.9600.

Chapter 3

3.12.6. Procedure for synthesis of lactone 38
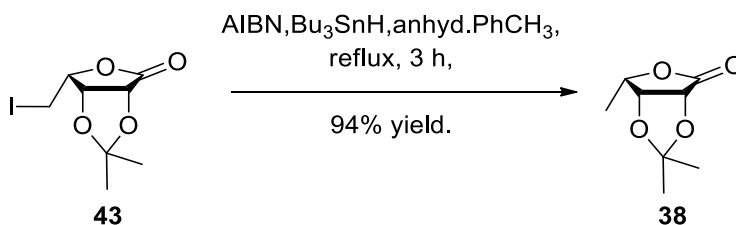
In a two neck round bottom flask, equipped with a water circulation condenser and continuous nitrogen flow; was placed a solution of **43** (0.017 mol) in anhyd toluene (60 mL) under magnetical stirring. To this solution, AIBN (0.008 equiv) and tributyltin hydride (1.10 equiv) were added under constant stirring. This reaction mass was refluxed for 3 h. Progress of the reaction was monitored by TLC. After complete consumption of the starting (3 h) the solvent was distilled under reduced pressure. The residue was purified by column chromatography (ethyl acetate: hexane 2:8) to afford pure **38** as a colourless crystalline solid (2.7 g, 94% yield). R_f (ethyl acetate:hexane 2:8) = 0.63; $[\alpha]^{26.2}_D$ = -44.0 (*c* 0.25, CHCl$_3$); mp 77 ˚C; IR (KBr) cm^{-1} 2994, 2963, 2940, 1776; ^{1}H NMR (400 MHz, CDCl$_3$) δ 1.34 (s, 3H), 1.42 (s, 3H), 1.43 (d, *J* = 6.8 Hz, 3H), 4.55 (dq, *J* = 6.8 Hz, *J* = 3.6 Hz, 1H), 4.64 (dd, *J* = 5.2 Hz, *J* = 3.6 Hz, 1H), 4.75 (d, *J* = 5.6 Hz, 1H); ^{13}C NMR (100 MHz, CDCl$_3$) δ 13.6, 26.0, 26.8, 76.0, 76.6, 77.5, 114.0, 174.1. HRMS (TOF MS ES+) *m/z* calculated for C$_8$H$_{12}$O$_4$Na [M + Na]$^+$ 195.0633, found 195.0634.

3.12.7. Procedure for synthesis of lactol 44
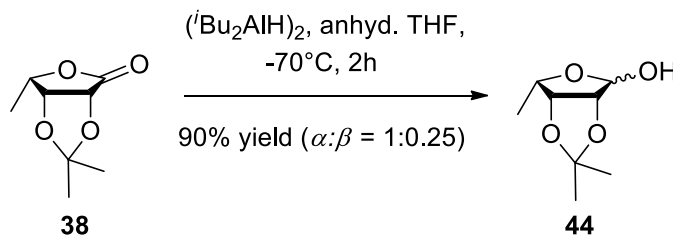
In a two neck round bottom flask was placed a solution of **38** (0.015 mol) in anhyd THF (20 mL) under N$_2$ atmosphere. To this, approx. 1M solution of (^{i}Bu$_2$AlH)$_2$ in THF (2.20 equiv) was added dropwise using a syringe under mechanical stirring, at -70°C. The reaction mass was stirred for 2 h at the same temperature. Progress of the reaction was monitored using TLC. The temperature of the reaction mixture was now set to -50°C and the reaction was

quenched with methanol (5 mL). Next, the pH of the reaction mixture was adjusted to 3.0 with cold approx.. 10% H_2SO_4. THF was evaporated under reduced pressure on rotavap and the aqueous layer was extracted with ethyl acetate (150 mL× 3). The combined organic layers were dried over Na_2SO_4 and the volatile solvent was distilled under reduced pressure to afford an anomeric mixture of **44** as a colourless viscous liquid (2.3 g, 90% yield) $\alpha:\beta$ = 1:0.25 (determined by ^1H NMR). R_f (ethyl acetate:hexane 2:8) = 0.33; IR (Neat) cm^{-1} 3435, 2988, 2940; ^1H NMR (400 MHz, CDCl$_3$) (major **44**) δ 1.32 (d, J = 6.5 Hz, 3H), 1.34 (s,3H), 1.47 (s,3H), 1.82 (bs, 1H), 4.32 (qd, J = 6.4 Hz, J = 3.2 Hz, 1H), 4.60-4.64 (m, 2H), 5.35 (s, 1H); ^1H NMR (400 MHz, CDCl$_3$) (minor **44**) δ 1.32 (d, J = 6.5 Hz, 3H), 1.38 (s, 3H), 1.54 (s,3H), 3.00 (bs, 1H), 3.66 (qd, J = 6.4 Hz, J = 3.2 Hz, 1H), 3.92 (d, J = 12.0 Hz, 1H), 4.53 (qd, J = 10.8 Hz, J = 3.2Hz, 1H); ^{13}C NMR (100 MHz, CDCl$_3$) (major **44**) δ 13.4, 24.8, 26.0, 75.9, 80.9, 86.0, 100.7, 112.3; ^{13}C NMR (100 MHz, CDCl$_3$) (minor **44**) δ 13.2, 25.0, 25.8, 71.7, 79.0, 80.9, 96.6, 112.9. HRMS (TOF MS ES+) m/z calculated for $C_8H_{14}O_4Na$ [M + Na]$^+$ 197.0790, found 197.0790.

3.12.8. Procedure for synthesis of diol 45a and 45b
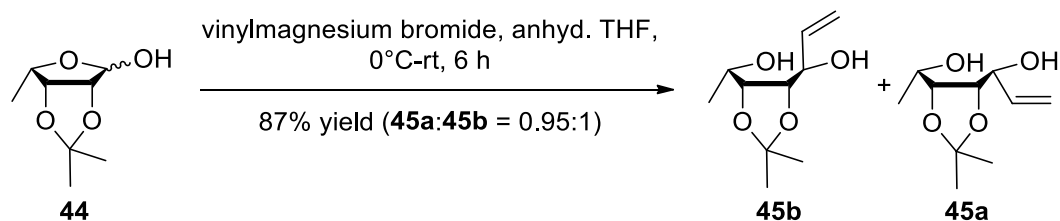
In a two neck round bottom flask was placed approx. 1 M solution of vinylmagnesium bromide (5.00 equiv) in THF under nitrogen atmosphere. To this lactol **44** (0.012 mol) in anhyd THF was added dropwise at 0°C. The reaction mix was allowed to warm at rt and was stirred for 6 h at the same temperature. Progress of the reaction was monitored using TLC. The reaction was quenched with saturated aq. ammonium chloride at 0°C. THF was evaporated under reduced pressure on rotavap and the aqueous layer was extracted with ethyl acetate (100 mL× 3). The combined organic layers were dried over Na_2SO_4 and the volatile solvent was distilled under reduced pressure. The residue was purified by column chromatography (ethyl acetate:hexane 2:8 to 3:7) to afford a diastereomeric mixture of **45a** & **45b** as a light yellow viscous liquid (2 g, 87% yield) $\alpha:\beta$ = 0.95:1 (determined by ^1H NMR).

45b (β isomer):   R$_f$ (ethyl acetate:hexane 4:6) = 0.73; [α] $^{22.6}$ D = -6.0 (c 0.10, CHCl$_3$); IR (Neat) cm^{-1} 3341, 3080, 2982, 2934, 2878, 1643; ^{1}H NMR (400 MHz, CDCl$_3$) δ 1.30 (d, J = 6.4 Hz, 3H), 1.40 (s,3H), 1.56 (s,3H), 2.93 (bs, 1H), 3.20 (bs, 1H), 4.03 (dd, J = 7.2 Hz, J = 2.8 Hz, 1H), 4.08 (dd, J = 6.4 Hz, J = 2.8 Hz, 1H), 4.13 (dd, J = 7.2 Hz, J = 3.1 Hz, 1H), 4.35-4.36 (m 1H), 5.27 (dt, J = 10.4 Hz, J = 1.2 Hz, 1H), 5.40 (dt, J = 17.2 Hz, J = 1.2 Hz, 1H), 5.94 (dddd, J = 17.2 Hz, J = 10.4 Hz, J = 6.4 Hz, J = 5.6 Hz, 1H); ^{13}C NMR (100 MHz, CDCl$_3$) δ 21.0, 24.6, 26.7, 65.3, 70.3, 79.4, 80.6, 108.3, 117.1, 137.6. HRMS (TOF MS ES+) m/z calculated for C$_{10}$H$_{18}$O$_4$Na [M + Na]$^+$ 225.1103, found 225.1104.

45a (α isomer): R$_f$ (ethyl acetate:hexane 4:6) = 0.55; [α] $^{22.6}$ D = -14.0 (c 0.16, CHCl$_3$); IR (Neat) cm^{-1} 3319, 3088, 2980, 2936, 2891, 1643; ^{1}H NMR (400 MHz, CDCl$_3$) δ 1.31 (d, J = 6.5 Hz, 3H), 1.38 (s,3H), 1.52 (s,3H), 2.70 (bs, 1H), 3.13 (bs, 1H), 4.00-4.04 (m, 2H), 4.20-4.22 (m, 1H), 4.50 (bs, 1H), 5.28 (dt, J = 10.6 Hz, J = 1.5 Hz, 1H), 5.43 (dt, J = 17.3 Hz, J = 1.6 Hz, 1H), 6.01 (dddd, J = 15.8 Hz, J = 10.4 Hz, J = 5.2 Hz, J = 1.6 Hz, 1H); ^{13}C NMR (100 MHz, CDCl$_3$) δ 21.1, 25.0, 27.2, 65.1, 70.7, 79.4, 80.4, 108.0, 116.4, 137.6. HRMS (TOF MS ES+) m/z calculated for C$_{10}$H$_{18}$O$_4$Na [M + Na]$^+$ 225.1103, found 225.1104.

3.12.9. Procedure for synthesis of thiosugar 36a and 36b
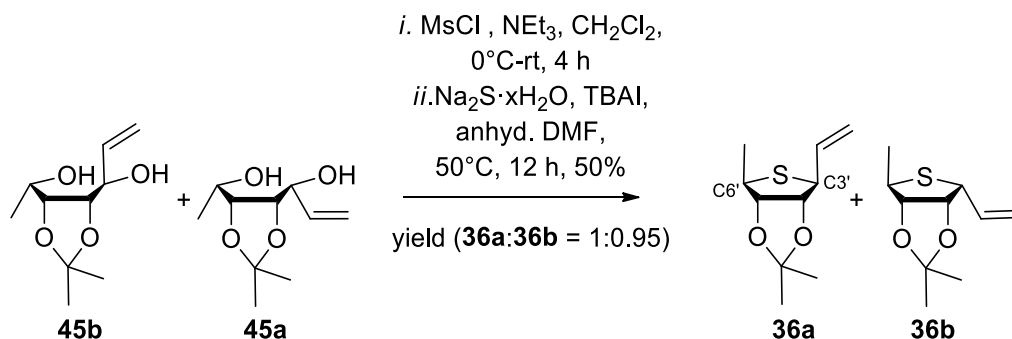
In a two neck round bottom flask was placed a crude diastereomeric mixture of diol (**45a** & **45b**) (0.01 mol) in anhyd. CH$_2$Cl$_2$ (10 mL) was added under N$_2$ atmosphere. To this solution, triethylamine (3.00 equiv) was added. Mesyl chloride (2.50 equiv) was added dropwise at 0 °C. The temperature of the reaction mixture was gradually increased from 0 °C to rt. After consumption of **45a** & **45b** as followed by TLC (4 h), the reaction was quenched with saturated aq. sodium bicarbonate (20 mL). The compound was extracted with CH$_2$Cl$_2$ (30 mL × 3). The combined organic layers were washed with brine. The organic layer was dried over

Chapter 3

Na$_2$SO$_4$ and the volatile solvent was distilled under reduced pressure to obtain light brown viscous liquid which was used for the next reaction without further purification.

In a two neck round bottom flask, equipped with chilled water circulation condenser was placed the solution of the above residue in anhyd DMF (80 mL) under magnetical stirring. To this solution, TBAI (0.20 equiv) and Na$_2$S·xH$_2$O (1.20 equiv) was added under constant stirring. This reaction mass was heated at 50°C for 12 h. Progress of the reaction was monitored by TLC. To the reaction mixture water (100 mL) was added and the aqueous layer was extracted with diethyl ether (100 mL× 3). The combined organic layers were washed with brine. The organic layer was dried over Na$_2$SO$_4$ and the volatile solvent was distilled under reduced pressure to obtain light brown viscous liquid. The residue was purified by column chromatography (diethyl ether: hexane 1:9) to afford pure **36a** and **36b** as a colourless viscous liquid (600 mg, 50% yield) (α:β = 1:0.9, determined by ^{1}H NMR).

36b (α isomer): R$_f$ (diethyl ether:hexane 1:9) = 0.60; [α] $^{22.6}$ D = -16.4 (c 0.07, CHCl$_3$); IR (Neat) cm^{-1} : 2955, 2924, 2851, 1462, 1262, 1080; ^{1}H NMR (400 MHz, CDCl$_3$) δ 1.25 (s,3H), 1.31 (d, J = 6.8 Hz, 3H), 1.46 (s, 3H), 3.34 (sx, J = 6.8 Hz, J = 1.6 Hz, 1H), 3.85 (dd, J = 8.4 Hz, J = 5.6 Hz, 1H), 4.32 (dd, J = 6.8 Hz, J = 1.6 Hz, 1H), 4.50 (t, J = 6.4 Hz, 1H), 5.08 (d, J = 10.4 Hz, 1H), 5.24 (d, J = 16.8 Hz, 1H), 5.77 (dddd, J = 16.8 Hz, J = 10.4 Hz, J = 8.4 Hz, J = 8 Hz, 1H); ^{13}C NMR (100 MHz, CDCl$_3$) δ 19.9, 24.4, 26.6, 46.0, 54.3, 86.8, 88.3, 112.7, 116.7, 134.8. HRMS (TOF MS ES+) m/z calculated for C$_{10}$H$_{16}$O$_2$SH [M + H]$^+$ 201.0949, found 201.0957.

36a (β isomer): R$_f$ (diethyl ether:hexane 1:9) = 0.71; [α] $^{22.6}$ D = -8.0 (c 0.15, CHCl$_3$); IR (Neat) cm^{-1} : 2957, 2924, 2868, 2855, 1454, 1371, 1257, 1211; ^{1}H NMR (400 MHz, CDCl$_3$) δ 1.31 (s,3H), 1.32 (d, J = 7.6 Hz, 3H), 1.54 (s, 3H), 3.33 (qd, J = 7.6 Hz, J = 1.6 Hz, 1H), 4.05 (dd, J = 8.8 Hz, 4.4 Hz, 1H), 4.54 (dd, J = 5.6 Hz, J = 1.6 Hz, 1H), 4.76 (t, J = 5.2 Hz, 1H), 5.18 (dd, J = 10.0 Hz, J = 1.6 Hz, 1H), 5.29 (d, J = 16.8 Hz, 1H), 5.98 (dddd, J = 16.8 Hz, J = 10.0 Hz, J = 8.8 Hz, J = 6.8 Hz, 1H); ^{13}C NMR (100 MHz, CDCl$_3$) δ 20.1, 24.7, 26.2, 48.1, 53.5, 85.0, 90.3, 111.3, 118.0, 133.0. HRMS (TOF MS ES+) m/z calculated for C$_{10}$H$_{16}$O$_2$SH [M + H]$^+$ 201.0949, found 201.0957.

Chapter 3

3.12.10.   Procedure for synthesis of protected phenol 46
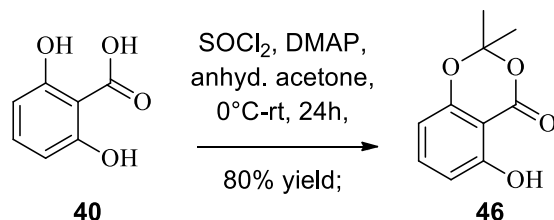
In a two neck 250 mL round bottom flask was placed 2,6-dihydroxybenzoic acid **40** (0.03 mol) in dimethoxyethane (DME) (26 mL) under N_2 atmosphere. To this solution, dimethylamino pyridine (DMAP) (0.05 equiv) was added under mechanical stirring. The resulting solution was cooled in an ice-salt bath and anhyd. acetone (1.25 equiv) and thionyl chloride (1.30 equiv) were added to it dropwise, consecutively. The reaction mixture was stirred at the same temperature for an hour and then was gradually allowed to warm at rt. After 24 h stirring at rt, the reaction was quenched with saturated aq. sodium bicarbonate. The compound was extracted with diethyl ether (100 mL × 3). The organic layer was dried over Na_2SO_4 and the volatile solvent was distilled under reduced pressure. The residue was purified by column chromatography (ethyl acetate:hexane 5:95) to afford pure **46** as colourless crystals (5 g, 80% yield). mp 40 ˚C (reported 59-65 °C, hexane);[70] R_f (ethyl acetate:hexane 10:90) = 0.63; IR (KBr) cm^{-1}: 3204, 3065, 2996, 2941, 1692, 1632, 1586, 1465, 1385; ^{1}H NMR (400 MHz, CDCl$_3$) δ 1.75 (s, 6H), 6.45 (dd, , J = 8.4 Hz, , J = 0.8 Hz, 1H), 6.64 (dd, , J = 8.4 Hz, , J = 0.8 Hz, 1H), 7.42 (t, , J = 8.4, 1H), 10.34 (s, 1H); ^{13}C NMR (100 MHz, CDCl$_3$) δ 25.6 (2C), 99.3, 107.1, 107.2, 110.8, 137.9, 155.6, 161.4, 165.4.

3.12.11. Procedure for synthesis of triflate 47
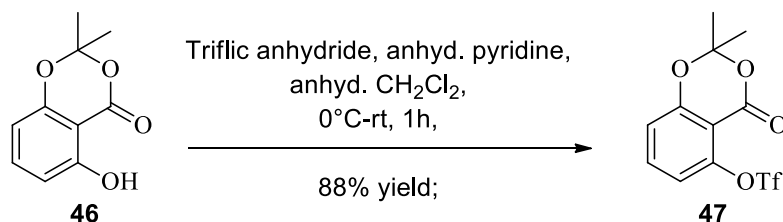
In a two neck 500 mL round bottom flask was placed protected phenol **46** (0.026 mol) in anhd. CH$_2$Cl$_2$ (50 mL) under N_2 atmosphere. To this solution, anhyd. pyridine (3.70 equiv) was added dropwise under mechanical stirring. The resulting solution was cooled in an ice-salt bath and triflic anhydride (1.20 equiv) was added to it dropwise. The reaction mixture

was then was gradually allowed to warm at rt and the progress of the reaction was monitored on TLC. After 1 h the reaction was diluted with diethyl ether (100 mL) and water (100 mL) and the compound was extracted with diethyl ether (100 mL × 3). The organic layer was dried over Na_2SO_4 and the volatile solvent was distilled under reduced pressure. The residue was purified by column chromatography (ethyl acetate:hexane 10:90) to afford pure triflate **47** as colourless crystals (7 g, 88% yield). mp 120 ˚C (reported 115-118 °C;[70] R_f (ethyl acetate:hexane 10:90) = 0.91; IR (KBr) cm^{-1} 2924, 2853, 1746, 1620, 1578, 1474, 1439; ^{1}H NMR (400 MHz, CDCl$_3$) δ 1.77 (s, 1H), 7.00 (d, *J* = 8.0, 1H), 7.06 (dd, *J* = 8.4 Hz, *J* = 0.8 Hz, 1H), 7.61 (t, *J* = 8.4, 1H); ^{13}C NMR (100 MHz, CDCl$_3$) δ 25.5 (2C), 106.8, 108.3, 116.6, 117.8, 117.9, 120.3, 136.3, 148.6, 157.1, 157.4.

3.12.12. Procedure for synthesis of protected styrene 48
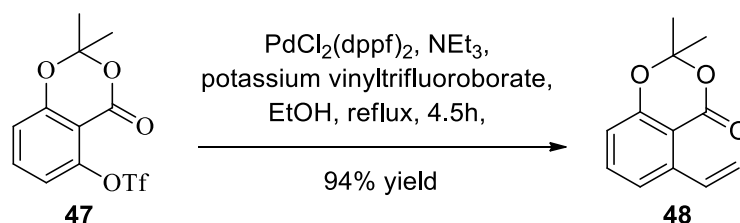
In a two neck RBF equipped with a water circulation condenser, PdCl$_2$(dppf)$_2$ (5 mol%) and triethyl amine (1.30 equiv) were added to a stirring solution of potassium vinyltrifluoroborate (1.10 equiv) in absolute ethanol (100 mL) under N$_2$ atmosphere. To this was then added triflate **47** (0.016 mol) under mechanical stirring. The resulting reaction mixture was refluxed for 4.5h. The progress of the reaction was monitored on TLC. After complete consumption of the starting material, the reaction mixture was then cooled to rt, ethanol was distilled out completely on rotavap under reduced pressure. The residue was then diluted with water (100 mL) and the aqueous layer was extracted with diethyl ether (100 mL × 3). The organic layer was dried over Na$_2$SO$_4$ and the volatile solvent was distilled under reduced pressure. The residue was purified by column chromatography (ethyl acetate: hexane 5:95) to afford pure protected styrene **48** as colorless oil (3 g, 94% yield).[71] R_f (ethyl acetate:hexane 20:80) = 0.23; IR (Neat) cm^{-1}: 3125, 2927, 2941, 2928, 1732, 1576, 1475, 1390, 1271; ^{1}H NMR (400 MHz, CDCl$_3$) δ 1.72 (s, 6H), 5.43 (dd, *J* = 11.2 Hz, *J* = 1.2 Hz, 1H), 5.72 (dd, *J* = 17.2 Hz, 1.2 Hz, 1H), 6.89 (dd, *J* = 8.0 Hz, *J* = 0.8 Hz, 1H), 7.28 (d, *J* = 6.8 Hz, 1H), 7.48 (t, *J* = 8.0

Hz, 1H), 7.72 (dd, J = 17.2 Hz, J = 11.2 Hz, 1H); ^{13}C NMR (100 MHz, CDCl$_3$) δ 25.6 (2C), 105.3, 110.9, 116.6, 117.8, 121.4, 135.3, 135.4, 142.3, 156.7, 160.4.

3.12.13. Procedure for synthesis of functionalized styrene intermediate39
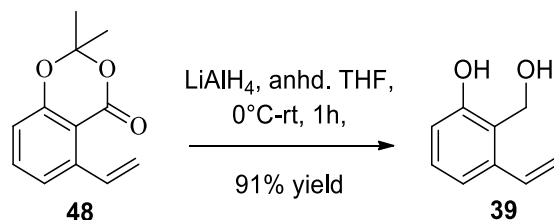
In a two neck 500 mL RBF containing a slurry of LiAlH$_4$ (1.50 equiv) in anhd. THF (50 mL), a solution of protected styrene **48** (0.014 mol) in anhd. THF (40 mL) was added dropwise under mechanical stirring and N$_2$ atmosphere at 0°C. The resulting reaction mixture was gradually allowed to warm at rt and stirred for an additional hour at rt. The progress of the reaction was monitored on TLC. After complete consumption of the starting material (1h), the reaction mixture was immersed in an ice bath and quenched with water dropwise. THF was distilled out completely on rotavap under reduced pressure. The compound was then extracted with ethyl acetate (100 mL× 3). The organic layer was dried over Na$_2$SO$_4$ and volatile solvent was distilled under reduced pressure to afford pure functionalized styrene intermediate **39** as colorless viscous liquid (2 g, 91% yield).[71] R$_f$ (ethyl acetate:hexane 2:8) = 0.68; IR (Neat) cm^{-1} 3280, 3183, 3086, 2963, 2924, 2853, 1572, 1454, 1265, 985; ^{1}H NMR (400 MHz, CDCl$_3$) δ 4.87 (s, 2H), 5.25 (dd, J = 10.8 Hz, J = 1.2 Hz, 1H), 5.49 (dd, J = 17.2 Hz, J = 1.2 Hz, 1H), 6.72 (d, J = 8.0 Hz, 1H), 6.79 (dd, J = 17.2 Hz, J =10.8 Hz, 1H), 6.91 (d, J = 7.6 Hz, 1H), 7.07 (t, J = 8.0 Hz, 1H), 7.72 (bs, 0.6 H); ^{13}C NMR (100 MHz, CDCl$_3$) δ 58.8, 114.9, 116.6, 117.6, 121.0, 128.0, 132.9, 136.5, 155.2.

3.12.14. Procedure for synthesis of mono-methylated alkene 49
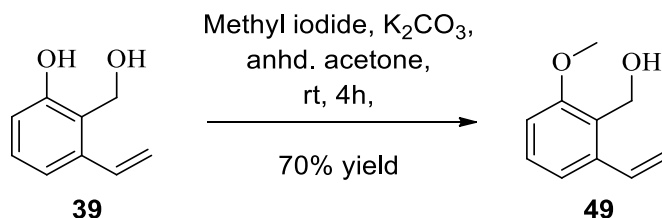
Chapter 3

In a two neck 500 mL RBF containing a solution of functionalized styrene intermediate **39** (0.011 mol) in anhd. acetone (80 mL), potassium carbonate (2.00 equiv) and methyl iodide (2.00 equiv) were added under mechanical stirring and N_2 atmosphere. The resulting reaction mixture was stirred at rt for 4 h. The progress of the reaction was monitored on TLC. After complete consumption of the starting material (4h) acetone was distilled out completely on rotavap under reduced pressure. The residue was diluted with water and the compound was then extracted with ethyl acetate (100 mL× 3). The organic layer was dried over Na_2SO_4 and the volatile solvent was distilled under reduced pressure. The crude residue was purified by column chromatography (ethyl acetate: hexane 2:8) to afford pure mono-methylated styrene **49**as colorless oil (1.3 g, 70% yield).[71]R_f (ethyl acetate:hexane 2:8) = 0.50; IR (Neat) cm^{-1} 3327, 3125, 2957, 2924, 2872, 2853, 1574, 1470, 1263, 1076;^{1}H NMR (400 MHz, CDCl$_3$) δ 3.87 (s, 3H), 4.80 (s,2H), 5.36 (dd, J = 11.2 Hz, J = 1.6 Hz, 1H), 5.66 (dd, J = 17.2 Hz, J = 1.2 Hz, 1H), 6.84 (d, J = 8.2 Hz, 1H), 7.09 (dd, J = 17.6 Hz, J = 11.2 Hz, 1H), 7.26 (dd, J = 8.4 Hz, J = 7.6 Hz, 1H); ^{13}C NMR (100 MHz, CDCl$_3$) δ 55.64, 56.80, 109.71, 117.52, 118.93, 126.17, 128.89, 134.16, 138.61, 158.00.

3.12.15. Procedure for synthesis of aromatic building block 37
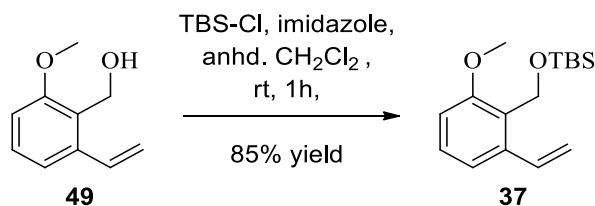
In a two neck 500 mL RBF containing a solution of mono-methylated styrene **49** (0.007 mol) in anhd. CH$_2$Cl$_2$ (80 mL), imidazole (3.05 equiv) and tertiarybutyldimethylsilyl chloride (TBS-Cl) (1.20 equiv) were added under mechanical stirring and N_2 atmosphere. The progress of the reaction was monitored on TLC. After complete consumption of the starting material (1h) reaction mixture was immersed in an ice bath and quenched with saturated aq. ammonium chloride solution. The compound was then extracted with CH$_2$Cl$_2$ (100 mL× 3). The organic layer was dried over Na_2SO_4 and the volatile solvent was distilled under reduced pressure. The crude residue was purified by column chromatography (ethyl acetate: hexane 3:97) to afford pure aromatic building block **37** as colourless oil (1.7 g, 85% yield).[71] R_f (ethyl acetate:hexane 5:95) = 0.70; IR (Neat) cm^{-1} 3091, 2955, 2929, 2885, 2822, 1570, 1466,

1249, 1040 ; ^{1}H NMR (400 MHz, CDCl$_3$) δ -0.0001 (s, 6H), 0.84 (s, 9H), 3.77 (s, 3H), 4.77 (s, 2H), 5.26 (dd, J = 10.8 Hz, J = 1.6 Hz, 1H), 5.63 (dd, J = 17.6 Hz, J = 1.6 Hz, 1H), 6.74 (d, J = 8.0 Hz, 1H), 7.08-7.21 (m, 3H); ^{13}C NMR (100 MHz, CDCl$_3$) δ -5.20 (2C), 18.47, 25.99, 55.62, 55.97, 109.95, 116.00, 118.36, 126.39, 128.59, 135.06, 139.71, 157.42.

3.12.16. Procedure for synthesis of protected thiovaritriols 50a and 50b and self-coupled product 51
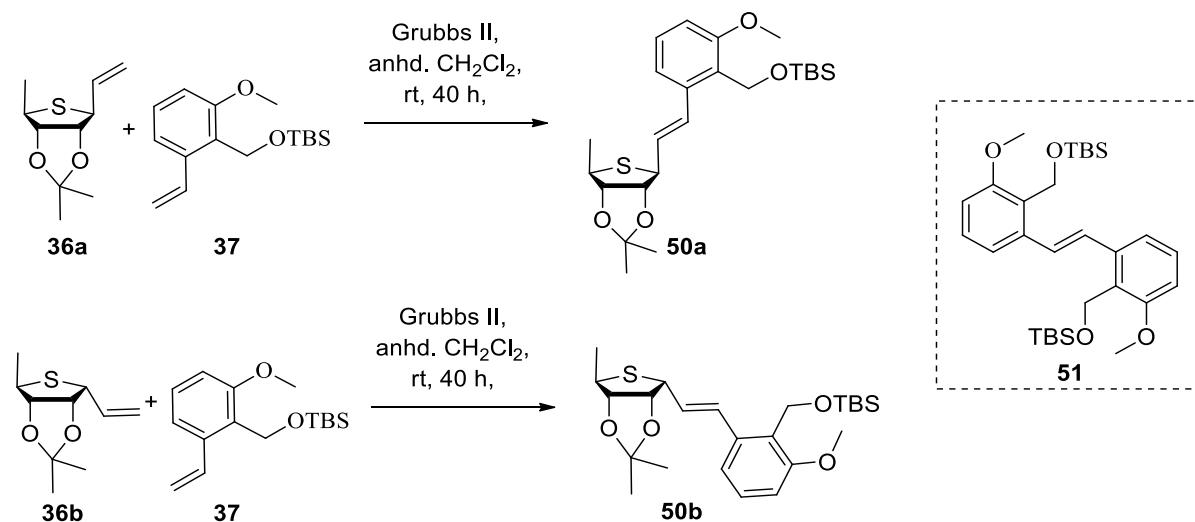
In a two neck, 25 mL RBF equipped with a water circulation condenser was placed aromatic building block **37** (1.00 equiv) under N$_2$ atmosphere. To this was then added thiosugar **36a/36b** (0.625 mmol) in anhd. CH$_2$Cl$_2$ (5 mL) and Grubbs IInd generation catalyst (5 mol%). The resulting reaction mixture was refluxed for 40 h. The progress of the reaction was monitored on TLC. Then, CH$_2$Cl$_2$ was distilled out completely on the rotavap under reduced pressure. The crude residue was then purified by column chromatography (Diethyl ether: hexane 5:95) to afford pure self-coupled aromatic product **51** as white sticky liquid (50 mg, 26% yield) & recovered aromatic building block **37** (50 mg, 29% yield); (diethyl ether acetate/ petroleum ether = 1/9) pure protected thiovaritriol **50a/50b** as a colourless viscous liquid (80 mg, 42% yield).

Protected thio-varitriol **50b**: R$_f$ (Diethyl ether:hexane 1:9) = 0.88; [α] $^{22.6}$ $_D$ = -7.5 (c 0.08, CHCl$_3$); IR (Neat) cm^{-1} 2916, 2864, 1560, 1466, 1218, 1084; ^{1}H NMR (400 MHz, CDCl$_3$) δ -0.02 (6H), 0.82 (s, 9H), 1.26 (s, 3H), 1.34 (d, J = 6.8 Hz, 3H), 1.48 (s, 3H), 3.40 (sx, J = 6.8

Hz, J = 5.6 Hz, 1H), 3.74 (s, 3H), 4.06 (dd, J = 8.4 Hz, J = 5.6 Hz, 1H), 4.35 (t, J = 5.6, 1H), 4.60 (t, J = 5.6 Hz, 1H), 4.73 (s, 2H), 6.07 (dd, J = 15.6 Hz, J = 8.4 Hz, 1H), 6.7 (d, J = 8.0, 1H), 7.00 (dd, J = 15.6 Hz, J = 7.2 Hz, 2H), 7.12 (t, J = 8.0 Hz, 1H); ^{13}C NMR (100 MHz, CDCl$_3$) δ -6.2 (2C), 17.4, 18.0, 24.4, 25.0 (3C), 26.7, 46.0, 54.1, 54.6, 54.9, 87.2, 88.4, 108.9, 112.6, 117.8, 125.4, 127.5, 128.3, 129.6, 137.4, 156.4. HRMS (TOF MS ES+) m/z calculated for C$_{24}$H$_{38}$O$_4$SSi [M + K]$^+$ 489.1897, found 489.2113.

Protected thio-varitriol **50a**: R$_f$ (Diethyl ether:hexane 1:9) = 0.81; [α] $^{22.6}$ $_D$ = -4.2 (c 0.24, CHCl$_3$); IR (Neat) cm^{-1} : 2910, 2852, 1530, 1450, 1210, 1070; ^{1}H NMR (400 MHz, CDCl$_3$) δ -0.00 (s, 6H), 0.82 (s, 9H), 1.24 (s, 3H), 1.31 (d, J = 7.6 Hz, 3H), 1.49 (s, 3H), 3.28 (qd, J = 7.3 Hz, J = 1.2 Hz, 1H), 3.74 (s, 3H), 4.18 (dd, J = 9.2 Hz, J = 4.4 Hz, 1H), 4.48 (dd, J = 5.6 Hz, J = 1.6 Hz, 1H), 4.71-4.75 (m, 3H), 6.2 (dd, J = 16.0 Hz, J = 9.2 Hz, 1H), 6.69 (dd, J = 7.6 Hz, J = 1.2 Hz, 1H), 6.91 (d, J = 15.6 Hz, 1H), 7.08-7.17 (m, 2H); ^{13}C NMR (100 MHz, CDCl$_3$) δ -6.2 (2C), 19.3, 23.6, 25.0 (3C), 25.3, 47.3, 52.5, 54.6, 54.9, 84.3, 89.4, 108.8, 110.2, 118.0, 125.3, 125.4, 127.4, 129.8, 137.6, 156.2. HRMS (TOF MS ES+) m/z calculated for C$_{24}$H$_{38}$O$_4$SSi [M + Na]$^+$ 473.2158, found 473.2159.

Self-coupled aromatic product **51**: IR (Neat) cm^{-1} 2955, 2926, 2896, 2855, 1578, 1468, 1250, 1055; ^{1}H NMR (400 MHz, CDCl$_3$) δ -0.00 (s, 6H), 0.84 (s, 9H), 3.79 (s, 3H), 4.85 (s, 2H), 6.75 (dd, J = 8.0 Hz, J = 1.2 Hz, 1H), 7.18-7.26 (m, 3H); ^{13}C NMR (100 MHz, CDCl$_3$) δ -5.2 (2C), 18.4, 25.9 (3C), 56.7, 56.0, 109.8, 118.5, 126.7, 128.6, 128.7, 139.7, 157.4. HRMS (TOF MS ES+) m/z calculated for C$_{30}$H$_{48}$O$_4$Si$_2$ [M + Na]$^+$ 551.3091, found 551.2989.

3.12.17. Synthesis of 3'-*epi*-thiovaritriol 3
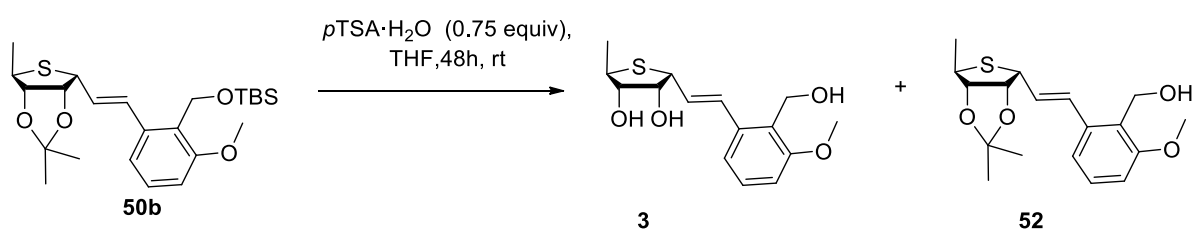
In a single neck RBF was placed **50b** (25 mg) under N$_2$ atmosphere in THF (approx. 1.5 mL). To this pTSA·H$_2$O (0.75 equiv) was added in portions over the period of 48h. At 0h pTSA·H$_2$O (0.30 equiv) was added. At 7h another portion of pTSA·H$_2$O (0.30 equiv) was added. At 12h another portion of pTSA·H$_2$O (0.15 equiv) was added. Similarly, At 24h

another portion of pTSA·H$_2$O (0.01 mmol) was added. The resulting reaction mixture was stirred at rt for 7h. The progress of the reaction was monitored on TLC. Then, THF was distilled out completely on the rotavap under reduced pressure. The crude residue was then dissolved in CH$_2$Cl$_2$ purified by column chromatography (ethyl acetate: hexane 1:1) to afford pure **52** as a white viscous liquid (3 mg, 16% yield) & (ethyl acetate: hexane 1:0) to afford pure **3** as a white viscous liquid (10 mg, 61% yield).

3: R$_f$ (ethyl acetate:hexane 1:0) = 0.50; $[\alpha]^{22.6}_D$ = -39.2 (c 0.05, CHCl$_3$); IR (Neat) cm^{-1} 3339, 2966, 2916, 2845, 1728, 1577, 1447, 1255, 1084, 1013, 802; ^{1}H NMR (400 MHz, CDCl$_3$) δ 1.307 (d, J = 7.2 Hz, 3H), 2.20 (t, J = 7.6 Hz, 1H), 2.43 (t, J = 8.0 Hz, 1H), 3.25-3.27 (m, 1H), 3.781 (s, 3H), 3.87-3.88 (m, 1H), 3.99 (s, 2H), 4.29 (t, J = 6.8 Hz, 1H), 4.64 (d, J = 12 Hz, 1H), 4.77 (d, J = 12 Hz, 1H), 5.96 (dd, J = 8.4 Hz, J = 15.6 Hz, 1H), 6.74 (d, J = 8 Hz, 1H), 6.84 (d, J = 15.2 Hz, 1H,), 7.02 (d, J = 8 Hz, 1H), 7.17 (t, J = 8 Hz, 1H).

52: R$_f$ (ethyl acetate:hexane 1:1) = 0.50; ^{1}H NMR (400 MHz, CDCl$_3$) δ 1.26 (s, 3H), 1.34 (d, 3H, J = 7.2 Hz), 1.49 (s, 3H), 3.58 (sx, J = 6.8 Hz, J = 5.6 Hz, 1H), 3.80 (s, 3H), 4.05 (dd, J = 6.8 Hz, J = 5.6 Hz, 1H), 4.36 (dd, J = 6.8 Hz, J = 5.6 Hz, 1H), 4.60 (dd, J = 5.7 Hz, J = 5.6 Hz, 1H), 4.70 (s, 2H), 6.04 (dd, J = 15.6 Hz, J = 8.4 Hz, 1H), 6.75 (d, J = 16.0 Hz, 1H), 6.91 (d, J = 15.6 Hz, 1H), 7.00 (d, J = 8.0 Hz, 1H), 7.15 (d, J = 8.0 Hz, 1H).

3.13. Spectra

LR-S2-23-02 DMSO-D6 PMR
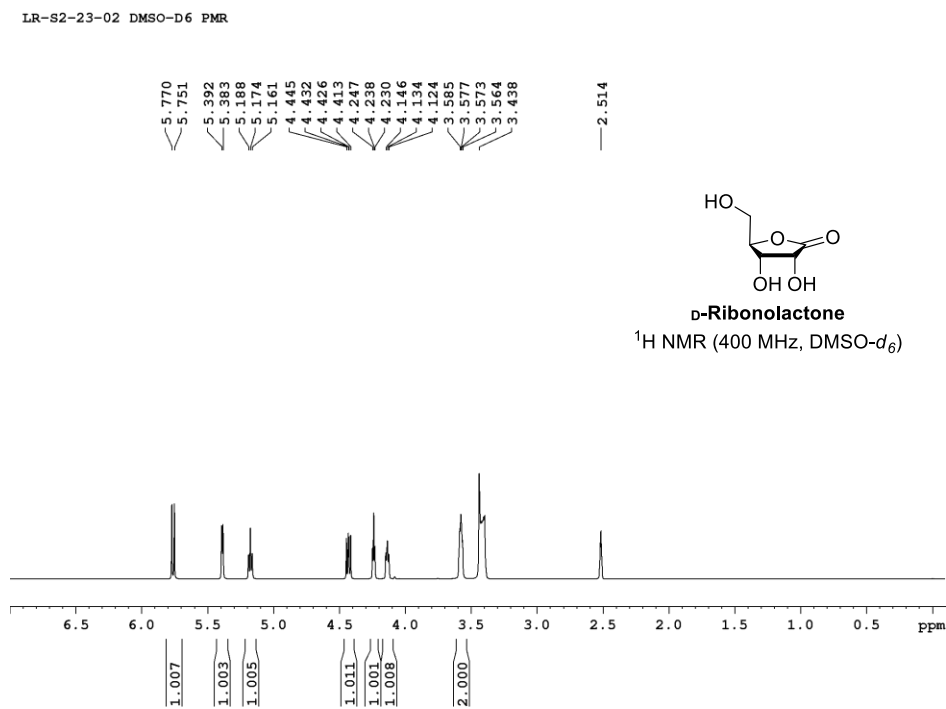
Figure 3.29: ^{1}H NMR spectrum of D-ribonolactone.
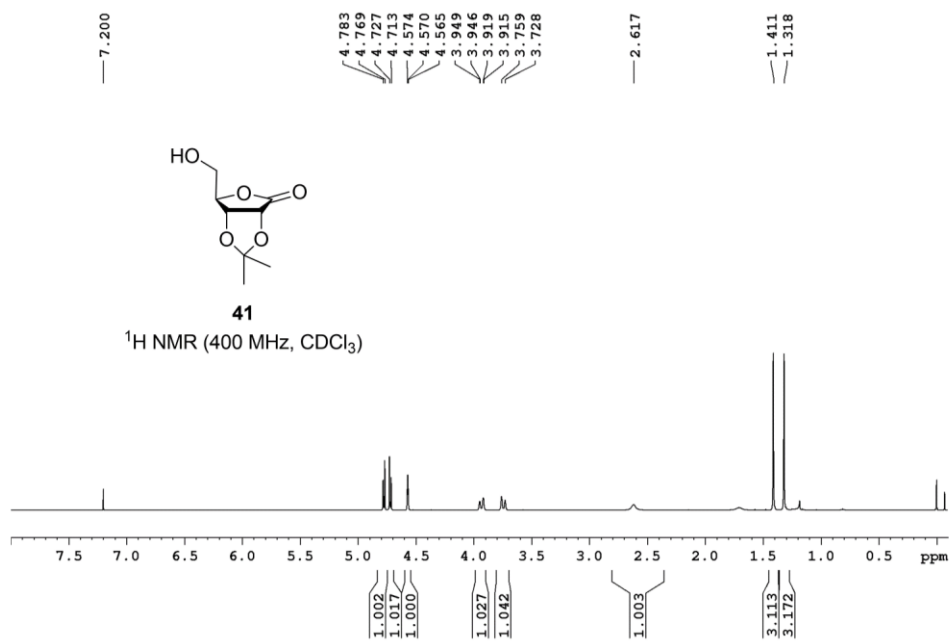
Figure 3.30: ^{1}H NMR spectrum of **41**.
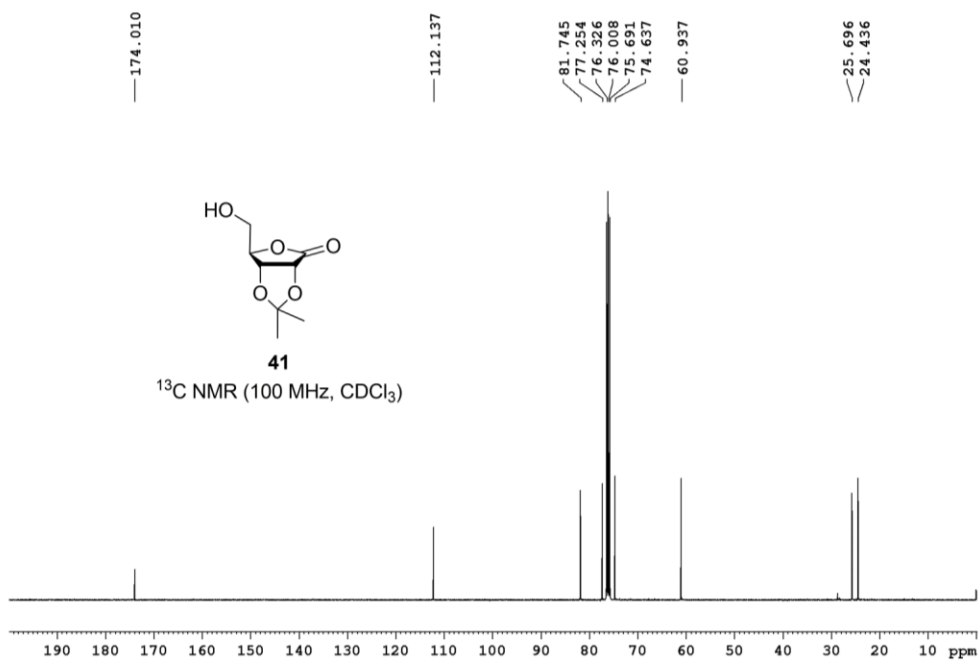
Figure 3.31: ^{13}C NMR spectrum of **41**.
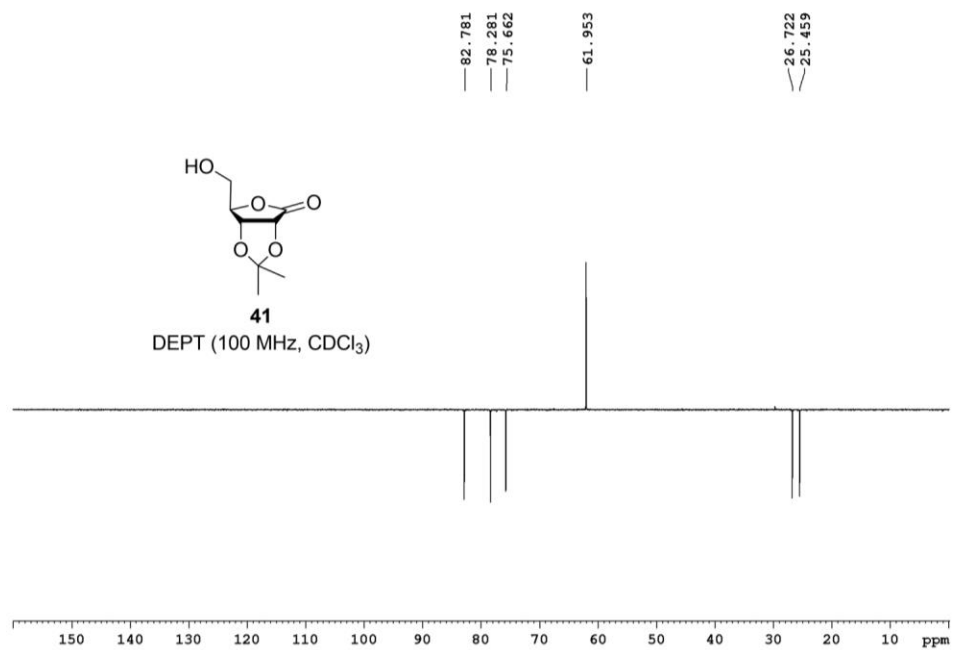
Figure 3.32: DEPT spectrum of **41**.
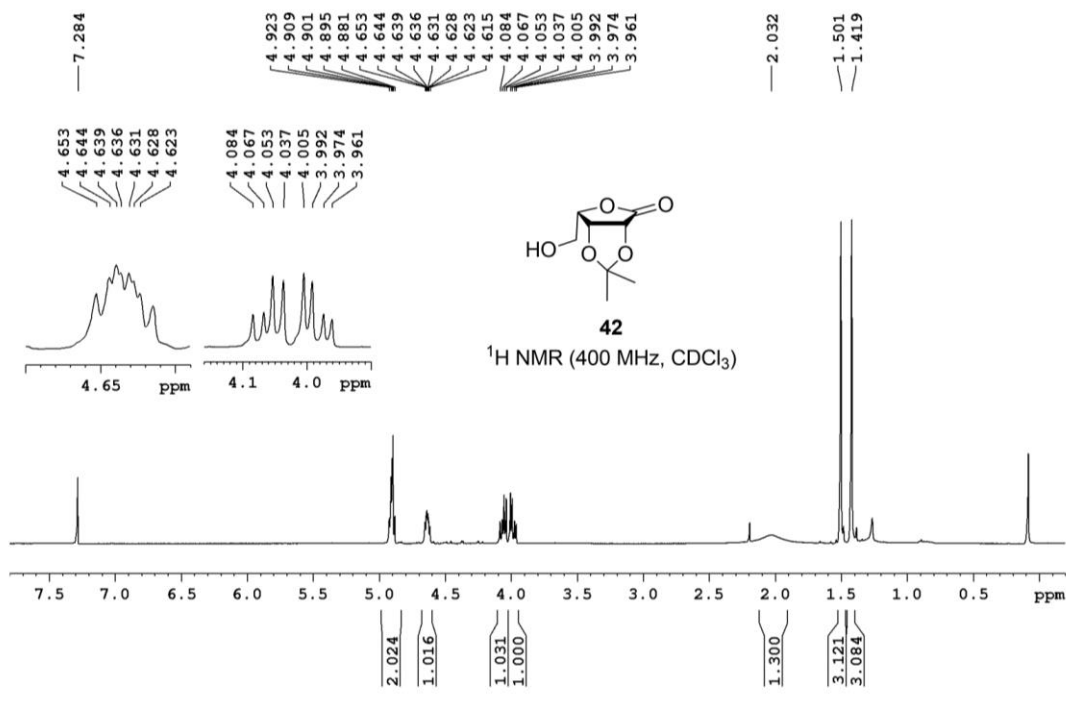
Figure 3.33: ^{1}H NMR spectrum of **42**.
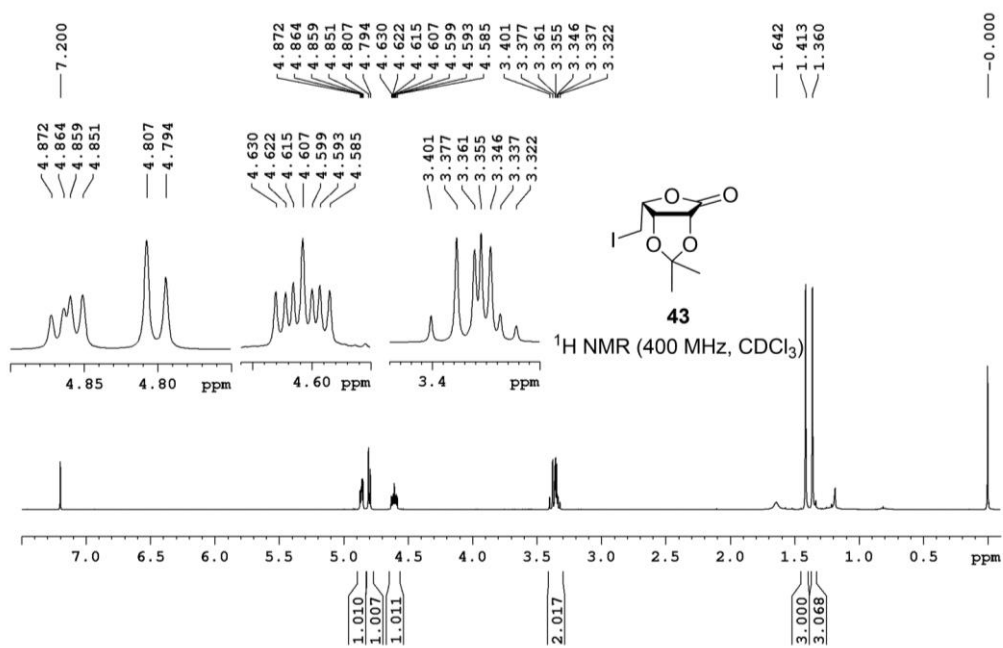
Figure 3.34: ^{1}H NMR spectrum of **43**.
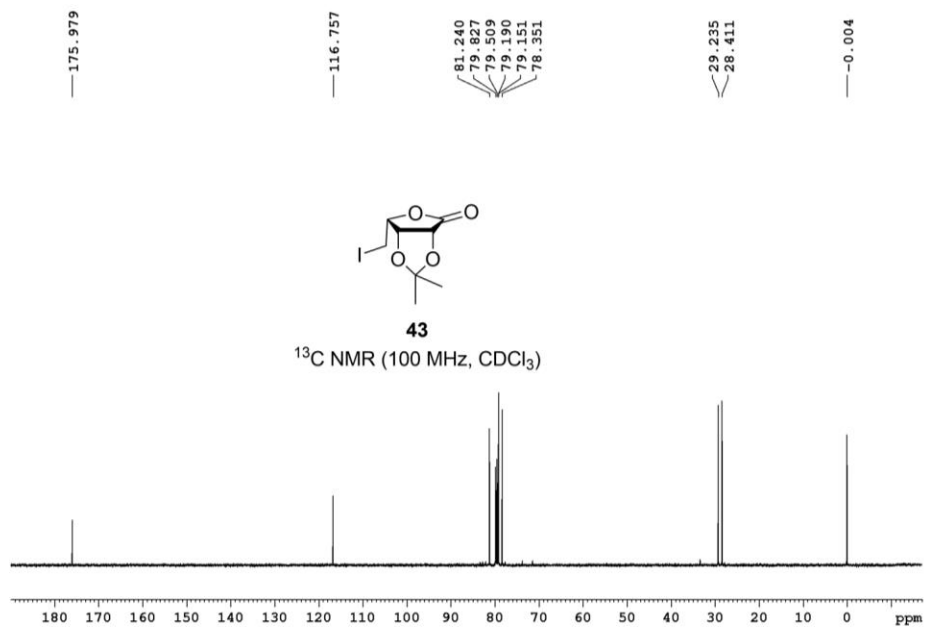
Figure 3.35: ^{13}C NMR spectrum of **43**.
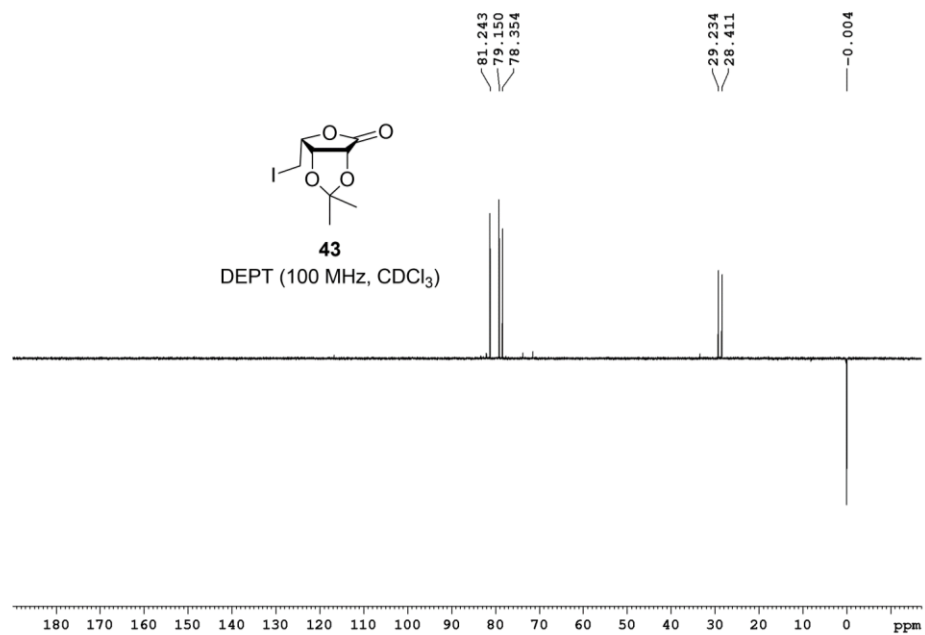
Figure 3.36: DEPT spectrum of **43**.
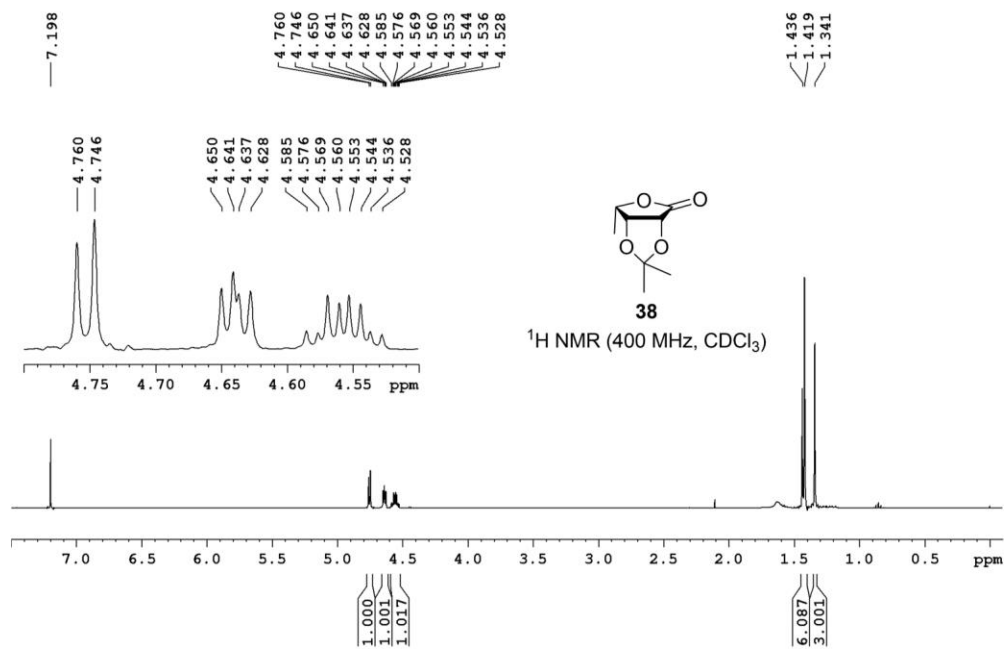
Figure 3.37: ^{1}H NMR spectrum of **38**.
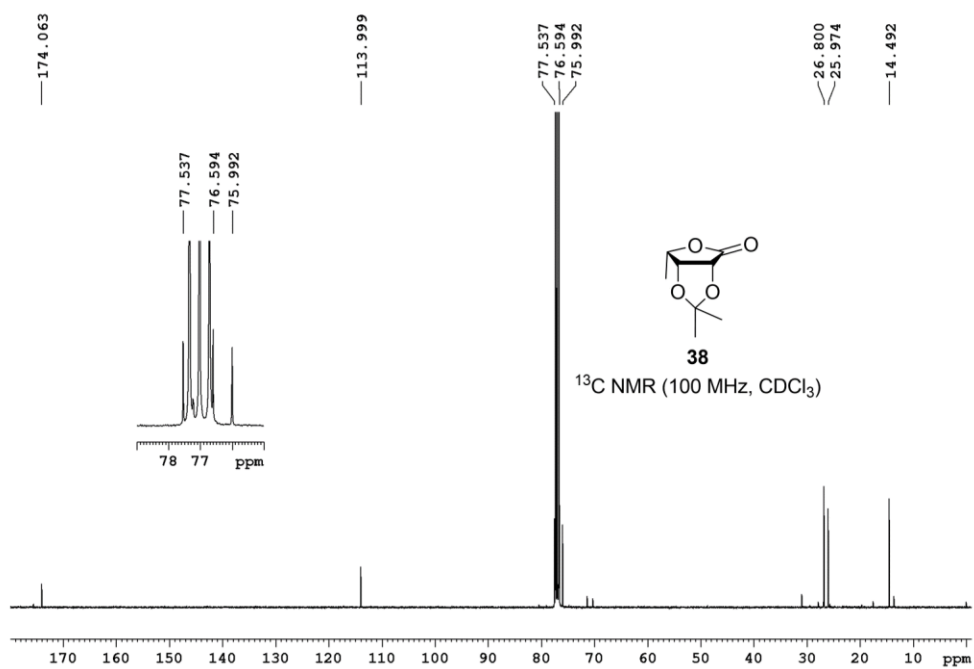
Figure 3.38: ^{13}C NMR spectrum of **38**.
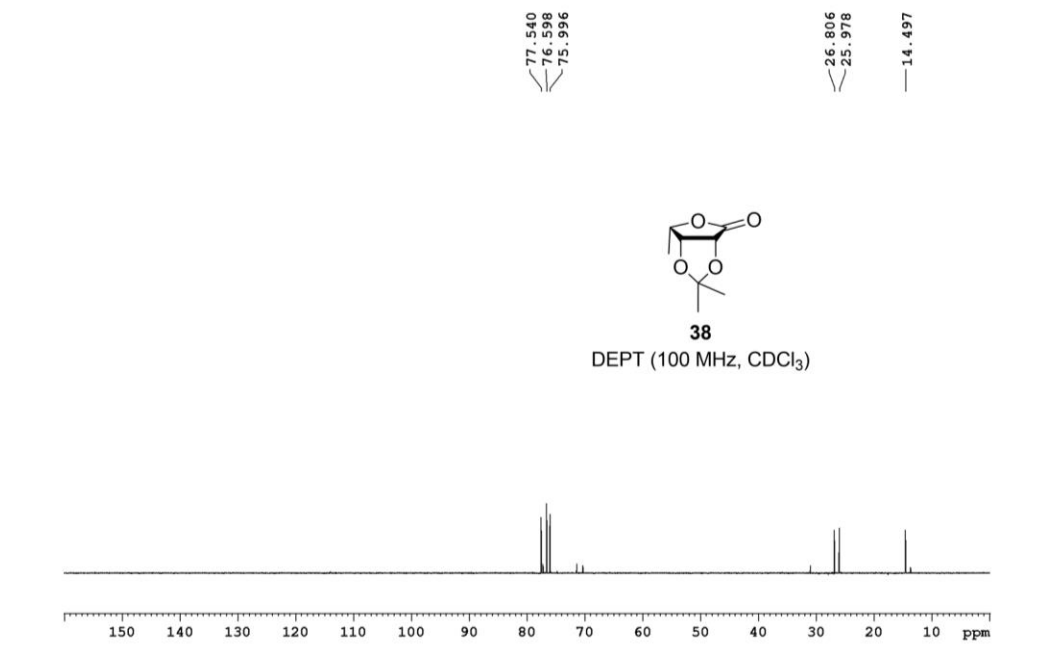
Figure 3.39: DEPT spectrum of **38**.
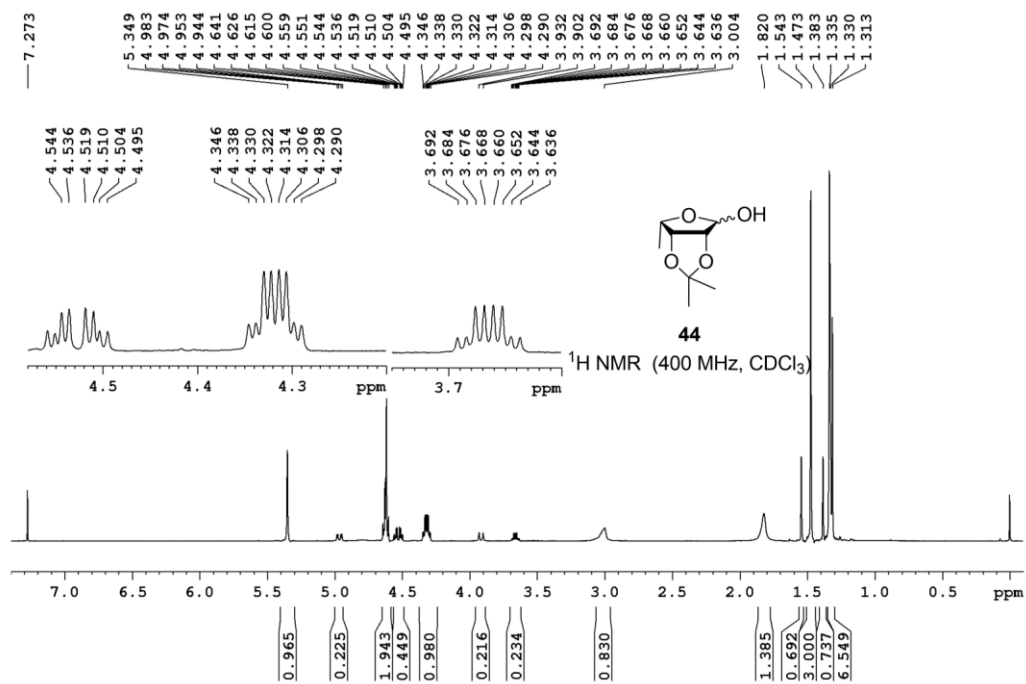
Figure 3.40: ¹H NMR spectrum of **44**.
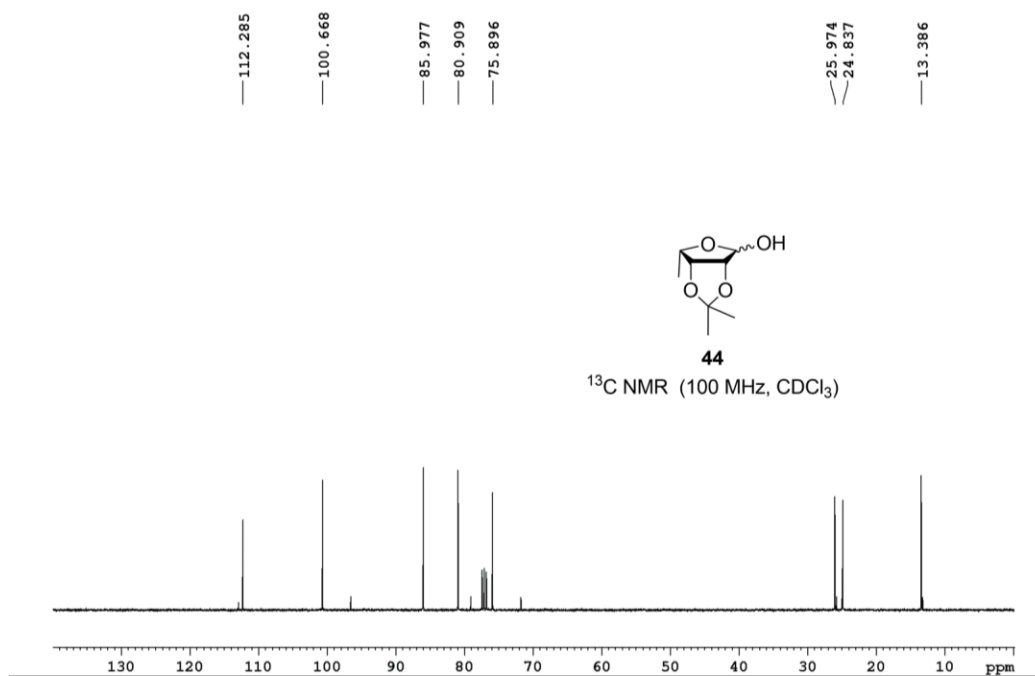
Figure 3.41: ^{13}C NMR spectrum of **44**.
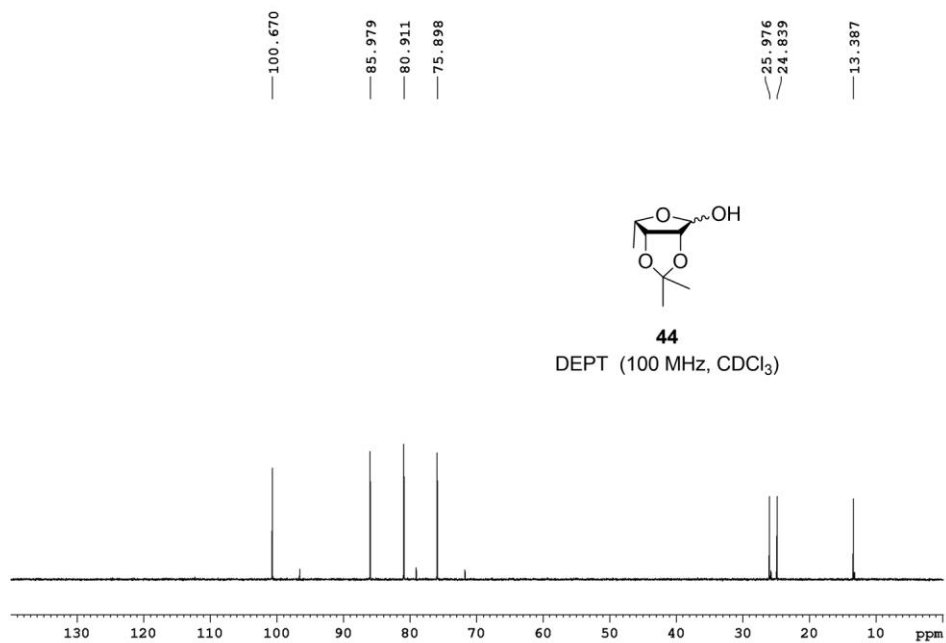
Figure 3.42: DEPT spectrum of **44**.
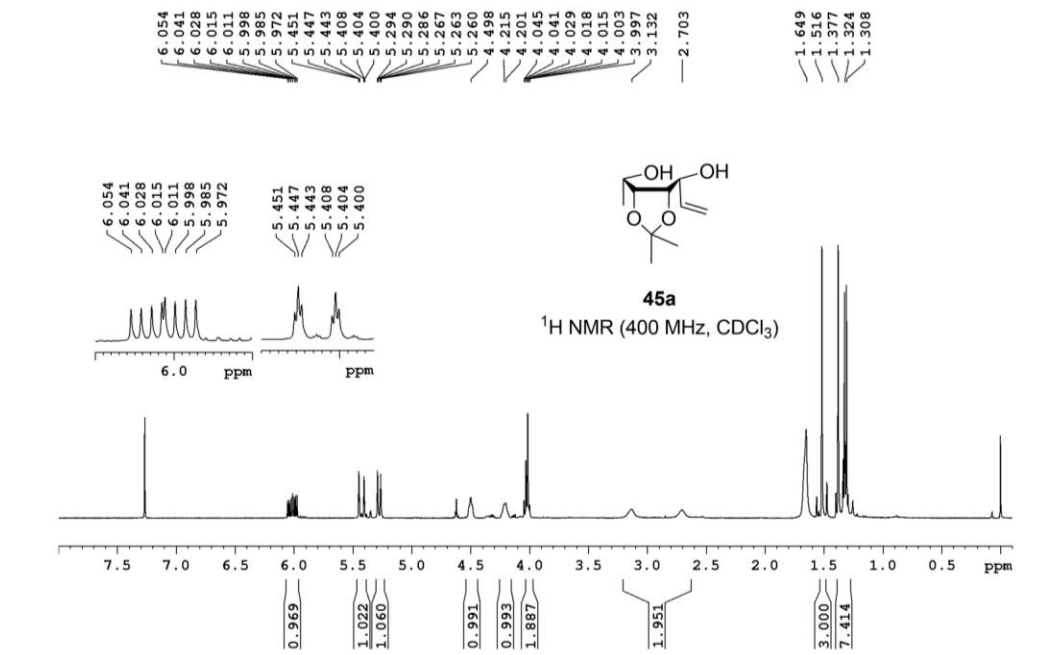
Figure 3.43: ^{1}H NMR spectrum of **45a**.
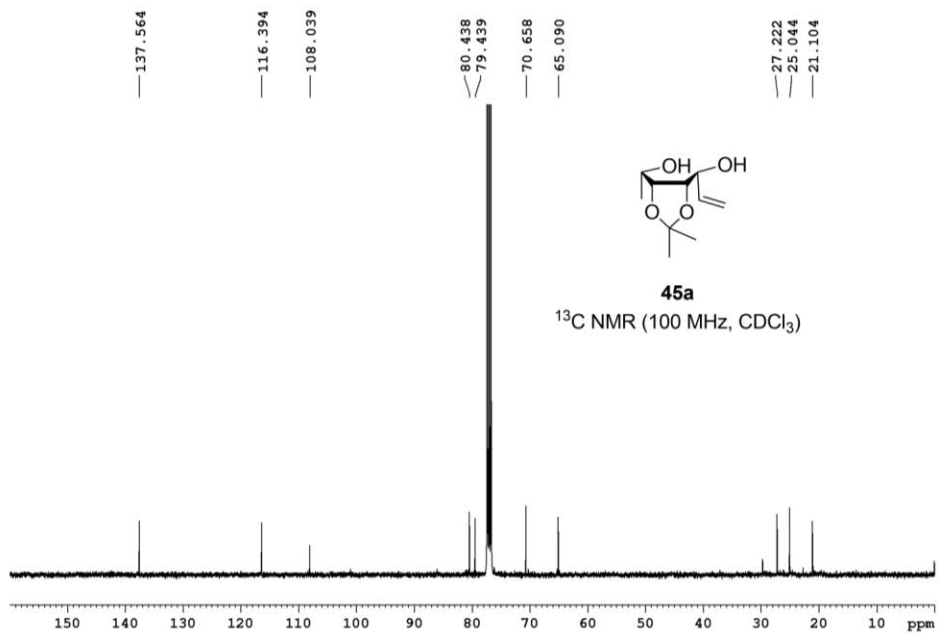
Figure 3.44: ^{13}C NMR spectrum of **45a**.
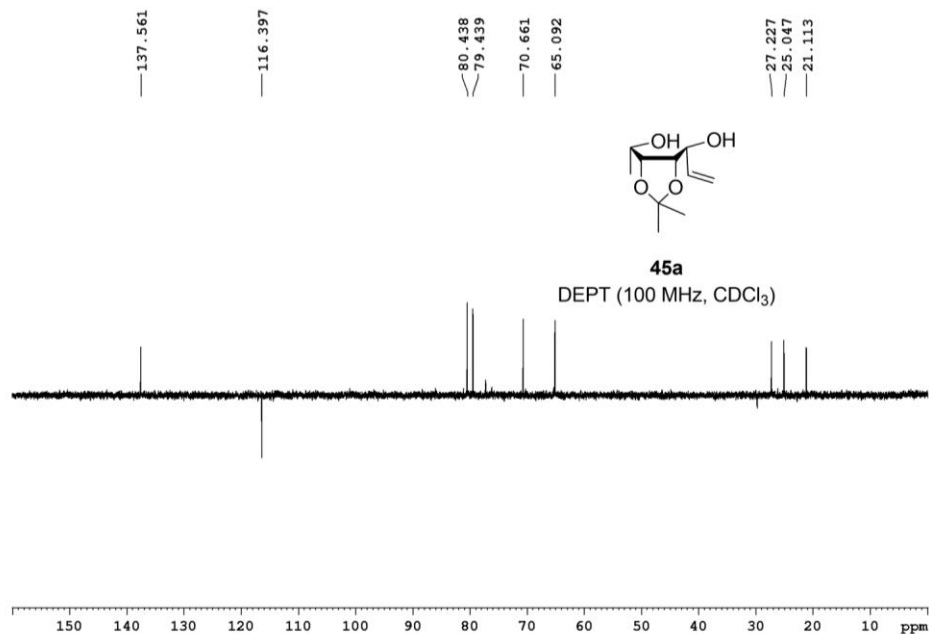
Figure 3.45: DEPT spectrum of **45a**.
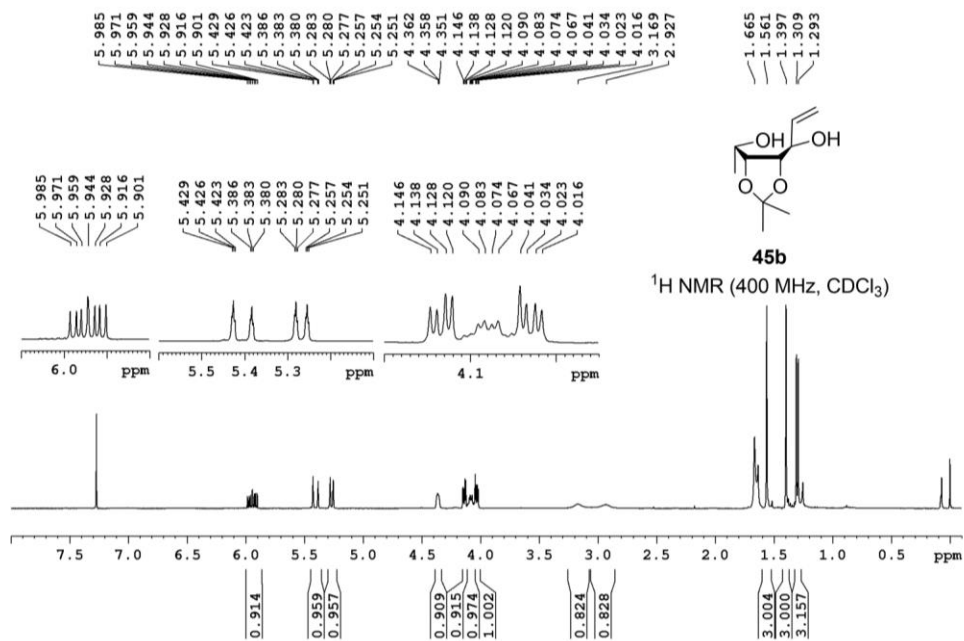
Figure 3.46: ^{1}H NMR spectrum of **45b**.
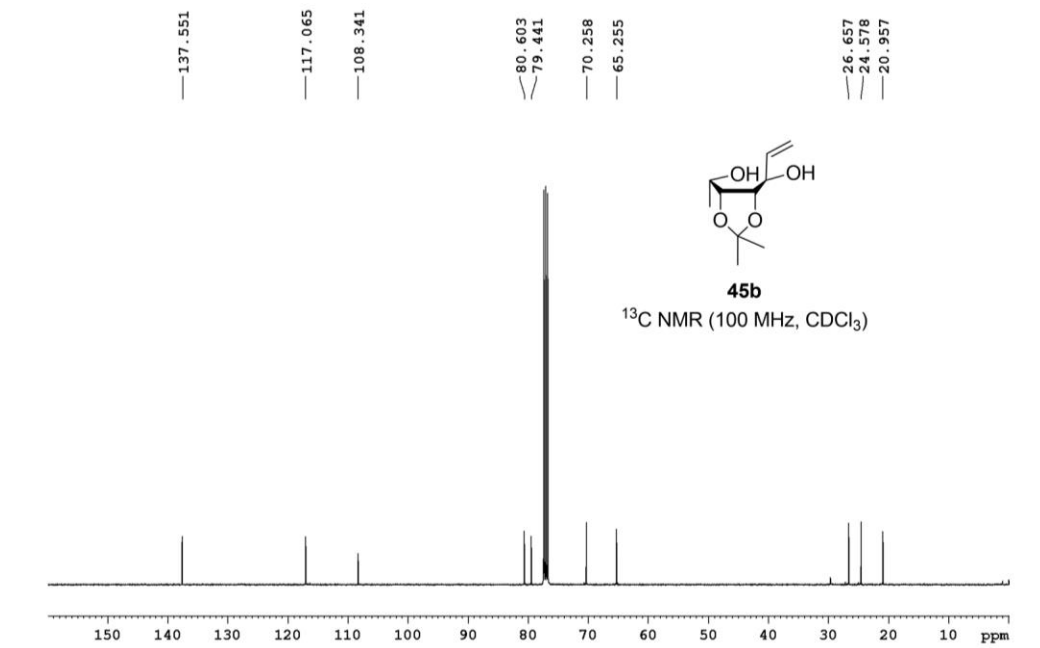
Figure 3.47: ^{13}C NMR spectrum of **45b**.
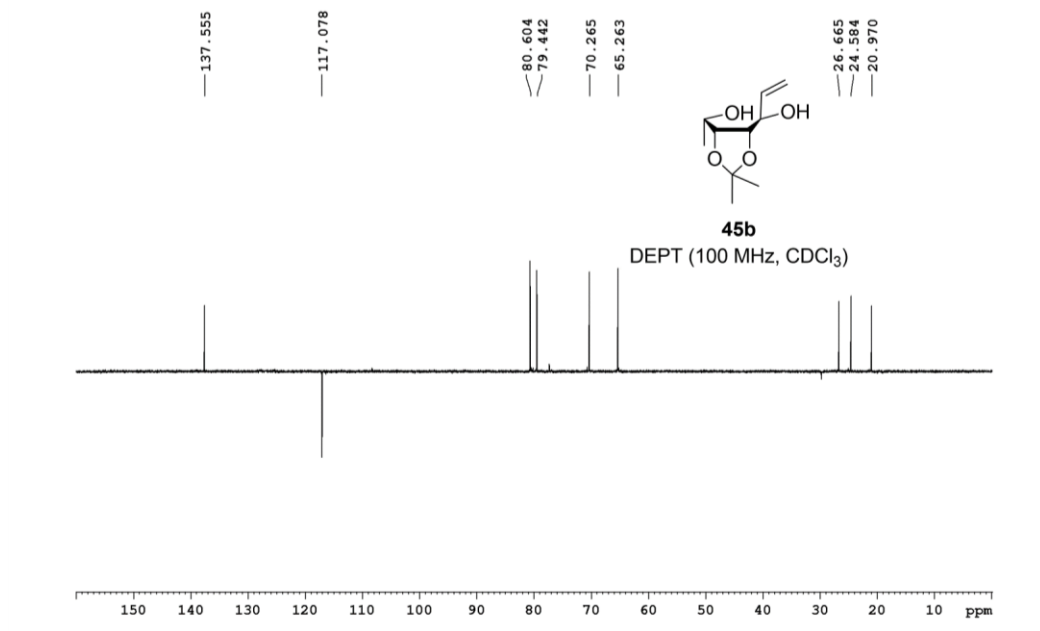
Figure 3.48: DEPT spectrum of **45b**.
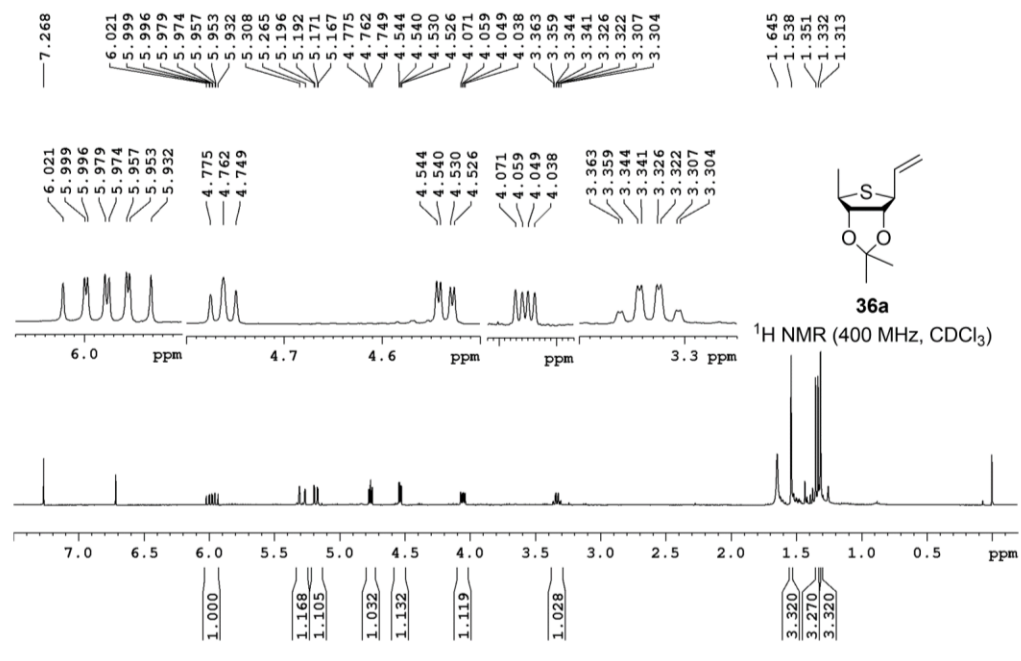
Figure 3.49: ^{1}H NMR spectrum of **36a**.
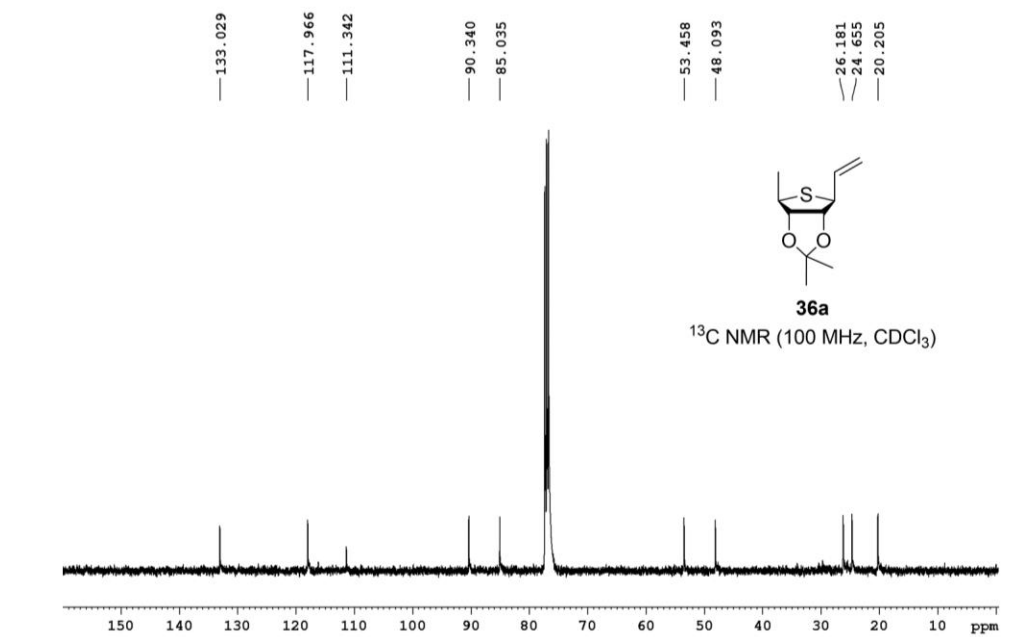
Figure 3.50: ^{13}C NMR spectrum of **36a**.
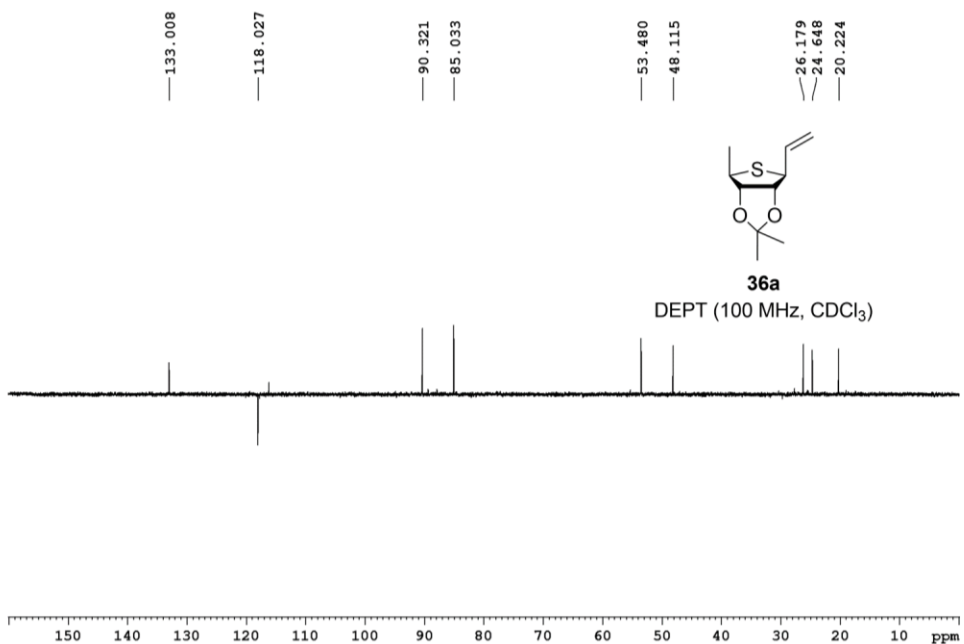
Figure 3.51: DEPT spectrum of **36a**.
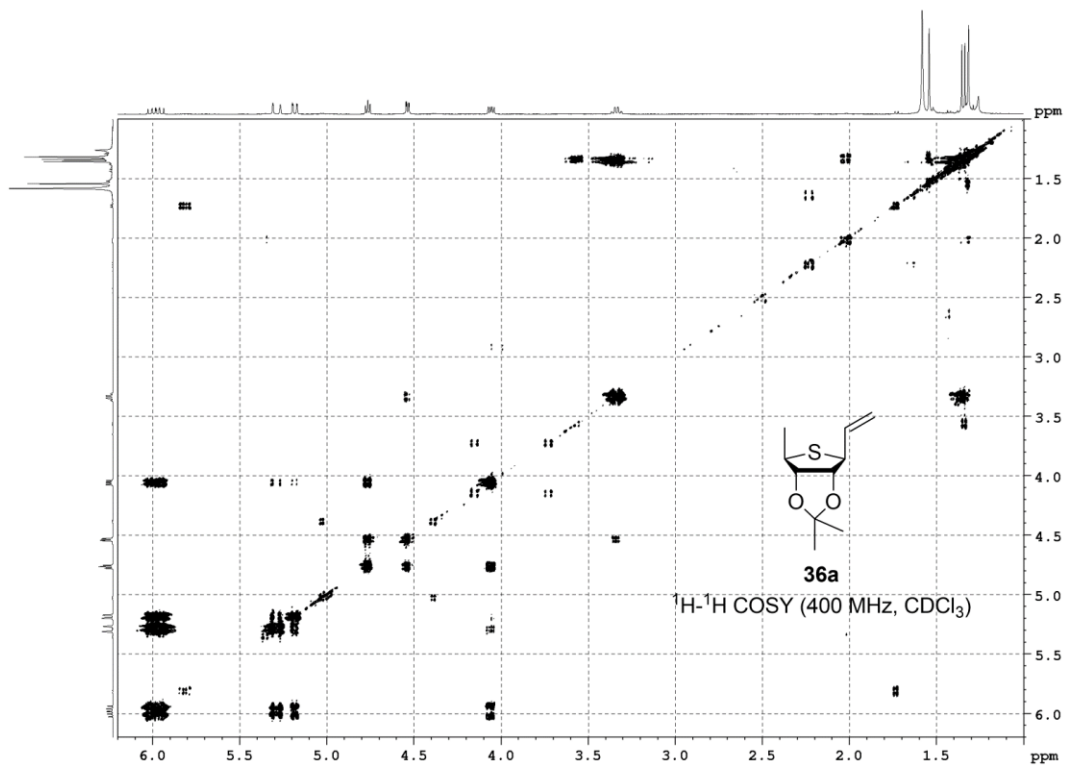
Figure3.52: ^{1}H-^{1}H COSY of spectrum of **36a**.
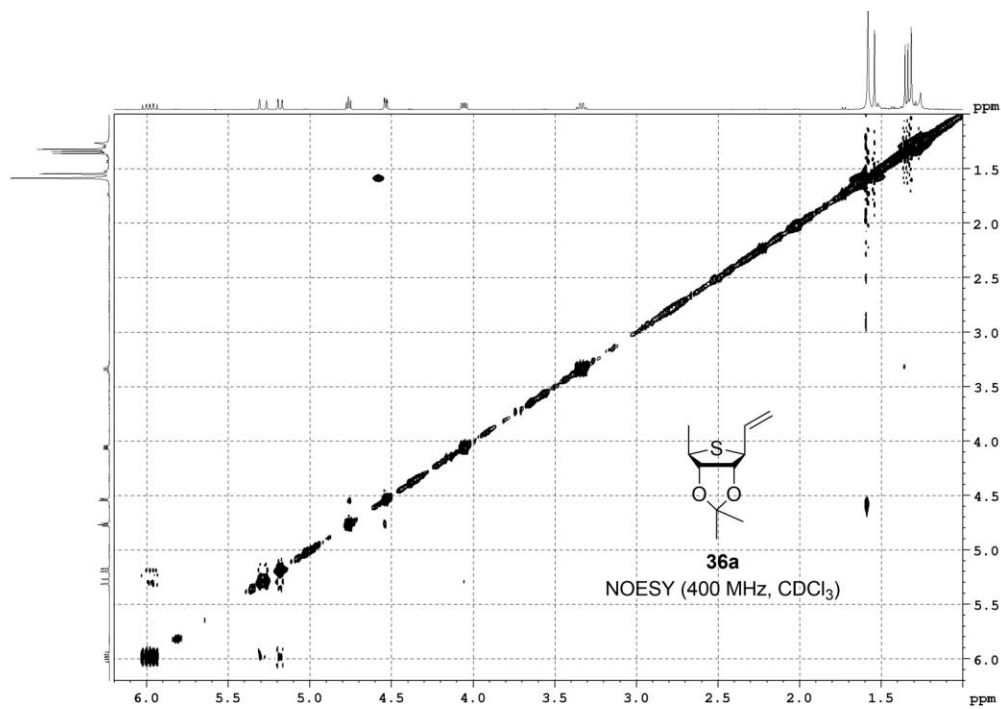
Figure3.53: NOESY spectrum of**36a**.
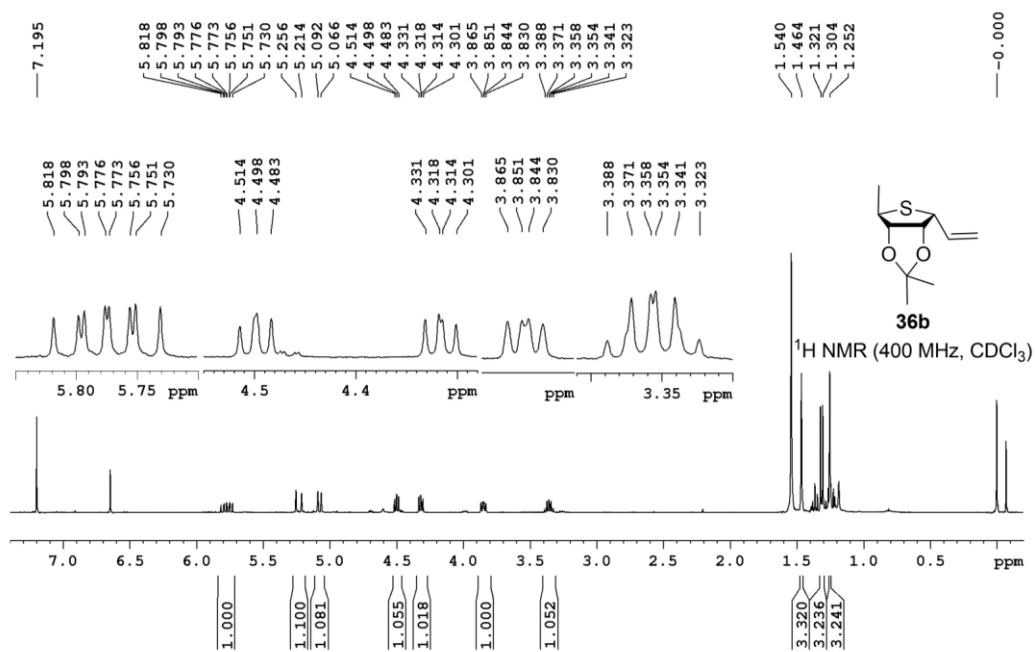
Figure 3.54: ^{1}H NMR spectrum of **36b**.
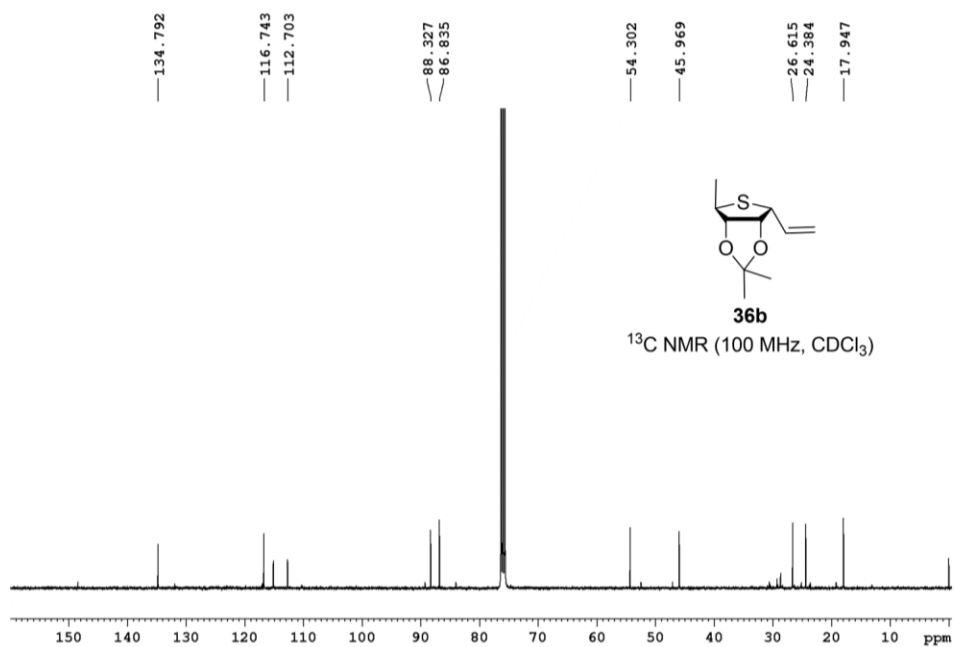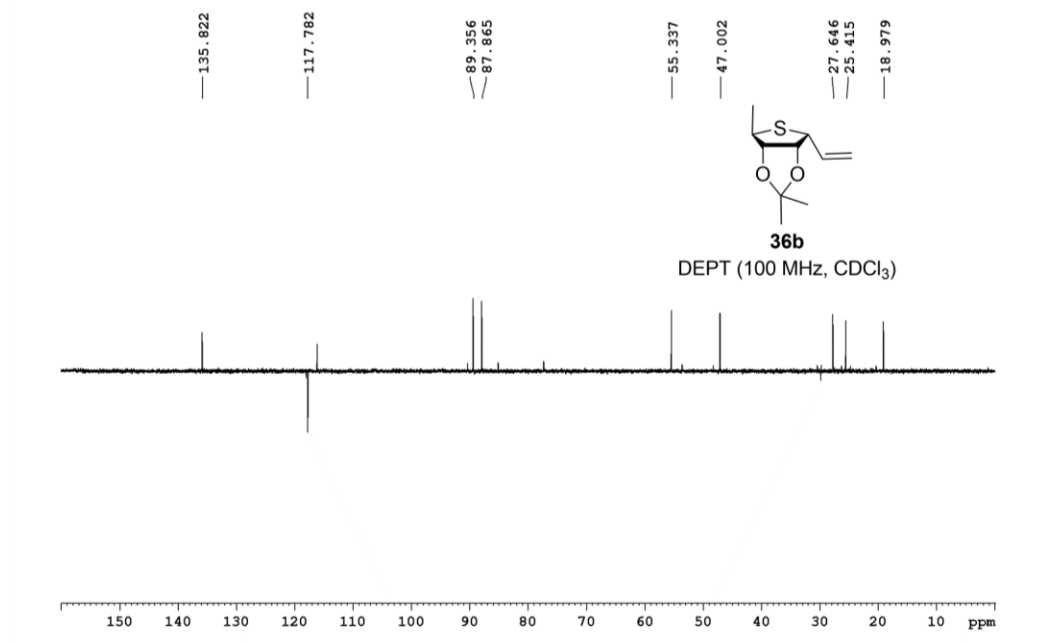
Figure 3.55: ^{13}C NMR spectrum of **36b**.
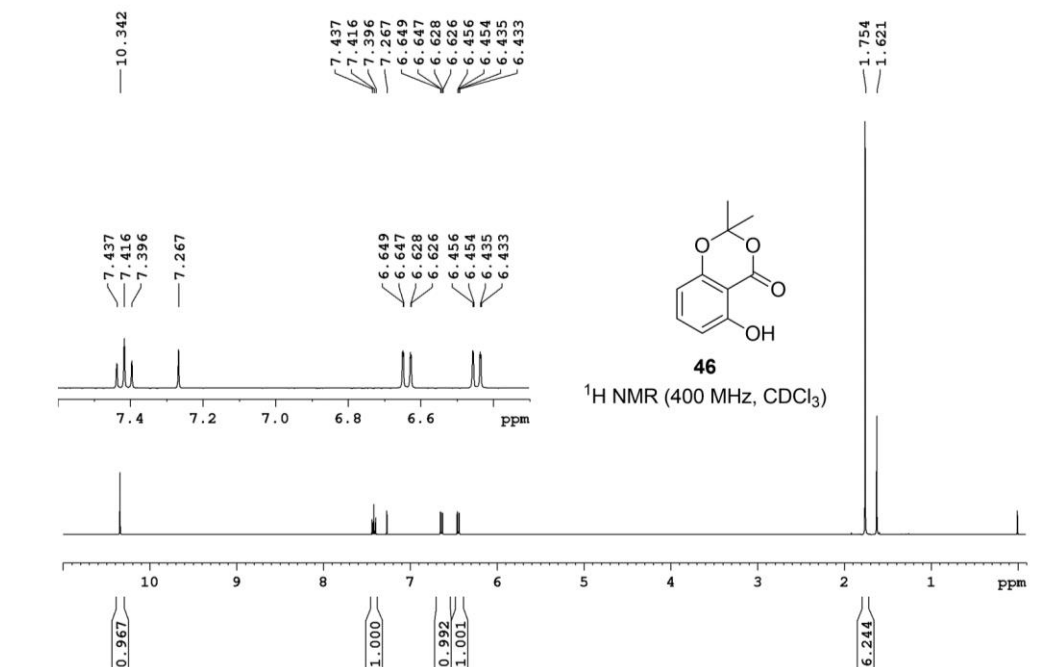

Figure 3.56 DEPT spectrum of **36b**.

Figure 3.57: ^{1}H NMR spectrum of **46**.
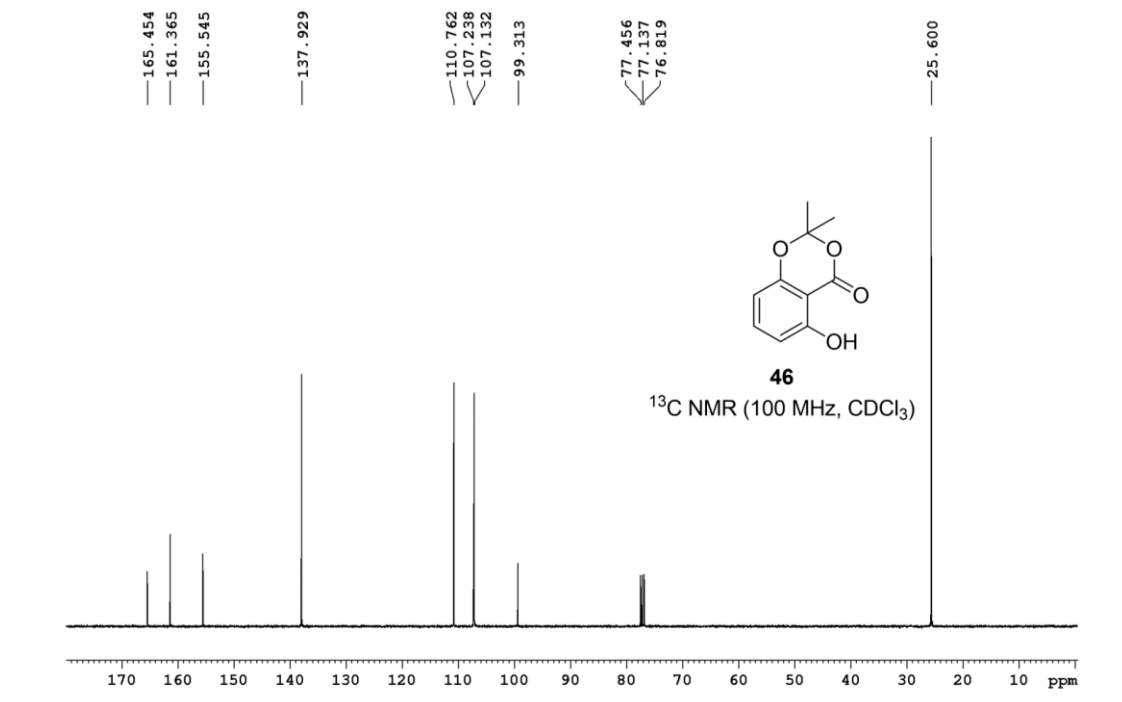
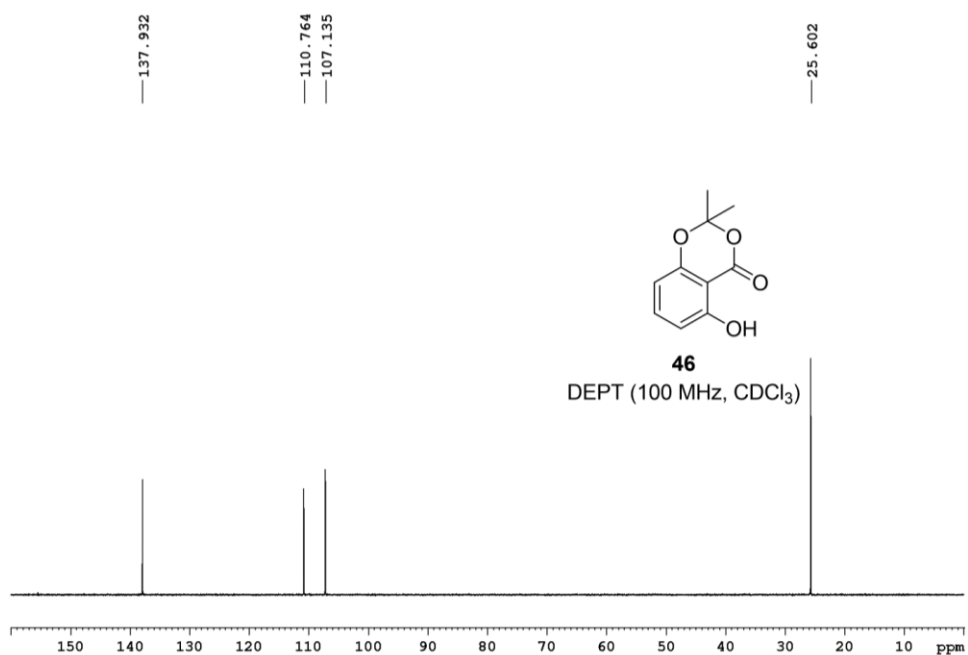**Figure 3.58:** ^{13}C NMR spectrum of **46**.
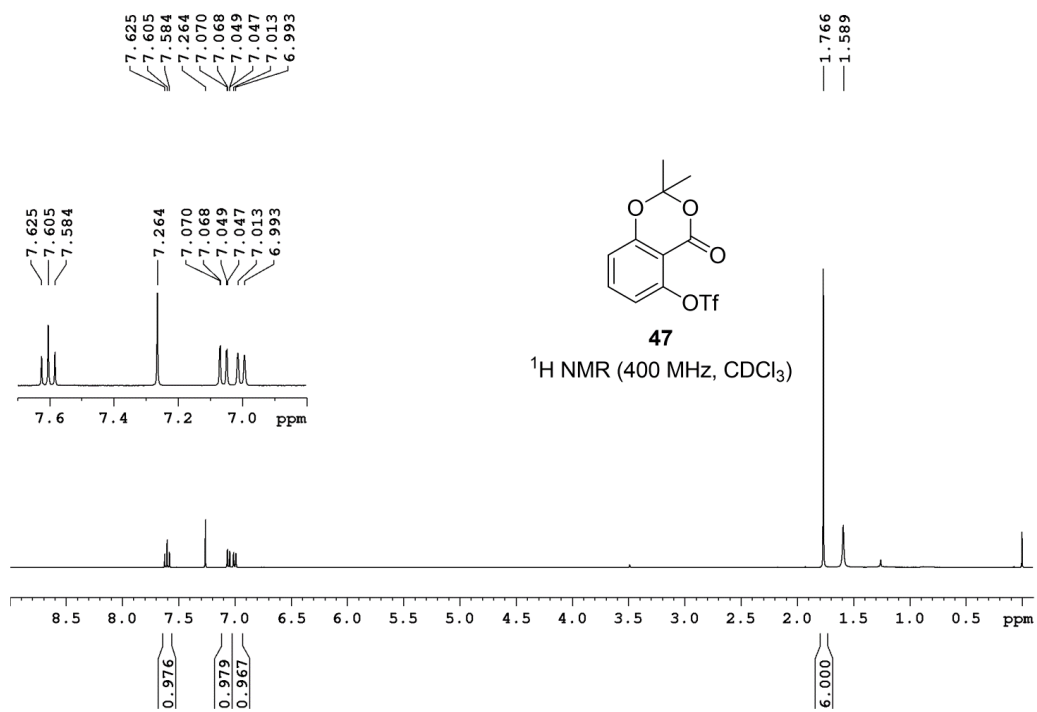
Figure 3.59: DEPT spectrum of **46**.

Figure 3.60: ^{1}H NMR spectrum of **47**.

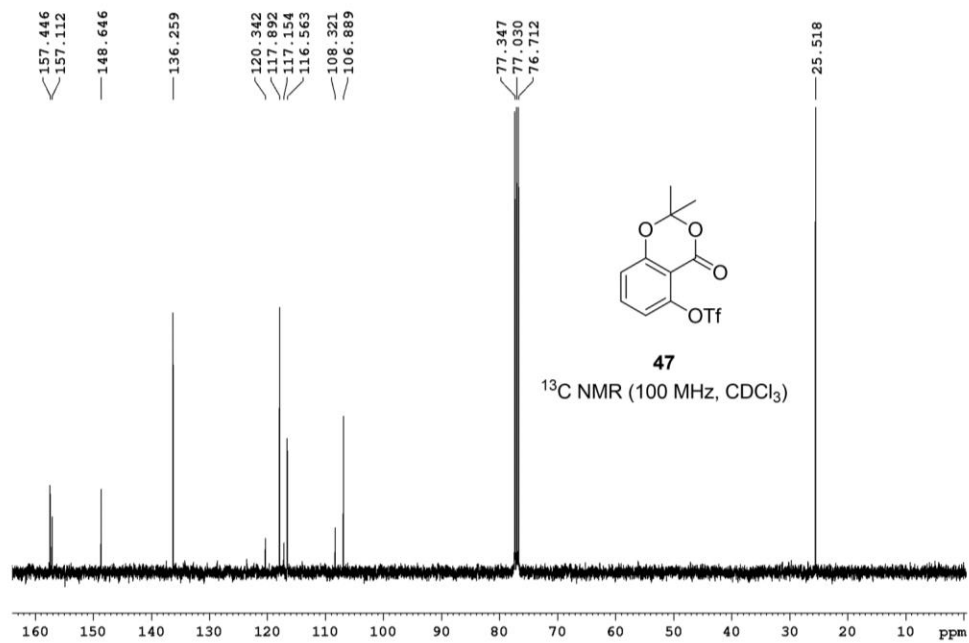**Figure 3.61:** ^{13}C NMR spectrum of **47**.
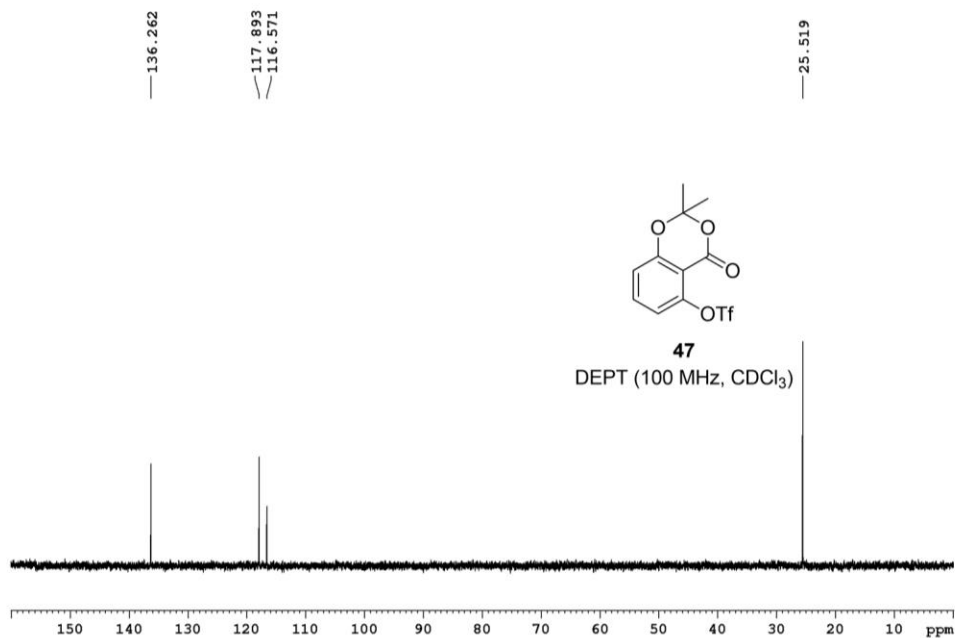
Figure 3.62: DEPT spectrum of **47**.
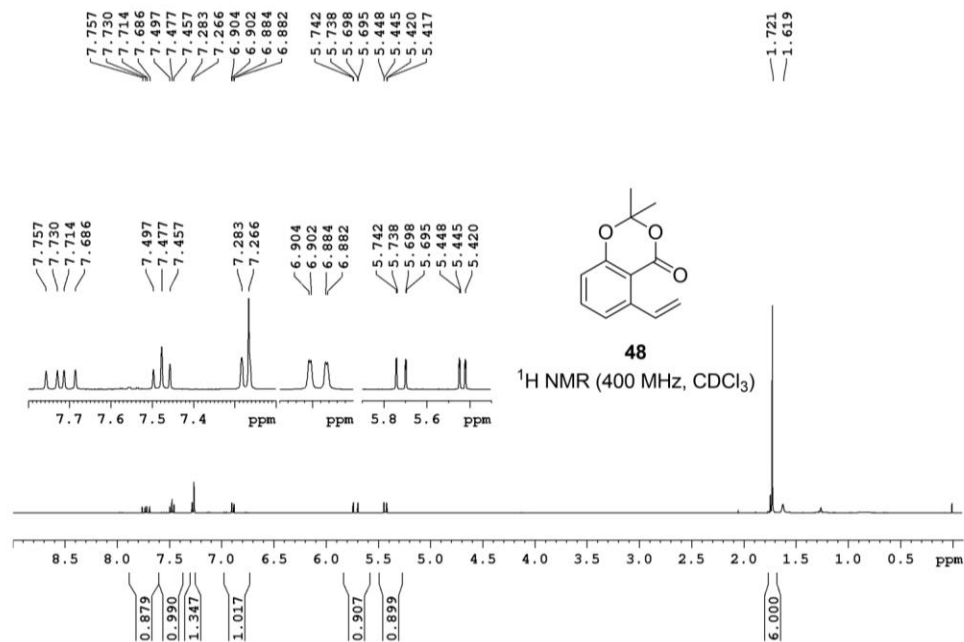
Figure 3.63: ^{1}H NMR spectrum of **48**.
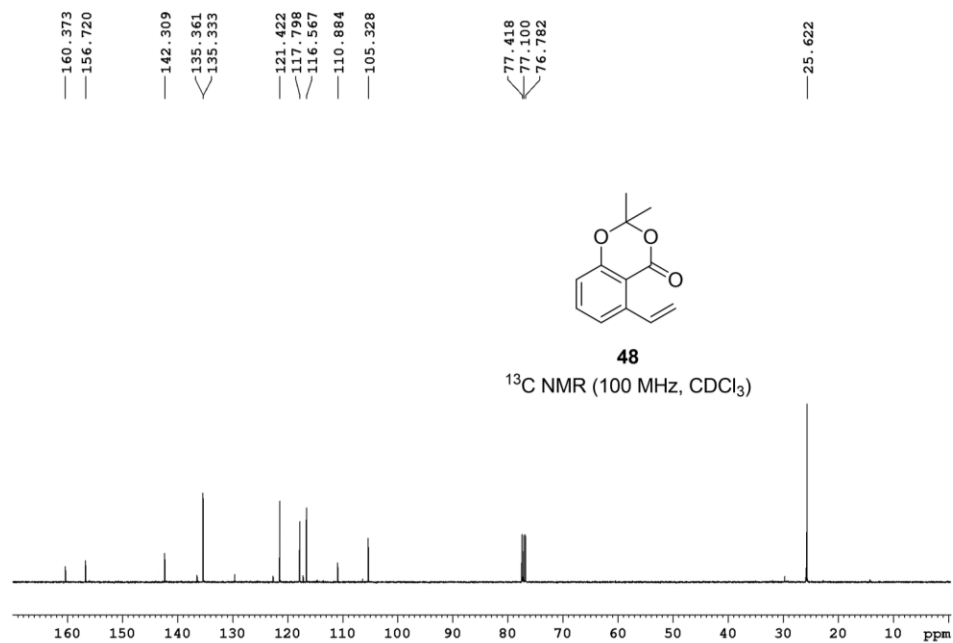
Figure 3.64: ^{13}C NMR spectrum of **48**.
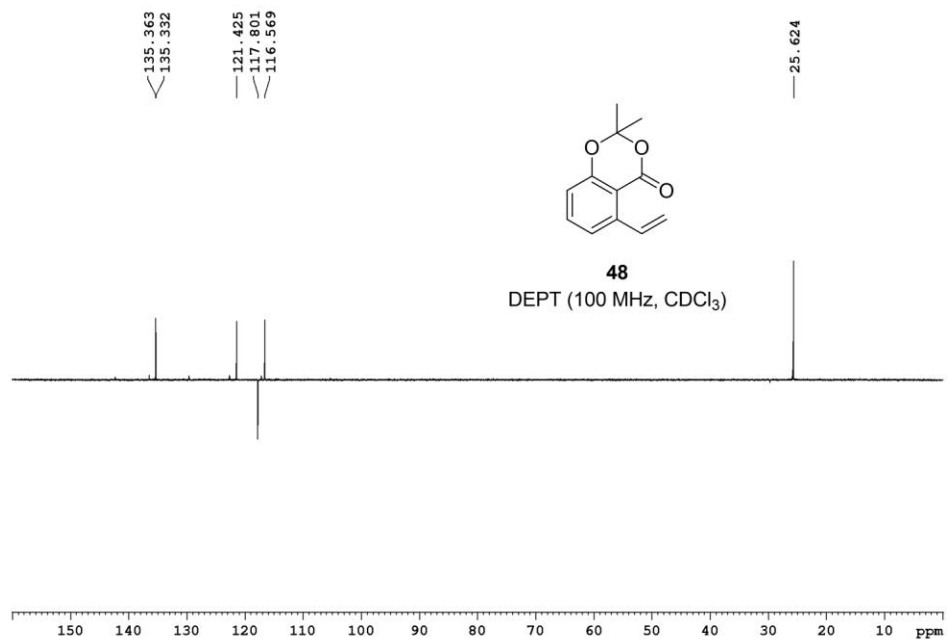
Figure 3.65: DEPT spectrum of **48**.
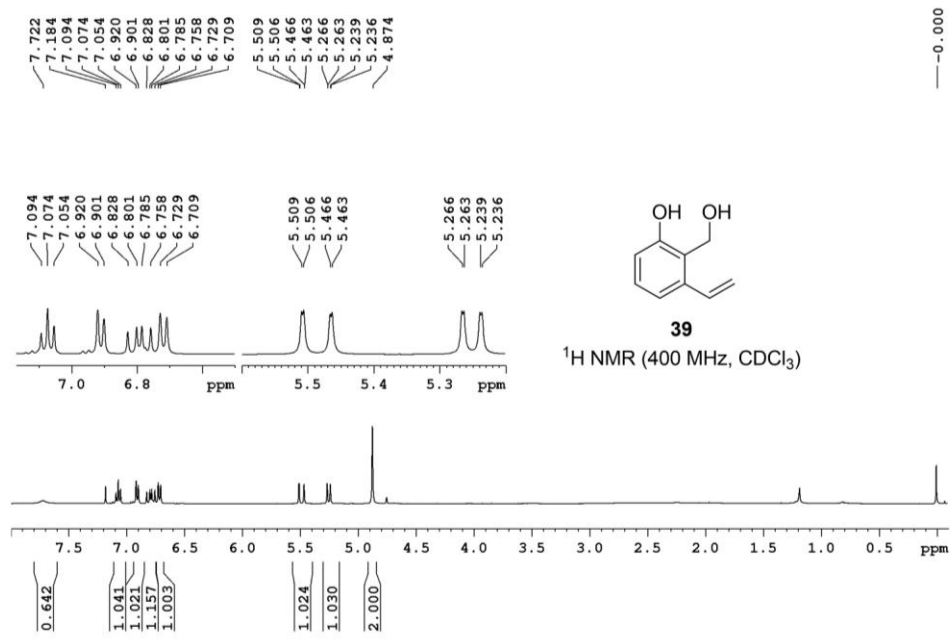
Figure 3.66: ^{1}H NMR spectrum of **39**.
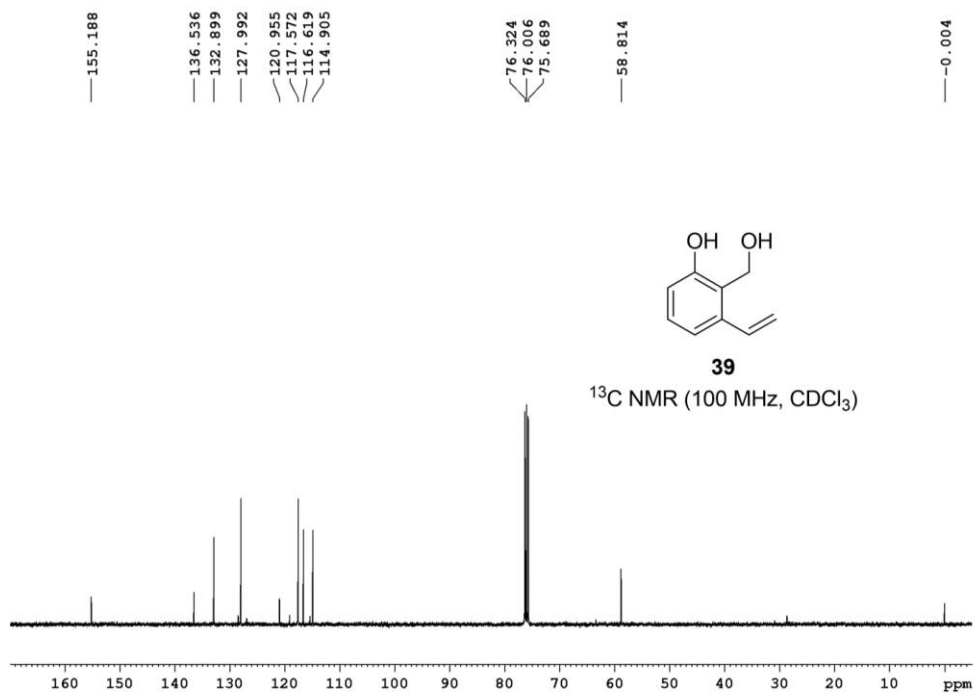
Figure 3.67: ^{13}C NMR spectrum of **39**.
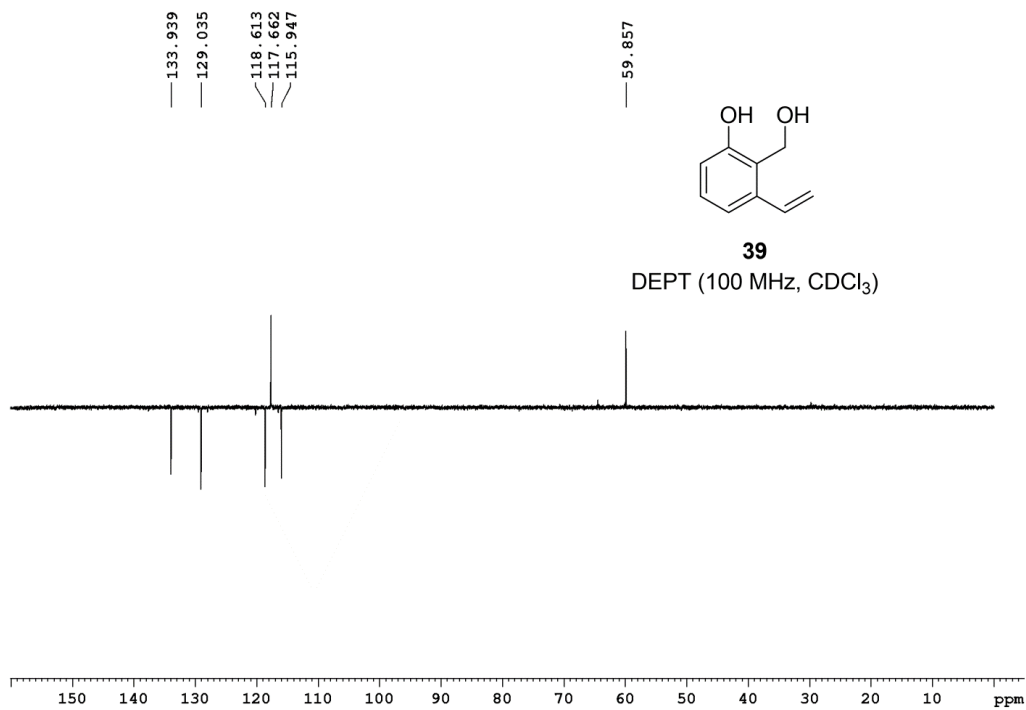
Figure 3.68: DEPT spectrum of **39**.
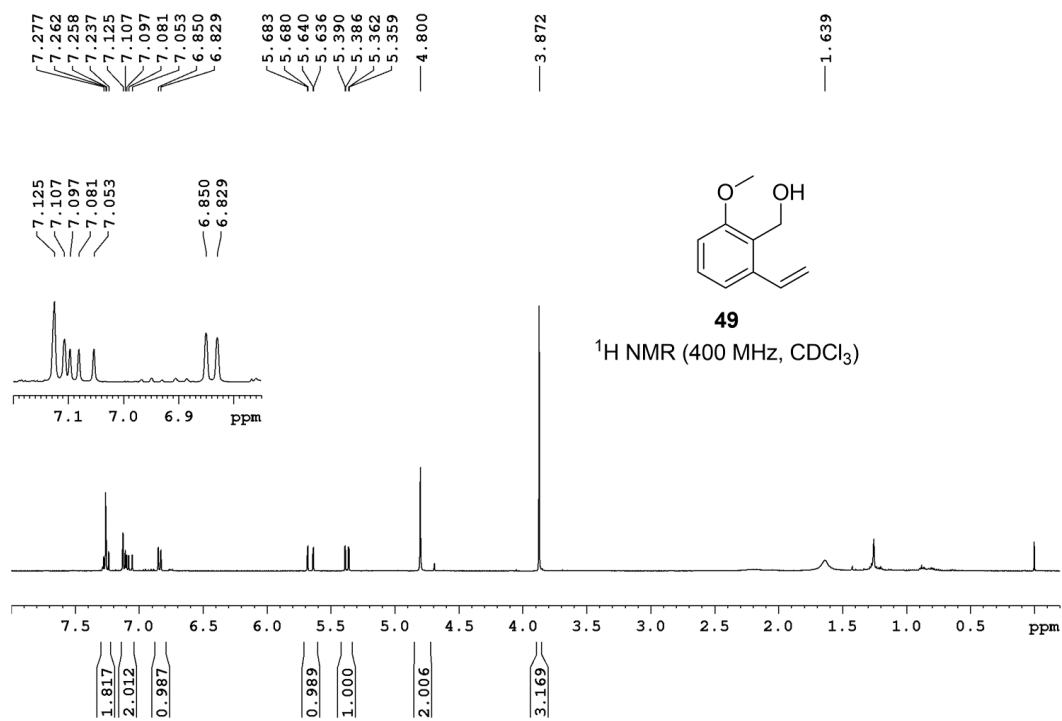
Figure 3.69: ^{1}H NMR spectrum of **49**.
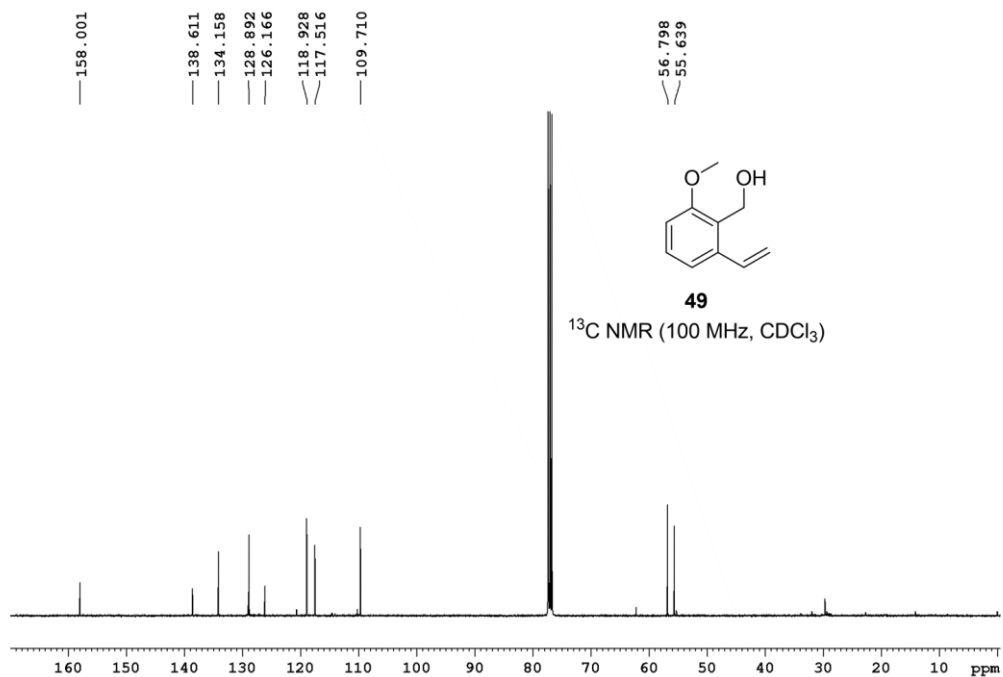
Figure 3.70: ^{13}C NMR spectrum of **49**.
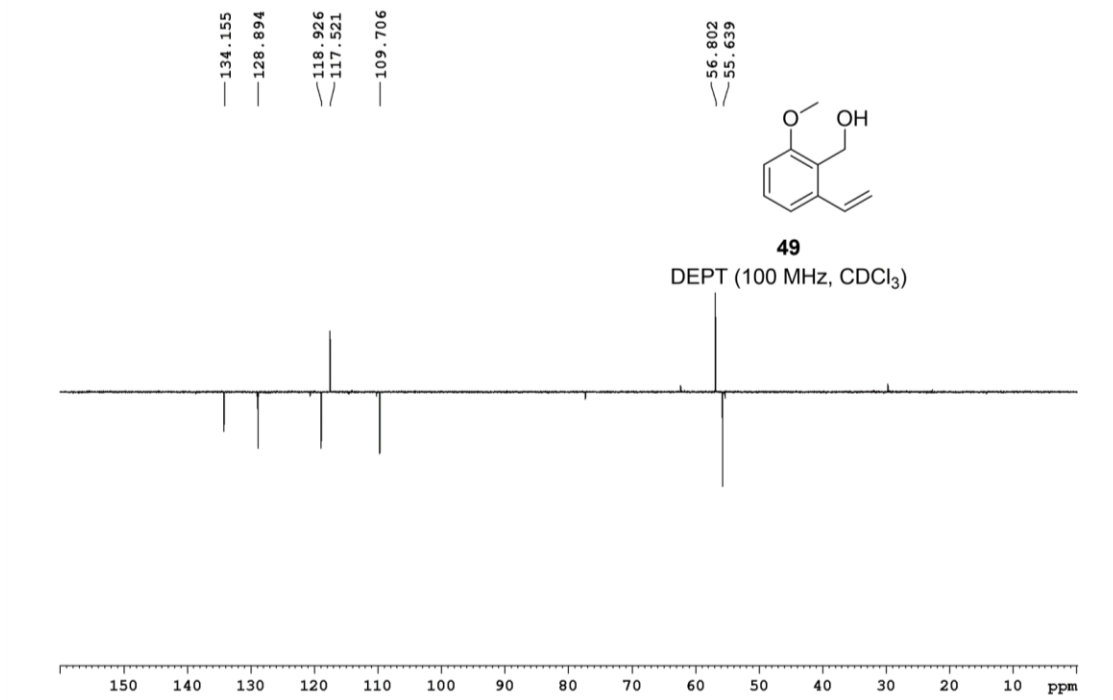
Figure 3.71: DEPT spectrum of **49**.
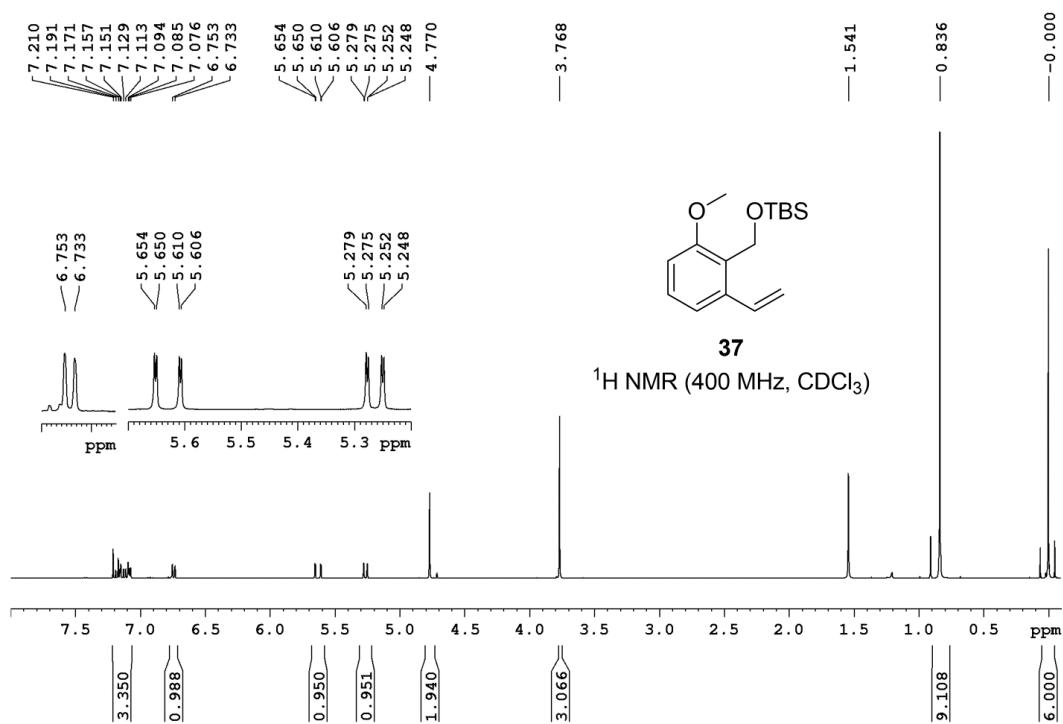
Figure 3.72: ^{1}H NMR spectrum of **37**.
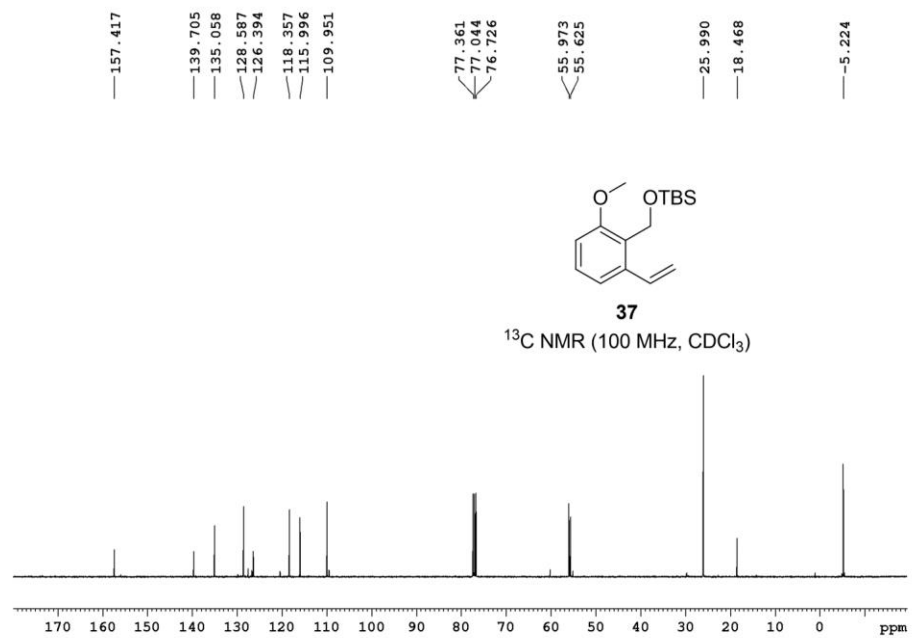
Figure 3.73: ^{13}C NMR spectrum of **37**.
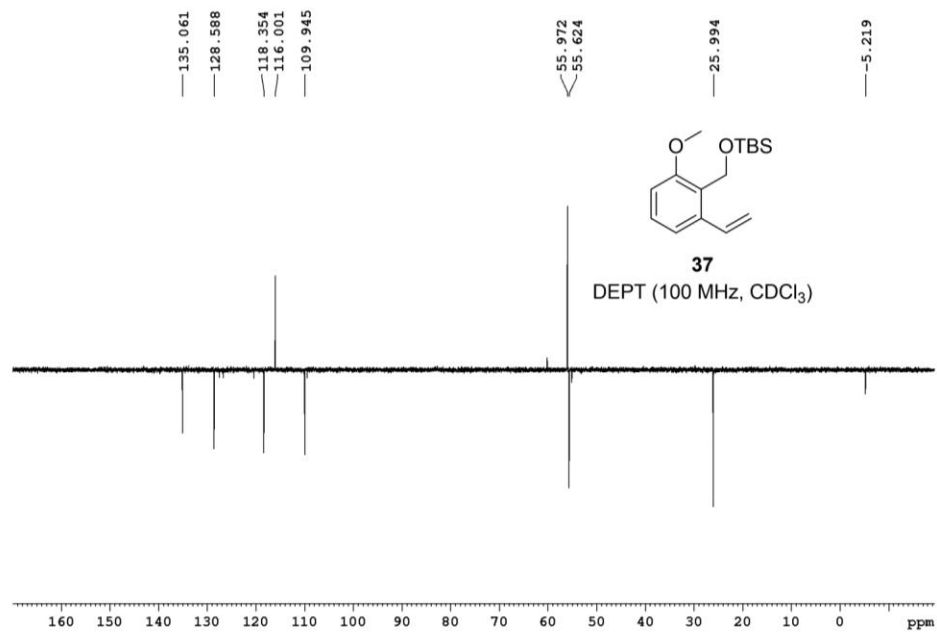
Figure 3.74: DEPT spectrum of **37**.

Figure 3.75: [^1]H NMR spectrum of **50a**.
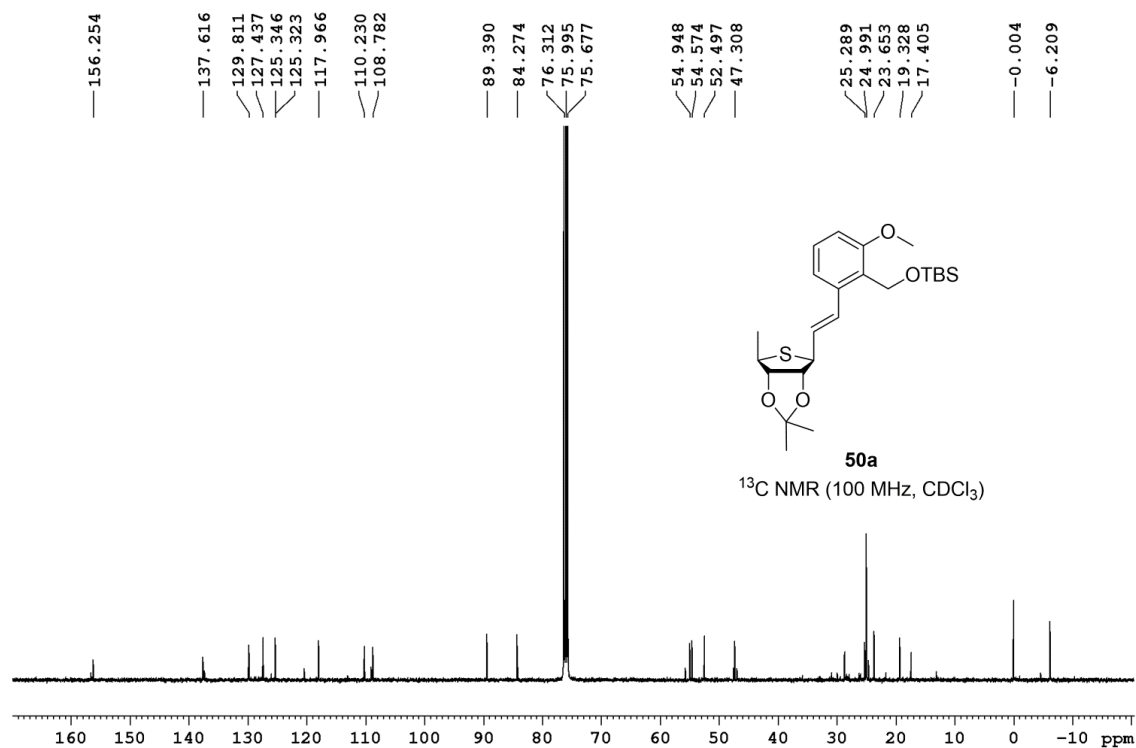
Figure 3.76: [^13]C NMR spectrum of **50a**.
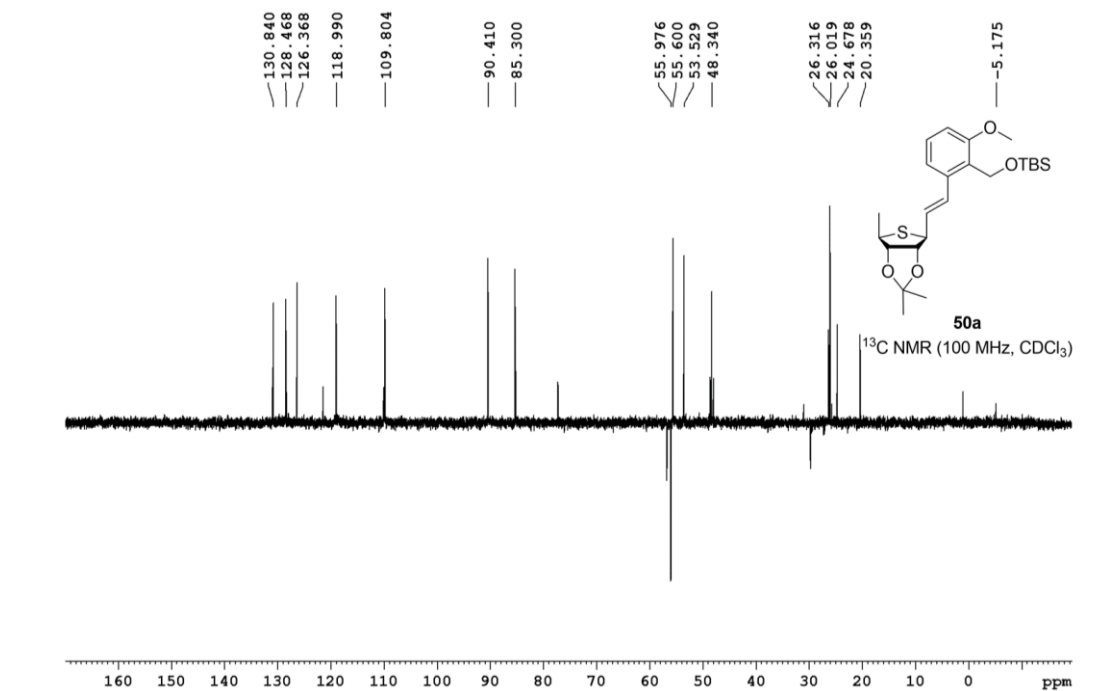
Figure 3.77: DEPT spectrum of **50a**.
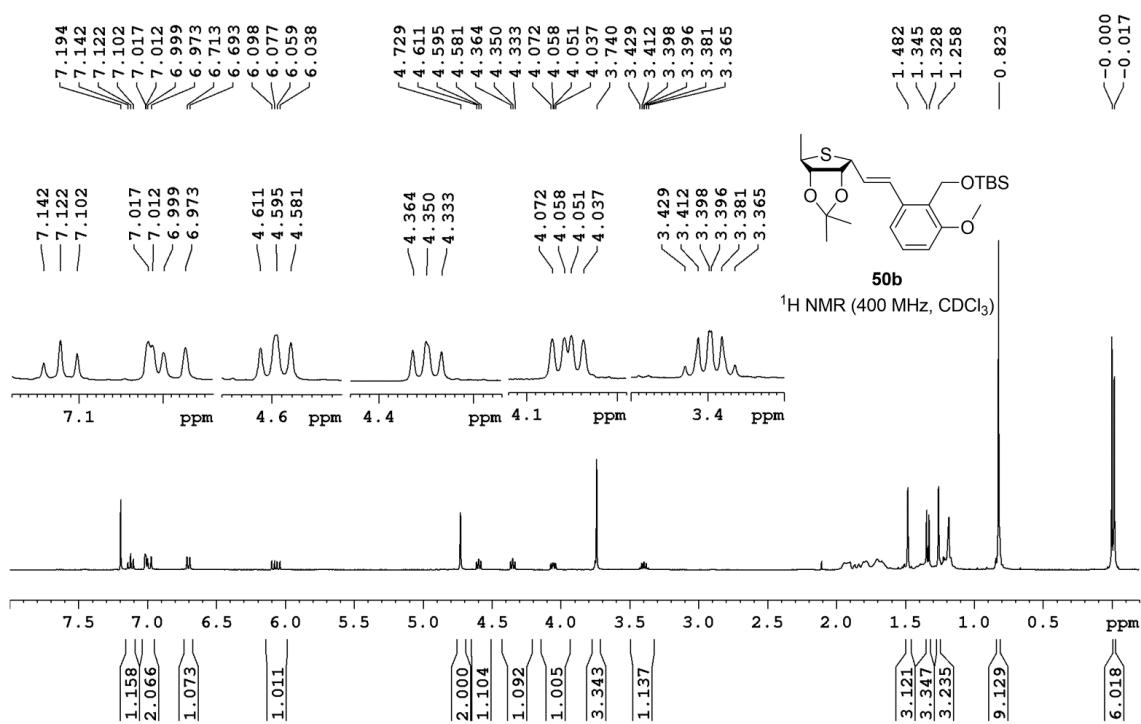
Figure 3.78: ¹H NMR spectrum of **50b**.
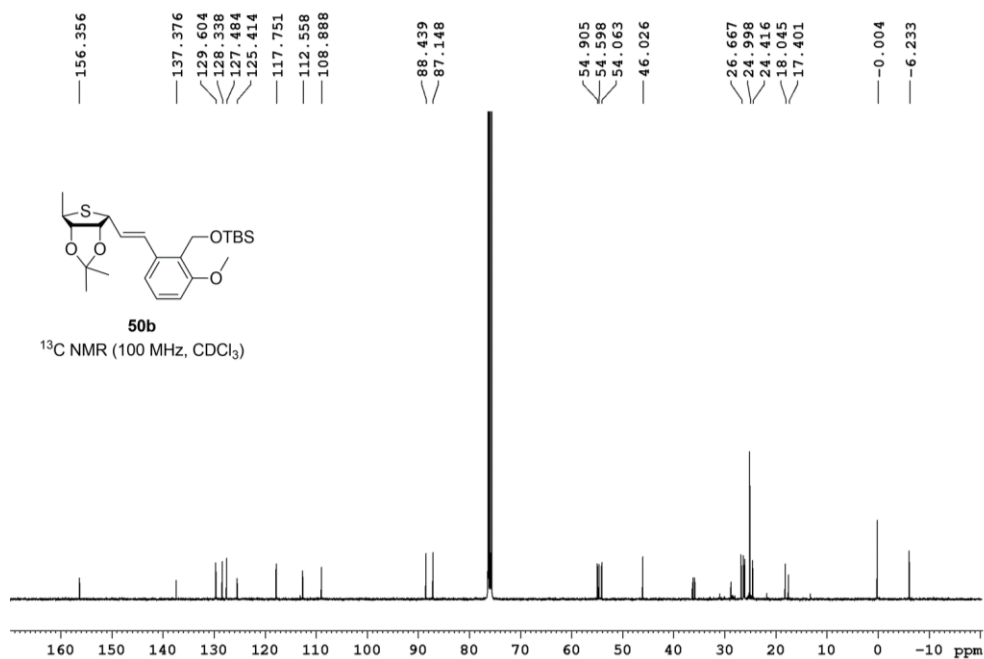
Figure 3.79: ^{13}C NMR spectrum of **50b**.
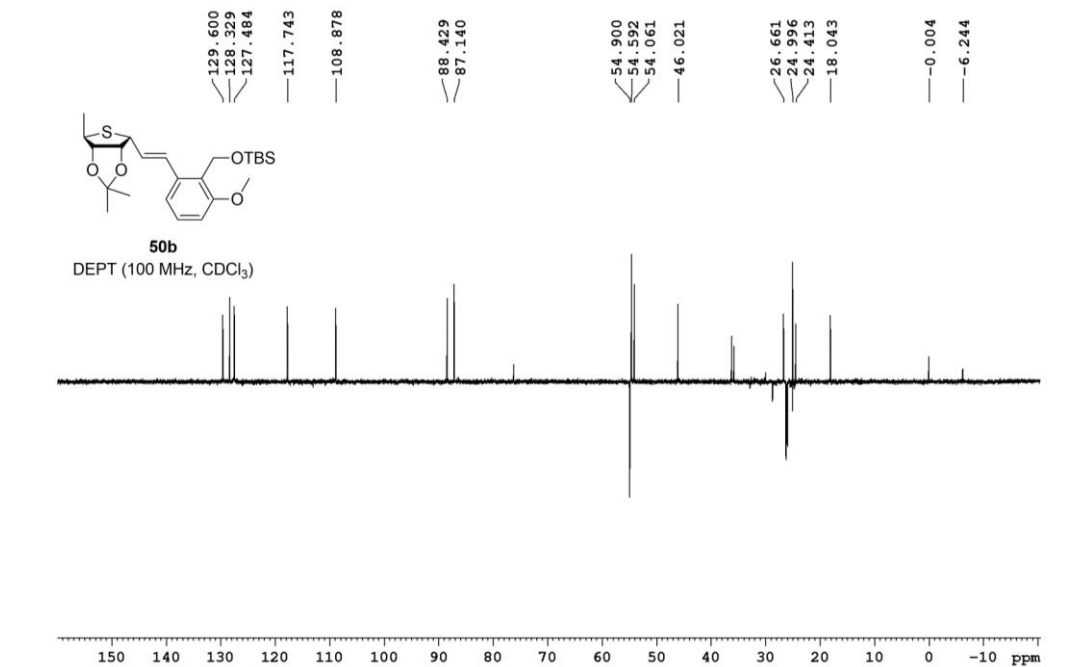
Figure 3.80: DEPT spectrum of **50b**.
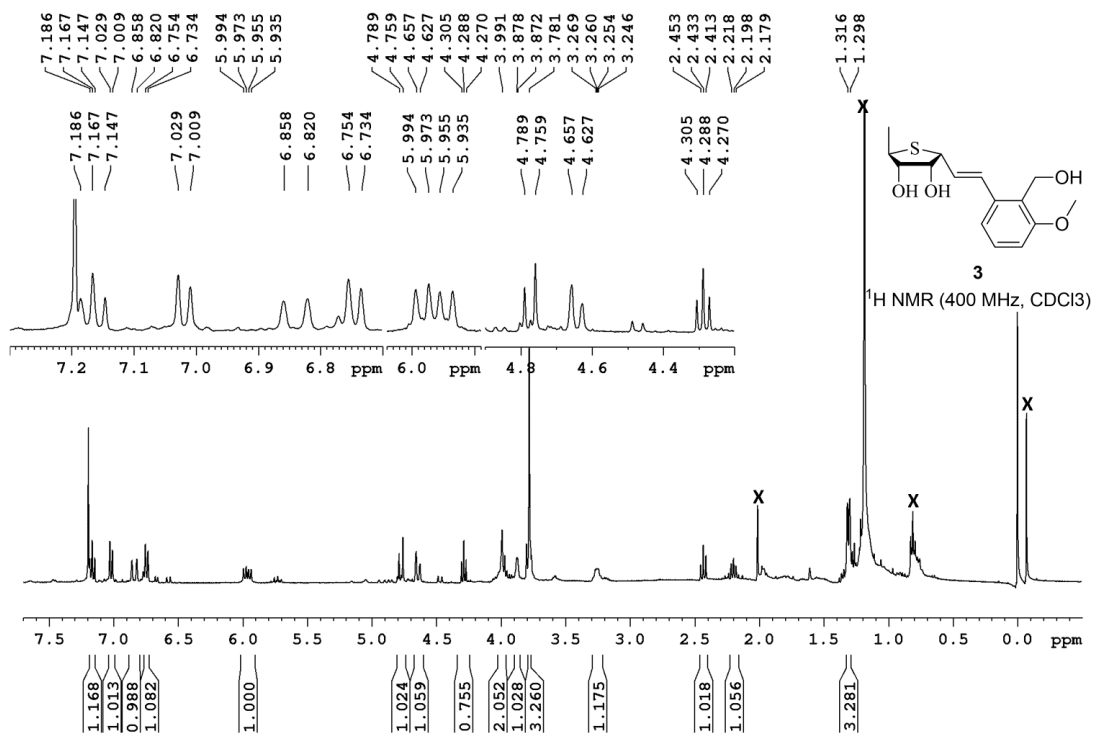
Figure 3.81: ^{1}H NMR spectrum of **3**.
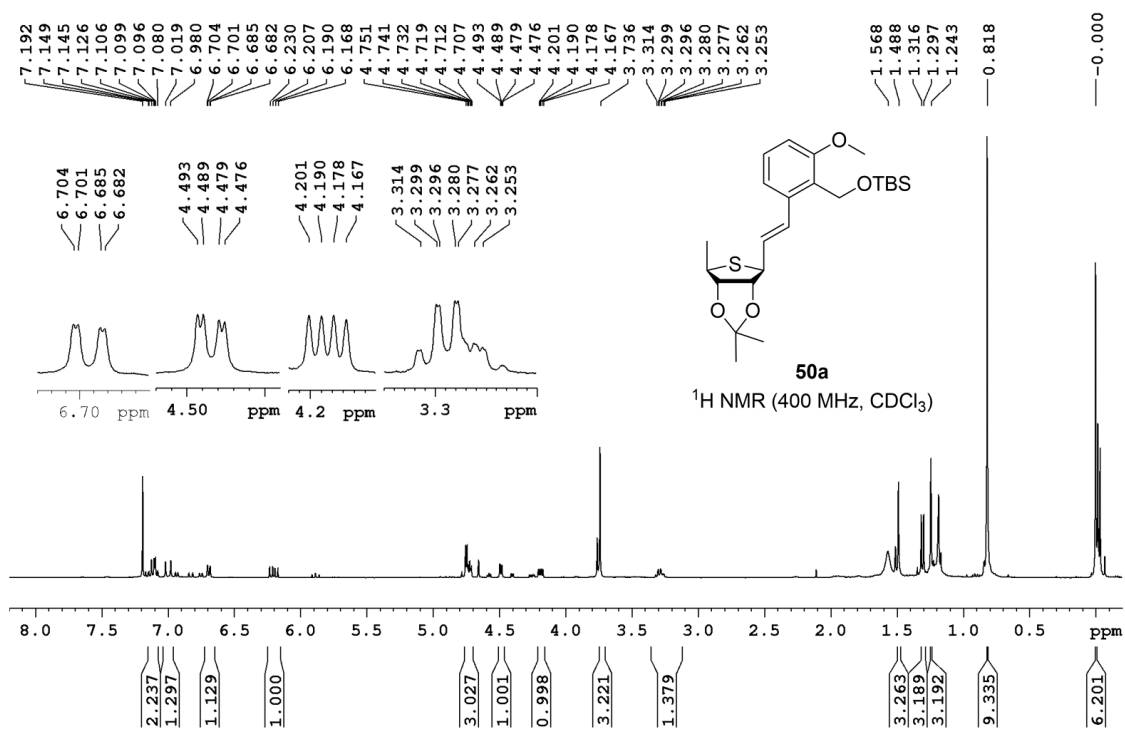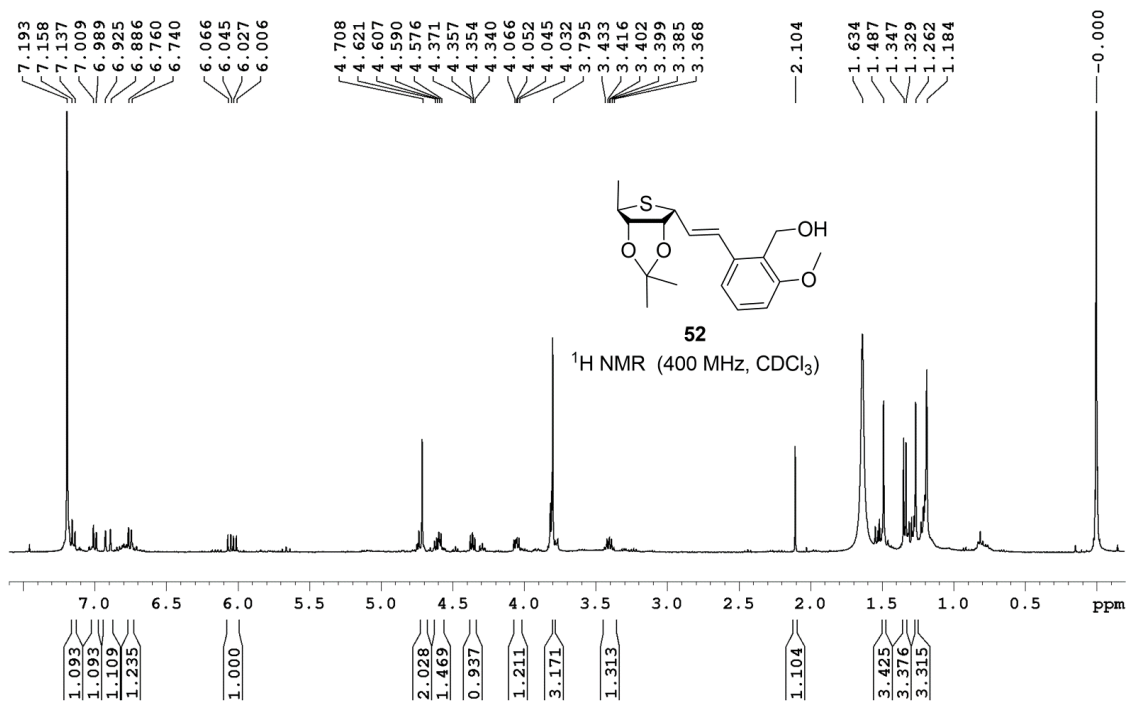

Figure 3.82: ^{1}H NMR spectrum of **52**.

Chapter 3

3.14. References

(1)   Nagar, P. R.; Gajjar, N. D.; Dhameliya, T. M. In Search of SARS CoV-2 Replication Inhibitors: Virtual Screening, Molecular Dynamics Simulations and ADMET Analysis. *J. Mol. Struct.* **2021**, *1246*, 131190. https://doi.org/10.1016/j.molstruc.2021.131190.

(2)   Wang, Y.; Li, P.; Solanki, K.; Li, Y.; Ma, Z.; Peppelenbosch, M. P.; Baig, M. S.; Pan, Q. Viral Polymerase Binding and Broad-Spectrum Antiviral Activity of Molnupiravir against Human Seasonal Coronaviruses. *Virology* **2021**, *564*, 33–38. https://doi.org/10.1016/j.virol.2021.09.009.

(3)   Tian, L.; Qiang, T.; Liang, C.; Ren, X.; Jia, M.; Zhang, J.; Li, J.; Wan, M.; YuWen, X.; Li, H.; Cao, W.; Liu, H. RNA-Dependent RNA Polymerase (RdRp) Inhibitors: The Current Landscape and Repurposing for the COVID-19 Pandemic. *Eur. J. Med. Chem.* **2021**, *213*, 113201. https://doi.org/10.1016/j.ejmech.2021.113201.

(4)   Malmstrøm, J.; Christophersen, C.; Barrero, A. F.; Oltra, J. E.; Justicia, J.; Rosales, A. Bioactive Metabolites from a Marine-Derived Strain of the Fungus *Emericella Variecolor. J. Nat. Prod.* **2002**, *65*, 364–367. https://doi.org/10.1021/np0103214.

(5)   Majik, M.; Tilvi, S.; Parvatkar, P. Recent Developments Towards the Synthesis of Varitriol: An Antitumour Agent from Marine Derived Fungus *Emericella Variecolor. Curr. Org. Synth.* **2014**, *11*, 268–287. https://doi.org/10.2174/15701794106661311241342200.

(6)   Patil, S. M.; Maruthi, K. R.; Bajpe, S. N.; Vyshali, V. M.; Sushmitha, S.; Akhila, C.; Ramu, R. Comparative Molecular Docking and Simulation Analysis of Molnupiravir and Remdesivir with SARS-CoV-2 RNA Dependent RNA Polymerase (RdRp). *Bioinformation* **2021**, *17*, 932–939. https://doi.org/10.6026/97320630017932.

(7)   Focosi, D.; Anderson, A. O.; Tang, J. W.; Tuccori, M. Convalescent Plasma Therapy for COVID-19: State of the Art. *Clin. Microbiol. Rev.* **2020**, *33*, 1–17. https://doi.org/10.1128/CMR.00072-20.

(8)   Xi, Y. Convalescent Plasma Therapy for COVID-19: A Tried-and-True Old

Strategy*Signal Transduct. Target. Ther.* **2020**, *5*, 203. https://doi.org/10.1038/s41392-020-00310-8.

(9)   Hasan, M.; Parvez, M. S. A.; Azim, K. F.; Imran, M. A. S.; Raihan, T.; Gulshan, A.; Muhit, S.; Akhand, R. N.; Ahmed, S. S. U.; Uddin, M. B. Main Protease Inhibitors and Drug Surface Hotspots for the Treatment of COVID-19: A Drug Repurposing and Molecular Docking Approach. *Biomed. Pharmacother.* **2021**, *140*, 111742. https://doi.org/10.1016/j.biopha.2021.111742.

(10)   Kabinger, F.; Stiller, C.; Schmitzová, J.; Dienemann, C.; Kokic, G.; Hillen, H. S.; Höbartner, C.; Cramer, P. Mechanism of Molnupiravir-Induced SARS-CoV-2 Mutagenesis. *Nat. Struct. Mol. Biol.* **2021**, *28*, 740–746. https://doi.org/10.1038/s41594-021-00651-0.

(11)   Rafi, M. O.; Bhattacharje, G.; Al-Khafaji, K.; Taskin-Tok, T.; Alfasane, M. A.; Das, A. K.; Parvez, M. A. K.; Rahman, M. S. Combination of QSAR, Molecular Docking, Molecular Dynamic Simulation and MM-PBSA: Analogues of Lopinavir and Favipiravir as Potential Drug Candidates against COVID-19. *J. Biomol. Struct. Dyn.* **2022**, *40*, 3711–3730. https://doi.org/10.1080/07391102.2020.1850355.

(12)   Skariyachan, S.; Gopal, D.; Chakrabarti, S.; Kempanna, P.; Uttarkar, A.; Muddebihalkar, A. G.; Niranjan, V. Structural and Molecular Basis of the Interaction Mechanism of Selected Drugs towards Multiple Targets of SARS-CoV-2 by Molecular Docking and Dynamic Simulation Studies- Deciphering the Scope of Repurposed Drugs. *Comput. Biol. Med.* **2020**, *126*, 104054. https://doi.org/10.1016/j.compbiomed.2020.104054.

(13)   Du, Y.; Chen, X. Favipiravir: Pharmacokinetics and Concerns About Clinical Trials for 2019-nCoV Infection. *Clin. Pharmacol. Ther.* **2020**, *108*, 242–247. https://doi.org/10.1002/cpt.1844.

(14)   Cai, Q.; Yang, M.; Liu, D.; Chen, J.; Shu, D.; Xia, J.; Liao, X.; Gu, Y.; Cai, Q.; Yang, Y.; Shen, C.; Li, X.; Peng, L.; Huang, D.; Zhang, J.; Zhang, S.; Wang, F.; Liu, J.; Chen, L.; Chen, S.; Wang, Z.; Zhang, Z.; Cao, R.; Zhong, W.; Liu, Y.; Liu, L. Experimental Treatment with Favipiravir for COVID-19: An Open-Label Control

Study. *Engineering* **2020**, *6*, 1192–1198. https://doi.org/10.1016/j.eng.2020.03.007.

(15) Mulamoottil, V. A.; Majik, M. S.; Chandra, G.; Jeong, L. S. Recent Advances in Synthesis and Biological Activity of 4′-Thionucleosides. In *Chemical Synthesis of Nucleoside Analogues*; John Wiley & Sons, Inc.: Hoboken, NJ, USA, 2013; Vol. 17, pp 655–697. https://doi.org/10.1002/9781118498088.ch14.

(16) Kim, Y.; Jedrzejczak, R.; Maltseva, N. I.; Wilamowski, M.; Endres, M.; Godzik, A.; Michalska, K.; Joachimiak, A. Crystal Structure of Nsp15 Endoribonuclease from SARS-CoV-2. *Protein Sci.* **2020**, *29*, 1596–1605. https://doi.org/10.1002/pro.3873.

(17) Norgan, A. P.; Coffman, P. K.; Kocher, J.-P. A.; Katzmann, D. J.; Sosa, C. P. Multilevel Parallelization of AutoDock 4.2. *J. Cheminform.* **2011**, *3*, 12. https://doi.org/10.1186/1758-2946-3-12.

(18) Morris, G. M.; Huey, R.; Lindstrom, W.; Sanner, M. F.; Belew, R. K.; Goodsell, D. S.; Olson, A. J. AutoDock4 and AutoDockTools4: Automated Docking with Selective Receptor Flexibility. *J. Comput. Chem.* **2009**, *30*, 2785–2791. https://doi.org/10.1002/jcc.21256.

(19) Patil, S. M.; Martiz, R. M.; Ramu, R.; Shirahatti, P. S.; Prakash, A.; Kumar, B. R. P.; Kumar, N. Evaluation of Flavonoids from Banana Pseudostem and Flower (Quercetin and Catechin) as Potent Inhibitors of α-Glucosidase: An in Silico Perspective. *J. Biomol. Struct. Dyn.* **2021**, *0*, 1–15. https://doi.org/10.1080/07391102.2021.1971561.

(20) Ortiz, C. L. D.; Completo, G. C.; Nacario, R. C.; Nellas, R. B. Potential Inhibitors of Galactofuranosyltransferase 2 (GlfT2): Molecular Docking, 3D-QSAR, and In Silico ADMETox Studies. *Sci. Rep.* **2019**, *9*, 17096. https://doi.org/10.1038/s41598-019-52764-8.

(21) Benetti, S.; De Risi, C.; Pollini, G. P.; Zanirato, V. Synthetic Routes to Chiral Nonracemic and Racemic Dihydro- And Tetrahydrothiophenes. *Chem. Rev.* **2012**, *112*, 2129–2163. https://doi.org/10.1021/cr200298b.

(22) Rodrigues, L.; Tilve, S. G.; Majik, M. S. Synthetic Access to Thiolane-Based Therapeutics and Biological Activity Studies. *Eur. J. Med. Chem.* **2021**, *224*, 113659.

https://doi.org/10.1016/j.ejmech.2021.113659.

(23)   Müller-Kuhrt, L. Putting Nature Back into Drug Discovery. *Nat. Biotechnol.* **2003**, *21*, 602–602. https://doi.org/10.1038/nbt0603-602.

(24)   Sánchez-Eleuterio, A.; García-Santos, W. H.; Díaz-Salazar, H.; Hernández-Rodríguez, M.; Cordero-Vargas, A. Stereocontrolled Nucleophilic Addition to Five-Membered Oxocarbenium Ions Directed by the Protecting Groups. Application to the Total Synthesis of (+)-Varitriol and of Two Diastereoisomers Thereof. *J. Org. Chem.* **2017**, *82*, 8464–8475. https://doi.org/10.1021/acs.joc.7b01211.

(25)   Benetti, S.; De Risi, C.; Pollini, G. P.; Zanirato, V. Synthetic Routes to Chiral Nonracemic and Racemic Dihydro- and Tetrahydrothiophenes. *Chem. Rev.* **2012**, *112*, 2129–2163. https://doi.org/10.1021/cr200298b.

(26)   Chavan, S. P.; Chittiboyina, A. G.; Ramakrishna, G.; Tejwani, R. B.; Ravindranathan, T.; Kamat, S. K.; Rai, B.; Sivadasan, L.; Balakrishnan, K.; Ramalingam, S.; Deshpande, V. H. An Unusual Stereochemical Outcome of Radical Cyclization: Synthesis of (+)-Biotin. *Tetrahedron* **2005**, *61*, 9273–9280. https://doi.org/10.1016/j.tet.2005.07.070.

(27)   Volkmann, R. A.; Kelbaugh, P. R.; Nason, D. M.; Jasys, V. J. 2-Thioalkyl Penems: An Efficient Synthesis of Sulopenem, a (5*R*,6*S*)-6-(1(*R*)-Hydroxyethyl)-2-[(*cis*-1-oxo-3-thiolanyl)thio]-2-penem Antibacterial. *J. Org. Chem.* **1992**, *57*, 4352–4361. https://doi.org/10.1021/jo00042a010.

(28)   Ghosh, A. K.; Thompson, W. J.; Holloway, M. K.; McKee, S. P.; Duong, T. T.; Lee, H. Y.; Munson, P. M.; Smith, A. M.; Wai, J. M.; Darke, P. L.; Zugay, J. A.; Emini, E. A.; Schleif, W. A.; Huff, J. R.; Anderson, P. S. Potent HIV Protease Inhibitors: The Development of Tetrahydrofuranylglycines as Novel P2-Ligands and Pyrazine Amides as P3-Ligands. *J. Med. Chem.* **1993**, *36*, 2300–2310. https://doi.org/10.1021/jm00068a006.

(29)   Ponce, A. M.; Overman, L. E. A New Method for Stereocontrolled Synthesis of Substituted Tetrahydrothiophenes. *J. Am. Chem. Soc.* **2000**, *122*, 8672–8676.

https://doi.org/10.1021/ja001975m.

(30)   Young, R. J.; Shaw-Ponter, S.; Thomson, J. B.; Miller, J. A.; Cumming, J. G.; Pugh, A. W.; Rider, P. Synthesis and Antiviral Evaluation of Enantiomeric 2′,3′-Dideoxy- and 2′,3′-Didehydro-2′,3′-Dideoxy-4′-Thionucleosides. *Bioorg. Med. Chem. Lett.* **1995**, *5*, 2599–2604. https://doi.org/10.1016/0960-894X(95)00472-6.

(31)   Jana, G.; Viso, A.; Díaz, Y.; Castillón, S. Stereoselective Synthesis of Homochiral Substituted Tetrahydrothiophenes by Electrophile-Promoted Thioetherification. *European J. Org. Chem.* **2003**, *2003*, 209–216. https://doi.org/10.1002/1099-0690(200301)2003:1<209::AID-EJOC209>3.0.CO;2-S.

(32)   Bilokin, Y. V.; Melman, A.; Niddam, V.; Benhamú, B.; Bachi, M. D. Synthesis of Thiabicyclic Heterocycles Through Free Radical Cyclization of *β*-Thioacrylates. *Tetrahedron* **2000**, *56*, 3425–3437. https://doi.org/10.1016/S0040-4020(00)00247-7.

(33)   Batra, H.; Moriarty, R. M.; Penmasta, R.; Sharma, V.; Stanciuc, G.; Staszewski, J. P.; Tuladhar, S. M.; Walsh, D. A.; Datla, S.; Krishnaswamy, S. A Concise, Efficient and Production-Scale Synthesis of a Protected ʟ-Lyxonolactone Derivative: An Important Aldonolactone Core. *Org. Process Res. Dev.* **2006**, *10*, 484–486. https://doi.org/10.1021/op050222n.

(34)   Tanabe, G.; Matsuda, Y.; Oka, M.; Kunikata, Y.; Tsutsui, N.; Xie, W.; Balakishan, G.; Amer, M. F. A.; Marumoto, S.; Muraoka, O. Highly Diastereoselective Route to *α*-Lucosidase Inhibitors, Neosalacinol and Neoponkoranol. *J. Org. Chem.* **2016**, *81*, 3407–3415. https://doi.org/10.1021/acs.joc.5b02894.

(35)   Kotoulas, S. S.; Kojić, V. V.; Bogdanović, G. M.; Koumbis, A. E. Synthesis and Cytotoxic Evaluation of Novel Pyrimidine Deoxyapiothionucleosides. *Bioorg. Med. Chem. Lett.* **2013**, *23*, 3364–3367. https://doi.org/10.1016/j.bmcl.2013.03.091.

(36)   Danquigny, A.; Aït Amer Meziane, M.; Demailly, G.; Benazza, M. Short Synthesis of Hydroxylated Thiolane and Selenolane Rings from Mono-Benzylated Pentitols and Aldoses Dithioacetals bis-Thionocarbonates as Bis-Electrophilic Substrates. *Tetrahedron***2005**, *61*, 6772–6781. https://doi.org/10.1016/j.tet.2005.05.008.

(37) Jeong, L. S.; Choe, S. A.; Gunaga, P.; Kim, H. O.; Lee, H. W.; Lee, S. K.; Tosh, D. K.; Patel, A.; Palaniappan, K. K.; Gao, Z.-G.; Jacobson, K. A.; Moon, H. R. Discovery of a New Nucleoside Template for Human A3 Adenosine Receptor Ligands: D-4'-Thioadenosine Derivatives without 4′-Hydroxymethyl Group as Highly Potent and Selective Antagonists. *J. Med. Chem.* **2007**, *50*, 3159–3162. https://doi.org/10.1021/jm070259t.

(38) Siriwardena, A. H.; Chiaroni, A.; Riche, C.; El-Daher, S.; Winchester, B.; Grierson, D. S. (1*R*,2*S*,4*S*,7a*R*)-1,2-Dihydroxy-7-thia-3a-thioniaperhydropentalene chloride: A New, Biologically Active Pyrrolizidine Alkaloid Analogue. *ChemInform* **2010**, *24*. https://doi.org/10.1002/chin.199305175.

(39) Cerè, V.; Peri, F.; Pollicino, S. Regio- and Stereospecific Me₃SiI-Promoted Intramolecular Displacement of Hydroxy Group by Sulfide. 2. Polyhydroxylated Thiepane Ring Contraction to Thiolane or Thiane Derivatives. Synthesis of Enantiopure Polyalcohols. *J. Org. Chem.* **1997**, *62*, 8572–8574. https://doi.org/10.1021/jo9711448.

(40) Arcelli, A.; Cerè, V.; Peri, F.; Pollicino, S.; Sabatino, P. Synthesis and Biological Activity of the (−)-(2*R*,3*S*,4*S*)-3-Azido-4-Methoxy-2-(1′*S*-Methoxy-2′-Azido)Ethyl-Thiolane. *Tetrahedron: Asymmetry* **2000**, *11*, 1389–1395. https://doi.org/10.1016/S0957-4166(00)00071-9.

(41) Kuszmann, J.; Sohár, P. 1,6-Anhydro-1(6)-Thio-L-Iditol and L-Mannitol, and Some Derivatives Thereof. *Carbohydr. Res.* **1977**, *56*, 105–115. https://doi.org/10.1016/S0008-6215(00)84241-X.

(42) Kumar, V.; Shaw, A. K. First Total Synthesis of (+)-Varitriol. *J. Org. Chem.* **2008**, *73*, 7526–7531. https://doi.org/10.1021/jo8013534.

(43) Garegg, P. J.; Samuelsson, B. Novel Reagent System for Converting a Hydroxy-Group into an Iodo-Group in Carbohydrates with Inversion of Configuration. Part 2. *J. Chem. Soc. Perkin Trans. 1* **1980**, No. 2866, 2866. https://doi.org/10.1039/p19800002866.

(44) Papageorgiou, C.; Benezra, C. A Facile Synthesis of Optically Pure Valerolactone and

β-Hydroxy Valerolactone from a Common Sugar-Derived Precursor. *Tetrahedron Lett.* **1984**, *25*, 6041–6044. https://doi.org/10.1016/S0040-4039(01)81755-X.

(45) Garegg, P. J.; Regberg, T.; Stawiński, J.; Strömberg, R. A Phosphorus Nuclear Magnetic Resonance Spectroscopic Study of the Conversion of Hydroxy Groups into Iodo Groups in Carbohydrates Using the Iodine–Triphenylphosphine–Imidazole Reagent. *J. Chem. Soc., Perkin Trans. 2* **1987**, *3*, 271–274. https://doi.org/10.1039/P29870000271.

(46) Unsworth, W. P.; Stevens, K.; Lamont, S. G.; Robertson, J. Stereospecificity in the Au-Catalysed Cyclisation of Monoallylic Diols. Synthesis of (+)-Isoaltholactone. *Chem. Commun.* **2011**, *47*, 7659. https://doi.org/10.1039/c1cc11805f.

(47) Sánchez-Eleuterio, A.; García-Santos, W. H.; Díaz-Salazar, H.; Hernández-Rodríguez, M.; Cordero-Vargas, A. Stereocontrolled Nucleophilic Addition to Five-Membered Oxocarbenium Ions Directed by the Protecting Groups. Application to the Total Synthesis of (+)-Varitriol and of Two Diastereoisomers Thereof. *J. Org. Chem.* **2017**, *82*, 8464–8475. https://doi.org/10.1021/acs.joc.7b01211.

(48) Fernandez, A.-M.; Plaquevent, J.-C.; Duhamel, L. Optically Pure Dihydroxy *γ*-Alkylated *γ*-Butyrolactones Starting from ʟ-Tartaric Acid: Application to Formal and Total Syntheses of Natural Products. *J. Org. Chem.* **1997**, *62*, 4007–4014. https://doi.org/10.1021/jo970117e.

(49) Prasad, K. R.; Chandrakumar, A. Stereoselective Syntheses of *γ*-Alkyl (Aryl)-*α,β*-Dihydroxy-*γ*-Butyrolactones and Naturally Occurring Lipid Guggultetrol. *Tetrahedron* **2007**, *63*, 1798–1805. https://doi.org/10.1016/j.tet.2006.12.037.

(50) Mailar, K.; Choi, W. J. The First Asymmetric Synthesis of Marliolide from Readily Accessible Carbohydrate as Chiral Template. *Carbohydr. Res.* **2016**, *432*, 31–35. https://doi.org/10.1016/j.carres.2016.06.005.

(51) Wolf, J.; Jarrige, J.-M.; Florent, J.-C.; Grierson, D. S.; Monneret, C. New 2′-C -Branched-Chain Sugar Nucleoside Analogs with Potential Antiviral or Antitumor Activity. *Synthesis.* **1992**, *1992*, 773–778. https://doi.org/10.1055/s-1992-26224.

(52)   Buchanan, J. G.; Edgar, A. R.; Power, M. J. C-Nucleoside Studies. Part I. Synthesis of [2,3,5-tri-*O*-Benzyl-*α*(and *β*)- D-ribofuranosyl]ethyne. *J. Chem. Soc., Perkin Trans. 1* **1974**, 1943–1949. https://doi.org/10.1039/P19740001943.

(53)   Chandra, G.; Majik, M. S.; Lee, J. Y.; Jeong, L. S. Stereoselective Synthesis of Fluoro-Homoneplanocin A as a Potential Antiviral Agent. *Org. Lett.* **2012**, *14*, 2134–2137. https://doi.org/10.1021/ol300667q.

(54)   Jeong, L. S.; Lee, H. W.; Jacobson, K. A.; Kim, H. O.; Shin, D. H.; Lee, J. A.; Gao, Z.-G.; Lu, C.; Duong, H. T.; Gunaga, P.; Lee, S. K.; Jin, D. Z.; Chun, M. W.; Moon, H. R. Structure−Activity Relationships of 2-Chloro- N6 -Substituted-4′-Thioadenosine-5′-Uronamides as Highly Potent and Selective Agonists at the Human A₃Adenosine Receptor. *J. Med. Chem.* **2006**, *49*, 273–281. https://doi.org/10.1021/jm050595e.

(55)   Serpico, L.; De Nisco, M.; Cermola, F.; Manfra, M.; Pedatella, S. Stereoselective Synthesis of Selenium-Containing Glycoconjugates via the Mitsunobu Reaction. *Molecules* **2021**, *26*, 2541. https://doi.org/10.3390/molecules26092541.

(56)   Zeng, J.; Vedachalam, S.; Xiang, S.; Liu, X.-W. Direct C -Glycosylation of Organotrifluoroborates with Glycosylfluorides and Its Application to the Total Synthesis of (+)-Varitriol. *Org. Lett.* **2011**, *13*, 42–45. https://doi.org/10.1021/ol102473k.

(57)   Clemens, R. T.; Jennings, M. P. An Efficient Total Synthesis and Absolute Configuration Determination of Varitriol. *Chem. Commun.* **2006**, *25*, 2720. https://doi.org/10.1039/b603931f.

(58)   Kumar, V.; Shaw, A. K. First Total Synthesis of (+)-Varitriol. *J. Org. Chem.* **2008**, *73*, 7526–7531. https://doi.org/10.1021/jo8013534.

(59)   Gunaga, P.; Kim, H. O.; Lee, H. W.; Tosh, D. K.; Ryu, J.-S.; Choi, S.; Jeong, L. S. Stereoselective Functionalization of the 1′-Position of 4′-Thionucleosides. *Org. Lett.* **2006**, *8*, 4267–4270. https://doi.org/10.1021/ol061548z.

(60)   Jeong, L. S.; Choe, S. A.; Gunaga, P.; Kim, H. O.; Lee, H. W.; Lee, S. K.; Tosh, D.

K.; Patel, A.; Palaniappan, K. K.; Gao, Z.-G.; Jacobson, K. A.; Moon, H. R. Discovery of a New Nucleoside Template for Human A₃ Adenosine Receptor Ligands: D -4′-Thioadenosine Derivatives without 4′-Hydroxymethyl Group as Highly Potent and Selective Antagonists. *J. Med. Chem.* **2007**, *50*, 3159–3162. https://doi.org/10.1021/jm070259t.

(61) Liang, C.-W.; Choi, W. J.; Jeong, L. S. Synthesis of 2-Alkynyl Substituted 4′-Thioadenosine Derivatives and Their Binding Affinities at the Adenosine Receptors. *Arch. Pharm. Res.* **2008**, *31*, 973–977. https://doi.org/10.1007/s12272-001-1254-x.

(62) Cong, L.; Zhou, W.; Jin, D.; Wang, J.; Chen, X. Synthesis and Antitumor Activity of 5′-Deoxy-4′-Thio-L-Nucleosides. *Chem. Biol. Drug Des.* **2010**, *75*, 619–627. https://doi.org/10.1111/j.1747-0285.2010.00967.x.

(63) Lin, Z.; Xu, X.; Zhao, S.; Yang, X.; Guo, J.; Zhang, Q.; Jing, C.; Chen, S.; He, Y. Total Synthesis and Antimicrobial Evaluation of Natural Albomycins against Clinical Pathogens. *Nat. Commun.* **2018**, *9*, 3445. https://doi.org/10.1038/s41467-018-05821-1.

(64) O'Boyle, N. M.; Banck, M.; James, C. A.; Morley, C.; Vandermeersch, T.; Hutchison, G. R. Open Babel: An Open Chemical Toolbox. *J. Cheminform.* **2011**, *3*, 33. https://doi.org/10.1186/1758-2946-3-33.

(65) Kim, S.; Chen, J.; Cheng, T.; Gindulyte, A.; He, J.; He, S.; Li, Q.; Shoemaker, B. A.; Thiessen, P. A.; Yu, B.; Zaslavsky, L.; Zhang, J.; Bolton, E. E. PubChem in 2021: New Data Content and Improved Web Interfaces. *Nucleic Acids Res.* **2021**, *49*, D1388–D1395. https://doi.org/10.1093/nar/gkaa971.

(66) Ramachandran, B.; Kesavan, S.; Rajkumar, T. Molecular Modeling and Docking of Small Molecule Inhibitors against NEK2. *Bioinformation* **2016**, *12*, 62–68. https://doi.org/10.6026/97320630012062.

(67) Williams, J. D.; Kamath, V. P.; Morris, P. E.; Townsend, L. B. D-Ribonolactoneand 2,3-Isopropylidene (D-Ribonolactone). *Org. Synth.* **2005**, *82*, 75. https://doi.org/10.15227/orgsyn.082.0075.

(68) Batra, H.; Moriarty, R. M.; Penmasta, R.; Sharma, V.; Stanciuc, G.; Staszewski, J. P.;

Tuladhar, S. M.; Walsh, D. A.; Datla, S.; Krishnaswamy, S. A Concise, Efficient and Production-Scale Synthesis of a Protected ʟ-Lyxonolactone Derivative: An Important Aldonolactone Core. *Org. Process Res. Dev.* **2006**, *10*, 484–486. https://doi.org/10.1021/op050222n.

(69) Fan, A.; Jaenicke, S.; Chuah, G.-K. A Heterogeneous Pd–Bi/C Catalyst in the Synthesis of ʟ-Lyxose and ʟ-Ribose from Naturally Occurring d-Sugars. *Org. Biomol. Chem.* **2011**, *9*, 7720. https://doi.org/10.1039/c1ob06116j.

(70) Rountree, J. S. S.; Murphy, P. V. Synthesis of a Novel Polyhydroxylated Salicylic Acid Lactone Framework. *Org. Lett.* **2009**, *11*, 871–874. https://doi.org/10.1021/ol802852r.

(71) Kumar, V.; Shaw, A. K. First Total Synthesis of (+)-Vatriol. *J. Org. Chem.* **2008**, *73*, 7526–7531. https://doi.org/10.1039/C6SC05627J.

Appendix I

List of publications:

1. **Rodrigues, L**.; Majik, M. S.*; Tilve, S. G. Wahidulla, S. Synthesis of (-)-Elemoxide, a Commercially Important Fragrance Compound. *Tetrahedron Letters* **2018**, *59*, 3413-3415.

2. **Rodrigues, L.**; Majik, M. S.* Progress towards the Total Syntheses of *Lycopodium* Alkaloid, Lycopladine A. *Asian Journal of Organic Chemistry* **2019**, *8*, 1-14.

3. **Rodrigues, L.**; Tilvi, S.; Fernandes, M. S.; Harmalkar, S. S.; Tilve, S. G.; Majik, M. S.* Isolation and Identification of Tyrosinase Inhibitors from Marine Algae *Enteromorpha* sp. *Letters in Organic Chemistry* **2020***, 18*, 353 – 358.

4. **Rodrigues, L.**; Tilve, S. G; Majik, M. S.* Synthetic Access to Thiolane-based Therapeutics and Biological Activity Studies. *European Journal of Medicinal Chemistry* **2021**, *224*, 113659-113690.

5. Majik, M. S.*; **Rodrigues, L**.; Tilve, S. G.; Nada, H.; Lee, K. Design, Synthesis, Bioactivity and Molecular Docking Analysis of Elemane-based Sesquiterpenes as Tyrosinase Inhibitor *(Manuscript under preparation).*

6. **Rodrigues, L**.; Tilve, S. G.; Majik, M. S.* Towards the Synthesis of Protected Thiovaritriol: A Strategic Approach for Enhancing Biological Activity *(Manuscript under preparation).*

Appendix II

Participation and presentation at National & International conferences:

1. **L. Rodrigues**, S. G. Tilve, M. S. Majik, "Conversion of Elemol to Commercially Important Sesquiterpenes: Synthetic studies and Biological activities" presented at Recent Development in Chemical Sciences (RDCS-2018), Mumbai (8-9 March 2018).

2. **L. Rodrigues**, S. G. Tilve, M.S. Majik "Melanogenesis Inhibitory Activity Guided Isolation of 4-Hydroxycoumarin and Ergosterol from *Enteromorpha* sp" presented at 17th Prof. K.V. Thomas Endowment Seminar & 2nd International Symposium on New Trends in Applied Chemistry (NTAC-2019) organized by Sacred Heart College (Autonomous) at Crowne Plaza, Kochi from (January 14-15, 2019).

3. **L. Rodrigues**, S. G. Tilve , M.S. Majik, "Synthetic & Bio-activity Studies of Economically Significant Terpenes" presented at a One Day Symposium on Green Chemistry for Better Sustainability organised by Dnyanprassarak Mandal's College and Research Centre Assagao, Bardez-Goa (September 27, 2019).

4. **L. Rodrigues**, S. G. Tilve , M.S. Majik, "Synthetic & Bio-activity Studies of Economically Significant Terpenes" presented at Two-day Workshop on Material Science between University of Porto, University of Coimbra & Goa University organized by Directorate of International Coorporation and Exchange (DICE) & Directorate of Research Development and Resource Mobilization (DRDRM) (November 18-19 , 2019).

5. **L. Rodrigues**, S. G. Tilve , M.S. Majik, "Synthetic Transformation of Elemol to Bio-active Terpenes: Synthesis & Bio-activity Studies" presented at National Conference on New Frontiers in Chemistry-from Fundamentals to Applications (NFCFA-2019) organized by Department of Chemistry, BITS Pilani, K. K. Birla, Goa Campus (December 20-22, 2019).

Symposiums/Workshops attended:

1. Attended and participated in One Day National Seminar on "Recent Trends in Organic Chemistry" at the School of Chemical Sciences, Goa University, Goa (19th August 2017)

2. Participated in the skill development workshop on "Chemical Analysis of Biomolecules and Computation" organized by the Department of Biotechnology, Goa University (23rd -24th November 2017)

3. Attended One Day Seminar on "Recent Trends in Structural Chemistry" organized by the School of Chemical Sciences, Goa University (19th February 2019)

4. Attended and participated in the "17th Annual Convention cum Workshop in Chemistry" organized by Association of Chemistry Teachers-Goa and Government College of Arts, Science and Commerce, Khandola, Marcela-Goa (23rd February 2019).

5. Attended and participated in the "Syngenta Agroscience Symposium: Sustainable Chemistry & Technology" organized by Syngenta Biosciences Pvt. Ltd., Goa (4th November 2019).